Structural analysis of the major light-harvesting complex II by electron paramagnetic resonance (EPR): comparison between monomers and trimers.

Dissertation

zur Erlangung des Doktorgrades Dr. rer. nat.

eingereicht an der Johannes Gutenberg-Universität, Mainz

Carsten Dietz

geb. in Wetzlar

Mainz, Dezember 2012

Structural analysis of the major light-harvesting complex II by electron paramagnetic resonance (EPR): comparison between monomers and trimers.

Dissertation

zur Erlangung des Grades eines ‚Doktor rerum naturalium (Dr. rer. nat.)'

der Fachbereiche

- 08 Physik, Mathematik und Informatik
- 09 Chemie, Pharmazie und Geowissenschaften
- 10 Biologie
- Universitätsmedizin

eingereicht in Fachbereich 10 der Johannes Gutenberg-Universität Mainz

Max Planck Graduate Center

mit der

Johannes Gutenberg-Universität, Mainz

Angefertigt am Institut für allgemeine Botanik

vorgelegt von

Carsten Dietz

Mainz, Dezember 2012

Diese Arbeit wurde im Zeitraum Nov. 2008 bis Dez. 2012 im Fachbereich Biologie in Mainz am Institut für allgemeine Botanik angefertigt.

Amtierender Dekan:

Gutachter

1. Gutachter:

2. Gutachter:

Datum der mündlichen Prüfung: 06.03.2013

Contents

1. Introduction

1.1. Photosynthesis and the photosystem II (PSII) supercomplex

Photosynthesis fuels all biochemical cycles and converts 10^{11} tons of carbon into biomass each year (Field *et al*., 1998). One key factor for this high efficiency is the light reaction that takes place in the thylakoid membrane of the chloroplasts. This membrane can be subdivided into the stacked grana and stroma thylakoids. The photosystems (PS) are distributed heterogeneously (Green and Dunford, 1996); the grana stacks contain PSII, whereas PSI is located in stroma thylakoids (Figure 1.1).

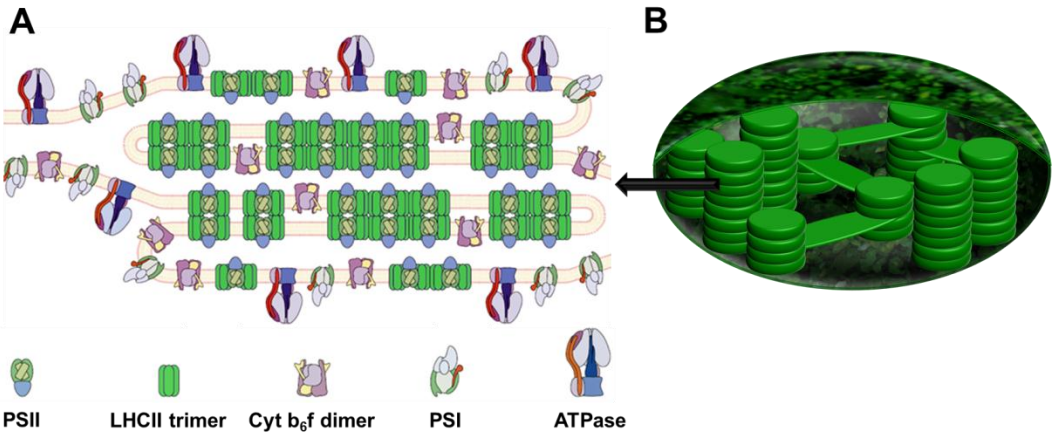

Figure 1.1: View inside a chloroplast (B) and topography of thylakoid stacks with lateral heterogen distributed protein parts of the photosynthesis light-reaction (A). Revised figure; A: Allen and Forsberg (2001).

The light reaction is essential to capture and store sunlight energy, to reduce plastoquinone, to oxidize water, to develop a transmembrane pH gradient, and to transfer electrons to the PSI, where the electrochemical potential is used to reduce reduction equivalents. In particular the PSII supercomplex plays an important role in this energy-conserving mechanism (Figure 1.2). It consists of 25 different protein subunits (Hankamer *et al*., 1997) that can be divided into the core complex and the peripheral antenna. The core complex contains the proteins of the reaction center D1 and D2, the two core antenna proteins CP47 and CP43, cytochrome b-559, several extrinsic proteins as well as small proteins of unknown function (Hankamer *et al*., 1997). Plants are able to collect sunlight

with high efficiency, caused by a perfect composition of peripheral antenna. These consist of several protein-pigment complexes, known as light-harvesting complex II (LHCII) proteins that are associated with the photosystems and transfer sunlight energy to the reaction centers of the PSII (Bassi *et al*., 1997). The absorption of sunlight excites the electrons of the pigments and the energy is transferred within femto- and picoseconds to the reaction centers. The quantum yield of this process is impressively high, which has been shown in bacterial photosystems because these high organized structures (Deisenhofer, 1985; Mc Dermott, 1995) convert the excited molecule state with perfect quantum efficiency into a stable electric potential (Zinth, 1998; Sundström, 2000). The major light harvesting complex II was the main topic of this work, thus, further detailed information relate explicitly to this protein-pigment complex.

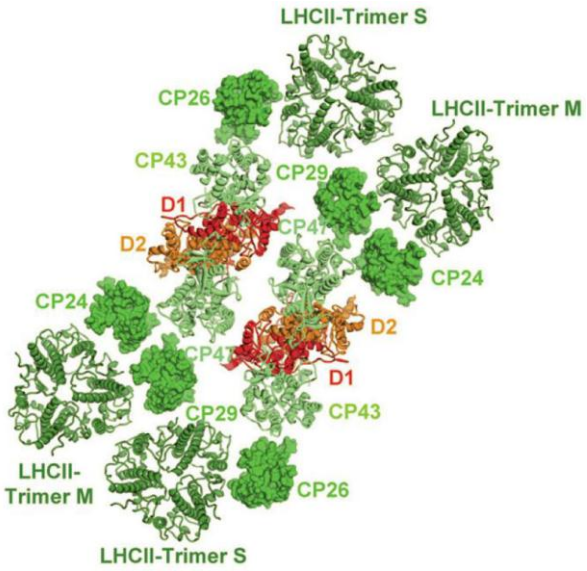

Figure 1.2: PSII supercomplex of higher plants consisting of the core complexes (D1, D2, CP43, CP47), minor (CP24, CP26, CP29) and major light harvesting complexes (LHCII; S: strong bound; M: moderate bound). Figure was taken from Schmid *et al*. (2008). PSII was assembled with chimera (Pettersen *et al*., 2004) using the D1, D2, CP43, and CP47 protein from the structure of the dimeric cyanobacterial PSII (pdb entry 2AXT) and the trimeric LHCII of higher plants (pdb entry 2BHW). Composition bases on electron microscope data from Dekker and Boekema (2005).

1.2. The major light harvesting complex II (LHCII)

The LHCII is the most abundant membrane protein on earth that accounts for approximately 30 % of all thylakoid membrane protein (Peter and Thornber, 1991) and is associated with the dimeric PS core complex via three minor Lhcb proteins (Caffari *et al*., 2009). Each monomer binds 18 chromophores non-covalently, including 50 % of the plants chlorophyll. These chromophores warrant absorption of solar radiation over much of the visible spectrum and increase the quantum yield of PSII to the factor 100.

1.2.1. LHCII biogenesis

The LHC super gene family, located in the nucleus, comprises more than 30 members and encodes the major light-harvesting chlorophyll *a/b*-binding (LHC) proteins, the minor antenna complexes of PSII (Camm and Green, 2004), the antenna complexes of PSI (Jansson *et al*., 1999) as well as photoprotective stress-response proteins (Meyer and Kloppstech, 1984; Adamska, 1997) and the PsbS protein (Wedel *et al*, 1992; Kim *et al*., 1992). The high amount of LHCII within plants is a result of the number of genes that code for Lhcb1, Lhcb2 and Lhcb3 (Schmid *et al*, 2008) and whose products are the three isoforms of LHCII. The polypeptide sequence, structure and function of these chl-protein complexes are similar (Jannson, 1999) and highly conserved; 91.8 % of the amino acids in pea (*Pisum sativum*) and *Arabidopsis thaliana* are identical and a comparison of the isoforms showed 56.6 % identity, whereas variations relate to the termini and the lumenal loop (Standfuss and Kühlbrandt, 2004). Studies of various plants showed that these Lhc isoforms are expressed in parallel (Zolla *et al*., 2002, 2003 and 2007; Storf *et al*., 2004; Timperio and Zolla, 2005). Encoded proteins are a prominent example of post-translationally targeted membrane proteins (Falk and Sinning, 2010), show similar molecular weights between 25 and 28 kDa and consist of approximately 232 amino acids (Jansson, 1994; Standfuss and Kühlbrandt, 2004). In the end they can form homo- or heterotrimers of the LHCII (Jansson, 1994; Jackowski *et al*., 2001).

However, after translation LHCP is transported to the chloroplasts and imported into their stroma by the TOC/TIC import machinery (Soll and Schleif, 2004; Kessler and Schnell, 2009). In the stroma, the chloroplast signal recognition particle (cpSRP) attaches to the hydrophobic LHCP (Figure 1.3), forming a soluble transit complex, which prevents aggregation (Bals *et al*., 2010; Falk and Sinning, 2010). The cpSRP is a heterodimeric complex consisting of a 54 kDa GTPase (cpSRP54) and a 43 kDa novel protein component (cpSRP43) that is limited to chloroplasts (Schünemann, 2007).The cpSRP43, which acts as unique chaperone (Falk and Sinning, 2010) consists of protein-protein interaction domains, three chromodomains, and four ankyrin repeats (Klimyuk *et al*., 1999; Stengel, 2008). The interaction with the LHCP is located in a conserved region (L18 region) between the two transmembrane helices (Tu *et al*., 2000) that acts as an internal targeting signal (Grudnik *et al*., 2009; Cross *et al*. 2009). A tyrosin hook in the ankyrin repeat of cpSRP43 interacts with a DPLG motif within the LHCII (Stengel *et al*., 2008). In order to transport the LHCP to the thylakoid membrane cpSRP54 interacts with the membrane-bound GTPase, cpFtsY (Jaru-Ampornpan *et al*., 2007; Stengel *et al*., 2007; Marty *et al*., 2009). Nonhydrolyzable GTP stabilizes a cpSRP–cpFtsY–Alb3 complex and supports GTP hydrolysis in releasing cpSRP from its receptor in the GDP-bound

conformation (Henry, 2010). The interaction of Alb3, which functions as a translocase (Moore *et al.*, 2000 and 2003) with cpSRP-targeting components stimulates GTP hydrolysis and LHC release from cpSRP, but the timing of these events and the involved protein interactions are not understood (Henry, 2010). Furthermore, the explicit time point of attaching the cofactors and folding process as well as trimerization is unknown.

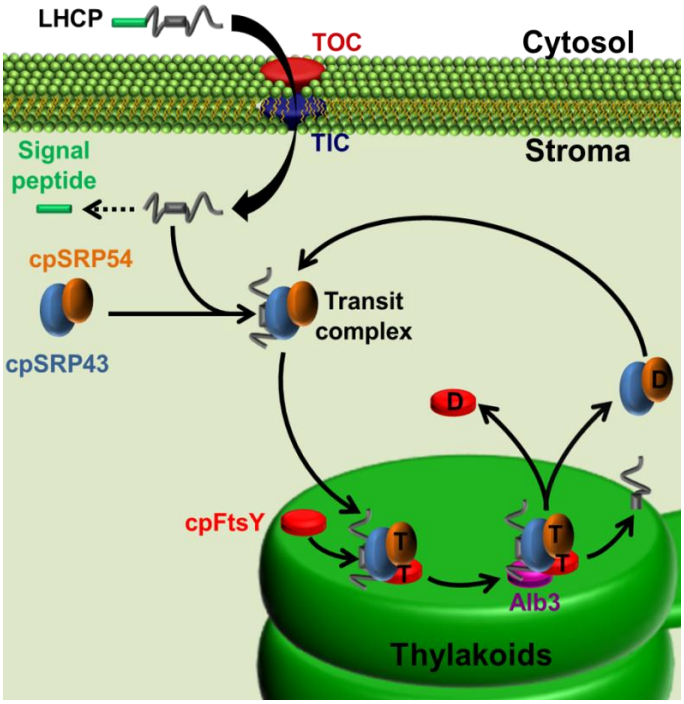

Figure 1.3: During the cpSRP pathway the precursored LHCP is imported into the stroma by a TOC/TIC translocase. After processing to its mature size cpSRP43 interacts with the LHCP, forming a soluble transit complex. The interaction with GTPases, cpSRP54 and its lipid-bound receptor cpFts tranfers the complex to the thylakoid membrane, where both GTPases are boundto GTP (T). The complex attaches to Alb3 stabilized by non-hydrolyzed GTP. LHCP is imported into the thylakoid membrane by hydrolysis of GTP to GDP (D) and accompanied by a released of cpSRP. Figure was reproduced after Henry (2010).

1.2.2. Molecular structure of LHCII

The electron microscopic structure of the LHCII was one of the first with an atomic resolution (Henderson *et al.*, 1990; Popot and Engelmann, 2000) and a major step for LHCII scientific work. In 1991 the first three-dimensional structure of the LHCII was published (Kühlbrandt and Wang, 1994), improved three years later to a resolution of 3.4 Å (Kühlbrandt *et al.*, 1994), in 2004 to 2.72 Å (Liu *et al.*, 2004) and in the end it cumulates in a structure, showing an almost atomic resolution of 2.5 Å (Standfuss *et al.*, 2005). Three LHCII monomers form homo- or heterotrimers (Figure 1.4). The high similarity between Lhcb1, b2, and b3 suggest that the three-dimensional structures of the three subtypes are virtually identical (Barros and Kühlbrandt, 2009). A comparison of the LHCII structure from pea (Standfuss *et al.*, 2005) and spinach (Liu *et al.*, 2004) showed

an approximately perfect overlap between the residues 14 to 231. The rms deviation between all main chain atoms in this range is only 0.40 Å (Barros and Kühlbrandt, 2009).

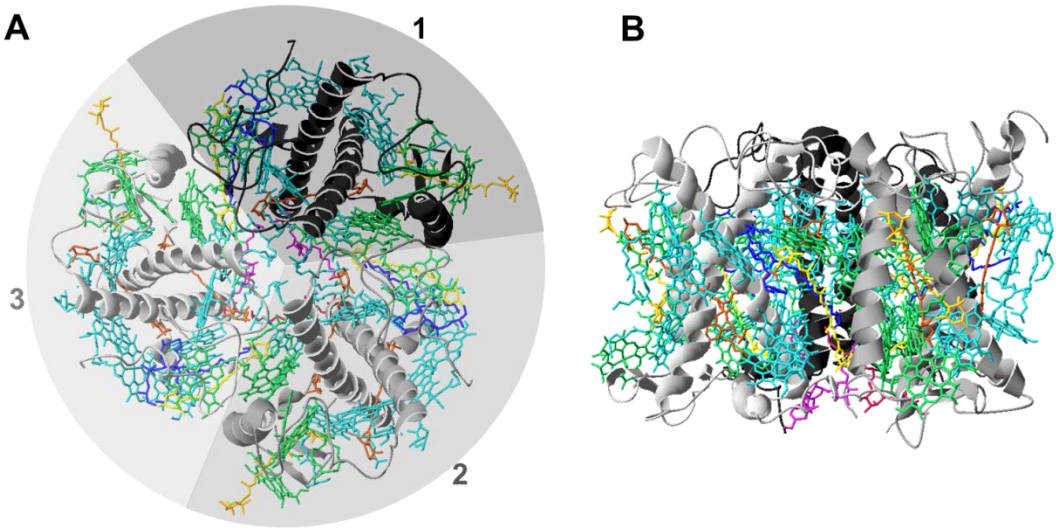

Figure 1.4: Three dimensional structure of a fully-pigmented LHCII trimer at a resolution of 2.5 Å. A: Topview of the complex that consists of three monomers (each monomer is numbered). B: Sideview of the complex. Figure was constructed with pdb viewer (entry 2BHW; Standfuss *et al*., 2005).

Each monomer of the complex consists of the three transmembrane α-helices H1, H3 and H4 as well as the two short amphipathic helices H2 and H5 (Figure 1.5).

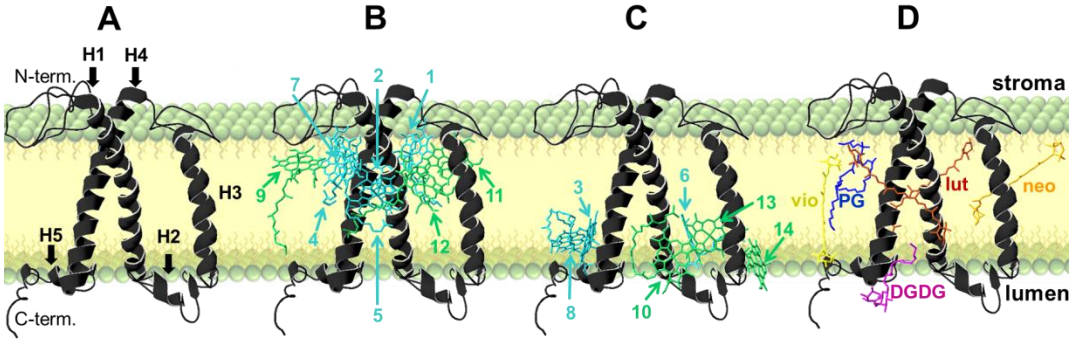

Figure 1.5: Sideview of the LHCII monomeric structure at a resolution of 2.5 Å. A: Three α-helices are spanning the membrane (H1, H3, H4) and the amphipathic helices are the linker between H1 and H3 (H2), respectively H4 and the C-terminus (H5). Chlorophylls are attached in a stromal (B) and lumenal (C) arrangement. D: Each monomer binds the xanthophylls lutein (lut), neoxanthin (neo), violaxanthin (vio) and the lipids PG and DGDG. Figure was constructed with pdb viewer (entry 2BHW; Standfuss *et al*., 2005).

Attached chromophores are eight chl *a*, six chl *b*, two lutein (lut), one neoxanthin (neo), and one violaxanthin (vio) molecules per monomer. For the coordination of the central ligands seven amino-acid residues, two backbone carbonyls, four water molecules, and the phosphodiester group of the lipid PG were identified (Liu *et al*., 2004). These chlorophylls are organized in two levels. Near the stroma site five chl *a* and three chl *b* molecules form an elliptic ring around the helices H1 and H4, whereas three chl *a* and three chl *b* molecules are located close to the lumenal site. It seems that they act as primary collectors in order to transfer absorbed energy to stromal chl (Liu *et al*., 2004). Both lut molecules, bound to the central binding sites L1 and L2, form a network, and support the linkage between H1 and H4. The lut 1 molecule combined with chls 1, 2, and 3 is arranged in a perfect symmetry to the corresponding lut 2 with the chls 4, 5 and 6 (Figure 1.6). This arrangement seems to be highly conserved and optimal for light harvesting, energy transmission, and photoprotection (Barros and Kühlbrandt, 2009). Lut in position L1, crossing the helix cross seems to be essential for the stability of the LHCII, whereas lut in position L2 might be replaced by vio during the xanthophyll cycle (Bassi and Caffari, 2000). The binding site N1 for neo is located close to the chl *b* rich region of H3. Neo is held in position by a single hydrogen bond between the tip of an OH group and tyr112 (Barros and Kühlbrandt, 2009) and represents an exceptional standing among carotenoids. Neo is bound as a cis stereoisomer, whereas the other three carotenoids are bound in their all-trans conformation but the significance of this feature is still unknown (Barros and Kühlbrandt, 2009). In the last decade experiments with the recombinant LHCII could show that the reconstitution without neo works but seems to effect changes within the complex (Hobe *et al*., 2000; Bender, 2004) because neo-free monomers showed trimer-typical CD spectra (Trostmann, 2004; Dietz, 2008). Mozzo *et al*. (2008) proposed that in neo-free complexes lut-lifetime in position L2 decreases and furthermore, the efficiency of energy transfers from chls to carotenoids. This might be essential during triplet quenching (1.2.3.3) because neo seems to function as an O_2 barrier to protect lut in position L2. Another suggestion is an essential role of neo during non-photochemical quenching (Liu *et al*., 2004). In contrast, Barros and Kühlbrandt (2009) proposed that its exposed position might support interactions with other membrane proteins in the photosynthetic apparatus.

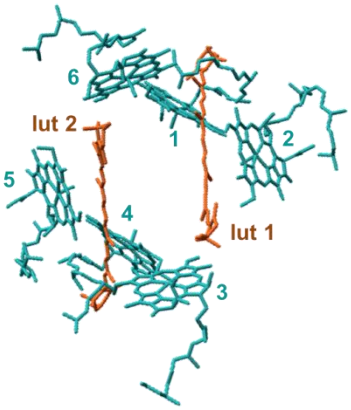

Figure 1.6: Topview to lut 1 with the chl 1, 2 and 3 that show a perfect symmetry to the corresponding lut 2 with chl 4, 5 and 6. Figure was prepared with pdb viewer (entry 2BHW; Standfuss *et al.* 2005).

Within the N-terminal domain is a five amino acid (ac) long sequence (ac 16-21) WYGPDR that is essential for trimerization (Hobe *et al*., 1995). Both aromatic amino acids at the positions 16 (Trp) and 17 (Try) seem to interact hydrophobically with amino acids in the neighboring monomers. Furthermore, this sequence interacts with lipids. PG is essential to form trimers (Trémoliéres *et al*., 1981) and stabilizes them caused by the hydrophobic characteristic; it seems to act as molecular glue between subunits (Nußberger *et al*., 1993). Besides its key role during trimerization, PG might be essential for the formation of grana stacks (Trémoliéres and Siegenthaler, 1998) and the coordination of the chl 7 (Barros and Kühlbrandt, 2009). The function of the other lipid DGDG by contrast is currently unknown (Standfuss *et al*., 2005) and variable positions were detected in LHCII crystal structures of spinach (Liu *et al*., 2004) and pea (Standfuss *et al*., 2005). However, further interactions that support trimerization were identified at the C-terminal domain. The non-polar Trp 222 seems to interact with the helix H3 respectively the pigments chl 10 and vio (Barros and Kühlbrandt, 2009).

1.2.3. Functions and regulation processes of LHCII

The LHCII maximizes the efficiency of the PSII immensely by collecting and transferring solar energy to the core complexes. The ability to absorb solar radiation efficiently requires chromophores that are attached to the protein. *In vivo* the absorption wavelength of chromophores depends on the chemical environment: on one hand the partial charge of surrounding amino acids and the deflection of chl side groups, on the other hand the arrangement within surrounding proteins. The closer the chl molecules, the higher the tendency for dipol-dipol interactions or exchange interactions. These interactions lower the energy level and thus, lead to a red shift of the absorption maxima. The fastest energy transfer between pigments was measured at room temperature. The fastest chl *b* to chl *a* transfer occurred with a lifetime of 150-200 femtoseconds (Connelly *et al*., 1997; Trinkunas *et al*., 1997; Kleima *et al*., 1997; Gradinaru *et al*., 1998), whereas energy transfer between the chl *a* was measured with >1 picosecond (Visser *et al*., 1996; Trinkunas *et al*., 1997; Kleima *et al*., 1997). These fast processes do not depend on slow redox processes; energy transfer is radiationless (Förster transfer). The arrangement of the chromophores enables a perfect exciton transfer from the light harvesting antennas to the core complexes. The conversion of light energy into electrochemical potential requires two photosystems working in close collaboration (Allen and Forsberg, 2001) but an efficient absorption of solar radiation also includes risks and is complicated to manage. High efficiency absorption under constant light conditions is one thing, but in nature light

levels can differ within seconds, caused by changes in cloud cover, or the sudden exposure of a shaded leaf to bright sunlight. Furthermore, almost all green plants are sessile and cannot move into the shadow. Therefore, finely tuned regulation processes are required for a perfect adaptation to constantly changing weather conditions.

1.2.3.1. State transition

Both PS are wired in series, thus, the flow rate of electrons through both PS must be adapted (Hill and Bendall, 1960; Duysena and Amesz, 1962). However, PS I uses blue, red and far-red light, whereas PSII uses more blue than red light and does not use far-red light at all (Allen and Forsberg, 2001). Besides these differences the light conditions vary during each day. To ensure an equalized flow rate of electrons, a regulation process called state transition (qT) is used, which regulates the distribution of absorbed excitation energy between the two photosystems under varying environmental conditions and/or metabolic demands (McConnell *et al.*, 2002). If electrons are accumulated at plastoquinone, the N-terminal domain of LHCII apoprotein gets phosphorylated by a protein kinase. Phosphorylated LHCII leaves PSII, attaches to PSI to act as its light-harvesting antenna and to increases the absorption of light (state 2). In this way the supply of electrons from PSII to plastoquinone decreases, whereas the electron flow out to PSI increases. If the amount of electrons at plastoquinone becomes too low,

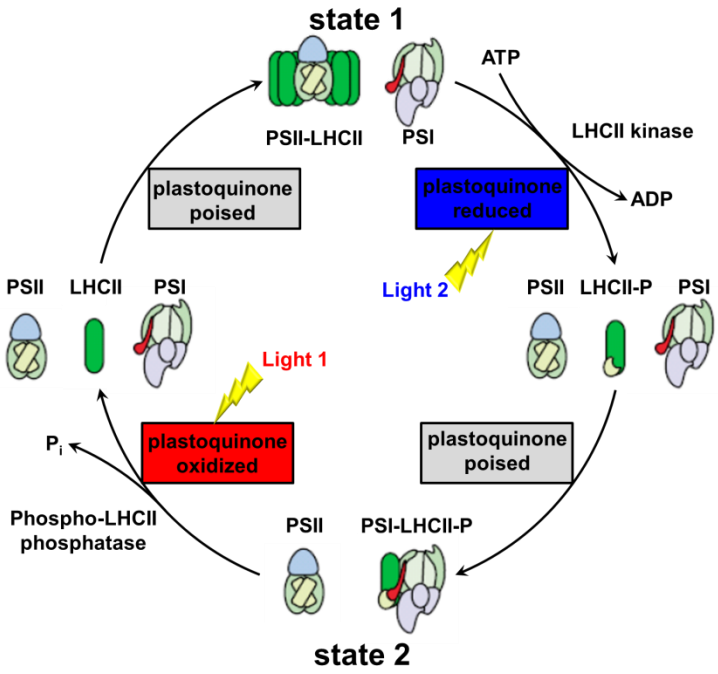

Figure 1.7: Mechanism of state transition (modified fig. from Allen and Forsberg, 2001). State 1: LHCII trimer is attached to PSII. If the amount of electrons at the plastoquinone increases under high-light conditions, the LHCII will be phosphorylated by a kinase. The phosphorylated LHCII binds to the PSI (state 2). An electron deficit at the plastoquinone leads to a dephosphorylation of the LHCII.

the kinase will be switched off and a phosphoprotein phosphatase converts LHCII back to its non-phosphorylated state; LHCII leaves PSI and binds to PSII (state 1).

1.2.3.2. Non-photochemical quenching

Plants require a regulation mechanism that adapts within minutes or seconds to changing light conditions (Standfuss *et al*., 2005). The non-photochemical quenching, known as NPQ (Demming-Adams, 1990) is a non-photochemistry process that includes the quenching of chlorophyll fluorescence by conversion into heat (Krause and Weis, 1991). The molecular mechanism is discussed controversially but common suggestions are that this quenching is energy dependent (qE), the ΔpH in the thylakoids can be seen as a volume knob, and xanthophylls play a key role.

Under high-light conditions the photosynthetic electron transport chain is very active and protons accumulate in the thylakoid lumen, leading to a drop of the lumenal pH value. The ΔpH seems to have two effects (Holt *et al*., 2005; Zaks *et al*., 2012): The first effect is the activation of the xanthophyll cycle (Gilmore and Yamamoto, 1992; Horton and Ruban, 1992; Pfündel and Bilger, 1994). The pH sensitive lumenal violaxanthin (vio) de-expoxidase (VDE) enzyme (Hager, 1969; Demming-Adams, 1990; Pfundel and Bilger, 1994; Hieber *et al*., 2000) floats in the lumen until the pH drops below 6. Then it binds to the thylakoid membrane and uses ascorbate to convert vio to the intermediate antheraxanthin and finally to zeaxanthin (zea), which has the lowest ionization potential of the three xanthophyll-cycle carotenoids (Dreuw *et al*., 2003). The second effect is the protonation of the acidic residues E122 and E226 of PsbS (Li *et al*., 2002 and 2004; Niyogi *et al*, 2004), which seems to provide the side of quenching because zea is bound and interacts with the LHCII, forming an chl-zea heterodimer that quenches excited chl (Holt *et al*., 2005). However, besides this newest

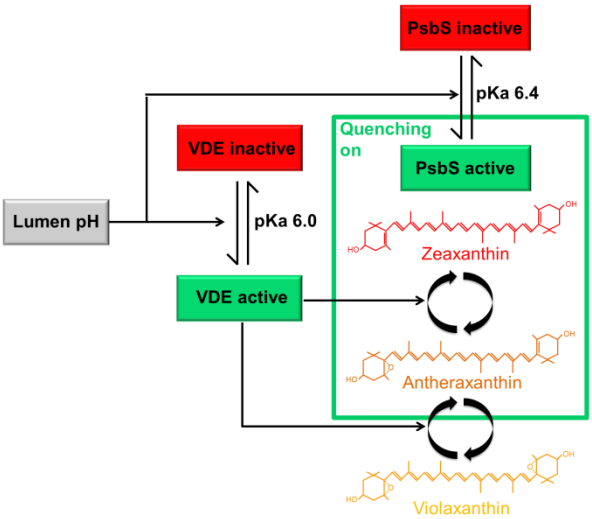

Figure 1.8: Schematic of qE activating system. If the pH drops, PsbS gets activated by protonation and active violaxanthin de-epoxidase (VDE) converts violaxanthin to zeaxanthin. Modified figure after Zaks *et al.* (2012)

hypothesis four others exist, that are partially suggest a conformational change of the LHCII.

Standfuss *et al*. (2005) support the suggestion that NPQ can be divided in a slow and fast component (Niyogie *et al*., 1998). The slow component (activated within minutes) is related to the xanthophyll-cycle. The fast component (induced within seconds) is activated by a drop of the pH value in the thylakoids and seems to be independent of the xanthophyll cycle. According to the slow component they proposed that the vio leaves its binding site and is converted to zea, which attaches to the vio binding site. Due to its more extended π system it accepts energy from the nearby chl 8. The energy cannot escape and is dissipated as heat. A conformational change of the LHCII does not take place.

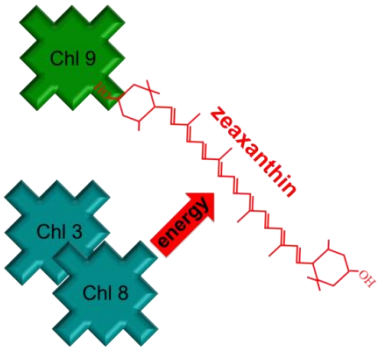

Figure 1.9: Hypothetic mechanism of NPQ after Standfuss *et al.* (2005). Excessive energy is transferred from chl 8 to zea, which is bound to the vio binding site of the LHCII.

Barros and Kühlbrandt (2009) also proposed a mechanism without a conformational change of the LHCII but including the PsbS dimer, which is almost similar to Holt *et al*. (2005) and Zask *et al*. (2012). A drop of the pH value activates the xanthophyll cycle. Vio is converted to zea but then zea goes into the lipid phase of the membrane. At the same time the PsbS dimer monomerizes and uncovers its zea binding site. Zea binds to the PsbS monomers, which interacts with minor and major light harvesting complexes. Such a zea-chl heterodimer acts as an effective quencher and dissipates extensive energy as heat.

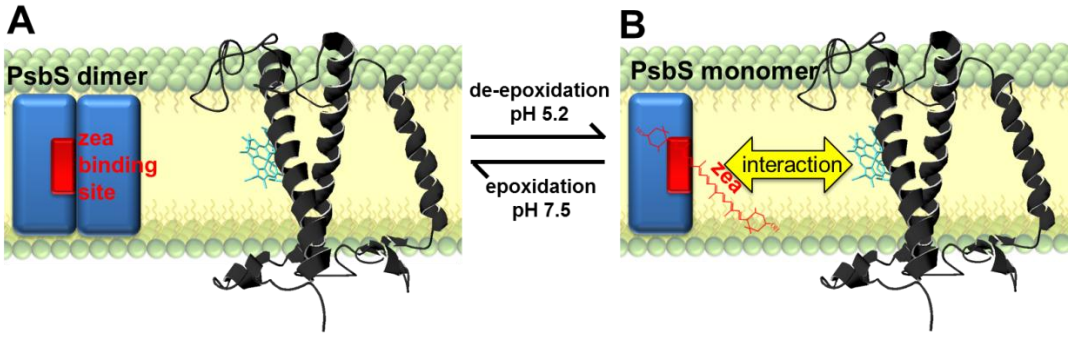

Figure 1.10: Hypothesis of NPQ after Barros and Kühlbrandt (2009). De-epoxidation leads to the conversion of vio to zea and monomerization of the PsbS dimer. Zea attaches to its binding site with the PsbS monomer and interacts with minor and major light harvesting complexes.

In contrast, Pascal *et al*. (2005) and Ruban *et al*. (2007) suggest a mechanism including a conformational change that is triggered by a twist of neo. Due to this twist lut gets closer to the chl 1, 2 and 7, resulting in changed energy levels of these pigments. Instead of transferring excitation energy to the core complexes it is absorbed by lut and dissipated as heat. Furthermore, the neo twist might affect a repositioning of the chl *b* molecules 10 and 13, leading to heat dissipation of excessive light energy (Pascal *et al*., 2010).

Figure 1.11: Hypothetic mechanism of NPQ after Pascal *et al*. (2005) and Ruban *et al*. (2007). A twist of neo leads to a reorientation of lut to surrounded chl molecules 1, 2 and 7 (A) and to a repositioning of the chl *b* molecules 10 and 13 into a dissipating formation(B).

The last hypothesis was proposed by Liu *et al*. (2004). They suggest a direct interaction of the de-epoxidase and the LHCII including a conformational change. In detail, the pH value drops and activates the xanthophyll cycle. LHCII-attached vio is directly converted to zea and lumen-exposed amino acids get protonated, which triggers a conformation change of the helices 2 and 5. This conformational change reorients the chlorophylls 8 and 14 to promote the energy transfer to zea, which dissipates excessive energy as heat.

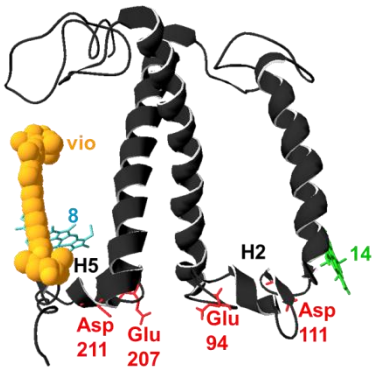

Figure 1.12: Hypothetic mechanism of NPQ after Liu *et al*. (2004). If the pH value decreases, lumen exposed amino acids get protonated, which triggers a conformational change of the helices H2 and H5 and thus, a reorientation of the chls 8 and 14.

1.2.3.3. Triplet quenching and relevance of the carotenoids

Besides NPQ, the fastest response to excess light conditions is triplet quenching within the antenna complexes by the carotenoid molecules (Salvadori *et al*, 2012) that act as direct quenchers of triplet chl to prevent the production of high reactive singlet oxygen (Frank

and Cogell, 1996). Caused by their low lying triplet state, energy is not sufficient to excite other molecules and is therefore dissipated as heat. Several triplet states of the carotenoids and their specific interactions with nearby chls were detected (Van der Vos *et al*., 1991). Among the carotenoids lutein could be identified as a chl triplet quencher by using optical and EPR spectroscopies (Di Valentin *et al*., 2009; Lampoura *et al*., 2002; Mozzo *et al*., 2008). Further investigations showed that in LHCII two photoprotective pairs of pigments are formed: chl 2 with lut 1 and chl 5 with lut 2 (Salvadori *et al*, 2012). The distance between these pairs is smaller than 3.7 Å, thus they fulfill all requirements for efficient triplet quenching.

1.2.4. The recombinant LHCII

The voltage-dependent anion channel (Engelhardt *et al*., 2007), the mammalian G protein-coupled receptor (Michalke *et al*., 2010), bacteriorhodopsin (Huang *et al*., 1981), and the LHCII are membrane proteins that could be analyzed *in vitro*. Initial knowledge of the LHCP gen was reached by the isolation (Broglie *et al*., 1981) and sequencing (Coruzzi *et al*., 1983) of its cDNA. After gene isolation (Cashmore *et al*., 1984) a recombinant overexpression in *E. coli* (Paulsen *et al*., 1990) and refolding by mixing the apoprotein with its cofactors was established, leading to a full functioning complex (Plumley and Schmidt, 1987; Paulsen *et al*., 1990). Usually membrane proteins tend to aggregate and precipitate in the absence of membranes and *in vitro* refolding barely works. Therefore, overexpression in bacteria combined with a complete refolding represents a valuable chance to learn more about membrane protein function in general because the LHCII as the most abundant membrane protein on earth can be seen as a model system. During the last two decades a lot of information about the refolding process (Booth and Paulsen, 1996; Reinsberg *et al*., 2000; Horn and Paulsen, 2002 and 2004; Horn *et al*., 2007) and principles of trimerization (Hobe *et al*., 1995) was obtained by fluorescence or circular-dichroism spectroscopy. Site-directed mutagenesis of the recombinant LHCII combined with site-directed spin labeling facilitated electron paramagnetic resonance measurements (Bender, 2004) and therefore, structural analysis of a solubilized membrane protein. Besides measurements of the refolded protein also the refolding process was monitored and revealed a two-stage model (Dockter *et al*., 2008). In a faster phase (30s-150s) the chl *a* molecules attach to the protein and a large part of the secondary structure forms. The slower phase (30 s-900 s) comprises the binding of chl *b* and the final condensation of the complex, juxtaposing the α-helices.

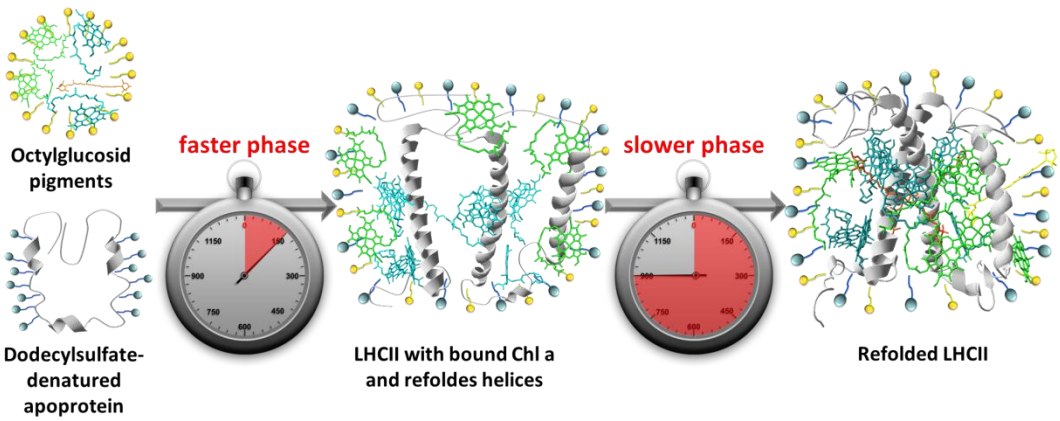

Figure 1.13: The refolding process of the LHCII can be divided into a faster phase (30-150 seconds) in which large part of the secondary structure forms and a slower phase (30-900 seconds) that includes the final condensation of the complex. Figured was prepared after Dockter *et al*. (2008).

1.2.5. Electron paramagnetic resonance (EPR) as an alternative technique for structural information

X-ray crystallography is currently the most favoured technique to monitor the three-dimensional structure of proteins. Compactly folded structures that do not change their structure during the crystallization process are best suited for X-ray, whereas flexible subunits escape a defined resolution. Furthermore, monitored conformations might not always represent the catalytic or functional state (Perozo *et al*., 1999; Fanucci *et al*., 2003). Alternative techniques to analyze proteins in solution are cryo-electron microscopy, nuclear magnetic resonance (NMR), and electron paramagnetic resonance (EPR). Cryo-electron microscopy enables to determine molecules and cell components *in vivo* but chemically unfixed preparations are sensitive to radiation and might get destroyed. NMR is the most popular method to monitor the intramolecular dynamics of proteins but liquid NMR spectroscopy is limited to molecules below 25-30 kDa and therefore, not suited for the LHCII. Solid-state NMR by contrast can be used for larger proteins and was established for the LHCII but led to further problems caused by the necessary protein concentration and therefore, aggregation problems (Dietz, 2008). However, EPR is an alternative spectroscopic method that bases in comparison to NMR on the detection of electron spins and is therefore, much more sensitive. This offers the possibility to get more information about the dynamic and interaction of a protein under functional conditions (Hubbel *et al*., 2000; Steinhoff, 2002). However, for this purpose chemically stable spin labels at defined positions within the protein are needed. Pioneer

research about spin labels was published three decades ago (Forrester *et al.*, 1968; Rozantsev, 1970; Balaban, 1971; Rozantev and Scholle, 1971; Aurich and Heiss, 1976; Janzen, 1971). Several nitroxide radical labels were analyzed (Keana, J. F. W., 1977); leading to a large number of nitroxide free radicals that are chemically stable. Studies showed that most stable nitroxide free radicals are secondary amine N-oxides in which there are no hydrogens attached to the α-carbon atoms (Keana, J. F. W., 1978). Such a stable label is PROXYL iodacetamide (PROXYL-IAA), which binds specifically to the sulfhydryl group of cysteine. The LHCII is best suited for EPR analyses because the recombinant protein can be modified by site-directed mutagenesis to attach spin labels to engineered cysteine residues replacing other amino acids without a functional impact. Two popular EPR-techniques (Figure 1.15) in order to study the protein dynamics are double electron electron resonance (DEER) and electron spin echo envelopment (ESEEM).

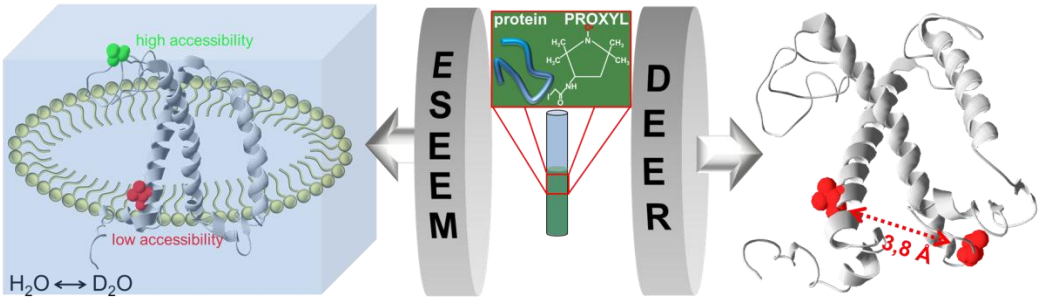

Figure 1.14: Two popular EPR techniques are DEER EPR to measure the distance between two attached spin labels (red balls) and ESEEM EPR to measure the accessibility of a spin label to the environment.

DEER offers a couple of possibilities: firstly to measure the distance between two spin labels, secondly the distance distribution enables statements on the rigidity or flexibility of the measured positions, and thirdly a series of double labeled molecules enables modeling of the protein structure by determining the distances between labels (Hubbel *et al.*, 1998). The maximum detectable distances are 8 nm (Figure 1.15). ESEEM by contrast provides additional information because it is used to measure the accessibility of a spin label to the

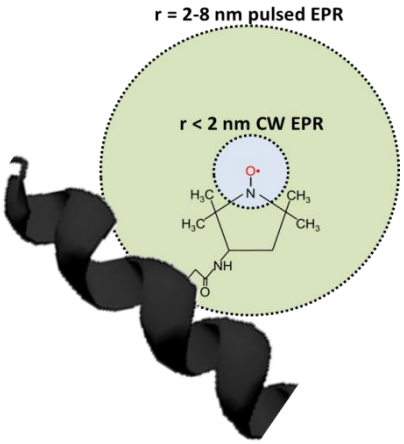

Figure 1.15: Site-directed labeling of a protein enables to define the distance between two spin labeles by measuring the diplor interactions. CW EPR is used for distances below 2 nm and pulsed EPR for distances between 2 and 8 nm.

environment. According to a membrane protein, it is therefore possible to distinguish between labeled amino acids that are either deep inside the hydrophobic part of the membrane or exposed to the hydrophobic environment. Besides several proteins, which were analyzed by EPR during the last two decades, EPR was established to the LHCII eight years ago (Bender, 2004). Since 2004, further samples were prepared and the method was refined continuously (Seimetz, 2004; Dockter, 2005 and 2009; Jeschke *et al*., 2005; Hebel, 2007; Dietz, 2008; Müller, 2008; Dockter *et al*., 2008; Volkov *et al*., 2010). Thereby, a lot of information about the terminal domains, the rigid core and loop regions in a monomeric and trimeric assembly of the LHCII in aqueous solution were collected.

1.3. Purpose of this work

In this work site-directed spin labeling of the LHCII was to be continued to get a deeper view inside membrane protein function by using EPR spectroscopy techniques. Previous data revealed the high potential but also the complexity of EPR measurements of a membrane protein. On one hand EPR is an excellent method to analyze rigid and flexible parts of the LHCII in aqueous solution and to compare measured distances with the crystal structure, on the other hand sample preparation includes several pitfalls, resulting in a loss of signal and/or contradictions between experimentally measured and theoretically predicted distances that occurred preferably in monomeric samples.

The significance of EPR measurements for protein analyses increases as the sensitivity of EPR spectrometer is constantly improved and pitfalls during sample preparation are avoided. Thus, it appeared necessary to analyze and optimize all sample preparation steps in detail. In combination with the establishment of the stronger Q-band EPR spectrometer the intention was to increase the detection limit to a level that allows measuring low concentrated protein samples, which was required to model and compare the incompletely resolved N-terminal domain in both assembly states. For this purpose it appeared necessary to establish a reproducible method for the production of heterogeneous trimers, whose signals are automatically reduced because they consist of one double labeled monomer and two unlabeled monomers. A further important step to study the natural dynamic and conformation of the LHCII, which also required high EPR sensitivity, was a unidirectional insertion of the refolded protein into liposomes. Several experiments were conducted a few years ago but failed (Boggasch, 2006; Yang *et al.*, 2006). This project was resumed with the intention to mimic regulation mechanisms, for example a pH gradient over the membrane and its influence to the lumenal loop region. Simultaneously

it appeared worthwhile to analyze this region under varied conditions in detergent micelles because the conformation of the lumenal loop during NPQ is controversially discussed (1.2.3.2) and EPR measurements of the detergent-solved LHCII are still established.

2. Material and methods

2.1. Equipment

Adsorption Spectrometer

UV-2101 PC	Shimadzu Corporation, Japan
V-550	Jasco labor and data technique GmbH, Groß-Umstadt
Microplate Reader	Tecan Infinite M1000
Eppendorf photometer	Eppendorf Vetrieb Germany GmbH, Wessling-Berzdorf

Autoclave

Varioclave Typ 500 H+P	Labor technique GmbH, munich

Camera

Canon Power Shot A710IS digital	Canon Germany GmbH, Krefeld

CD Spectrometer

J-810-S	Jasco labor and data technique GmbH, Groß-Umstadt

Pelletier element: Modell CDF-426S/426L

Software: Spectra Manager, Version 1.6

Cell disruption

French Pressure Cell Press	SLM Aminco, SLM Instruments

Centrifuges

Cooling centrifuges

J2HS; rotors: JLA-10500, JA-20.50	Beckmann Instruments, munich
Mikro 22 R; rotors: 1015, 1016 und 1195	Hettich Zentrifugen, Tuttlingen
Rotina 38 R; rotors: 1792 und 1789-L	Hettich Zentrifugen, Tuttlingen

Table centrifuges	
Mikro 12-29; rotor: 2029	Hettich Zentrifugen, Tuttlingen
Ultra centrifuges	
Optima XL-100K, XL-90K and XL-80K	Beckmann Instruments, munich
Rotors: SW60Ti, SW41Ti, SW40Ti and SW28Ti	
Cycler/Rotator	
Culture cycler type rotator	Bachofer GmbH, Reutlingen
EPR Spectrometer	
Spectrometer: Elexsys EX 580	Bruker BioSpin GmbH, Rheinstetten
Resonator: Split Ring ER4118X-MS3	
Resonator Q-Band	Self-construction AG Jeschke, ETH Zurich, switzerland
Amplifier: high-power TWT (150 W)	
Temperature control: Oxford CF935	Oxford Instruments, UK
Cryostat, ITC4 temperature controller	
Software: DEER-Analysis2006: www.mpip-mainz.mpg.de/~jeschke/ distance.html	
Extruder	
LiposoFast-Basic Extruder	Avestin, Mannheim
Membrane: Polycarbonate 100 nm	
Fluorescence Spectrometer	
Fluoromax 2	ISA SPEX Jobin Yvon, Grasbrunn
Cooling: Ministat Compatible Control	Huber Kältemaschinenbau GmbH, Offenburg
Software: Datamax Software, version 2.24	

Gel electrophoresis

Gel gating system: Midget system	Pharmacia LKB Biotechnology, Piscataway
Voltage source	Bio-Rad Power-Pac 3000, USA
Cooling: Haake G, Haake D1, Modell Fisons	Firma Haake Messtechnik GmbH, Karlsruhe
Gel dryer: 2003 Slab Gel Dryer	LKB Bromma

Gel documentation

VersaDoc™ Imaging System 3000	Bio-Rad, munich
Software: Quantity One	

Heating cabinet

Memmert	Memmert, Schwalbach

HPLC - analytic

Mixer: LG-1580-04 Quaternay Gradient Unit	Jasco labor and data technique GmbH, Groß-Umstadt
Pump: Pu-1580 Intelligent	
Detector: Diode Array Detector MD-1515	
Column: Chromolith SpeedROD RP-18e	
Software: Jasco-PDA, BROWIN, Version 1.5	

HPLC – preparative

Pumps: Modell 510, 501	Waters Millipore, Milford, MA, USA
Interface: System Interface Module	Waters Millipore, Milford, MA, USA
Detectors: Absorption: SP-6V; Fluorescence: RF 535	Gynothek GmbH, Gemering; Shimadzu Corporation, Kyoto, Japan
Column: Waters Bondapak C18; 125 Å; 10 µm; 30 x 300 mm	Waters Millipore, Milford, MA, USA

Software: Max 829	Waters Millipore, Milford, MA, USA
Incubator	
Certomat	H/B, Braun Biotech International, Melsungen
Laminar flow	
Laminar flow	SLEE Semiconductor Technik GmbH, Mainz
Magnetic stirrer	
Heidolph MR 3001 K8	HeidolphElektro, Kelheim
IKAMAG KMO2 basic	IKA, Labortechnik, Staufen
Mixer	
Heavy Duty Blendor	BlendorWaring, USA
PCR-Cycler	
Primus 25 Legal PCR-System Modell 5524	MWG-Biotech, Ebersberg
pH-Meter	
INOLab pH Level 2	WTW GmbH, Weilheim
Refractometer	
Hand refractometer HR900A	Krüss Optronic GmbH (Hamburg)
Rotary evaporator	
Heidolph VV 2000	Heidolph Elektro, Kelkheim
Ultrasonicator	
SONOREX Super	Bandelin, Berlin
Vibra Cell high intensity ultrasonic processor VC600	Sonics and Materials, Danbury, USA

Vortex	
IKA MS2 Minishaker	IKA Labortechnik, Staufen
Water bath	
Thermomix MM	H/B, Braun Biotech International, Melsungen
Water boiler	
HB4 basic	IKA, Labortechnik Staufen
Weighing machine	
BP 2100S	Sartorius AG, Göttingen
Analytik A200S	Sartorius AG, Göttingen

2.2. Chemicals

2.2.1. Solvents

All used solvents were purchased from Merck (Darmstadt), Riedel de Häen (Hannover) and Carl Roth (Karlsruhe). The purity of acetone was increased by distillation under ambient pressure. In order to recycle used acetone, it was distilled two times. Peroxides within diethyl ether were removed by adding KOH, boiling for two hours under reflux and one distillation.

2.2.2. Gases

Nitrogen was purchased from Widmann Gas (Gase Center Herbarth, Budenheim) and used for the drying process of pigments as well as circulating the detector of the CD spectrometer.

2.2.3. Further chemicals

All other chemicals (quality p.a.) were purchased from the companies: Amersham Pharmacia Biotech (Freiburg); Alfa Aesar (Karlsruhe); Avanti Polar-Lipids (Hamburg); Biomol (Hamburg); BioRad Laboratories (Munich); Boehringer (Mannheim); Macherey-Nagel (Düren); MobiTec (Göttingen); New England BioLabs Inc. (Schwalbach); PEQLAB Biotechnologie GmbH (Erlangen); Serva (Heidelberg); Sigma-Aldrich (Deisenhofen)

2.3. Protein standards

For denaturing gel electrophoresis the SDS7 (Sigma-Aldrich) and protein test mixture 6 (Serva) were used. According to the SDS7 standard, proteins were dissolved in a buffer, consisting of 62.5 mmol/l Tris/HCl (pH 6.8), 2 % sodiumdodecylsulfate (SDS), 5 % ß-mercaptoethanol (ß-me), 10 % glycerol, and 0.001% bromphenol blue. According to the protein test mixture 6, standard proteins were dissolved in a buffer consisting of 125 mmol/l Tris/HCl pH 6.8, 2 % SDS ,15 % glycerol, 10 mmol/l DTT, 0.025 % bromophenol blue, 0.025 % Orange G. Before using protein standards were boiled for 2 min. at 100°C.

Table 2.1: Composition and molecular weights of the protein standard SDS7.

Molecular weight	Protein
67.0 kDa	Albumin bovine
45.0 kDa	Albumin egg
36.0 kDa	Glyceraldehyd-3-phosphate dehydrogenase, rabbit
29.0 kDa	Carbonic anhydrase bovine
24.0 kDa	Trypsinogen, bovine pancreas
20.1 kDa	Trypsin inhibitor, soybean
14.2 kDa	α-Lactalbumin, bovine milk

Table 2.2: Composition and molecular weights of the protein test mixture 6.

Molecular weight	Protein
97.4 kDa	Phosphorylase B
67.0 kDa	Albumin bovine
45.0 kDa	Albumin egg
29.0 kDa	Carbonic anhydrase bovine
21.0 kDa	Trypsin inhibitor, soybean
12.5 kDa	Cytochrome C
6.5 kDa	Trypsin inhibitor, bovine lung

2.4. Labels

2.4.1. Fluorescence label

DY731-maleimide (DYOMICS, USA)

Specifications: $C_{44}H_{53}N_4O_{10}S_2Na$; molecular weight: 885.04 g/mol; max. absorption (ethanol): 736 nm; max. emission (ethanol): 759 nm; molar extinction-coefficient: 225000 [cm^{-1} x M^{-1}]; soluble in water, methanol, DMF, DMSO; light sensitive.

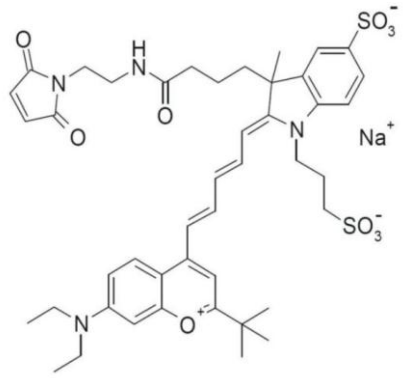

Figure 2.1: Structural formula of DY731.

2.4.2. EPR label

3-(2-Iodoacetamido)-PROXYL, free radical - PROXYL-IAA (Sigma-Aldrich)

Specifications: $C_{10}H_{18}IN_2O_2$; molecular weight: 325.17 g/mol; soluble in DMSO, DMF, water, ethanol; light sensitive.

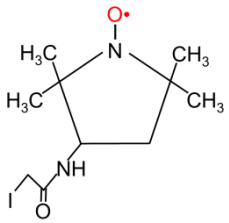

Figure 2.2: Structural formula of PROXYL-IAA.

2.5. Bacterial strains

2.5.1. JM101

Chemo-competent bacteria cells of the *E. coli* expression strain JM101 were purchased from NEB (Bad Schwalbach). The production of chemo-competent cells as well as the transformation efficiency was done like described in Müller (2008).

2.5.2. XL1-Blue

Super-competent bacteria cells of the *E. coli* strain XL1-Blue were part of the "Quickchange® II site-directed mutagenesis kit" and purchased from Stratagene (La Jolla, USA). All cells were thawed on ice, divided into aliquots, frozen in liquid nitrogen, and stored at -80°C. Directly before using, aliquots were thawed on ice.

2.6. Construction of new Lhcb1 mutants

All newly constructed mutants are derivatives of the mature *Lhcb1* gene (*lhcb*1*2, AB80; Cashmore, 1984) from pea (*Pisum sativum*) and were inserted into the multiple cloning site of the expression vector pDS12-RBSII (Bujard *et al*., 1987). The pDS12-RBSII vector including the *Lhcb1* consists of 4241 nucleotides. The plasmid is figured out and described in Figure 2.3.

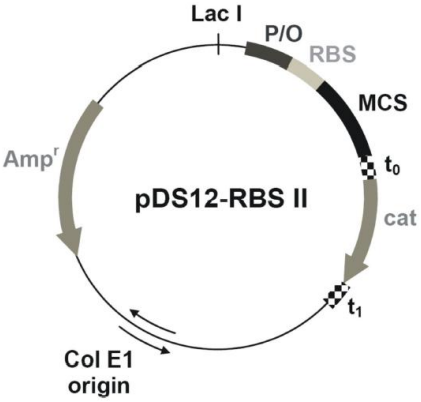

Figure 2.3: Schematic overview of the expression vector pDS12-RBSII. Col E1: origin of replication; Amp^r: ß-lactamase gene for ampicillin resistance; Lac I: Lac repressor gene; P: T5 promotor P_{N25}, O: *E. coli* lac operator; RBS: ribosome binding-site; MCS: multiple cloning-site; t_0 and t_1: terminators; cat: gene for chloramphenicol acetyltransferase for chloramphenicol resistance. Modified figure after Heinemann (1999).

For the construction of the mutants the plasmid of suitable clones was isolated and the DNA concentration analyzed (2.6.1). Replacements of amino acids were done by using the "Quikchange® II site-directed mutagenesis kit" (2.6.2) and protein tags as well as additional amino acids were introduced by using the "Phusion Site-Directed Mutagenesis kit" (2.6.3). PCR products were transformed in *E. coli* (2.6.4). Finally new mutants were sequenced (2.6.5) and stored as gylcerol stocks (2.6.6).

2.6.1. Plasmid isolation and DNA quantification

Material:

peqGOLD plasmid miniprep kit I (PEQLAB Biotechnologie, Erlangen)

LB-amp plates	1 % Tryptone	Liquid LB media	1 % Tryptone
	0.5 % Yeast		0.5 % Yeast
	1 % NaCl (pH 7.5)		1 % NaCl (pH 7.5)
	1.5 % Agar		1 % Tryptone
	100 µg/ml Ampicillin		

Method:

For plasmid isolation, bacteria of *E. coli* strain JM101 were separated overnight on Luria-Bertani (LB)-ampicillin (amp)-plates at 37°C. One culture was picked and overnight grown in 15 ml liquid LB-medium at 37°C, containing 100 mg/ml amp. The plasmid DNA was isolated by using the "peqGOLD plasmid miniprep kit I" (PEQLAB Biotechnologie, Erlangen). In contrast to the manufacturer´s instructions the elution of the DNA from the silica columns was done by using 70 µl sterile aqua bidest in two steps (first step: 50 µl, second step: 20 µl).

The yield of DNA was quantified photometrically at 260 nm, and the purity analyzed by the absorption maxima at 280 nm as well as 320 nm. The DNA concentration was calculated by: c (DNA) [ng/µl] = (E_{260} – E_{320}) x 50 ng/µl. Pure DNA has a E_{260}/E_{280} quotient of 1.8, RNA of 2.0. Contamination leads to a decrease of the quotient.

2.6.2. Mutagenesis reaction by using the "Quikchange® II site-directed mutagenesis kit"

Material:

Isolated plasmid-DNA pDS12-RBSII with *Lhcb1*; Quikchange® II site-directed mutagenesis kit (Stratagene, Santa Clara USA); Sense and antisense primer

NZCYM-Broth EZ-mix	22,45 g/l NZCYM-Broth-EZ
	12,5 mmol/l $MgSO_4$
	3,6 g/l D-Glucose

LB-amp plates (2.6.1)

Liquid LB-media (2.6.1)

Table 2.3: Overview of the expression rate of all codons in *E. coli* after Hernaut and Dachin, 1996. Green: high rate (>20 %); yellow: acceptable rate (5-20 %); orange: critical rate (3-5 %); red: inacceptable rate (<2 %).

	T			C			A			G		
T	TTT	29.08	Phe	TCT	32.41	Ser	TAT	35.23	Tyr	TGT	38.85	Cys
	TTC	70.93	Phe	TCC	26.56	Ser	TAC	64.77	Tyr	TGC	61.15	Cys
	TTA	3.44	Leu	TCA	4.79	Ser	TAA	-	Stopp	TGA	-	Stopp
	TTG	5.47	Leu	TCG	7.39	Ser	TAG	-	Stopp	TGG	100	Trp
C	CTT	5.56	Leu	CCT	11.23	Pro	CAT	29.77	His	CGT	64.25	Arg
	CTC	8.03	Leu	CCC	1.63	Pro	CAC	70.23	His	CGC	32.97	Arg
	CTA	0.083	Leu	CCA	15.25	Pro	CAA	18.65	Gln	CGA	1.07	Arg
	CTG	76.67	Leu	CCG	71.89	Pro	CAG	81.35	Gln	CGG	0.8	Arg
A	ATT	33.49	Ile	ACT	28.08	Thr	AAT	17.25	Asn	AGT	4.52	Ser
	ATC	65.94	Ile	ACC	53.6	Thr	AAC	82.75	Asn	AGC	24.33	Ser
	ATA	0.97	Ile	ACA	4.67	Thr	AAA	78.55	Lys	AGA	0.62	Arg
	ATG	100	Met	ACG	12.65	Thr	AAG	21.45	Lys	AGG	0.29	Arg
G	CTT	39.77	Val	GCT	27.54	Ala	GAT	46.05	Asp	GGT	50.84	Gly
	GTC	13.45	Val	GCC	16.14	Ala	GAC	53.95	Asp	GGC	42.83	Gly
	GTA	19.97	Val	GCA	24.01	Ala	GAA	75.35	Glu	GGA	1.97	Gly
	GTG	26.81	Val	GCG	32.3	Ala	GAG	24.65	Glu	GGG	4.36	Gly

Table 2.4: List of all used mutagenesis primers and their specifications.

Name	Sequence	length	Description
LHCII-S3Cfw	5'-TTA AGC ATG CGT AAA TGT GCT ACC ACC AAG AAA GTA GC-3'	38 nt	Replacement S3C
LHCII-S3C rv	5'-GCT ACT TTC TTG GTG GTA GCA CAT TTA CGC ATG CTT AA-3'	38 nt	Replacement S3C
LHCII-K7C fw	5'-GC ATG CGT AAA TCT GCT ACC ACC TGT AAA GTA GCG AGC TCT GG-3'	43 nt	Replacement K7C
LHCII-K7C rv	5'-CC AGA GCT CGC TAC TTT ACA GGT GGT AGC AGA TTT ACG CAT	43 nt	Replacement K7C

	GC-3’		
LHCII-S11Cfw	5’-CC ACC AAG AAA GTA GCG TGC TCT GGA AGC CC-3’	31 nt	Replacement S11C
LHCII-S11Crv	5’-GG GCT TCC AGA GCA CGC TAC TTT CTT GGT GG-3’	31 nt	Replacement S11C
LHCII-S34Cfw	5’-CC GGT GAG TCT CCA TGC TAC TTG ACT GGA GAG TTC CCC-3’	38 nt	Replacement S34C
LHCII-S34Crv	5’-GGG GAA CTC TCC AGT CAA GTA GCA TGG AGA CTC ACC GG-3’	38 nt	Replacement S34C
Lhcb1-S59C for (+)	5’-GCT GAC CCA GAG ACA TTC TGC AAG AAC CGT GAG C-3’	34 nt	Replacement S59C
Lhcb1-S59C rv (-)	5’-G CTC ACG GTT CTT GCA GAA TGT CTC TGG GTC AGC-3’	34 nt	Replacement S59C
Lhcb1 V90C Stra fw	5’-C CCA GAG CTT TTG TCT CGC AAC GGT TGT AAA TTC GGC GAA GC 3’		Replacement V90C
Lhcb1 V90C Stra rv	5’-GC TTC GCC GAA TTT ACA ACC GTT GCG AGA AAC GAA CTC TGG G-3’		Replacement V90C
Lhcb1 V96C fw	5'-GGT GTT AAA TTC GGC GAA GCT TGC TGG TTC AAG GCA GGA TC-3'	41 nt	Replacement V96C
Lhcb1 V96C rv	5`-GAT CCT GCC TTG AAC CAG CAA GCT TCG CCG AAT TTA ACA CC-3`	41 nt	Replacement V96C
Lhcb1 S102C fw	5'-GTG TGG TTC AAG GCA GGA TGT CAA ATC TTT AGT GAG GGT GG-3'	41 nt	Replacement S102C
Lhcb1 S102C rv	5'-CCA CCC TCA CTA AAG ATT TGA CAT CCT GCC TTG AAC CAC AC-3'	41 nt	Replacement S102C
LHCII S106C fw	5`-GGA TCT CAA ATC TTT TGT GAG GGT GGA CTT GAT TAC TTG GG-3’		Replacement S106C
LHCII S106C rv	5’-CC CAA GTA ATC AAG TCC ACC CTC ACA AAA GAT TTG AGA TCC-3’		Replacement S106C

Lhcb1 L113C fw	5'-GGT GGA CTT GAT TAC TGC GGC AAC CCA AGC TTG G-3'	34 nt	Replacement L113C
Lhcb1 L113C rv	5'-CCA AGC TTG GGT TGC CGC AGT AAT CAA GTC CAC C-3'	34 nt	Replacement L113C
LHC2 I124C fw	5'-GGT CCA TGC TCA AAG CTG TCT TGC CAT ATG GGC C-3'	34 nt	Replacement I124C
LHC2 I124C rv	5'-GGC CCA TAT GGC AAG ACA GCT TTG AGC ATG GAC C-3'	34nt	Replacement I124C
LHCII V138Cfw	5`-ATC TTG ATG GGA GCT TGC GAA GGT TAC CGT ATT C-3`	34 nt	Replacement V138C
LHCII V138Crv	5`-CAA TAC GGT AAC CTT CGC AAG CTC CCA TCA AGA T-3`	34 nt	Replacement V138C
LHCII I143Cfw	5`-GAA GGT TAC CGT TGT GCC GGT GGG CCT-3`	27 nt	Replacement I143C
LHCII I143Crv	5`-AGG CCC ACC GGC ACA ACG GTA ACC TTC-3`	27 nt	Replacement I143C
LHCII-A174Cfw	5`-GAT GAT CCA GAA GCA TTC TGT GAA TTG AAG GTG AAG GAA CTC-3`	42 nt	Replacement A174C
LHCII-A174Crv	5`-GAG TTC CTT CAC CTT CAA TTC ACA GAA TGC TTC TGG ATC ATC-3`	42 nt	Replacement A174C

Method:

In comparison to traditional methods (restriction and ligation) the "Quikchange® II site-directed mutagenesis kit" was used to replace specific amino acids caused by a faster process (Dockter, 2009). Almost all mutagenesis preparations led to very good yields, thus, costs were reduced by using half volumes of PCR-mixture (Table 2.5) as well as XL1-blue super competent cells. All ingredients of a 25 µl mixture excluding the polymerase were mixed on ice and shaken. Finally the polymerase was added and carefully mixed without shaking to ensure its high activity.

Table 2.5: Composition of an 25 µl PCR mixture

Material	Amount/Concentration
Template	25 ng
Primer	62.5 ng sense + 62.5 ng antisense
dNTP mix Stratagene	0.5 µl
DNA polymerase Pfu Ultra HF	1.25 U
Reaction buffer	2.5 µl
dH_2O steril	ad 25 µl

According to the set-up instruction the sizes of the sense as well as antisense primers were between 25 and 45 nucleotides and had a melting temperature (T_m) of at least 78°C. The mutation was located in the middle of each primer, whereas the rest was complementary to the sense respectively antisense strain. For the replacement of amino acids highly expressed codons in *E. coli* were preferred (Table 2.3). All designed primers were purchased from the company biomers (Ulm). All used primers are listed in Table 2.4. The polymerase chain reaction (PCR) was done in accordance to the set-up instructions that are described in Table 2.6.

Table 2.6: PCR program for mutagenesis reaction after Stratagene

Cycles	Temperature	Time	Description
-	110°C	-	Preheating the lid
1x	95°C	30 s	Activation
16x	95°C	30 s	Denaturing
	55°C	1 min	Annealing
	68°C	5 min	Amplification
-	4°C	infinite	Storage

The PCR product is by contrast to the mature DNA non-methylated. Therefore, the restriction enzyme DpnI (10 U) was added to each mixture and incubated for one hour at 37°C in order to digest template DNA. After that, mutated DNA was transformed into supercompetent XL1-blue cells. For this purpose a 25 µl XL1-blue aliquot was thawed on ice, 0.5 µl DNA added, and the mixture incubated on ice for 30 min. In the next step, the mixture was heat shocked for 45 s at 42°C in a water bath and 250 µl NZCYM-Broth ET-mix was added. In order to increase the amount of new clones, the growth phase after transformation in super competent cells was increased from 1 h to 2 h and finally this mixture was plated on LB-amp plates and incubated overnight at 37°C. The next day, one separated bacteria culture was picked and overnight grown in 15 ml liquid LB-medium at 37°C containing 100 mg/ml amp. The XL1-blue DNA was isolated (2.6.1), the concentration analyzed and transformed into chemo-competent *E. coli* JM101 cells (2.6.4), the insertion checked by DNA sequencing (2.6.5) and finally glycerol stocks prepared (2.6.6).

2.6.3. Mutagenesis reaction by using the "Phusion Site-Directed Mutagenesis kit"

Material:

Isolated plasmid-DNA pDS12-RBSII with *Lhcb1*; "Phusion Site-Directed Mutagenesis kit" (Finnzymes); Phosphorylated sense and antisense primers; LB-amp plates (2.6.1); Liquid LB-media (2.6.1)

Table 2.7: List of all used phosphorylated mutagenesis primers and their specifications.

Name	Sequence	length	Description
LHCII C Strep Fw	5`-Phosphate-CCG CAG TTC GAA AAA TAA CCC GGG AAA TAA ACA CTC TTA TAT TTA TAT GTT-3`	51 nt	Insertion of a C-terminal strep tag II
LHCII C Strep Rv	5`-Phosphate-GTG GCT CCA ACC ACC TTT TCC GGG AAC AAA GTT CTT GG-3`	36 nt	Insertion of a C-terminal strep tag II
LHCII His-	5`-Phosphate- CAG TTC GAA AAA TAA	48 nt	Insertion of a C-

Strep Fw	CCC GGG AAA TAA ACA CTC TTA TAT TTA TAT GTT -3`		terminal strep tag II behind the his_6 tag
LHCII His-Strep Rv	5`-Phosphate-CGG GTG GCT CCA ATG GTG ATG GTG ATG GTG TTT TCC GG-3`	38 nt	Insertion of a C-terminal strep tag II behind the his_6 tag
LHCII Strep-His FW	5`-Phosphate-CCG CAG TTC GAA AAA CAC CAT CAC CAT CAC CAT TAA CC-3`	38 nt	Insertion of C-terminal strep tag II in front of a his_6 tag
LHCII Strep-His Rv	5`-Phosphate-GTG GCT CCA ACC ACC TTT TCC GGG AAC AAA GTT GGT GG-3`	38 nt	Insertion of C-terminal strep tag II in front of a his_6 tag
LHCII-His3NterFW	5`-Phosphate-CAT CAC CAT CGT AAA TCT GCT ACC ACC AAG AAA G-3`	34 nt	Insertion of a N-terminal his_6 tag
LHCII-His3NterRv	5`-Phosphate-GTG ATG GTG CAT GCT TAA TTT CTC CTC TTT AAT GAA TTC-3`	39 nt	Insertion of a N-terminal his_6 tag
hNC79S_tS_fw	5'-Phosphate-GGT AGC AGC TAA CCC GGG AAA TAA ACA C-3'	28 nt	Insertion of a C-terminal SSPGSS motif
LHCII-c-term-tS-rv	5'-Phosphate-AGG GCT GCT TTT TCC GGG AAC AAA GTT-3'	27 nt	Insertion of a C-terminal SSPGSS motif

Method:

The “Phusion Site-Directed Mutagenesis kit” was used to insert specific nucleotides into the expression vector. Designed primers were complementary to the sense, respectively antisense strain. The additional nucleotides were divided equally to the 5`ends of both primers. The 5`ends were phosphorylated to allow a ligation of the linearized modified plasmid (Figure 2.4). According to the set-up instructions, the annealing temperature, which depends on the length and T_m of the primers should be between 65-72°C.

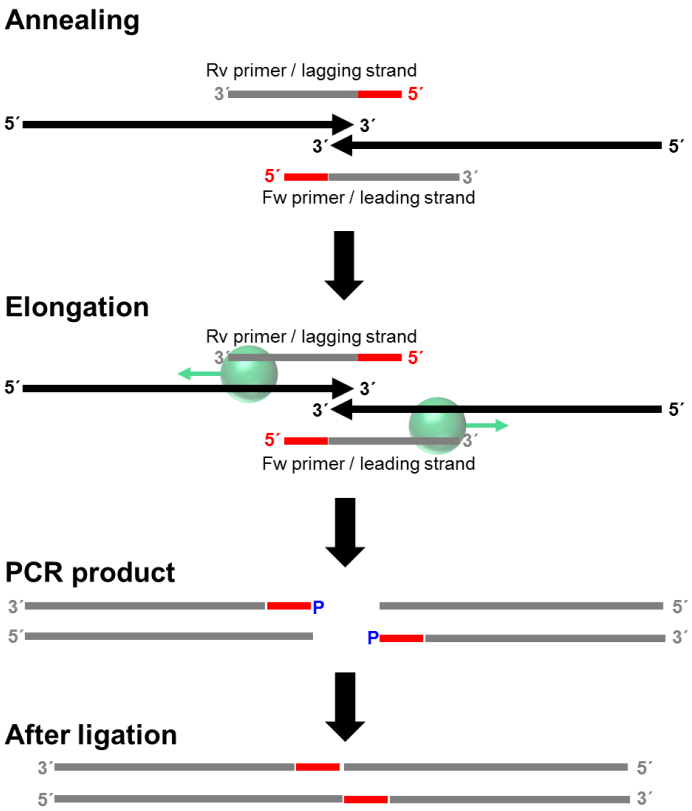

Figure 2.4: Overview of muatgenesis PCR and ligation in order to construct new mutants with additional amino acids. The additional sequence is divided equally between both primers. After denaturation both phosphorylated primers, consisting of a complementary (grey line) and mentioned additional (red line) sequence bind to the sense, respectively antisense strain. Several cycles of annealing and elongation lead to a linear PCR product with phosphyorylated 5` ends, which are needed for ligation. After ligation the additional sequence is introduced into the new mutated plasmid

All designed primers were purchased from the company biomers (Ulm). All used primers are listed in (Table 2.7).

The composition of the PCR mixture was in most cases identical to the set-up instructions. Caused by the low amount of template, DpnI digestion was not necessary. However, in some critical cases the amount of template was increased and a DpnI digestion prepared, analogously to 2.6.2.

Table 2.8: Composition of an 50 µl PCR mixture.

Material	Amount/Concentration
Template	1.5 ng
Primer	0.5 µmol/l sense + 0.5 µmol/l antisense
dNTP mix Finnzymes	1.0 µl
DNA polymerase Pfu Ultra HF	2.5 U

5x reaction buffer	10.0 µl
dH_2O sterile	ad 50 µl

The polymerase chain reaction (PCR) was done in accordance to the set-up instructions (Table 2.9).

Table 2.9: PCR program for mutangesesis reaction after Finnzymes.

Cycles	Temperature	Time	Description
-	110°C	-	Preheating the lid
1x	98°C	1 min	Activation
36x	98°C	10 s	Denaturing
	67/70°C	30 s	Annealing
	72°C	150 s	Amplification
1x	72°C	5 min	Final Amplification
-	4°C	infinite	Storage

Subsequently 5 µl Quick ligation buffer and 0.5 µl Quick T4 DNA ligase were added to 5 ml of the PCR product and incubated for 5 min at room temperature. The ligated product was transformed into chemo-competent *E. coli* JM101 cells (2.6.4), the insertion checked by DNA sequencing (2.6.5), and finally, glycerol stocks prepared (2.6.6).

2.6.4. Transformation in *E. coli* JM101 cells

Material:

E. coli JM101 chemo-competent cells; LB-amp plates (2.6.1); liquid LB-media (2.6.1)

Method:

In order to transform mutated DNA (2.6.2 and 2.6.3) into *E. coli* JM101 cells, 25 µl JM101 cells were thawed on ice, 25 ng XL1-blue or ligated DNA added, and 30 min. incubated on ice. The heat shock was done for 1 min. at 42°C in a water bath and then 250 µl liquid LB-media was added. The mixture was incubated for 1 h at 37°C, plated on LB-amp plates and incubated overnight at 37°C. The next day, a separated bacteria culture was picked and overnight grown in 15 ml liquid LB-medium at 37°C containing 100 mg/ml amp. Subsequently 10-13 ml of the culture were used to isolate the plasmid, measure the DNA concentration (2.6.1) and check the mutation by DNA sequencing (2.6.5), whereas 2x 400 µl were used to prepare glycerol stocks (2.6.6).

2.6.5. DNA sequencing

Material:

400 ng DNA; 1 µl sequencing primer

Method:

In order to sequence the isolated plasmid, a mixture consisting of 400 ng DNA, 1 µl primer, and dH_2O (ad 7 µl) was prepared and analyzed by the company GENterprise (Mainz). The used method bases on the chain termination method developed by Frederick Sanger (Sanger *et al*., 1977). The selection of the primer depended on the location of the mutation. All primers are listed in Table 2.10.

Table 2.10: Characteristics of the primers that were used for DNA sequencing. A: adenin; T: thymin; C: cytosin; G: guanin; nt: nucleotides; (+): forward primers; (-): reverse primers.

Name	Sequence	Length	Description
Ds23 (+)	5´-ATT TGC TTT GTG AGC GG-3`	17 nt	Binds 23 bp upstream the start codon
Ds178 (-)	5´-GGA GTT CTG AGG TCA TTA CTG G-3´	22 nt	Binds 178 bp downstream the stopp codon (reverse primer)

Seq105 (-)	5'-CC ATC ATC TTG TAT TAG TGA ACC-3'	23 nt	Binds 105 bp downstream the stopp codon (reverse primer)
Seq195 (+)	5'-ACA TTT CCC CGA AAA GTG-3'	18 nt	Binds 195 bp upstream the start codon

2.6.6. Glycerol stocks

Material:

400 µl *E. coli* JM101 overnight culture; 600 µl 80 % glycerol

Method:

In order to store all new mutants as glycerol stocks, 400 µl of the final *E. coli* JM101 overnight culture (2.6.4) were mixed with 600 µl 80 % glycerol and frosted at -80°C.

2.7. Preparative biochemical methods

2.7.1. Extraction of pigments

Material:

Leaves of *Pisum sativum*; acetone; distilled diethylether; 5 mol/l NaCl, Nitrogen 5.0

Extraction buffer	1 mol/l Tris/HCl pH 7.8
	1 mmol/l DTT
	330 mmol/l sorbitol

Method:

Total pigment extract as well as single pigments were isolated from pea (*Pisum sativum*). Seeds were incubated in water bubbled with air overnight, put under vermiculit and grown

under long day conditions at 20°C. After 13 days, plants were harvested in their dark phase by collecting and cutting all leaves. Plant material (1 kg) was mixed (Waring Blendor) with 1.5 l extraction buffer and filtrated through three layers of cotton. The filtrate was collected in 500 ml beakers and centrifuged at 4°C and 10000 rpm (Beckmann cooling centrifuge; rotor: JLA-10500). The green pellet was used to extract the pigments by adding 500 ml acetone. After a second centrifugation step (10 min., 4°C, 10000 rpm), the green solution was transferred into a separating funnel, covered with diethyl ether and mixed carefully by inverting . In order to transfer pigments into the ether phase, polarity of the acetone phase was increased by adding water and 5 mol/l NaCl. The uncolored water phase was disposed of after each mixing step. All steps were repeated until all of the acetone-water mixture was removed and until all pigments were transferred to the diethyl-ether phase.

Dissolved pigments were stored at -20°C overnight to get rid of residual water. For this purpose ice crystals were removed by filtrating and pigments were dried in the rotary evaporator, kept dark and stored on ice. The concentration (2.7.3) and composition (2.7.4) of the pigment extract was analyzed by dissolving them in water-free acetone.

2.7.2. Extraction of single pigments

Material:

Acetone; 1,4-dioxan; 5 mol/l NaCl; distilled diethylether; Nitrogen 5.0

Method:

In order to separate pigments, the chlorophylls of the total extract, dissolved in water-free acetone were precipitated. For this purpose the pigment solution in acetone was stirred and cooled on ice, while 0.15 volume 1,4-dioxan and subsequently 0.32 volume of distilled water were added with the help of a dropping funnel. The mixture was stored on ice without stirring for 1 h. After that, precipitated chlorophylls were centrifuged (10 min., 4°C, 10000 rpm; Beckmann, rotor JLA 10.500). The aqueous supernatant contained the xanthophylls.

The chlorophyll pellet and xanthophyll solution were separated into a funnel and diethyl ether was added to both parts. The further procedure was identical to the extraction of pigments (2.7.1). Dried pigments were stored at -20°C in the dark until they were further

processed. The chlorophylls were separated into chl *a* and *b* by using the preparative HPLC (2.7.2.2). Xanthophylls were saponified (2.7.2.1) and then separated into lutein, neoxanthin and violaxanthin by using the preparative HPLC (2.7.2.2).

2.7.2.1. Saponification of xanthophylls

Material:

Acetone; ethanol p.a.; KOH 60 % (w/v); 5 mol/l NaCl; distilled diethyl ether

Method:

In order to remove the last part of chlorophylls and lipids, the xanthophyll solution was saponified by adding KOH. For this purpose dried xanthophylls were dissolved in 50 ml ethanol p.a., 5 ml 60 % KOH was added and the mixture was incubated at 30°C in the dark overnight. The next day diethyl ether was added and the saponified, water soluble chlorophylls were removed with the help of water and NaCl. The yield of xanthophylls was increased by further extraction steps of the water solution with diethyl ether. At the end the xanthophyll solution was dried in the rotary evaporator.

2.7.2.2. Separation of the chlorophylls and xanthophylls by using the preparative HPLC

Material:

RP-HPLC with an C18 column; pigments; acetone, distilled diethyl ether; buffered water (0.1 mmol/l HEPES pH 7.0)

Detectors	Sp-6V		Shimadzu RF 535	
	Absorption	0.04	Excitation	435 nm
	Response	Standard	Emission	680 nm
			Response	Medium
			Range	2
			Sensitivity	high
Program:	For chlorophylls:		CHLMOD, Time 360 min.	

For Xanthophylls: XGRADFF

Table 2.11: Program of the acetone/water gradient in order to separate chlorophylls. Flow 5 ml/min.

Acetone [%]	Water [%]	Time [min.]	Timepoint [min.]
86	14	0	0
86	14	100	100
88	12	170	270
100	0	50	320

Table 2.12: Program of the acetone/water gradient in order to separate xanthophylls. Flow 5 ml/min.

Acetone [%]	Water [%]	Time [min.]	Timepoint [min.]
78	22	0	0
78	22	200	200
100	0	80	280

Method:

The dried chlorophylls were dissolved in 86 ml acetone and homogenized in a sonic bath. After that 14 ml water was added and the solution was centrifuged (8 min., 4°C, 8000 rpm; Beckmann, rotor JA25.50). The supernatant, containing the chlorophylls was loaded into the sample loop and the program was initialized (Table 2.11). Chl *b* was eluted after 70 min. and chl *a* after 90 min. The principle of the RP-HPLC is described in 2.7.4.

The dried xanthophylls were dissolved in 80 % acetone and homogenized in a sonic bath. After that they were loaded into the sample loop and the program was initialized (Table 2.12). Neoxanthin was eluted first, then violaxanthin and finally lutein.

All separated pigments were mixed with diethyl ether in a separating funnel, washed with water, and dried in a rotary evaporator. The amount and purity of pigments was checked by analytic HPLC (2.7.4). Finally pigment aliquots were prepared (2.7.6).

2.7.3. Chlorophyll concentration

Material:

80% acetone; pigments dissolved in water free acetone

Method:

The chlorophyll concentration was analyzed after Porra *et al*. (1989). A defined volume of pigments and 80 % acetone were mixed and the absorption measured at 750, 663.6, 646.6 nm. The chlorophyll concentration was calculated after:

Chl *a* = 12.25 • A663.6 – 2.55 • A646.6 = [µg/ml] • dilution factor

Chl *b* = 20.31 • A646.6 – 4.91 • A663.6 = [µg/ml] • dilution factor

2.7.4. Analysis of the pigment composition by using analytical HPLC

Material:

RP-HPLC with a Waters Bondapak column (C18; 125 Å; 10 µm; 30 x 300 mm); 100 % acetone (filtrated and degased); buffered aqua bidest. (0.2 mmol/l Tris/HCl pH 7.0); pigment extract in 80 % acetone; program: „ChromolithA“

Method:

The composition of the isolated pigments was monitored by using the reversed phase high performance chromatography (RP-HPLC) either after pigment isolation (2.7.1) or after butanol extraction (2.7.5). Separation by using RP-HPLC bases on two phases: a non-polar stationary phase (surfaced modified silicia column material) and a polar mobile phase (variable composition of an acetone-water mixture). Thus, after calibration of the column (two runs with 80 % acetone) pigments were separated depending to on their hydrophobicity because hydrophobic pigments had a longer retention time on the column. The elution was controlled by varying the composition of the mobile phase. Eluted

molecules were detected by UV-Vis spectroscopy and the pigment concentration was calculated by integration of the peak area.

2.7.5. Butanol extraction

Material:

100 % sec butanole; 5 mol/l NaCl; 70 % buffered acetone

Method:

Butanole extraction (after Martinson & Plumley) was used to calculate the pigment composition of refolded protein-pigment complexes. The extraction of the pigments was done like described in Dockter (2009).

2.7.6. Preparation of pigment aliquots

Material:

Isolated pigments; 100 % acetone; nitrogen 5.0

Method:

After analyzing the pigment composition (2.7.4) and chlorophyll concentration (2.7.3) the isolated pigments were dissolved in 100 % acetone, separated in aliquots and dried under a continuously nitrogen flow. All prepared aliquots were stored at -20°C in the dark.

2.7.7. Overexpression and isolation of LHCP from *E. coli* as inclusion bodies

Material:

Laminar flow; IPTG (1 mol/l)

LB-amp plates	1 % Tryptone	Liquid LB media	1 % Tryptone
	0.5 % Yeast		0.5 % Yeast
	1 % NaCl (pH 7.5)		1 % NaCl (pH 7.5)
	1.5 % Agar		1 % Tryptone
	100 µg/ml Ampicillin		
Lysis buffer	0.8 mg/ml DTT	Tris buffer	50 mmol/l Tris/HCl pH 8.0
	4 µg/ml DNaseI		1 mmol/l EDTA
Detergent buffer	200 mmol/l NaCl	Triton buffer	1 mmol/l EDTA
	1 % Desoxycholacid (w/v)		0,05 % Triton X100 (w/v)
	20 mmol/l Tris/HCl pH 7.5		20 mmol/l Tris/HCl pH 7.5
	1 % Nonidet P40 (w/v)		
	2 mmol/l EDTA		
	10 mmol/l ß-me		

Method:

In order to produce inclusion bodies, glycerol stocks (2.6.6) of concerned mutants were plated on LB-amp plates. An isolated bacterial culture was picked and used to inoculate a 800 ml liquid LB-amp bacterial culture, which was incubated at 37°C and 180 rpm on an incubation shaker overnight (12-14 h). After that, isopropyl-ß-thiogalactoside (IPTG) was added to the turbid solution to induce the production of protein. Four to five hours later, the bacterial culture was centrifuged (5 min., 8000 rpm, 4°C; Beckmann, rotor JLA-10500) and the pellet resuspended in 30 ml lysis buffer.

Bacteria cells were broken mechanically or thermally. For the mechanical procedure two to three rounds in the french press were performed. For the thermal procedure the mixture in lysis buffer was frozen (5 min.) in liquid nitrogen and thawed in the ultrasonic bath (15 min). After that the lysate was centrifuged (5 min., 8000 rpm, 4°C; Beckmann, rotor JA-20) and resuspended in 20 ml detergent buffer. This step was repeated until the pellet was nearly white. The white pellet was resuspended in 20 ml triton buffer and incubated in a shaker at 4°C overnight. The next day the solution was centrifuged (5 min., 8000 rpm,

4°C; Beckmann, rotor JA-20), the pellet resuspended in 5 ml Tris buffer, and the concentration analyzed photometrically.

2.7.8. Quantification of the protein concentration

Material:

A280 buffer	10 mmol/l Tris/HCl pH 6.7
	2 % Sodiumdodecylsulfate (SDS)
	1 mmol/l ß-me

Method:

The protein dilution was done by preparing three aliquots; each consisted of 10 µl protein solution and 990 µl A280 buffer, and a reference without protein. ß-me was added as a fresh solution. The absorption of these protein solutions was measured photometrically at 280 nm and the mean value defined. The protein concentration was calculated with the help of a LHCII standard curve (Hobe, 1995). Thus, the concentration was defined as:

0.1 (extinction at 280 nm) = 53 µg/ml protein

2.7.9. Labeling of LHCP

2.7.9.1. Labeling with SH-reactive spin labels

Material:

LHCP; 10 % LDS; 100 mmol/l natrium phosphate buffer pH 7.0; 100 mmol/l Tris-(2-cyanoethyl)phosphine (TCyEP) in dimethylformamide (DMF); 10 mg/ml PROXYL-IAA in dimethylsulfoxide (DMSO)

Method:

The labeling of the LHCP with PROXYL was done like described in Dockter (2011 and 2009)

2.7.9.2. Labeling with SH-reactive dyes

Material:

LHCP; 10 % LDS; 100 mmol/l natrium phosphate buffer pH 7.0; 100 mmol/l triscyanoethylphosphine (TCyEP) in dimethylformamide (DMF); 10 mmol/l DY731in dimethylsulfoxide (DMSO).

Method:

The labeling of the LHCP with Dy731 was done like described in Gundlach (2010).

2.7.9.3. Protein precipitation

Material:

LHCP; 100 mmol/l acetic acid; 100 % acetone; 70 % ethanol

2x Solubilization buffer	200 mmol/l Tris/HCl pH 9.0
	4 % SDS
	10 mmol/l ε-aminocapronic acid
	2 mmol/l benzamidine
	25 % sucrose (w/v)

Method:

Labeled protein was precipitated by adding 1/10 volume of 100 mmol/l acetic acid and 2.3 fold volume of acetone. This mixture was incubated on ice for 30 min. up to 2 hours and then centrifuged (14000 rpm, 4°C; 5 min., Beckmann, rotor JA-20). The protein pellet was washed with 70 % ethanol, dissolved in 2x solubilization buffer and the concentration analyzed (2.7.8). All labeled samples were stored in the dark at -20°C.

2.7.10. Protein refolding by using the detergent-exchange method

Material:

2x Solubilization buffer	200 mmol/l Tris/HCl pH 9.0
	4 % SDS
	10 mmol/l ε-aminocapronic acid
	2 mmol/l benzamidine
	25 % sucrose (w/v)

1 mol/l ß-me; ethanol p.a.; pigment extract; 10 % octylglucoside (OG); 2 mol/l KCl

Method:

The used detergent-exchange method is described for the reconstitution of 2 mg protein: 2 mg of the LHCII apoprotein was dissolved in 2.5 ml 2x solubilization buffer and diluted with 2.5 ml of aqua dest. In order to largely denature the protein, the mixture was boiled for 2-5 min., depending on the total volume. After cooling down to room temperature, disulfide bonds were cracked by adding 11 mmol/l ß-mercaptoethanol (ß-me). The threefold molecular excess of pigments (3333 µg) were dissolved in 333 µl ethanol p.a. by mixing and in the sonic bath. If single pigments were used, the total amounts of pigments was identical to the total pigment extract but in a first step lutein and further carotenoids were dissolved in ethanol and in a second step the chlorophylls. In the next step, the pigment solution was added under permanent vortexing and incubated for 5 min. at room temperature. Under permanent mix 1 % (717 µl) of a mild non-denaturing detergent (OG) as well as 717 µl 2 mol/l KCl were added and incubated on ice for 10 min., leading to insoluble KDS. At the same time pigments and protein came close together in OG detergent micelles, leading to a spontaneous refolding of the protein. The insoluble KDS was removed by centrifugation (5 min, 8000 g) and refolded monomers could be either purified by ultracentrifugation or they were used for a trimerization.

2.7.11. Trimerization of the LHCII by using liposomes

Material:

LHCII monomers; degased Bio-Beads (BioRad, munich)

Liposome buffer	50 mmol/l NaCl
	10 mmol/l Tris/HCl pH 7.5
	0.1 mmol/l EDTA

Method:

The trimerization in PG liposomes was used for LHCII monomers without a his_6 tag and for the production of heterogeneous trimers (liposome-his_6 tag method). 1 mg of refolded LHCII was mixed with a PG solution, which consisted of 2.5 mg PG (16:0) and 1 % OG dissolved in 1 ml liposome buffer. The detergent was absorbed with the help of Bio-Beads, leading to a pass of the monomers into the liposomes. The removal of the detergent was done in several steps to avoid aggregation. In a first step 50 mg of wet and degased Bio-Beads were added and the mixture incubated at 4°C for 2 h in the dark on a rotator. In a second step the solution (without the Bio-Beads) was mixed with 100 mg of fresh Bio-Beads and incubated at 4°C for 24 h on a rotator. The second step was repeated until all detergent was removed (solution did not foam any longer). Inside the liposomes the LHCII proteins came so close together that a spontaneous trimerization took place. This procedure took 3-4 days. In order to purify these trimers, liposomes were destroyed by adding 0.5 % LM, incubated on ice and finally the mixture was loaded onto sucrose gradient and ultra-centrifuged.

2.7.12. Immobilization and trimerization of the LHCII by using the his_6 tag/Ni^{2+} IDA Sepharose system

Material:

Chelating Sepharose Fast Flow (GE Healthcare, Schweden); 0.3 mol/l $NiCl_2$; 50 mmol Tris/HCl ph 7.5; 2 % SDS; 0.4 mol/l imidazole; 0.1 mol/l EDTA; 20 % ethanol

OG buffer	1 % OG (w/v)	Tx buffer	0.05 % Tx (w/v)
	0.1 mol/l Tris/HCl pH 9.0		0.1 mol/l Tris/HCl pH 7.5
	12.5 % sucrose		0.1 mg/ml PG
Elution buffer	0.05 % Tx (w/v)		
	0.1 mol/l Tris/HCl pH 7.5		
	0.1 mg/ml PG		
	0.3 mol/l imidazole		

Method:

The immobilization of LHCII monomers and regeneration of the column material was done like described in Dockter (2009 and 2012).

2.7.13. Immobilization of LHCII by using the Streptactin column

The strep tag II is an eight amino acids long motif that has a high affinity to Strep-Tactin-Sepharose. The system was developed by IBA (Göttingen) and bases on a non-covalent binding of the strep tag II to Strep-Tactin. Biotin (vit. H) is able to remove the strep tag II. The binding principle is described in the manual (strep tag II – IBA Göttingen) and in Dockter (2009).

2.7.13.1. Preparation of heterogeneous trimers

Material:

SP- or Mp Strep-Tactin-Sepharose (IBA, Göttingen); 0.5 % Tx pH 8.0; 0.1 % SDS; LHCII eluate of the Ni-column

Buffer W	150 mmol/l NaCl	Tx buffer	0.05 % Tx (w/v)
	0.1 mol/l Tris/HCl pH 8.0		0.1 mol/l Tris/HCl pH 7.5
			0.1 mg/ml PG

			10 % glycerol (w/v)
Elution buffer	0.05 % Tx (w/v)	Wash buffer	1 mmol/l Tris/HCl pH 8.0
	0.1 mol/l Tris/HCl pH 8.0		0.15 mol/l NaCl
	0.1 mg/ml PG		1 mmol/l EDTA
	2.5 mmol/l D-biotin		
	10 % glycerol (w/v)		

Method:

The strep tag II/streptactin system was used to purify heterogeneous trimers. Heterogeneous trimers were prepared by mixing unlabeled and refolded LHCII that contained a his_6 tag with labeled and refolded LHCII that contained a his_6 tag as well as a strep tag II in a ratio of 8:1. The used amount of protein was related to the reconstitution yield, which was monitored by native gel electrophoresis (2.8.1.2). After mixing both solutions, monomers were immobilized on the Ni-column (2.7.12), columns were sealed, and incubated overnight. The next day, trimerization was continued and simultaneously the Mp-strep columns prepared. The high binding capacity of this system was reduced, if refolded LHCII was used. Thus, the amount of Mp-strep column material was by contrast to the set up specifications calculated with 0.5 ml column material in relation to 500 µg protein that contained a strep tag II. Strep columns were equilibrated by adding two column volumes of buffer W and two column volumes of Tx buffer. After that, the Ni-column eluate was loaded onto the strep column material and washed with two column materials of Tx buffer. For the elution four column materials of elution buffer, containing D-biotin (freshly prepared) were added. The eluate was purified by using solely 0.6 mol/l sucrose gradients (2.7.14 - SW60) caused by the high amount of glycerol.

2.7.13.2. Optimization experiments

Optimization experiments were done to increase the yield of heterogeneous trimers. Varied components and the implementation of the experiments are described in 3.4. However, for a better understanding the procedure and sample preparation of one complicated experiment (Figure 3.39) is shown in Figure 2.5.

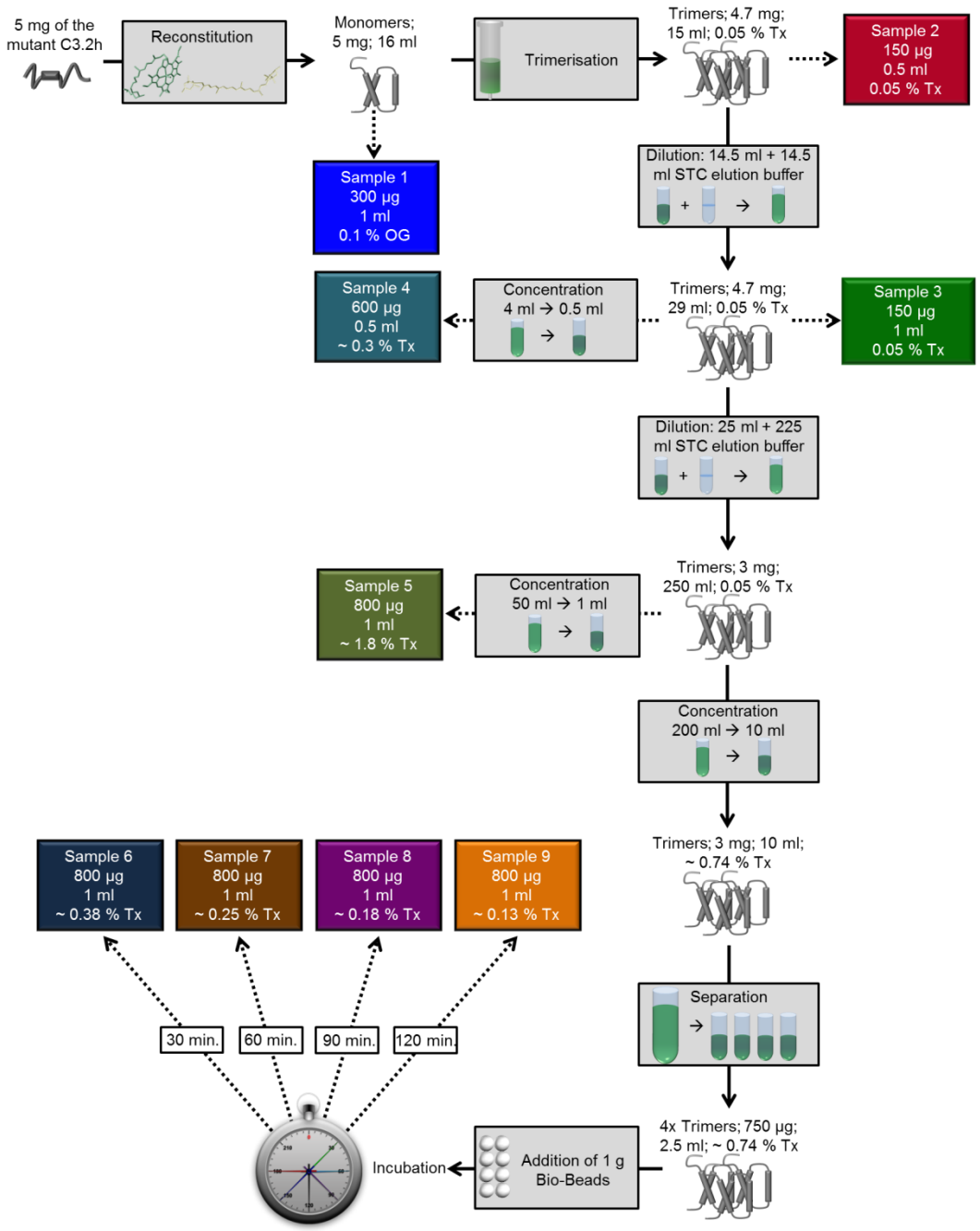

Figure 2.5: Experiment procedure in order to analyze the influence and removal of Tx to the purification quality of heterogeneous trimers. STC: strep tactin; concentration x ml → y ml: reduction of the volume by using amicons.

2.7.13.3. Regeneration of the Streptactin column

Material:

Elution buffer (2.7.13.1); 0.5 % Tx solution pH 8.0; buffer W (2.7.13.1); 0.1 % SDS

Regeneration buffer	0.1 mol/l Tris/HCl pH 8.0
	0.15 mol/l NaCl
	1 mmol/l EDTA
	1 mmol/l HABA

Method:

Experiments showed that the regeneration of the column material differed from the set up specifications. Thus, the description of the regeneration procedure is limited to the gentlest regeneration of the Mp-strep column material. For this purpose 2.5 ml of used column material was filled in a 15 ml Falcon tube, mixed with 5 ml elution buffer, and incubated at 4°C on a rotator overnight. The next day, the liquid supernatant was replaced by 10 ml 0.5 % Tx solution pH 8.0 and incubated at 4°C on a rotator overnight. If the column material was not white, the last step was repeated. The white column material was filled in an empty column and washed with two to five column volumes of buffer W. After that, four column volumes of regeneration buffer were added. The color should change into red caused by the binding of HABA to the column material. If a red coloring did to take place, the column material was destroyed. Usually five regeneration steps should be possible but the binding capacity and therefore, durability also depended on the storage time. HABA was removed from the column by adding four column volumes of wash puffer. Then, 2 column volumes of 0.1 % SDS were applied. Finally, two column volumes of buffer W were added and the material stored in buffer W at 4°C in the refrigerator.

2.7.14. Sucrose density gradient ultracentrifugation

Material:

Ultracentrifugation Beckmann Optima 100/90/80; rotors SW60, SW40/41, SW28; sucrose (0.55 mol/l for SW60, 0.3 mol/l for SW40/41, and 0.4 mol/l for SW28); 5 mmol/l Tris/HCl pH 7.8; 0.1 % n-dodecyl-ß-D-maltoside (LM).

Method:

Refolded monomers and trimers were purified by using ultracentrifugation. A buffered solution, consisting of a defined amount of sucrose and 0.1 % LM was mixed, filled into the gradient tubes, and frozen. During the defrosting gradients were formed. The best purification quality was reached by using 0.55 mol/l sucrose for the small SW60, 0.3 mol/l for the medium SW40/41, and 0.4 mol/l for the large SW28 gradients. For the purification of heterogeneous trimers 0.6 mol/l (SW60) were used, caused by the composition of these samples (contained 10 % glycerol). The frosting temperature was -20°C, one freeze-thaw cycle, and a defrosting temperature of 4.0°C. The top layer was removed and LHCII samples were applied carefully. All tubes were balanced and centrifuged under vacuum at 4°C. Small and medium gradients were centrifuged for 16-17 hours and the large for 24-26 hours. After the ultracentrifugation run, bands of free pigments, monomers, trimers, and aggregates (form the top to the bottom) should be formed. Monomers or trimers were collected by using a syringe, stored on ice in the dark, and analyzed.

2.7.15. Determination of the sucrose concentration by using refractometry

Material:

Light source (sunlight); hand refractometer

Method:

In order to determine the concentration of sucrose within the gradients, the gradient solution was drained progressively (20 fractions per gradient). The %-brix value measured refractometrically and the concentration calculated with the help of a standard curve (Figure 2.6).

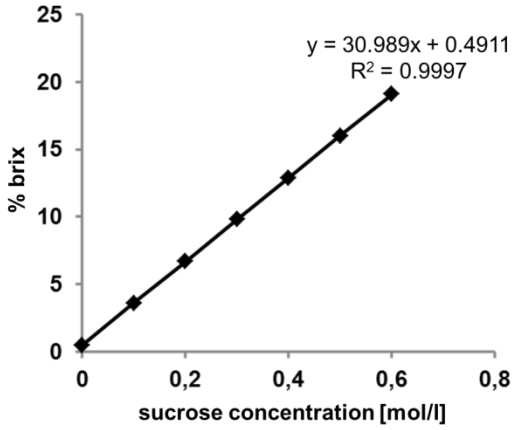

Figure 2.6: Standard curve in order to determine the sucrose concentration by using a refractometer.

2.7.16. Increase of the protein concentration

Material:

Amicon Ultra MW-30 (Millipore, Cork Irland)

Method:

Amicons were used to increase the protein concentration. Samples were filled into Amicons and centrifuged (4°C, 6000 rpm; Hettich refrigerated centrifuge) in 10 min. steps until the concentration was reached. Between each step adhesive protein on the membrane was dissolved by vortexing and the clear solution, which passed the membrane, was disposed. The final concentration was quantified after Butler and Kühlbrandt (1988).

2.7.17. Quantification of the LHCII concentration after Butler and Kühlbrandt (1988)

The concentration of LHCII monomers and trimers was calculated photometrically at 670 nm with the help of a molar extinction coefficient (ε_{LHCII} = 5.46 • 10^5 [cm^{-1} • M^{-1}]) that was analyzed by Butler and Kühlbrandt (1988). The LHCII solution was diluted with gradient solution in a ratio of 1:50. In this way absorptions (E) of three dilutions were

measured at 670 nm and the mean value was taken to calculate the protein concentration (c) with the formula:

$c_{LHCII} = E_{LHCII} / \varepsilon_{LHCII}$ [mol/l] • dilution factor

2.7.18. Preparation of EPR samples

Material:

Amicon Ultra MW-30; 80 % Deuterium glycerol (glycerol-d8, 98 atom % D, Isotec USA)

Deuterium buffer	5 mmol/l Tris/HCl pH 7.8
	275 mmol/l sucrose [w/v]
	in deuterium oxide (D_2O)

Method:

The protein concentration was increased to get a better signal to noise ratio in EPR measurements. Nevertheless, a higher concentration included a higher risk of aggregation. Thus, the concentration was increased to an optimized value. For X-band EPR a concentration of 150-200 µmol/l was chosen and for the more sensitive Q-band EPR a concentration between 50-100 µmol/l. For this purpose the volume and concentration of spin labeled, refolded, and purified LHCII samples was measured to calculate needed centrifugation steps. After that, samples were filled into Amicons and centrifuged (4°C, 6000 rpm; Hettich refrigerated centrifuge) in 10 min. steps until a volume of 200 µl was reached. Between each step adhesive protein on the membrane was dissolved by vortexing and the clear solution, which passed the membrane, was disposed. In order to replace the water against deuterium, 200 µl deuterium buffer was added and the volume reduced to 200 µl by centrifugation. This step was repeated four times and the volume reduced until the final concentration was reached. Finally the concentration was quantified after Butler and Kühlbrandt (1988) by using 1 µl of the high concentrated sample.

2.7.19. Directed insertion of the LHCII into liposomes

For a directed insertion of the LHCII into liposomes, the refolded protein was immobilized on Ni-column material, incubated with liposome solution (lipid to protein ratio 300:1), and the detergent was removed. The interactions between the protein and the column material based on the his_6 tag/Ni^{2+} IDA Sepharose column system (2.7.12). Two kinds of mutants were used. The first one had the his_6 tag at the N-terminal domain (hNC79Sh) and the second one at the C-terminal domain (C79Sh). This should support insertions into two different directions because after incubation with liposomes, the non-immobilized site of the protein should be directed to the inside of the liposomes. However, besides different liposome compositions, the detergent had to be removed to ensure a closed liposome sphere formation.

2.7.19.1. Preparation of liposomes

Material:

Liposome buffer (2.7.11); thylakoid lipids: DGDG, SQDG and PG in chloroform (Polar lipids); PG (Avanti)

Method:

Two kinds of liposomes were used for the insertion experiments. Firstly, liposomes consisting of PG (lipid to protein ratio 300:1) that were prepared like described in 2.7.11. Secondly, liposomes consisting of plant-extracted lipids. DGDG, PG, and SQDG were mixed in a ratio of 61.9 : 21.4 : 16.7 (w/w). The mixture was dried in the rotary evaporator and resolved in liposome buffer (concentration 1 or 2.5 mg/ml). After a treatment in the sonic bath, liposomes within the clear solution were sized uniformly (>100 nm) by an extruder (Avestin, Mannheim). Prepared liposomes were immediately used and not stored. The detailed procedure is described in Yang *et al*. (2006).

2.7.19.2. Removal of detergent by wash cycles

Material:

Chelating Sepharose Fast Flow treated with $NiCl_2$ (2.7.12); LHCII reconstitution (2.7.10); liposome solution (2.7.19.1); OG-buffer (2.7.12); imidazole; Bio-Beads (BioRad, munich)

Method:

500 µg of reconstituted protein was immobilized on 500 µl column material and washed with 500 µl OG buffer. In order to remove the detergent two different procedures were done. Firstly, a liposome solution series, containing a decreasing amount of detergent (0.1 %, 0.08 %, 0.06 %, 0.04 %) was prepared and loaded onto the column consecutively. A liposome solution with 0.04 % detergent and 0.3 mol/l imidazole was used for the elution. Secondly, the detergent was removed by Bio-Beads. Therefore, 4 ml liposome solution was loaded onto the column and the eluate was incubated with Bio-Beads. The recycled liposome solution was loaded onto the column again to replace the detergent against liposomes step by step. Totally four of these cycles were done until the immobilized LHCII was eluted by adding a fresh liposome solution, containing 0.3 mol/l imidazole. The experiment was done in the dark at 4°C. The eluate was checked by CD (2.8.2.3) and the insertion analyzed by an analytical trypsin digestion (2.7.19.4).

2.7.19.3. Removal of detergent by dialysis

Material:

Dialysis tube: ZelluTransRoth® (Carl Roth GmbH, Karlsruhe), material: regenerated cellulose, filter rate: 12 kDa, width: 25 mm, wall-thickness: 20 µm; Chelating Sepharose Fast Flow treated with $NiCl_2$ (2.7.12); LHCII reconstitution (2.7.10); liposome solution (2.7.19.1); OG-buffer (2.7.12); Bio-Beads (BioRad, munich)

Method:

In order to prepare the dialysis tube it was equilibrated for at least one hour in distillated water (80°C). During this time the reconstituted LHCII was immobilized on the Ni-column, washed with OG buffer and the column material suspended in 1.6 ml

(concentration: 2.5 mg/ml) of a liposome solution. This mixture was transferred into the dialysis tube. Both sites were sealed with clamps and the tube put into a flacon tube, containing liposome buffer and Bio-Beads. The dialysis took three days in the dark at 4°C on a rotator, whereas Bio-Beads were changed each day. After three days, the content of the dialysis tube was loaded onto an empty column and the LHCII was eluted. The eluate was checked by CD (2.8.2.3) and the insertion analyzed by an analytic trypsin digestion (2.7.19.4).

2.7.19.4. Analyses of the inserted LHCII by analytical trypsin digestion

Material:

Liposome buffer (2.7.19.1); Sparmix (2.8.1.1); Trypsin (Roche, Basel)

Trypsin buffer	10 mmol/l Tricine pH 8.0
	0.2 mmol/l EDTA

Method:

The insertion was checked by an analytical trypsin digestion. The protease trypsin splits the peptide bond after the basic amino acids lysine and arginine or after modified cysteine. The unfolded LHCII is degraded completely, whereas degradation of refolded LHCII is limited to the N-terminal domain (Boggasch, 2006). Therefore, the N-terminal domain of liposome inserted LHCII should be digested, if it was pointed to the outside of the liposome and should be by contrast not available, if it was pointed to the inside of the liposomes.

For the digestion different trypsin concentrations (0.001 mg/ml up to 10 mg/ml) were used. The eluate (2.7.19.2 and 2.7.19.3) was separated into various fractions and 1/9 volume of trypsin was added (final concentration 0.0001 mg/ml up to 1 mg/ml). The digestion took 30 min. at room temperature in the dark and was interrupted by adding half volume of sparmix and a boiling step. The negative control contained the same contents without protein. All samples were analyzed by discontinuous SDS polyacrylamide gel electrophoresis (2.8.1.1).

2.8. Analytic methods

2.8.1. Gel electrophoresis

2.8.1.1. Discontinuous SDS polyacrylamide gel electrophoresis after Laemmli (1970)

Material:

Midget gel chamber; glas and aluminum oxide plates; spacer; combs

SDS buffer	25 mmol/l Tris	Sparmix	4 % SDS
	192 mmol/l glycine		1.4 mol/l ß-me
	0.1 % SDS (v/v)		24 % glycerol
	0.5 mmol/l EDTA		100 mmol/l Tris/HCl pH 7.0
			20 mmol/l bromphenol blue

Table 2.13: Composition of the acrylamide solutions in order to prepare 10 gels. Sep: separating.

Stock solution	Sep. gel 15 %	Sep. gel 10 %	Stacking gel 4.5 %
30 % acrylamide / 1 % bisacrylamide	18 ml	27.4 ml	6 ml
1 mol/l Tris/HCl pH 8.8	22.6 ml	22.6 ml	-
1 mol/l Tris/HCl pH 6.8	-	-	5.2 ml
80 % glycerol	3.4 ml	3.4 ml	5 ml
Aqua dest.	11.2 ml	1.8 ml	23.4 ml
10 % APS	400 µl	400 µl	200 µl
TEMED	26 µl	26 µl	20 µl

Method:

The SDS polyacrylamide gel electrophoresis was used to separate proteins by their size. Gels had a defined gel matrix, which was reached by mixing acrylamide, bisacrylamide, the radical donator ammonium per sulfate (APS), and the catalysator N, N, N, N-

tetramethylethylendiamin (TEMED). Gels (0.75 mm thick) were prepared in a midget gel chamber and consisted of a 4.5 % stacking gel and a 10 % or 15 % separating gel. In a first step, the components of the separating gel were mixed, air bubbles removed by a water jet pump, APS and TEMED added, the gel chamber filled to 75 %, and the surface of each gel was coated with 400 µl water. In a second step (after the polymerization was finished), the components of the stacking gel were mixed, air bubbles removed, APS and TEMED was added, the gel chamber filled to 100 %, and a comb inserted into each gel. One hour later, combs were removed and gels stored under wet conditions in cellophane foil at 4°C. Proteins were mixed with ¼ volume of sparmix and boiled for 2 min. at 100°C in a water boiler to denature them. Gels were put into an electric gel chamber and covered with SDS buffer. In each gel pocket 1-2 µg protein was inserted and in one pocket 3 µl of a protein standard. The SDS had the function to cover the own charge of the proteins, leading to proteins with uniform negative charges. The separation was initiated by an electric field. An electric voltage of 70 volt was used until all proteins reached the separating gel and then increased to 200 volt.

2.8.1.2. Low denaturing gel electrophoresis after Peter and Thornber (1991)

Material:

Glycerol 80 %

LDS buffer	25 mmol/l Tris	Deriphat buffer	0.15 % deriphat
	192 mmol/l glycine		48 mmol glycine
	0.1 % LDS (v/v)		12 mmol/l Tris
	0.5 mmol/l EDTA		

Method:

The low denaturing gel electrophoresis was used to separate refolded LHCII samples under mild conditions. Caused by the sample size 10 % polyacrylamide gels were used and samples were mixed with 1/5 volume of glycerol to increase the density. In contrast to SDS gel electrophoresis the voltage was reduced (40 volt until the separation gel was reached, then 80 volt), samples were not denatured by boiling and adding SDS sparmix.

Instead of SDS running buffer LDS or deriphat running buffer was used, and samples were kept dark as well as cooled (4°C) during the procedure.

2.8.1.3. Recrystallization of deriphat after Paulsen

Material:

1-propanol; liquid deriphat 160C

Method:

For the low denaturing gel electrophoresis (2.8.1.2) solid state of deriphat was needed. However, this was not available; thus, liquid deriphat 160C was purified by recrystallization. The procedure is described in Dockter (2009).

2.8.1.4. Coomassie brilliant blue staining

Material:

Coomassie solution	175 mg Coomassie brilliant blue		
	50 ml ethanol	Discolorizer 1	20 % ethanol
	7 ml acetic acid		7 % acetic acid
	43 ml aqua dest	Discolorizer 2	10 % acetic acid

Method:

After separating proteins by using gel electrophoresis, protein bands could be stained by the triphenylmethan dye Coomassie brilliant blue. For this purpose gels were incubated for 20-40 min. in a Coomassie solution. During this process, the dye attached to cationic, hydrophobic parts of the protein. Surplus dye was removed by incubation (20-40 min.) in discolorizer 1 and subsequently in discolorizer 2 until staining was limited to protein bands. All gels were documented photometrically.

2.8.1.5. Densitometric analyses of gels

Material:

Versa Doc (BioRad); Software: Quantity one (BioRad); protein gel; BSA

Method:

The Versa Doc was used to monitor the protein amount of each protein band. Coomassie stained gels were excited and detected in the visible spectrum, whereas a defined amount of bovines serum albumin (BSA) was used to prepare a protein standard. Fluorescence dye (Dye731) labeled proteins were excited by UV-light and the fluorescence emission detected at 759 nm. Analyses were done with the help of the software Quantity One.

2.8.2. Spectroscopy

2.8.2.1. Absorption spectroscopy

In this technique the absorption of radiation is measured as a function of wavelength according to its interaction with a sample. Monochromatic light shines through the sample, which absorbs photons. The transmission of light intensity is detected and allows defining the concentration with the help of the Lambert-Beer law:

$E = -\log (I/I_0) = \varepsilon \bullet c \bullet d$

(E = extinction; I = intensity of incident light; I_0 = intensity of transmitted light; ε = extinction coefficient; c = concentration of the solution; d = width)

Absorption spectroscopy was used to determine the protein (2.7.8) as well as pigment concentration and the concentration of the detergent Triton X100.

2.8.2.2. Fluorescence emission spectroscopy

Parameters:

Extinction	470 nm
Emission detection	600-750 nm

Band width	3/3
Detector sensitivity	2
Correction	S/R
Integration time	0.1 sec.
Temperature	20°C

Method:

The fluorescence emission spectroscopy with front face technique was used to analyze refolded LHCII samples. Essential factors are the path length of the excitation beam through the sample and the concentration of the solution. Reabsorption of the emitting light leads to distorted fluorescence signals. Thus, the path length should be short and/or the concentration of the sample low. To ensure a short path length, the sample was excited, the emission was collected by a concave mirror, which was positioned in a 45° angle, and transferred over another mirror to the detector.

All refolded and purified samples in this work were measured with the Fluoromax 2. At 470 nm the chl *b* molecules were excited and the emission was detected between 600-750 nm. If all pigments were correctly bound to the LHCII, all exciting energy was transferred to chl *a*, leading to fluorescence signal that was limited to chl a. A fluorescence signal of chl *b* by contrast was an indication for free or incorrectly folded LHCII.

2.8.2.3. Circular dichroism spectroscopy

Parameters:

Band width	2 nm
Response	4 sec
Sensitivity	Standard
Measurement range	750-400 nm
Data pitch	1 nm
Scanning speed	100 nm/min.
Accumulation	1
Temperature	4°C

Method:

Circular dichroism (CD) spectroscopy is a technique to identify the configuration of natural substances. CD allows distinguishing the spatial arrangement of molecules between image and its mirror image. The measuring range between 180-250 nm provides information about the secondary structure of proteins, between 250-340 nm about the tertiary structure of proteins, and between 180-320 nm about the structure of RNA and DNA. The measuring range between 350-800 nm is used to get structural information of actives centers of proteins and enzymes. Circular dichroism is formed by a different absorption of right and left circular polarized light through a sample. If linear polarized light hits a solution that contains optically active substances, elliptically polarized light will be emitted. Such light is formed, if two plane waves of differing amplitude are related in phase by 90°. This phenomenon leads to different extinction coefficients of the optical active substance for left and right polarized light. The difference depends on the absorption of both light waves and can be positive or negative. After the light passes the sample a detector, which is synchronously connected to the modulator, measures the intensity of left turning and right turning light and subtracts the absorption of both turning lights. In principal CD can be seen as difference spectra. The measured difference $\Delta\varepsilon = \varepsilon_L - \varepsilon_R$ is given as ellipticity Θ (Lottspeich, 1998). The fact is given as:

$$\Theta(\lambda) = \text{const.}\ (\varepsilon_L - \varepsilon_R) \bullet c \bullet d\ [\text{degree cm}^2 / \text{dmol}]$$

The LHCII contains a lot of Chromophores (pigments). A tightly coupling of these Chromophores leads to an increase or decrease of electronic levels and thus, to positive or negative peaks. If the Chromophores are tightly located, their π electron-cloud can interact with each other. An energy transfer might result in an increase of the signal or in an excitonic split. These effects allow identifying the pigment binding and the distance of the pigments, represented by characteristically CD spectra.

Correctly folded and fully-pigmented LHCII monomers in LM micelles show characteristic peaks at 491(-) nm, 650(-) nm, 667(+) nm and 678(-) nm, whereas trimers are represented by a further peak at 472(-) nm.

2.8.2.4. Electron paramagnetic resonance spectroscopy

Theoretical background:

Electron paramagnetic resonance (EPR) is a method for structural analyses of solids and molecules in solution. The basis for EPR measurements are the characteristics of electrons. Each electron has a magnetic moment and a spin quantum number with magnetic components. If an electron is exposed to a magnetic field B_0, the magnetic moment of the electrons aligns itself parallel or antiparallel to the field. The difference between both states relate to the strength of the magnetic field. This effect is called Zeeman effect.

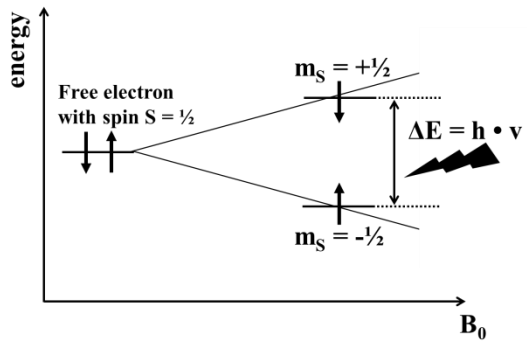

The energy difference between both states is defined as:

$\Delta E = E (m_s = +½) - E (m_s = -½) = h \bullet v = g_e \bullet ß_e \bullet B_0$

(g_e = 2.0023 g factor of a free electron; $ß_e = 9.27400899 \bullet 10^{-24}$ J/T Bohr magneton)

The absorption or emitting of electromagnetic radiation leads to a movement of an unpaired electron between both energy levels if the resonance conditions are met. The excited electron is able to relax into the lower energy level (free induction decay or FID). The relaxation time strongly depends on the environment. The lower the magnetic moment of the environment is, the longer is the relaxation time, and the better is the signal. The intensity of one free induction decay is too low to get a good signal. Therefore, several measurements are prepared because the signal to noise ratio increases proportional to the root of single measurements.

Distance analyses by using EPR (double electron electron resonance or DEER) requires two spins. In the ground state both have the same direction. One of these spins (puls spin) is emitted by electromagnetic radiation leading to changes of the magnetic environment around the second spin (observer spin). The dipole-dipole interaction between both spins

is proportional to $1/r^3$ and depends on the distance r. This can be measured by a characteristic absorption and leads to the primary data. The distance between both spins can be calculated by doing a Fourier transformation and a Tikhonov regularization of the primary data.

Experimental settings:

Four pulses DEER measurements were measured by Dr. Yevhen Polyhach and Tona von Hagens at the ETH Zürich (working group of Prof. Dr. Gunnar Jeschke). The temperature was constant at 50 K. Measurements were done in a modified Q-band spectrometer (34 GHz) and an X-band spectrometer (9.5 GHz). The pump frequency was at 34.3705 GHz, the observer frequency at 34.2705 GHz. The used pulses sequence was:

$\pi/2$ (observer) – τ_1 – π(observer) – τ_1 + t´ – π(pump) – (τ_2 – t´) – π(observer) – τ2 Echo

Further detailed information to the EPR specifications, ESEEM measurements and DEER measurements in X-band are described in Dockter *et al*. (2011). Experimental settings of the continuous wave EPR are described in Dockter (2009). DEER data were analyzed using the "Deer-Analysis" program. Experimental data were compared with theoretical data given by the software MMM2010.

3. Results

In this work, structural and conformational analyses of the major light harvesting complex II of higher plants (LHCII) were measured by Electron Paramagnetic Resonance (EPR) in order to get additional information of the protein-pigment complex in aqueous solution.

The wildtype as well as the unmodified recombinant LHCII consists of 232 amino acids and contains no unpaired electron. Therefore, it was necessary to label the apoprotein with a radical spin label. The most common and best suited EPR label for the LHCII is the PROXYL label (Dockter, 2009). PROXYL is a sulfhydryl group specific spin label that binds covalent to Cys residues. However, the wildtype LHCP contains only one Cys at position 79 and in order to get further information about different protein parts a specific labeling was required. Therefore, the recombinant apoprotein of the LHCII was PROXYL spin labeled as attaching the label to engineered Cys residues replacing either Val, Ser, Leu or Ile in LHCII complex. For this purpose, positions were chosen carefully to minimize the risk of these changes affecting the formation as well as conformation of the pigment-protein complex. Thus, in a first step these mutants were prepared by using molecular biology strategies (3.1) and in a second step they were characterized biochemically and biophysically (3.2).

Besides this, EPR measurements often require relatively high sample concentrations. Therefore, the protein purification and EPR sample production were optimized (3.3). Furthermore, these results were essential to develop a method for the production of heterogeneous trimers (3.4) which could be used for a comparison of the LHCII in a monomeric and trimeric assembly state.

In order to get closer to an *in vivo* similar environment, a directed insertion of the LHCII into liposomes was tested (3.5). In the end all kind of prepared and PROXYL labeled LHCII mutants were measured by EPR spectroscopy and compared with the X-ray structure (3.6).

3.1. Preparation of different recombinant LHCII mutants

In this work all experiments and measurements were done by using the recombinant version of the LHCII. The advantage was that changes of the *lhcb1* gen were well

established and despite these changes, they led to a full-functional LHCII in the end. Modifications included point mutations (3.1.1), more extended mutations (3.1.2) or the introduction of various affinity tags (3.1.3).

3.1.1. Production of single and double Lhcb1-Cys-clones

The wildtype version of the recombinant LHCII contains one cysteine at position 79. The most common labels (PROXYL and SH-reactive dyes) that were used in this work, bind covalently to the sulfhydryl group of a Cys. However, instead of position 79 specific labeling of the LHCII should be done and thus, Cys residues at desired positions were required. All new Lhcb1-Cys-clones were constructed by mutagenesis of the Lhcb1 gen. In contrast to the manufacture specifications half volumes of the mutagenesis kit were used to reduce costs. The results showed that all changes led to a sufficient quantity of new clones. On average, the yield was between 50-70 % in comparison to the standard procedure. If bacterial colonies did not grow, neither by using halved volumes nor by using the standard protocol, the tenfold amount of template had been used and the DpnI digestion was extended to 12 h.

For a better overview all new single (Table 3.1) and double (Table 3.2) Lhcb1-Cys clones that were prepared by me and by my diploma students were figured out in an overview.

Table 3.1: Overview of different single Cys mutants that were produced and used in this work.

Clone	Description	Producer
S3Csth	C79Sh with Cys at position 3 and C-terminal spacer, strep-, and his_6 tag	Lauf (2011)
K7Csth	C79Sh with Cys at position 7 and C-terminal spacer, strep-, and his_6 tag	Lauf (2011)
S11Csth	C79Sh with Cys at position 11 and C-terminal spacer, strep-, and his_6 tag	Lauf (2011)
stS11Ch	C79Sh with Cys at position 11, N-terminal strep tag II and C-terminal his_6 tag	Kaufmann (2010)
S34Csth	C79Sh with Cys at position 34 and C-terminal spacer, strep-, and his_6 tag	Lauf (2011)
S59Csth	C79Sh with Cys at position 59 and C-terminal	Lauf (2011)

	spacer, strep-, and his_6 tag	
stS59Ch	C79Sh with Cys at position 59, N-terminal strep tag II and C-terminal his_6 tag	Kaufmann (2010)
V90Ch	C79Sh with Cys at position 90 and C-terminal his_6 tag	Dietz (2008)
stV96Ch	C79Sh with Cys at position 96, N-terminal strep tag II and C-terminal his_6 tag	Berger (2010)
stS102Ch	C79Sh with Cys at position 102, N-terminal strep tag II and C-terminal his_6 tag	Berger (2010)
S106ChC	C79Sh with Cys at position 106 and C-terminal his_6 tag	Dietz (2008)
stL113Ch	C79Sh with Cys at position 113, N-terminal strep tag II and C-terminal his_6 tag	Berger (2010)
I124C	C79S with Cys at position 124	Dietz (2011)
V138C	C79S with Cys at position 138	Dietz (2011)
I143C	C79S with Cys at position 143	Dietz (2011)
A174C	C79S with Cys at position 174	Dietz (2011)

Table 3.2: Overview of different double Cys mutants that were produced and used in this work.

Clone	Description	Producer
S3C/S34Ch	C79Sh with Cys at positions 3, 34 and C-terminal his_6 tag	Dietz (2008)
S3C/S34Csth	C79Sh with Cys at positions 3, 34 and C-terminal spacer, strep-, and his_6 tag	Dietz (2012)
K7C/S34Ch	C79Sh with Cys at positions 7, 34 and C-terminal his_6 tag	Dietz (2008)
K7C/S34Csth	C79Sh with Cys at positions 7, 34 and C-terminal spacer, strep-, and his_6 tag	Lauf (2011)
S11C/S34Ch	C79Sh with Cys at positions 11, 34 and C-terminal his_6 tag	Dietz (2008)

S11C/S34Csth	C79Sh with Cys at positions 11, 34 and C-terminal spacer, strep-, and his_6 tag	Lauf (2011)
S3C/S59Csth	C79Sh with Cys at positions 3, 59 and C-terminal spacer, strep-, and his_6 tag	Lauf (2011)
K7C/S59Ch	C79Sh with Cys at positions 7, 59 and C-terminal his_6 tag	Dietz (2008)
K7C/S59Csth	C79Sh with Cys at positions 7, 59 and C-terminal spacer, strep-, and his_6 tag	Lauf (2011)
S11C/S59Ch	C79Sh with Cys at positions 11, 59 and C-terminal his_6 tag	Dietz (2008)
S11C/S59Csth	C79Sh with Cys at positions 11, 59 and C-terminal spacer, strep-, and his_6 tag	Lauf (2011)
stS11C/S59Ch	C79Sh with Cys at positions 11, 59, N-terminal strep tag and C-terminal his_6 tag	Kaufmann (2010)
S34C/S59Csth	C79Sh with Cys at positions 34, 59 and C-terminal spacer, strep-, and his_6 tag	Lauf (2011)
V90C/S106Ch	C79Sh with Cys at positions 90, 106 and C-terminal his_6 tag	Dietz (2008)
stV90C/L113Ch	C79Sh with Cys at positions 90, 113, N-terminal strep tag II and C-terminal his_6 tag	Berger (2010)
V90C/S123Ch	C79Sh with Cys at positions 90, 123 and C-terminal his_6 tag	Dietz (2008)
stV90C/I124Ch	C79Sh with Cys at positions 90, 124, N-terminal strep tag II and C-terminal his_6 tag	Berger (2010)
stV96C/I124Ch	C79Sh with Cys at positions 96, 124, N-terminal strep tag II and C-terminal his_6 tag	Berger (2010)
stS102C/I124Ch	C79Sh with Cys at positions 102, 124, N-terminal strep tag II and C-terminal his_6 tag	Berger (2010)
S106C/S160C	C79S with Cys at positions 106 and 160	Dietz (2010)
stL113C/I124Ch	C79Sh with Cys at positions 113, 124, N-terminal strep tag II and C-terminal his_6 tag	Berger (2010)

I124C/V138C	C79S with Cys at positions 124 and 138	Dietz (2011)
I124C/I143C	C79S with Cys at positions 124 and 143	Dietz (2011)
A174C/V196C	C79S with Cys at positions 174 and 196	Dietz (2011)

After mutagenesis and transformations in XL1 blue as well as subsequently JM101 cells, a DNA extraction kit was used to isolate the DNA. Changes of the amino acids were checked by sequencings (Genterprise genomics, Mainz). All produced single and double Cys mutants in *E. coli* JM101 cells were stored as glycerol stocks in a composition of 60 % glycerol and 40 % JM101 bacteria cell cultures at -70°C and used for the production of inclusion bodies (3.2).

3.1.2. Insertion of a tetra-Serine motif into the LHCII

In order to establish a possibility for site-specific spin labeling *in vivo* a mutant with a Ser-Ser-Pro-Gly-Ser-Ser motif (tetra-Serine) was constructed. Based on a publication (Halo *et al*., 2008) a membrane-passable dye containing two bis-boronic acid groups should be able to attach to this motif. Thereby labeling of the refolded LHCII - that is for example located in the thylakoid membrane - might be possible. Furthermore, such a dye could be modified by introduction of a radical spin label, establishing EPR measurements under *in vivo* conditions. However, the amino acid sequence of the LHCII did not contain such a tetra-Serine motif and thus, it had to be introduced. The best position for this motif seemed to be the terminal domains caused by a good accessibility and enough space for a large attached Dye. Inside the N-terminal domain the amino acids 10, 12, and 15 were chosen to create the tetra-Serine motif because changes were limited to three amino acids. Furthermore, the motif was added to the N-terminal as well as C-terminal domain by using the Phusion Site-Directed Mutagenesis Kit.

Table 3.3: Overview of Lhcb1 mutants with tetra-Serine motif

Clone	Description	Producer
A10S/S12P/P15S/C79Sh	C79Sh with tetra-Serine motif inside the N-terminal domain	Dietz (2010)
SSPGSS-NC79Sh	C79Sh with tetra-Serine motif attached to the N-terminus	Dietz (2010) Richard (2011)
hNC79S_ts	hNC79S with tetra-Serine motif	Richard (2011)

attached to the C-terminus

All new mutants were checked and stored as glycerol stocks as described in 3.1.1.

3.1.3. Addition of protein tags to the terminal domains of the LHCII

Some biochemical steps, for example immobilizations on column materials, required additional tags. The LHCII is a small protein, thus, changes should be kept as small as possible in order to do meaningful structural analyses. Thus, two kinds of protein tags were used: the hexahistidin tag (his_6 tag) as well as the streptactin tag II (strep tag II). Attachments of these tags were done by using the Phusion Site-Directed Mutagenesis Kit which allowed inserting amino acids into the lhcb1 genome with the help of designed primers.

Table 3.4: Overview of Lhcb1 mutants with additional tags

Clone	Description	Producer
hNC79S	Cys-free mutant with a N-terminal his_6 tag	Dietz (2009)
C79Shst	Cys-free mutant with a C-terminal his_6 and strep tag II	Dietz (2011)
C79Ssth	Cys-free mutant with a C-terminal strep II and his_6 tag	Dietz (2011)
C79Sst	Cys-free mutant with a C-terminal strep tag II	Dietz (2011)

All new mutants were checked and stored as glycerol stocks as described in 3.1.1.

3.2. Overexpression, refolding and characterization of LHCII mutants

The yield of overexpressed protein was on average 200-250 mg per liter bacteria culture. Bacterially expressed LHCII apoproteins were run on a denaturing SDS gel to check their purity (Figure 3.1). The LHCP including a his_6 tag formed a distinct band at 26 kDa and with an additional strep tag II at 26.8 kDa. Further bands (Figure 3.1 – left C3.2h line) indicated a contamination of foreign proteins caused by the disruption process of bacteria cells. However, the amount of foreign proteins differed, depending on the clone and disruption process, and could be decreased by intensive purification (Figure 3.1-middle and right C3.2h lines). SDS gel-electrophoresis was used to check and rough estimate the amount of protein, but the exact concentration was determined photometrically (UV-Vis spectroscopy) at 280 nm absorption.

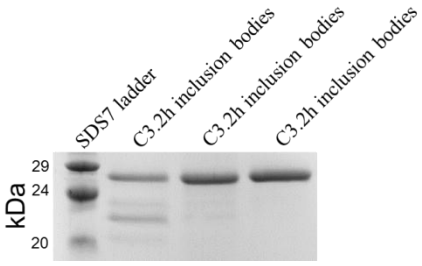

Figure 3.1: Coomassie stained 15 % denaturing SDS glycerol gel of C3.2h inclusion bodies.

The apoprotein was refolded by using the detergent-exchange method (Figure 3.2).

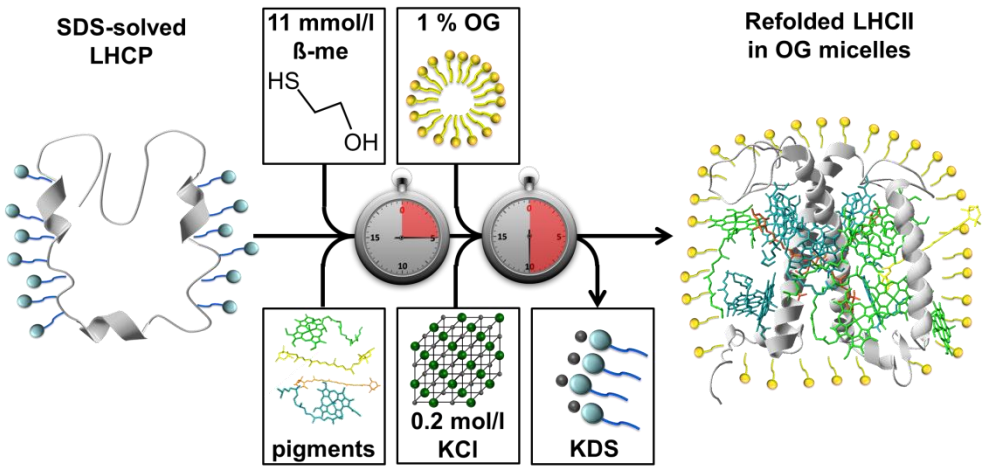

Figure 3.2: Schema of the detergent-exchange method in order to refold the LHCII apoprotein.

The yield of refolded protein varied between 40-70 %, depending on the used mutant. Trimers were formed in two different ways: firstly by using PG liposomes for tag-less mutants (Figure 3.3) and secondly by using a Ni-IDA Sepharose column (Figure 3.4).

After the trimerization process all samples were purified in sucrose gradients by ultracentrifugation.

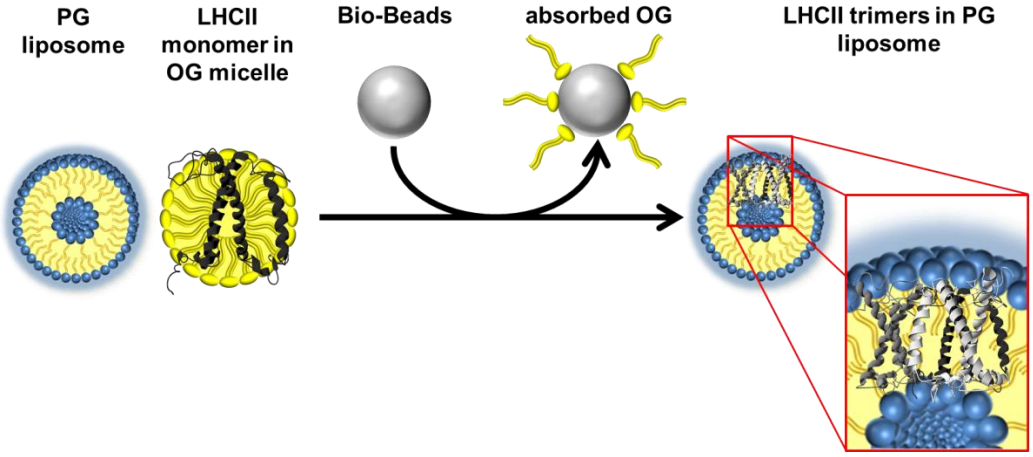

Figure 3.3: Trimerization process of tag-less LHCII monomers in PG liposomes. Bio-Beads were used to absorb the detergent (OG) of the micelles and to initiate the protein transfer into PG liposomes.

The trimerization yield for tag less mutants varied between 20-40 % and for his_6 tag mutants between 30-50 %. All used ultracentrifugation gradients consisted of 0.1 % LM, a mild non-ionic detergent, and sucrose (Figure 3.5). For the large (36 ml) gradients 0.4 mol/l sucrose, for the medium (10.8 ml) 0.25 mol/l sucrose, and for the small (4 ml) 0.55 mol/l sucrose was used (3.3.1) with one exception: for the purification of heterogeneous trimers small gradients with 0.6 mol/l sucrose had to be used caused by additional glycerol in the column eluate. Monomers that were used for EPR measurements were solely taken from purified reconstitution mixture because the monomeric band of trimerization purification could be contaminated by a small amount of trimers.

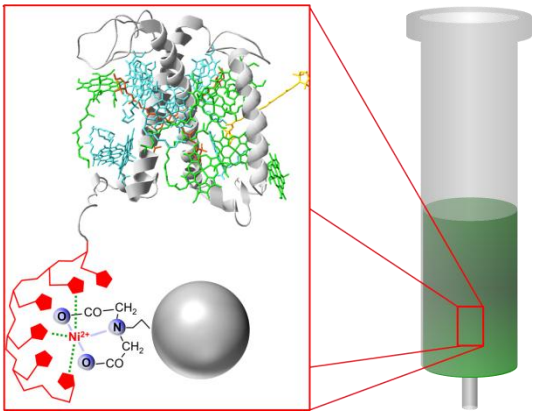

Figure 3.4: Immobilization process of LHCII monomers containing a his_6 tag (red) onto Ni-IDA Sepharose. Figure is not true-to-scale.

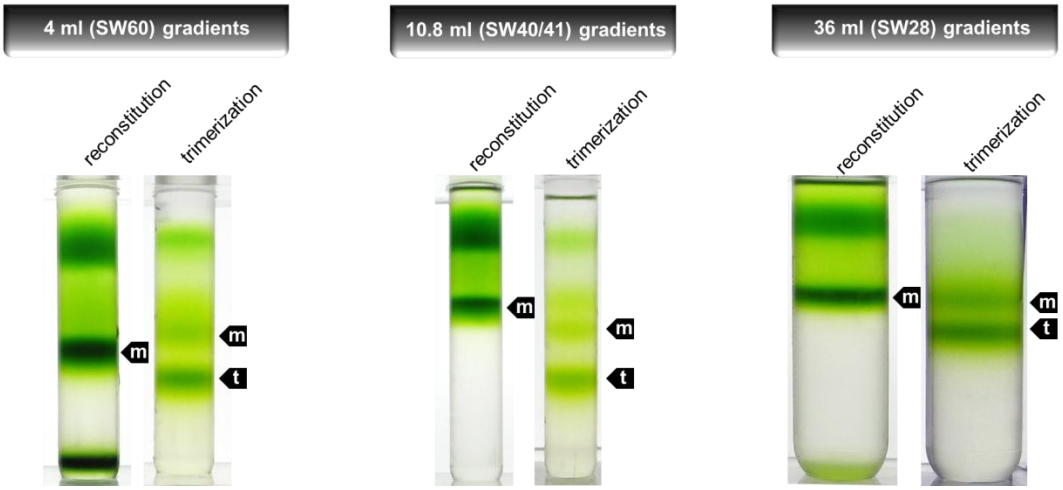

Figure 3.5: Typical purification of reconstituted monomers and trimers in sucrose gradients. Three kind of sizes were used: small 0.55 mol/l gradients (left); 0.25 mol/l gradients (middle); 0.4 mol/l gradients (right). m: monomers; t: trimers.

All isolated samples were kept dark on ice and analyzed biochemically (low denaturing 10 % glycerol gel electrophoresis) as well as biophysically (circular-dichroism and fluorescence-emission spectroscopy). In circular-dichroism spectroscopy (CD spectroscopy) monomers and trimers could be distinguished by their fingerprints. Typical peaks for fully-pigmented monomers in LM-detergent micelles were at 491 (-), 650 (-), 667 (+) and 678 (-) nm (- red line; Hobe, 1995). Trimers showed a further minimum at 472 (-) nm (Figure 3.6A - blue line). A couple of fully-pigmented trimers differed in their typical peaks (stL113C/I124Ch Figure 3.6A - magenta line; stV102C/I124Ch; stV90C/L113Ch; stI124Ch Figure 3.6A - green line).

In contrast neoxanthin free mutants showed modified spectra. The spectra of the monomeric mutants C3.2h, stV90C/I124Ch, stV96C/I124Ch and stV102C/I124Ch looked similar to the fully-pigmented complexes, but some monomeric mutants looked like trimers with a prominent 472 (-) peak (V90Ch; Figure 3.6B - blue line) and some others with a broader peak between 472 (-) and 491 (-) nm (stL113Ch and stV90C/L113Ch Figure 3.6B - green line; stL113C/I124Ch Figure 3.6B - magenta line). All spectra of neoxanthin free trimers were characterized by a deeper 472 (-) peak in relation to the 491 (-) peak (C3.2h Figure 3.6B - brown line; stL113C/I124Ch Figure 3.6B - yellow line).

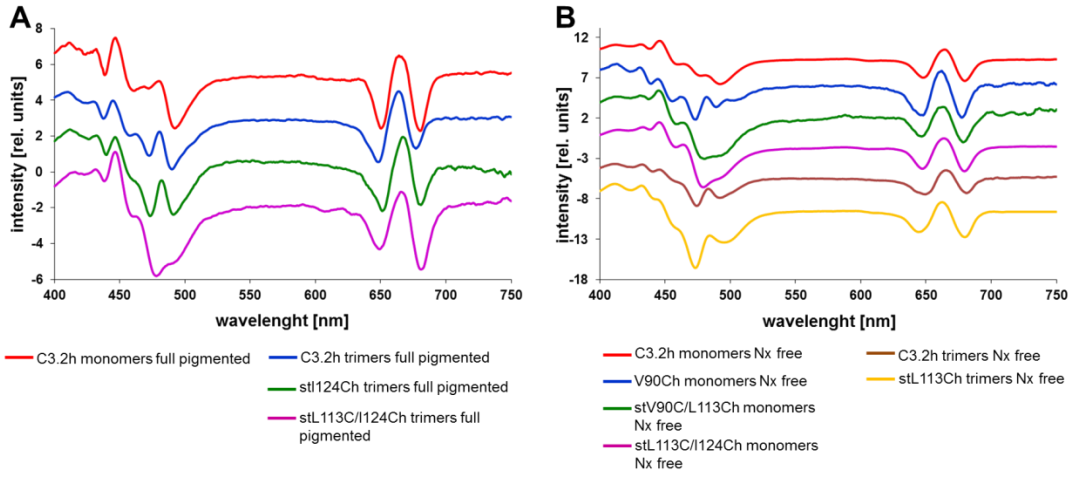

Figure 3.6: Typical CD-spectra of fully-pigmented LHCII monomers and trimers (A) and of neoxanthin free LHCII monomers and trimers (B).

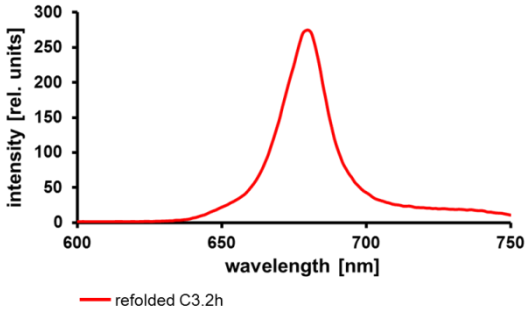

Figure 3.7: Fluorescence-emission spetrum of a full-functioning LHCII mutant.

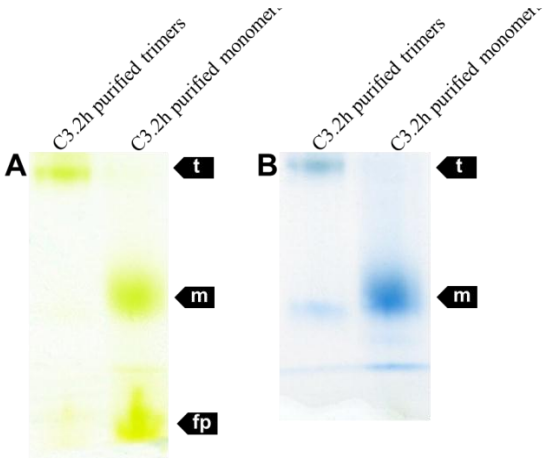

Figure 3.8: Low denaturing 10 % glycerol gel electrophoresis. t: trimers; m: monomers; fp: free pigments

Besides CD spectroscopy fluorescence-emission spectroscopy was used to check the refolding process of purified LHCII samples by detecting the energy transfer between pigments. For this purpose chl *b* was excited at 470 nm and the fluorescence was monitored between 600-750 nm. A full functioning LHCII showed a complete energy transfer from chl *b* to chl *a* leading to a fluorescence maximum at 680 nm without any chl *b* shoulder (Figure 3.7) at 653 nm (Rühle and Paulsen, 2004). Standard or particularly EPR samples showing a chl *b* shoulder were not used for further experiments. In order to define the protein concentration, absorption of the pigments at 670 nm was determined by UV-Vis spectroscopy and by the molar extinction coefficient of 546000 L • mol^{-1}• cm^{-1} (Butler and Kühlbrandt, 1988) the amount calculated. All refolded samples were loaded onto a partially denaturing 10 % glycerol gel,

leading to a typical separation into trimeric and monomeric bands (Figure 3.8- A). In the end all gels were Coomassie stained to identify protein bands.

3.3. Protein purifications and optimization of EPR samples

In this work structural analyses of the recombinant LHCII were done by using EPR spectroscopy. For this purpose single and double Cys-mutants had to be constructed in order to label them with the PROXYL spin label (3.1). The pigment-protein complexes constructed of these mutants were prepared and analyzed biochemically and spectroscopically (3.2). These procedures included several steps and thus, several pitfalls, until the refolded sample could be used for EPR spectroscopy. Most of these steps and protocols have been developed during the last ten years (Bender, 2004; Müller, 2008; Dietz, 2008; Dockter, 2009) but they should be adapted to current issues.

Firstly protein purification by using ultracentrifugation was analyzed in detail to increase the yield (3.3.1). Secondly an immobilization of refolded and ultracentrifugation-purified LHCII on the Ni-IDA Sepharose column (Ni-column) was required and thus optimized (3.3.2). The last two points of this chapter are related directly to EPR samples. The usage of stronger EPR spectrometer increased the detection limit of labeled protein but deviated distance peaks in comparison to the MMM-simulation (Multiscale modeling of macromolecular systems) as well as indications for a reduction of the PROXYL label were determined. Therefore, thirdly influences of all chemical ingredients to the PROXYL radical (3.3.3) were tested and fourthly high concentrated protein samples prepared and analyzed in order to find causes for these deviated distance peaks (3.3.4).

3.3.1. Optimization of protein purification by ultracentrifugation

For the production of EPR samples spin-labeled apoprotein had to be reconstituted using the detergent-exchange procedure to get monomers. LHCII trimers were then formed by immobilizing the monomers on Ni-IDA Sepharose (3.2). Finally, both monomers and trimers had to be purified by ultracentrifugation on a sucrose gradient. The gradient was formed by freezing and thawing a sucrose solution (freeze-thaw method) in an ultracentrifugation tube. Different conditions (number of freeze-thaw cycles, temperature

and sucrose concentration) could influence these formations. For the EPR measurements, the sample concentration needed to be increased to 300-400 µmol/l in a sample volume of 40 µl. Thus, a sufficient yield of purified protein was needed. A higher gradient volume allowed purifying a larger quantity of refolded protein but it was essential to ensure optimal sample quality for each gradient size. Therefore, all three sizes (small: 4 ml; medium: 10.8 ml and large: 36 ml) of gradients were analyzed in detail in order to find optimal conditions for the preparation of the gradients.

Finished gradients were divided into fractions and their sucrose concentration was analyzed by optical refractometry to determine the generation of a concentration gradient over the whole volume. Furthermore, a standard reconstitution and trimerization of the wildtype-similar mutant C3.2h was applied to the gradients. After a specific running time (SW60: 16 h at 392890 g; SW40 and 41 gradients: 16 h at 234745 g; SW28 gradients: 24 h at 141371 g) the isolated bands were collected and analyzed by CD spectroscopy, fluorescence-emission spectroscopy and low denaturing gel-electrophoresis (not figured out). An exemplary result of typical monomer and trimer spectra are shown in Figure 3.6 and Figure 3.7.

The number of freeze-thaw cycles could be identified as the most important factor to influence the concentration gradient and has a stronger effect in comparison to a higher gradient volume. In the small (4 ml) gradients a general tendency was discernible (Figure 3.9 A). The higher the number of freeze-thaw cycles the steeper was the concentration gradient (Figure 3.9 B), but the effect to the purification quality was less (Figure 3.10 A and B). In contrast the effect to the medium (10.8 ml) gradients was much higher. The course of the curve was not any longer linear; it became more exponential (Figure 3.9 C). This resulted in a longer pass of the sample through the gradient but not in a better resolution of bands (Figure 3.10 C and D). However, this kind of preparation was unsuitable for the biggest gradients (36 ml). The exponential course of the curve led to such a low sucrose concentration in the upper part of the gradient (Figure 3.9 E and F) that the applied samples sank deep into it and this resulted in a worse purification (Figure 3.10 E and F). Monomers and trimers could not be separated and formed a mixed band.

The effect of the freeze temperature was minor in comparison to the other variations. The course of the concentration gradient of the -70°C samples were similar to those that had been frozen at -20°C (Figure 3.9) independently of the gradient volume. Nevertheless, these small differences had an effect to the purification quality. The separation of monomer and trimer bands decreased as the gradient volume increased (Figure 3.10).

However, it seemed that separation quality increased as the samples passed a long distance within the gradient. Therefore, further variations were performed. A sucrose concentration of 0.55 mol/l instead of 0.6 mol/l for the small (4 ml), 0.25 mol/l instead of 0.3 mol/l for the medium (10.8 ml) and large (36 ml) gradients were analyzed. With regard to the small and medium gradients this step led to a better separation of mono- and trimers. The situation was different in the case of the large gradients because instead of a separation an undefined band containing mono- and trimers was formed.

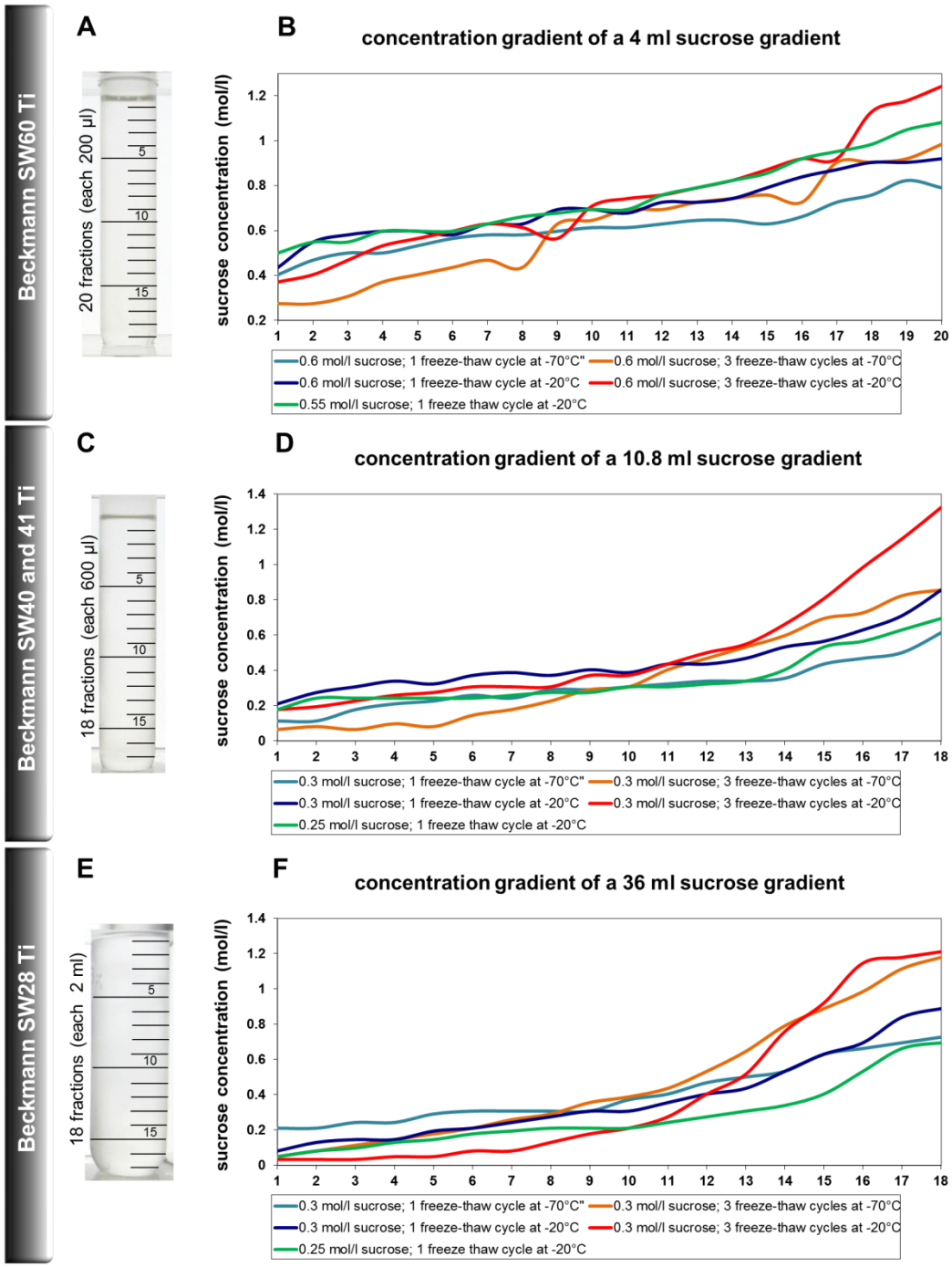

Figure 3.9: Concentration gradients of three sizes of sucrose gradients (A: 4 ml; C: 10.8 ml; E: 36 ml). The gradients were prepared by using the freeze-thaw method under varied conditions (freeze temp., number of freeze-thaw cycles, and sucrose concentration). The thawed gradients were divided into fractions and the sucrose concentration of each fraction determined by refractometry (B; D; F).

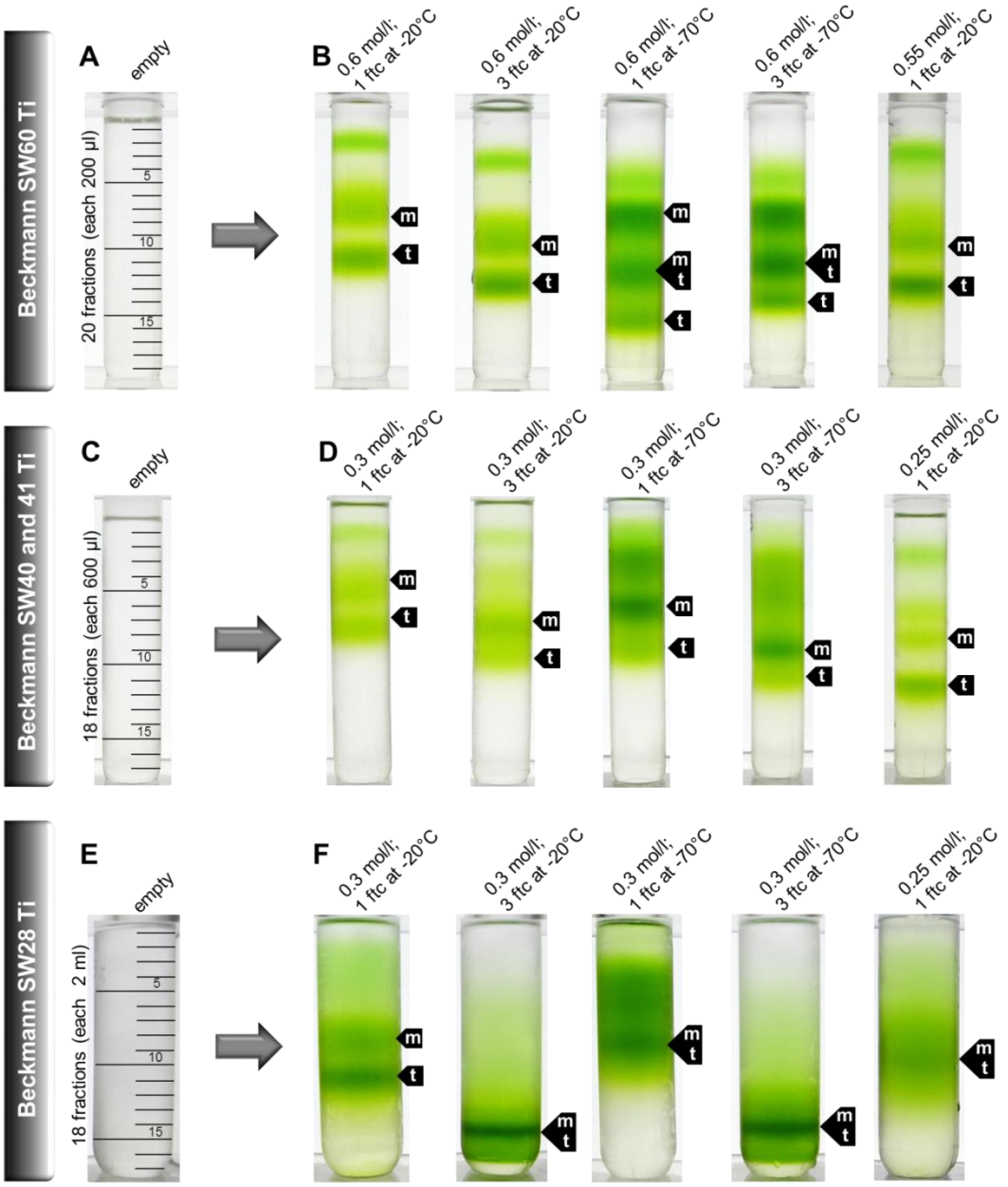

Figure 3.10: Separation ability of three sizes of sucrose gradients (A: 4 ml; C: 10.8 ml; E: 36 ml). Each gradient was prepared under varied conditions (freeze temp.; numbers of freeze-thaw cycles; sucrose concentration), loaded with a trimerization mixture, ultracentrifuged, and finally the quality of separation was analyzed. Running times: SW60: 16 h at 392890 g; SW40 and 41 gradients: 16 h at 234745 g; SW28 gradients: 24 h at 141371 g; m: monomers; t: trimers.

To establish a method that led to an acceptable purification with the large gradients a further experiment was enhanced. Recent results suggested that the most valuable influence to a good separation was the concentration of sucrose. Therefore, a

concentration ramp of sucrose, starting with 0.2 mol/l up to 0.4 mol/l in 0.05 mol/l steps, was performed. The sucrose concentration seemed to be more important than the covered distance of the sample through the gradient. The best isolation of mono- and trimers could be reached with a sucrose concentration of 0.4 mol/l (Figure 3.11).

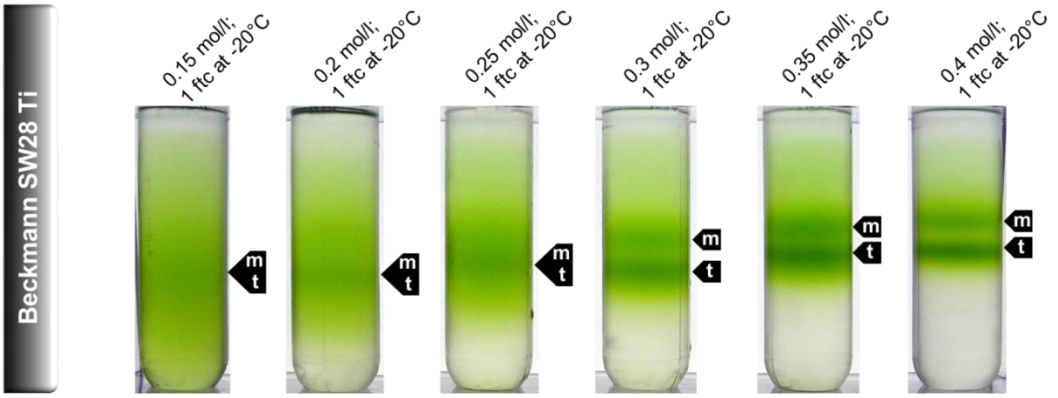

Figure 3.11: Separation ability of 36 ml gradients in relation to sucrose concentration. The freeze temperature and numbers of freeze-thaw were not variegated. Running time: 24 h at 141371 g; m: monomers; t: trimers.

However, these apparently satisfying results, were somewhat reduced by gel electrophoresis analysis. The isolated monomer sample of the gradient contained also a small amount of trimers. These results reinforced a correlation between the gradient volume and the separation quality. However, such a low contamination was also detected in smaller gradients and could not be eliminated entirely.

3.3.2. Rebinding of ultracentrifuge-purified LHCII samples onto the Ni-IDA Sepharose column.

A well-established method to form trimers is the immobilization of his_6 tagged monomers on the Ni-IDA column, in the end leading to a mixture of monomers and trimers. To isolate both assembly states, the mixture is subsequently ultracentrifuged in sucrose gradients. Some experimental approaches, for example the directed insertion of purified LHCII into liposomes (3.5) or a production of heterogeneous trimers (3.4, lipo-his method), required a rebinding of the samples to the Ni-column. The first immobilization of the LHCII functioned highly efficiently but the amount of rebound mono- or trimers by contrast was low. This problem was detected previously but could not be solved completely (Seimetz, 2004, Dockter 2005 and 2009, Plunger 2007). It was proposed that potential factors for a reduced amount of rebound protein could be the column material,

the degree of oligomerization, dissociated Ni^{2+} ions, the kind of detergent, and steric interference of the his_6 tagged C-terminal domain. Alternative column materials did not lead to an increase of rebound samples. However, it seemed that the re-immobilization of monomers in contrast to trimers worked a little bit better, which might be an indication for steric interferences. The kind of detergent was apparently the most important factor. The highest yield (26 %) of rebound LHCII was reached by diluting the purified samples in a mock reconstitution but this yield was not satisfactory (Dockter, 2009). Thus, these results were taken into account and further tests were prepared to improve the amount of rebound protein.

The N-terminal domain of the refolded LHCII is more flexible in comparison to the C-terminal domain (Dockter *et al.*, 2011); thus, a his_6 tag in this domain would be less prone to steric hindrance. Therefore, a new mutant with a his_6 tag attached to the N-terminus (hNC79S) was constructed (3.1.3) and its binding affinity was compared to the standard mutant (C79Sh) that had a C-terminal his_6 tag.

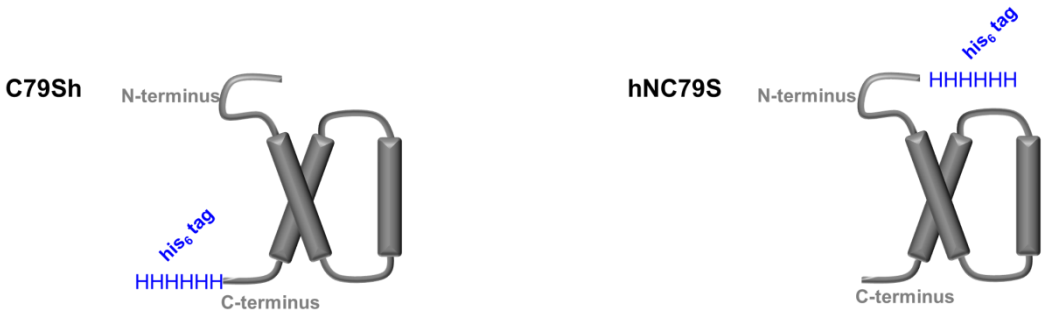

Figure 3.12: Two Cys-free LHCII mutants with an attached his_6 tag either at the C-terminal domain (left) nor at the N-terminal domain (right).

Both mutants were reconstituted and loaded onto a Ni-column. The first immobilization of both mutants seemed to be equal (Figure 3.13) but after ultracentrifugation the isolated monomeric and trimeric bands of the mutant C79Sh revealed a higher yield (Figure 3.14). All isolated samples were analyzed by CD- (Figure 3.14 B) and fluorescence-emission spectroscopy (data not shown). The concentration was measured photometrically (A670 absorption) and the yield was quantified. The yield of the mutant C79Sh was 1.7-fold higher than of the mutant hNC79S. In order to analyze the rebinding affinity to the Ni-column, the same protein amount of both mutants was loaded onto a second Ni-column. The intensity of the green color of the columns indicated low binding efficiencies (Figure 3.13). The yield of the mutant C79Sh was low and by contrast the yield of the mutant hNC79S was practically zero.

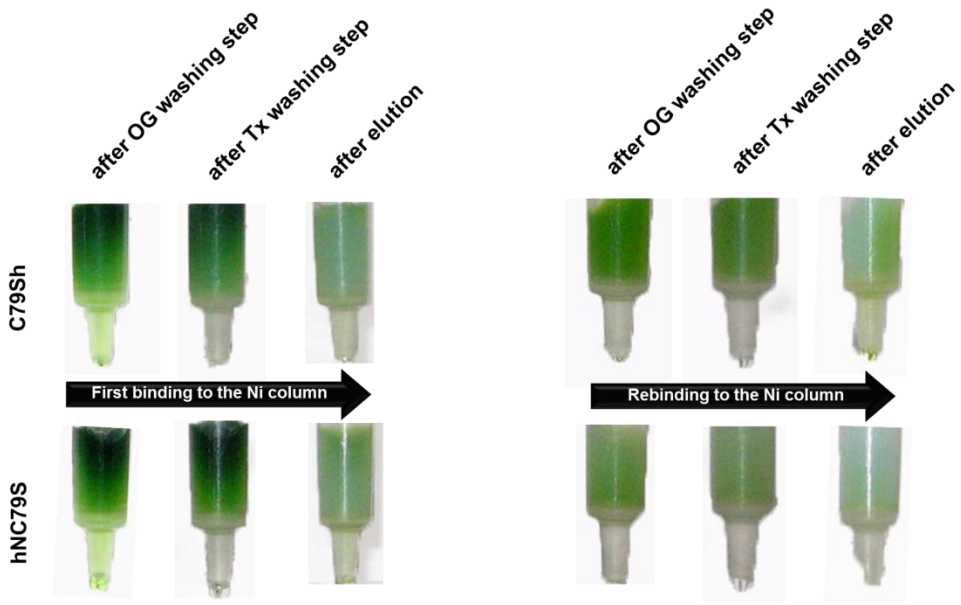

Figure 3.13: Binding and rebinding affinity to the Ni-column of the mutants C79Sh in comparison to hNC79S. Pictures of the columns were taken directly after each step.

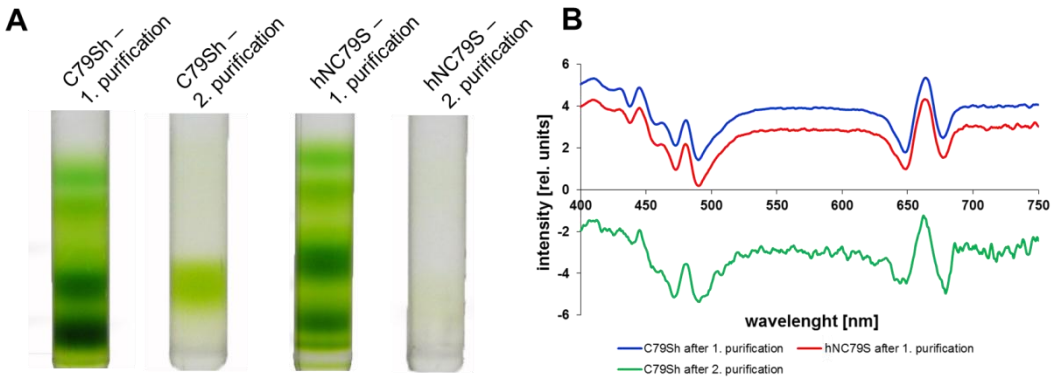

Figure 3.14: Ultracentrifugation gradients of the mutants C79Sh and hNC79S after the first and second purification (A). The monomeric (m) and trimeric bands (t) were collected and analyzed by CD (only the trimeric data are shown. B)

Overall it seemed that the low rebinding affinity of purified LHCII mutants to the Ni-column were not caused by steric interferences. Furthermore, a higher rebinding affinity of monomers in comparison to trimers that was proposed by Dockter (2009) was not observed (data not shown). In order to check if a contamination of the complex solution by Ni^{2+} might cause a low re-immobilization, $NiCl_2$ in different concentrations had been added to reconstituted LHCII-samples and the binding affinity was analyzed (Dockter, 2009). It was shown that the binding affinity decreased as $NiCl_2$ increased (Dockter,

2009). However, these results could not provide answers to the crucial question if Ni^{2+} was bound to the his_6 tag of LHCII mutants after elution.

Thus, two columns with varied compositions were prepared: Column 1 contained Ni^{2+} only in its upper half and column 2 in its lower half. The same amounts of purified LHCII trimers were loaded on both columns. If Ni^{2+} contaminates the his_6 tags of these trimers, they should preferably bind to the untreated part (Figure 3.15 column 1: lower part; column 2: upper part). In both cases the samples were immobilized on the Ni-IDA Sepharose part of the columns (data not shown) indicating that a Ni^{2+} contamination was unlikely.

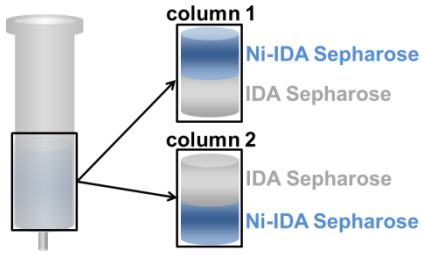

Figure 3.15: Two different compositions of IDA Sepharose columns in order to verify this part that is preferred by re-immobilization of purified LHCII samples.

To confirm these results three other columns were incubated with varied $NiCl_2$ concentrations: column 1 = 300 mmol/l, column 2 = 10 mmol/l, and column 3 without any $NiCl_2$. The same amount of purified LHCII samples had been loaded onto these columns and the rebinding affinity of each step was quantified photometrical. The results revealed that the higher the amount of Ni^{2+} on the columns was the greater was the binding affinity (Figure 3.16), confirming previously results.

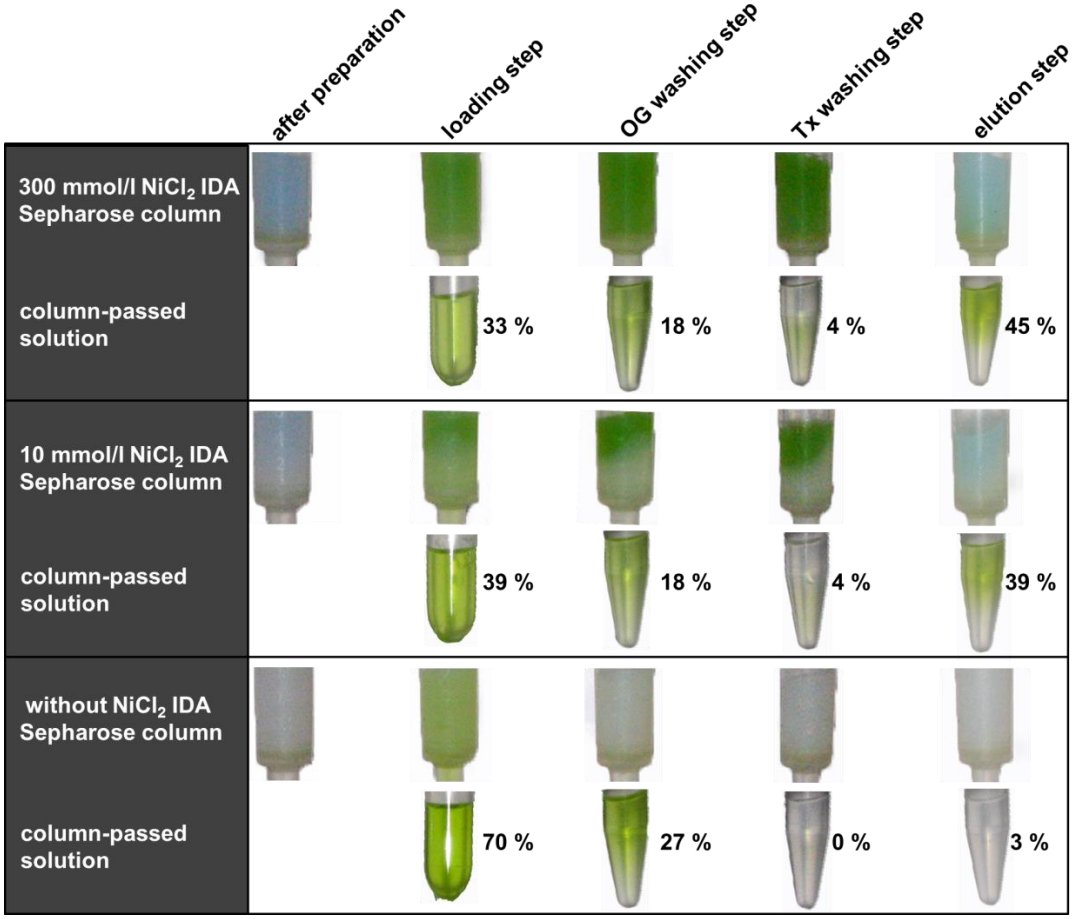

Figure 3.16: Correlation between the amount of Ni^{2+} on IDA Sepharose columns and the re-immobilization affintity of purified LHCII-samples. The percentage reflects the amount of protein in the column-passed solution.

Additional causes for the low binding affinity might be the detergent or the pH value. The pH value of purified samples is 7.8; by contrast the pH value is 9.0 during the refolding process. Therefore, master mixes of purified monomers and trimers were prepared and each divided into three fractions. Fractions one remained unchanged and served as a reference. The fractions two and three were centrifuged in 35 kDa amicons (centrifugation tubes with a membrane to reduce the volume) to get rid of the sucrose and were dissolved in LM solution with pH values of 9.0 (fractions two) and 10.0 (fractions three). Both solutions were loaded onto Ni-columns and the passed solution of each step was collected to determine the LHCII concentration.

The highest yield of rebound LHCII in the column eluate (26 %) was measured in fraction two of the trimers (Figure 3.17). The second purification confirmed these results; a clear

green trimeric band was identified in the gradient of the second purification. However, it seemed that the whole process went along with a degradation of refolded protein because in the gradient of the ultracentrifugation only 8 % of the previously loaded protein could be isolated. Thus, the pH value seemed to be one factor that caused the re-immobilization of purified LHCII-samples. Nevertheless, a yield of 26 % respectively 8% was low and included further optimization potential.

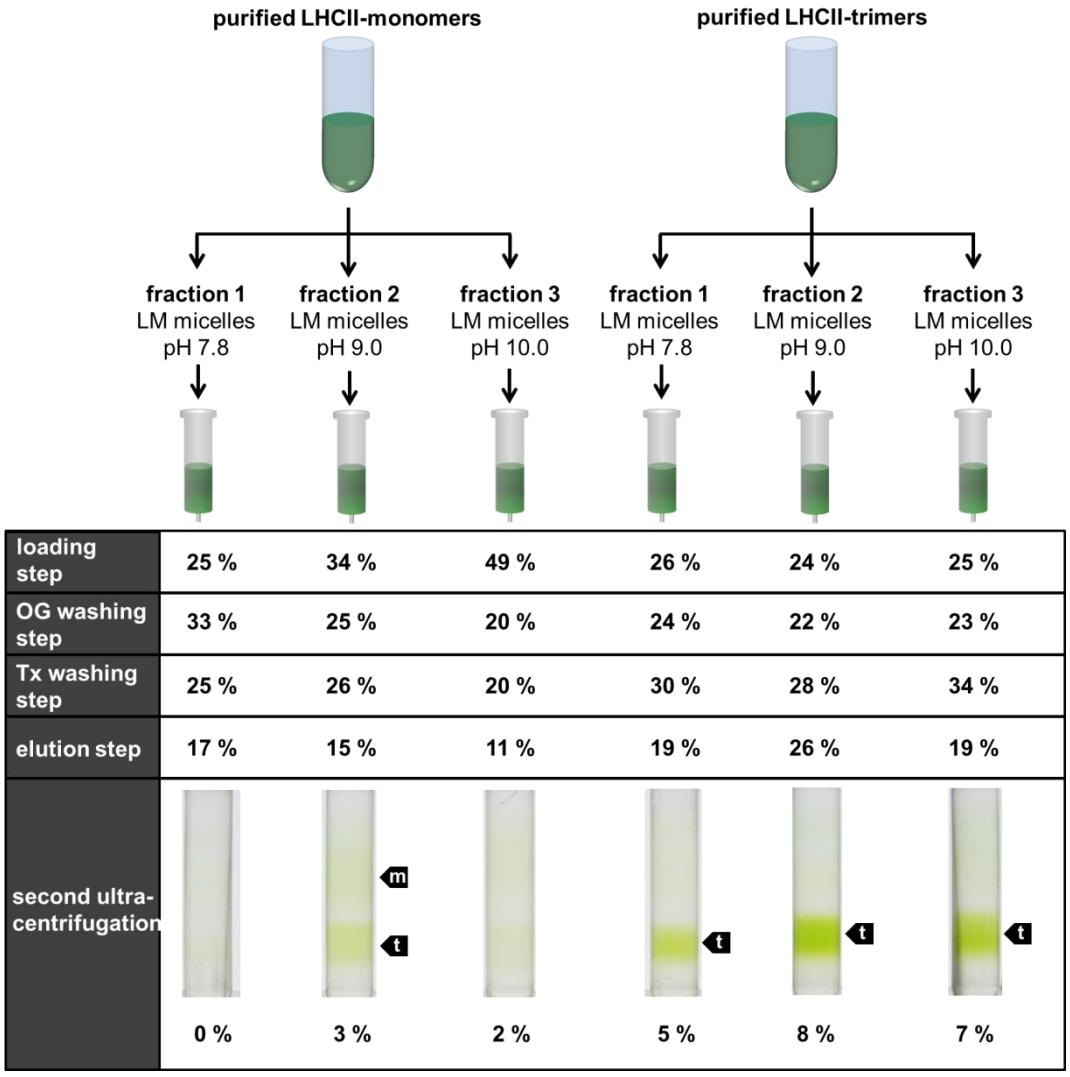

loading step	25 %	34 %	49 %	26 %	24 %	25 %
OG washing step	33 %	25 %	20 %	24 %	22 %	23 %
Tx washing step	25 %	26 %	20 %	30 %	28 %	34 %
elution step	17 %	15 %	11 %	19 %	26 %	19 %
second ultra-centrifugation	0 %	3 %	2 %	5 %	8 %	7 %

Figure 3.17: Re-immobilization of purified LHCII-samples on the Ni-column in relation to the pH value. The percentage reflects the amount of protein in the column-passed solution. m: monomers; t: trimers.

Another factor that might be involved in the rebinding affinity of LHCII samples is the detergent. In previous tests (Dockter, 2009) LM micelles, containing purified LHCII-

samples were replaced by 0.1 % OG micelles. However, this process included a lot of stress for the samples and thus, a huge loss was not surprising. Therefore, in this work the influence of detergent was analyzed under varied conditions and combined with the latest results according to the pH value. Instead of a completely replacement of detergent, a mixture of micelles was chosen. The purified LHCII-samples were separated from most of the sucrose by ultrafiltration and adjusted either pH 9.0 or to pH 10.0. The addition of 0.1% OG led to LM-OG mixed micelles. These solutions were loaded onto Ni-columns as it was done in the latest experiment but with one exception: The column material was doubled in volume (2 ml/1 mg protein) and the eluate of the loading step was re-applied to each column two times.

As previously, the highest yield was reached in fraction two of the trimers: 80 % of the protein was identified in the eluate but only 20 % of the trimers could be isolated from the ultracentrifugation gradient and remained completely intact. Nevertheless, it could be concluded that these modifications strongly influenced the re-immobilization affinity to the Ni-column because in contrast to the previous experiment all six samples led to clear green bands in the gradients of the second ultracentrifugation.

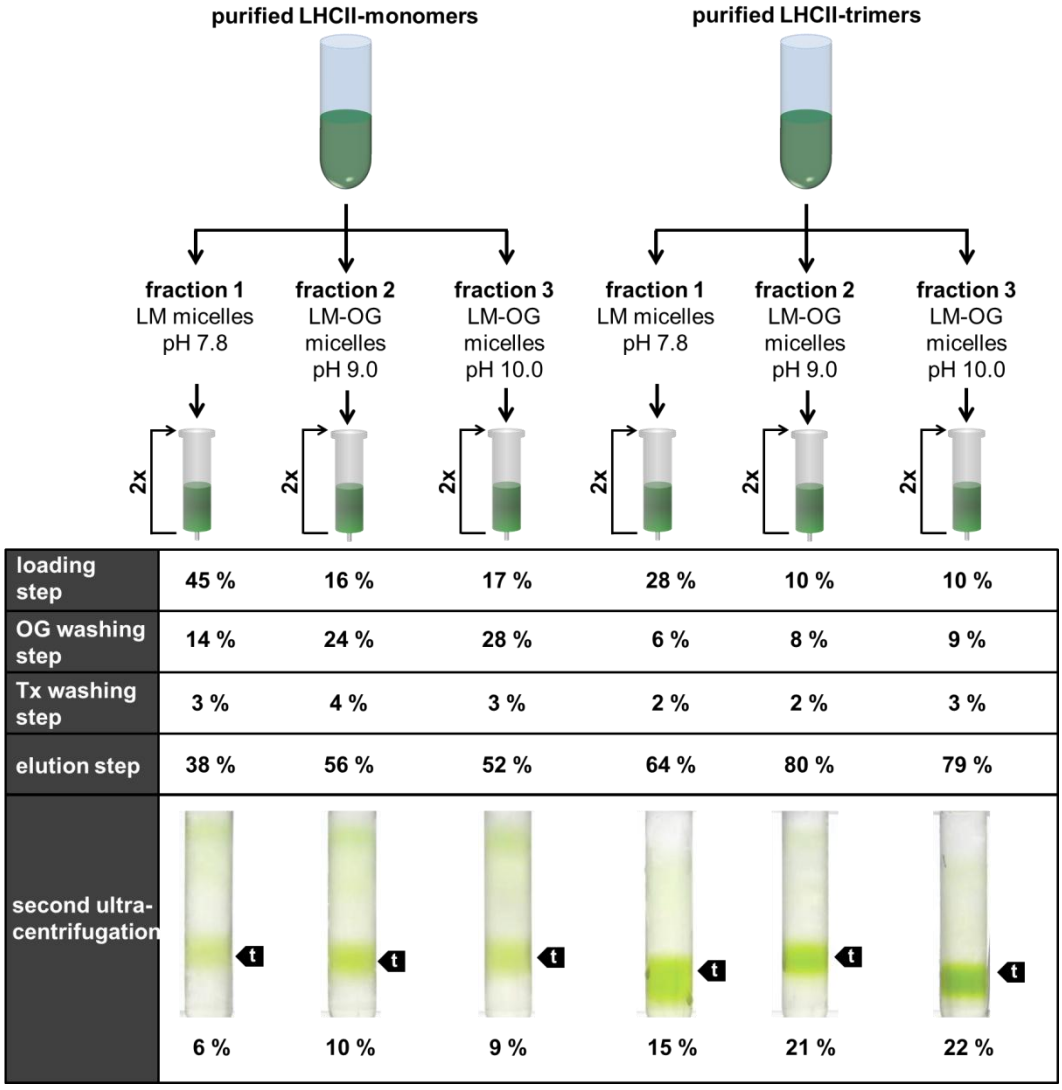

Figure 3.18: Re-immobilization of purified LHCII-samples on the Ni-column in relation to several modification steps (varied pH value and micelles, column volumes, and number of refill steps). The percentage reflects the amount of protein in the column-passed solution. The numbers next to the columns means that the passed solution of the loading step was refilled to the column two times. t: trimers.

Due to these promising results the column volume was increased one more time (3 ml/1 mg protein) and the eluates of the loading steps were re-applied to the columns four times instead of two times. According to the protein, purified LHCII trimers were divided into three fractions. Fraction one was dissolved in 0.1 % LM buffer (pH 7.8), fraction two was dissolved in 0.1 % OG buffer (pH 8.5), and fraction three in 0.1 % OG buffer (pH 9.0).

This time in each fraction the yield of re-immobilized protein was very high (Figure 3.19). During the elution steps 73 % (fraction 1) up to 85 % (fraction 2) of the LHCII trimers were detected. Furthermore, in the second purification step a maximum yield of 45 % absolutely clean LHCII trimers were measured (Figure 3.19 B, C). All of them showed typical trimeric spectra in CD and no chl *b* shoulder in the fluorescence-emission spectra indicating a perfect energy transfer.

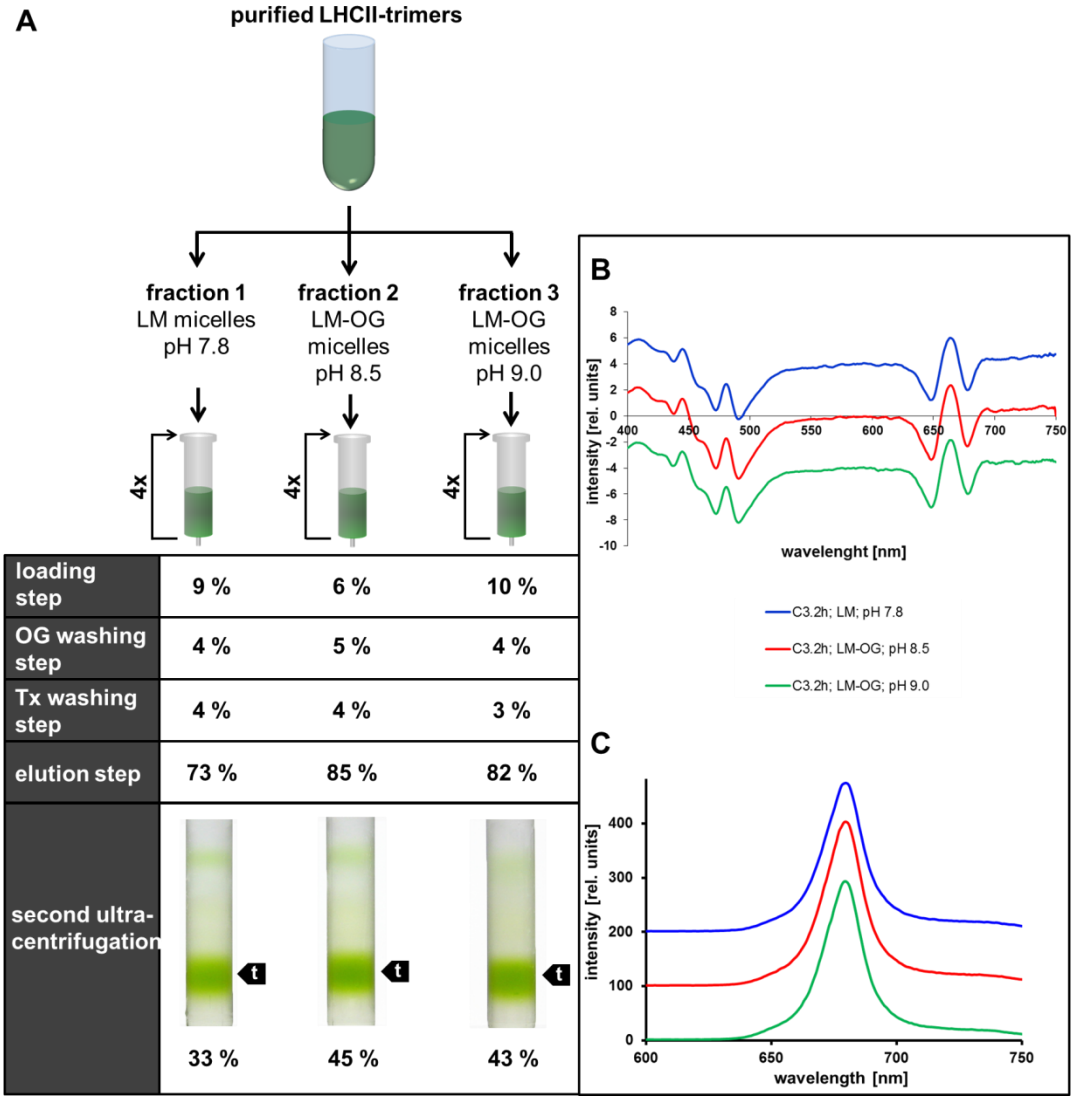

Figure 3.19: Re-immobilization of purified LHCII-samples on the Ni-column (A) in relation to several modification steps (varied pH value and micelles, column volumes, and number of refill steps). The percentage reflects the amount of protein in the column-passed solution. The numbers next to the columns means that the passed solution of the loading step was refilled to the column two times. The secondly purified samples taken from the ultracentrifugation gradients were analyses by CD spectroscopy (B) and fluorescence-emission spectroscopy (C). t: trimers.

Thus, it could be concluded that more than one factor seemed to influence the re-immobilization of purified LHCII samples. The exact cause was not identified but nevertheless, a preparation method could be developed to compensate the loss of trimers efficiently.

3.3.3. Chemical stability of the PROXYL-IAA label during sample production

Structural analysis of the LHCII by using EPR required a previously PROXYL labeling of the protein. PROXYL is a sulfhydryl group specific spin label that binds covalent to Cys residues (Figure 3.20). Several biochemical tests showed that the binding efficiency was above 90% (Dockter, 2009). Besides labeling efficiency the measuring sensitivity as well as the stability of the label were important factors which heavily influenced the quality of measurements. At the beginning of this work all measurements were done in an X-band EPR spectrometer. X-band is less sensitive than the currently used Q-band and requires a higher concentration of spin labels and thus, a higher protein concentration. Essentially, a high protein concentration included risks and it was better to keep the protein concentration as low as possible to avoid aggregation (3.3.4). During EPR measurements there was, however, growing evidence that some amount of the radical was reduced. Therefore, it was very important to check and at to ensure the stability of the PROXYL label. For this purpose the influence of several ingredients from labeling until the final product was finished, which might cause a reduction, were analyzed. Popular candidates were the reducing agents that were used during the labeling as well as reconstitution process and the pigments during the reconstitution. Thus, stock solutions were prepared, containing all ingredients that were needed for labeling respectively reconstitution with the exception of protein (mock solution) and the incubation times were varied.

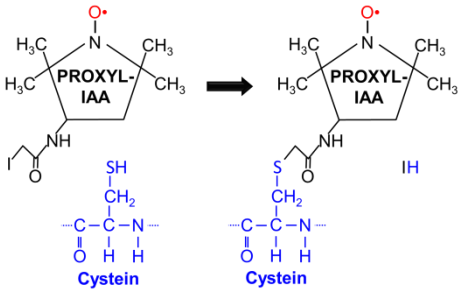

Figure 3.20: The PROXYL-IAA spin label binds irreversible to a sulfhydryl group of a cysteine (blue). The radical is labeled in red.

According to the labeling process, the mock labeling solution was divided into seven fractions that consisted of four and two mixtures respectively to calculate in the end the mean value of each measurement row. Three fractions served as references and thus, no reducing agent was added. They were incubated for zero, three and twelve hours. The

reducing agent tris-(-2-cyanoethyl)-phosphine (TCyEP) that is the standard reducing agent for protein labeling because it does not contain free sulfhydryl groups, was added to two fractions. These fractions where incubated for three and twelve hours. In comparison to TCyEP, ß-mercaptoethanol (ß-me) was added to two additional fractions and they were also incubated for three and twelve hours. In order to avoid any reactions, all samples of each fraction were frozen in liquid nitrogen after the individual incubation times and thawed immediately before they were measured by CW EPR.

The two fractions without any reducing agent and incubation time were defined as reference 1 (Figure 3.21) because all of the PROXYL label should be available in a radical state. The influence of the incubation time was monitored by the references 2 and 3. While three hours incubation time did not had an effect on the signal intensity, after twelve hours a loss of signal (13 %) was detectable. The decrease of the PROXYL signal was not higher by adding reducing agent. Neither the fractions containing TCyEP nor the fractions containing ß-me showed such a high decrease of the signal intensity. Therefore, these results indicated that the PROXYL label was oxidized by dissolved oxygen in the stock solution and perhaps, the reducing agents prevented this process.

Overall, during the labeling process an influence to the radical label was, although low, detectable but could not be the only cause for the detected loss of signal during EPR measurements.

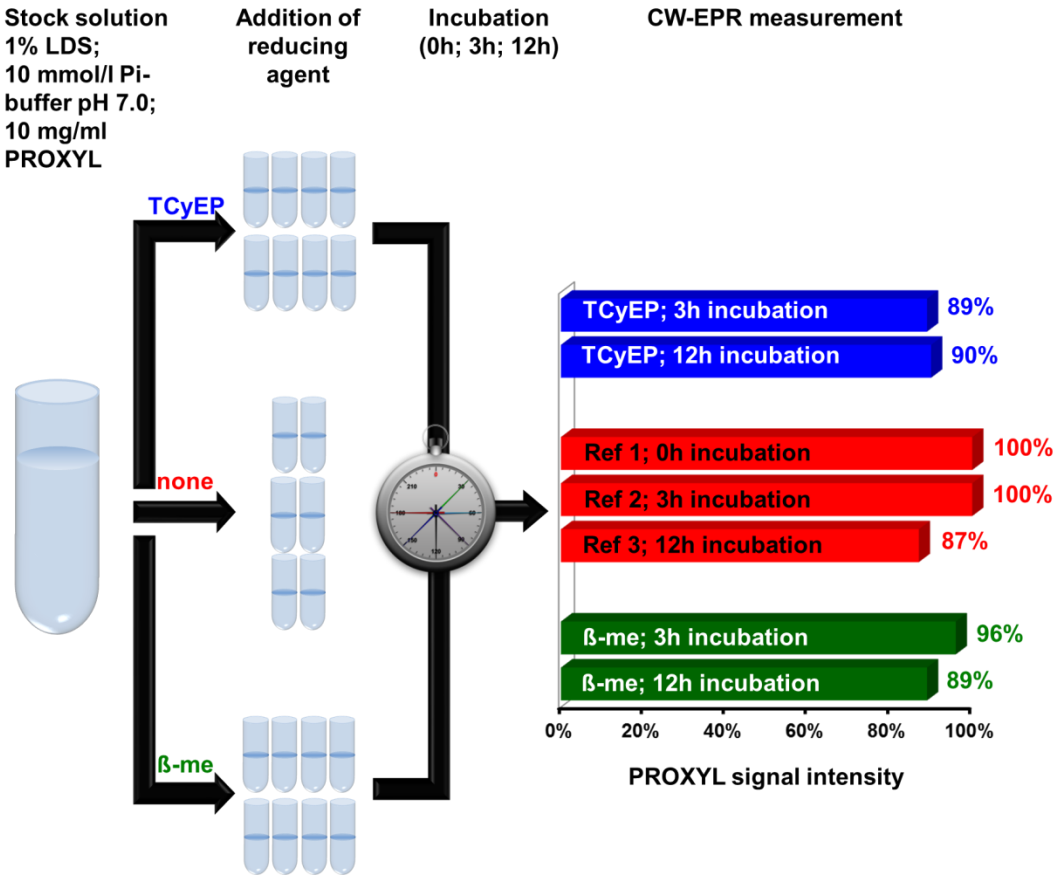

Figure 3.21: Influence of the reducing agent to the signal stability of the PROXYL radical during protein labeling. With the exception of protein, the stock solution contained all standard ingredients that are used for protein labeling procedure. This solution was divided into seven fractions of samples. Three of them were used as references (red) and incubated for 0, 3, and 12 hours. The usually used reducing agent TCyEP was added to two fractions (blue) and incubated for 3 and 12 hours. In comparison to TCyEP the reducing agent ß-me was added to two fractions (green) and also incubated for 3 and 12 hours. After the respective incubation time, all samples were frozen in liquid nitrogen and thawed immediately before the signal intensity of the PROXYL label was measured by CW EPR.

Besides the labeling process, further steps are required until the functional LHCII can be measured by EPR. The most important and critical step is the refolding process by using the exchange detergent method (Figure 3.2). During this process the reducing agent ß-me is added (c = 11 µmol/l), which might effect to the PROXYL label. However, further candidates might also be the pigments, perhaps combined with light energy.

Similar to the previous experiment, a mock reconstitution solution, containing an equivalent amount of 392 µmol/l PROXYL without protein was divided into six fractions. One half was used as reference and thus, did not contain any reducing agent. To the other half by contrast 11 µmol/l ß-me was added. According to the ingredients all mock

reconstitutions were prepared like described in Figure 3.2, but the procedures differed in the light conditions. 1/3 was reconstituted, as usually done, in the dark, 1/3 under daylight conditions and the last 1/3 was additionally exposed to UV light (10 min.) to simulate extremely the effect of light energy. All samples were frozen in liquid nitrogen after the reconstitution to stop any further reactions and thawed directly before the CW measurements to monitor the PROXYL signal intensity.

The signal intensity of Ref 1 (Figure 3.22) was set to 100% because this mixture contained no reducing agent and the reconstitution was done in the dark. Both other mixtures without reducing agent showed a slightly weaker signal, but neither the sunlight (Figure 3.22; Ref 2) nor the combination of sunlight and UV light (Figure 3.22; Ref 3) had a huge effect to the PROXYL signal. In contrast all samples containing ß-me led to weaker EPR signals. The mixtures that were prepared in the dark had a 13 % less signal, under sunlight conditions a 26 % less signal and the highest decrease of the PROXYL signal was detected in the samples that contained ß-me and was exposed to sun- and UV light. The influence of the pigments was not tested explicitly because they are essential for the reconstitution process and refolding would not work without them.

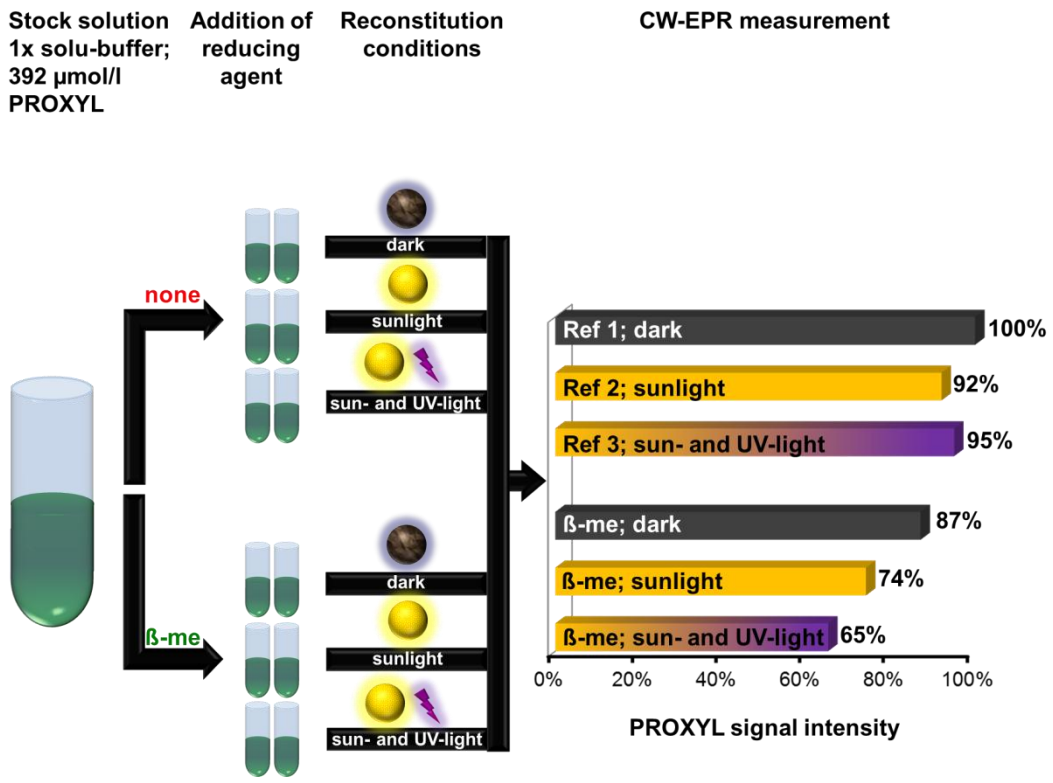

Figure 3.22: Influence of the reducing agent and light to the signal stability of the PROXYL radical during protein reconstitution. With the exception of protein, the stock solution contained all standard ingredients that are used for protein reconstitution. This solution was divided into six fractions of samples. One half were used as references did not contain any reducing agent and the other half contained the usually used ß-me (11 µmol/l). In order to check the influence of light, 1/3 of each part was reconstituted in dark, 1/3 under daylight conditions and 1/3 under daylight conditions as well as 10 min. exposed to UV-light. After the respective reconstitution time, all samples were frozen in liquid nitrogen and thawed immediately before the signal intensity of the PROXYL label was measured by CW EPR.

For protein labeling a reducing agent is absolutely essential to avoid disulfide bonds between Cys residues and a loss of signal has to be accepted. The situation is somewhat different for the reconstitution process. Actually all sulfhydryl groups of each Cys residues should be linked to PROXYL labels. Theoretically reducing agent should be not only inessential but also hindrance because it supports the reconstitution of unlabeled protein. In order to analyze the correlation between the reducing agents and reconstitution yield three kinds of mutants were compared: firstly a Cys-free mutant (C79Sh), secondly a single Cys and PROXYL labeled mutant (S12Ch), and thirdly a wild type similar single Cys mutant (C3.2h). Each stock solution was differed into six parts of equal volumes (Figure 3.23). After boiling and cooling down to room temperature 11 mmol/l ß-me was added to the reference, instead of reducing agent water to sample 1, 11 mmol/l TCyEP to the samples 2 and 3 and 11 mmol/l TCcEP (Tris-[2-carboxyethyl]phosphine) to the

samples 4 and 5. During the labeling process the reducing agents TCyEP as well as the alternative TCcEP are usually incubated for 1-2 hours, thus, half of the samples that contained one of these reducing agents were incubated for 2 hours. After that the reconstitutions were prepared by using the same aliquot of pigments for each mutant, and the mixtures were purified by ultracentrifugation. The yield of the isolated monomer bands were quantified photometrical. The average rate of yield of a standard reconstitution is between 50-60 % in relation to the used amount of apoprotein. In these experiments the yields of the references were set to 100 % for a better comparison.

The results clearly showed the correlation between the reducing agent and the yield of reconstitution, provided that the used mutant had a free cysteine. In comparison to the reference only 53 % of the apoprotein could be refolded without any reducing agent (Figure 3.23; C3.2h). However, Cys-free mutants (Figure 3.23; C79Sh) or PROXYL-labeled mutants (Figure 3.23; S12Ch) did not show a decrease of refolded protein. Other reducing agents (TCyEP or TCcEP) were less reliable and thus, less suitable but they also worked. Therefore, it seemed that a negative influence of reducing agent to the PROXYL label during reconstitution (Figure 3.22) could be avoided because it had not a great effect to the reconstitution yield of labeled mutants.

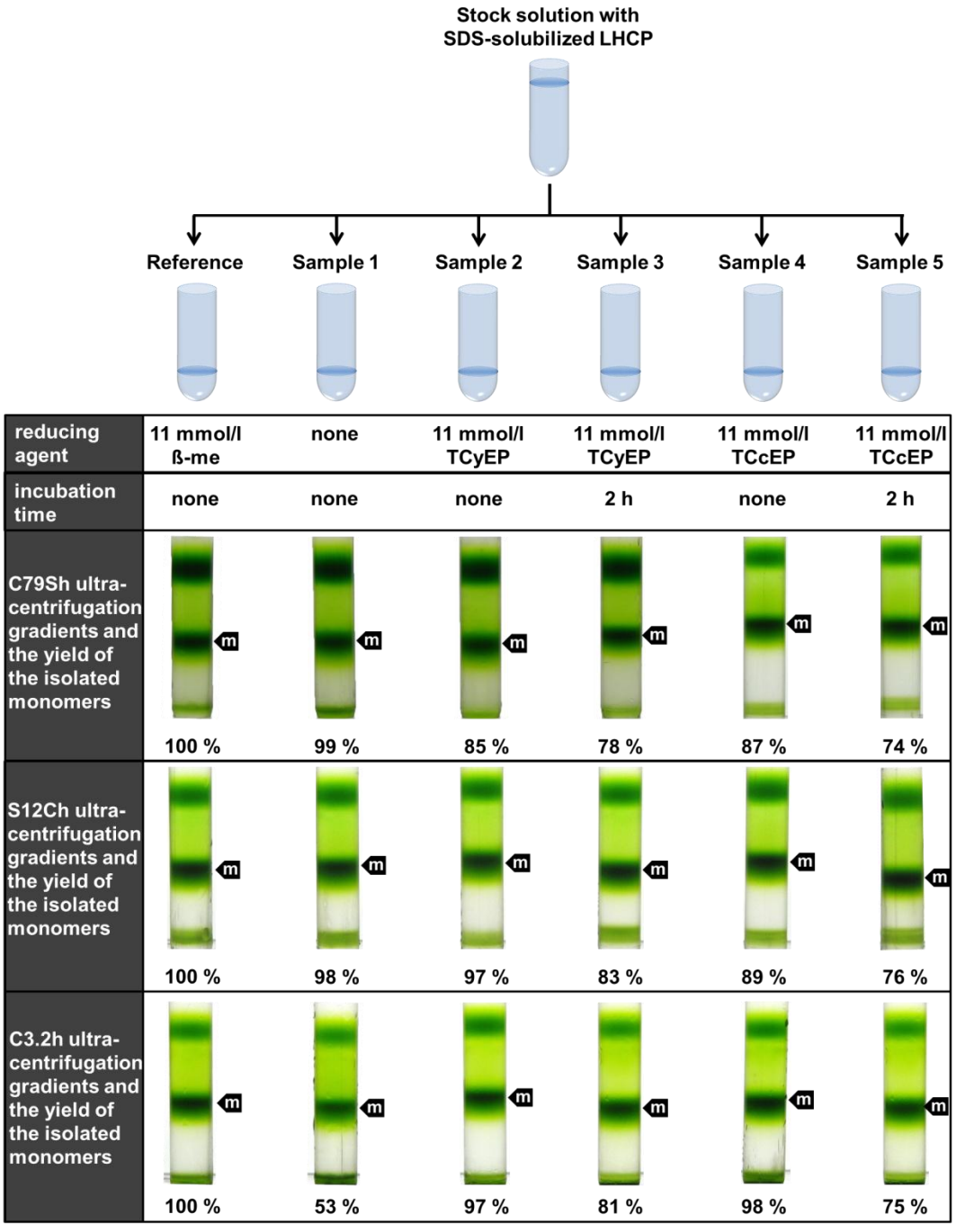

Figure 3.23: Reconstitution yield of three different LHC mutants in relation to the used reducing agents. Three kinds of mutants (C79Sh without any cysteine; PROXYL labeled S12Ch; C3.2h with an unlabeled cysteine at position 79) were used to prepare a stock solution. The stock solution was differed into six parts of equal volumes and the reducing agents were added as defined in the figure. After ultracentrifugation the yield of the isolated monomers was quantified photometrical and set in relation to the volume. For a better comparison the yield of the reference was set to 100 %. m: monomers.

3.3.4. Analyses of a potential aggregation and spontaneous trimerization of highly-concentrated EPR samples

EPR analyses of the PROXYL labeled and refolded LHCII required a sufficiently strong signal. After ultracentrifugation the protein concentration was between 2-8 µmol/l and this is undetectable by X-band EPR. Furthermore, it should be considered that a loss of PROXYL signal must be taken into account (3.3.3). Thus, the concentration of all samples had to be increased to 300-400 µmol/l (for X-band EPR), leading to further problems. The distance distributions of most samples, especially monomers, showed additional distance peaks that deviated from MMM simulation. Two explanations were a contamination of aggregates as well as a spontaneous trimerization. In both cases the PROXYL spin-labels on different complexes would come so close together that an undesired spin-spin signal is detectable.

An aggregation of the LHCII could be caused by a lot of factors and thus, was difficult to avoid generally. It was important to get some detailed information about this process. Spontaneous trimerization seemed to be unlikely because monomers, immobilized on a Ni-column, needed the lipid PG to form stable trimers and the average yield was usually 20-30 %, without PG less than 2 %. Trimers also form in liposomes due to the physical proximity of monomers in PG liposomes. Thus, an increase of the monomer concentration leads to a similar situation with the exception that PG liposomes were not added. Nevertheless, it could not be excluded that during the preparation of total extract (pigments) natural and plant´s own PG was isolated too which might support trimerization.

In order to check a potential risk of aggregation as well as a spontaneous trimerization the wildtype similar mutant C3.2h was reconstituted and purified by ultracentrifugation, leading to typical bands (Figure 3.24A – left gradient). The upper band contained free pigment, the lowest band aggregates, whereas the middle band (m) should contain purified monomers. This band was isolated from the gradient, the concentration determined photometrically (19 µmol/l), and analyzed by fluorescence emission (Figure 3.24B – blue line) as well as CD spectroscopy (Figure 3.24C – blue line). In the fluorescence-emission spectrum a perfect energy transfer from chl *b* to chl *a* was detected and the CD spectrum was identified as a typical monomer spectrum. Neither trimers nor aggregates were determined, which could be confirmed by the results of low denaturing gel electrophoresis (data not shown). The concentration of these monomers was increased up to 560 µmol/l as well as 820 µmol/l to check, whether this step might lead to aggregates or trimers. Neither the fluorescence emission (Figure 3.24B – red and green lines) nor the CD spectra (Figure 3.24C – red and green line) showed any indications for aggregates or trimers. Furthermore, the 820 µmol/l sample was diluted (to 40 µmol/l) by using a mock

reconstitution (reconstitution without protein) and purified a second time by ultracentrifugation in order to determine small amounts of potential trimers. The gradient (Figure 3.24A – right gradient) showed three bands. The upper band contained free pigments, the middle band monomers and the lowest band pigment aggregates. The middle band was isolated and analyzed by fluorescence emission (Figure 3.24B – black line) and CD spectroscopy (Figure 3.24C – black line). The fluorescence-emission spectrum showed a little chl *b* shoulder at 640 nm, whereas the CD spectrum was typical for monomers. These results could be confirmed by low denaturing gel electrophoresis (data not shown). Overall, this test was done twice and in both cases led to the same results.

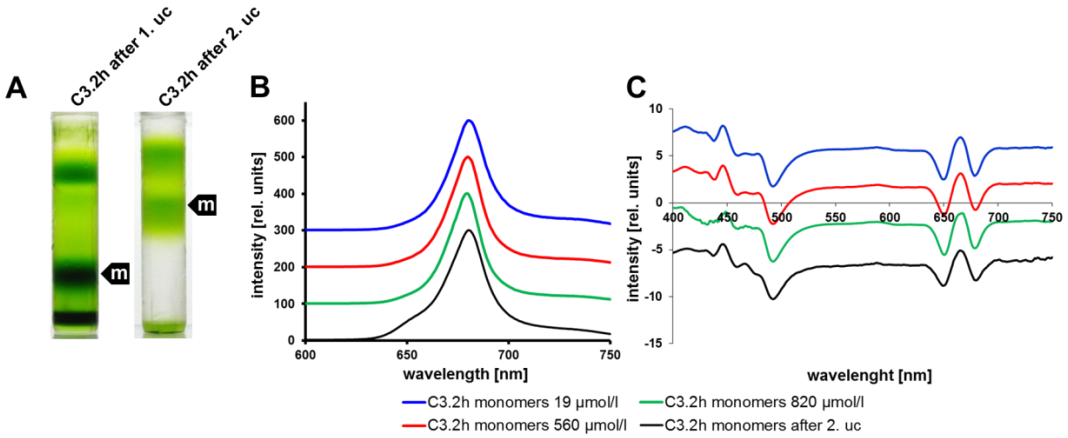

Figure 3.24: Different concentrations of the same reconstituted and purified (A) mutant C3.2h were analyzed by fluorescence-emission (B) and CD-spectroscopy (C) in order to check whether an increase of the concentration could support aggregation and/or a spontaneous trimerization. In a first step reconstituted monomers were purified by ultracentrifugation (A – left gradient), the monomers (m) isolated from the gradient, the concentration determined and then increased to 560 and 820 µmol/l. The highest concentrated monomers (820 µmol/l) were diluted by using a mock-reconstitution and this dilution purified a second time (A – right gradient). uc: ultracentrifugation; m: monomers.

It seemed that these EPR-determined artifacts could not be identified biochemically. Previous results showed that it was impossible to avoid the aggregation process because it depended on several factors: the composition of the total extract (pigments and lipids), the kind of mutant, the kind of preparation and as last the incalculable time when a crystallization nucleus was formed. In order to exclude the risk of a spontaneous trimerization the amount of the lipid PG, which worked as molecular glue and was essential to form stable trimers was reduced by degradation or by removal. To get rid of the PG two different ways were compared. Firstly: the enzyme phospholipase A_2 was tested. *In vivo* this eukaryotic enzyme is needed for the degradation of phosphatidylglycerols and production of prostaglandins. Thus, the isolated enzyme was used *in vitro* to attack the carboxy group of the C2-atom, leading to lysophospholipids (Figure 3.25). Secondly: instead of total extract HPLC-purified and thus, lipid-free total

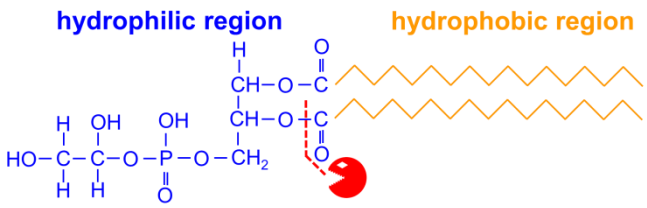

Figure 3.25: Phosphatidylglycerol that is part of membranes and an essential lipid to stabilize LHCII monomers within a trimeric assembly state. The phospholipase A2 attacks the carboxy group at the C2 atom, leading to a lysophospholipid.

extract was used. The wildtype similar mutant C3.2h was reconstituted on the one hand by using lipid free total extract and on the other hand by using standard total extracts (Figure 3.26). After dividing these monomers into five fractions (each 500 µg) they were immobilized on five different Ni-columns. The buffers of the Ni-columns differed in their ingredients. For the reference as well as the samples sp and 1 the standard OG buffer was used. In contrast the OG buffer for the samples 2 and 3 contained additionally 530 ng/ml respectively 10.6 µg/ml phospholipase A_2. All immobilized samples were incubated in OG buffer for 12 hours. After that the Tx washing step and elution was performed. For these steps both buffers were lacking PG with one exception: For the reference the standard buffers (containing 0.1 mg/ml PG) were used. After elution all samples were purified by ultracentrifugation and analyzed by CD- as well as fluorescence-emission spectroscopy. In order to check the amount of trimers all samples were loaded on a 10 % low denaturing glycerol gel and their yields were analyzed densitometrically.

In all gradients, with the exception of the reference, no trimer band was isolated (Figure 3.26). These results could be confirmed by the CD- and fluorescence-emission spectra (data not shown), leading to typical monomeric spectra and a total energy transfer from chl *b* to chl *a*. However, slight contaminations of trimers could be monitored by gel electrophoresis. The PG in the total extract was enough to form a small amount of trimers (Figure 3.26, sample 1). The addition of phospholipase could reduce this formation (Figure 3.26, sample 2 and 3) but the best way to avoid trimerization was reached by using PG-less total extract (Figure 3.26, sp sample). A small amount of trimers (3 %) was also detected in the sp sample but it should be noted that on one hand monomers are not immobilized on the Ni-column in order to prepare a monomeric EPR-sample and on the other hand that densitometric analyses should be seen more as an qualitatively rather than quantitative measure. Finally it was decided to prefer the usage of lipid-free total extract because in comparison to the usage of phospholipase, firstly the risk for a spontaneous trimerization was less and secondly results were more reproducible as well as cheaper.

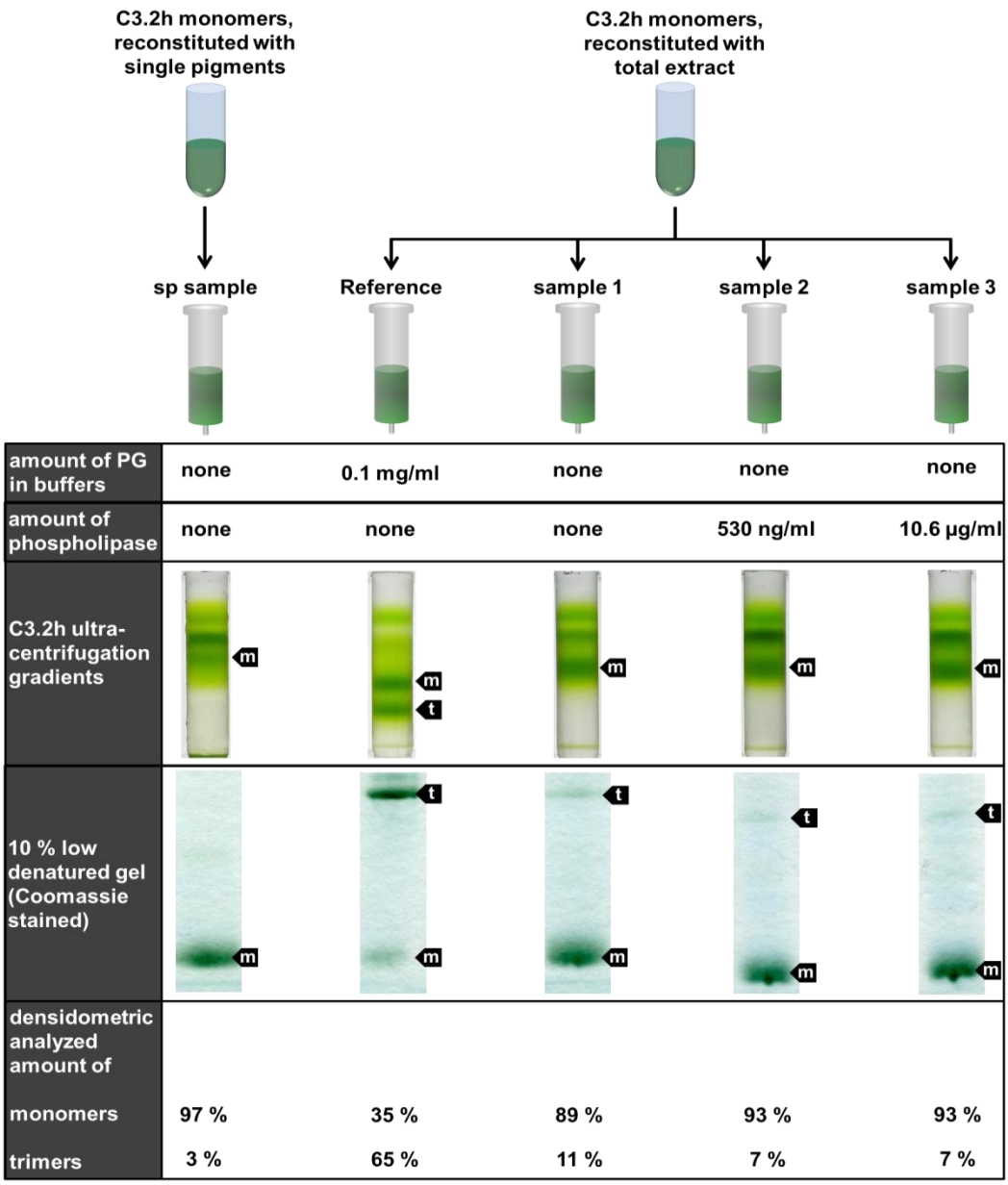

Figure 3.26: Correlation between the amount of PG and yield of trimerization. The apoprotein of the mutant C3.2h was reconstituted with PG-less single pigments and standard total extract. Each 500 µg of the monomers were immobilized on a Ni-column and treated with different OG-, Tx-, and elution buffers. After protein purification the labeled bands (m: monomers; t: trimers) of the gradients were isolated, then separated by low denaturing gel electrophoresis and finally the amounts of mono- and trimers were identified densitometrically.

These results were used to determine aggregation or a potential formation of trimers by EPR. In general a single labeled mutant in a monomeric assembly does not lead to an EPR signal because the distance between coupled electrons spins is too far apart. Coupled

electrons spins of a double labeled mutant in a monomeric assembly by contrast are detectable, but in a trimeric assembly each of the six spin labels would couple with every other one, leading to 15 different signals. Thus, the double labeled mutant V90C/S106Ch was used because of its special theoretical intra- and intermolecular distance distribution, which are far enough apart and thus, distinguishable. The intramolecular distance between the positions 90 and 106 is predicted as 1.5-3 nm (Figure 3.27 – blue solid line), whereas the intermolecular distances between the positions 90 are predicted as 6-7.5 nm (Figure 3.27 – blue dotted line) and between the positions 106 as 4-6 nm (Figure 3.27 – blue dashed line). EPR samples of this mutant were prepared by using lipid-free pigments as well as standard pigments. In order to check for aggregates or spontaneously formed trimers three different concentrations were used. All measured samples showed mainly a mean distance device between 2-3 nm (Figure 3.27C). Further distance peaks were monitored at 4.8 and 5.9 nm but were neither affected by the sample concentration nor by the used pigment composition during reconstitution. The distance distribution of the lipid free samples were slightly broader than those that were reconstituted with total pigment extract and had a lower total modulation depth (Figure 3.27B), indicating less coupled spins.

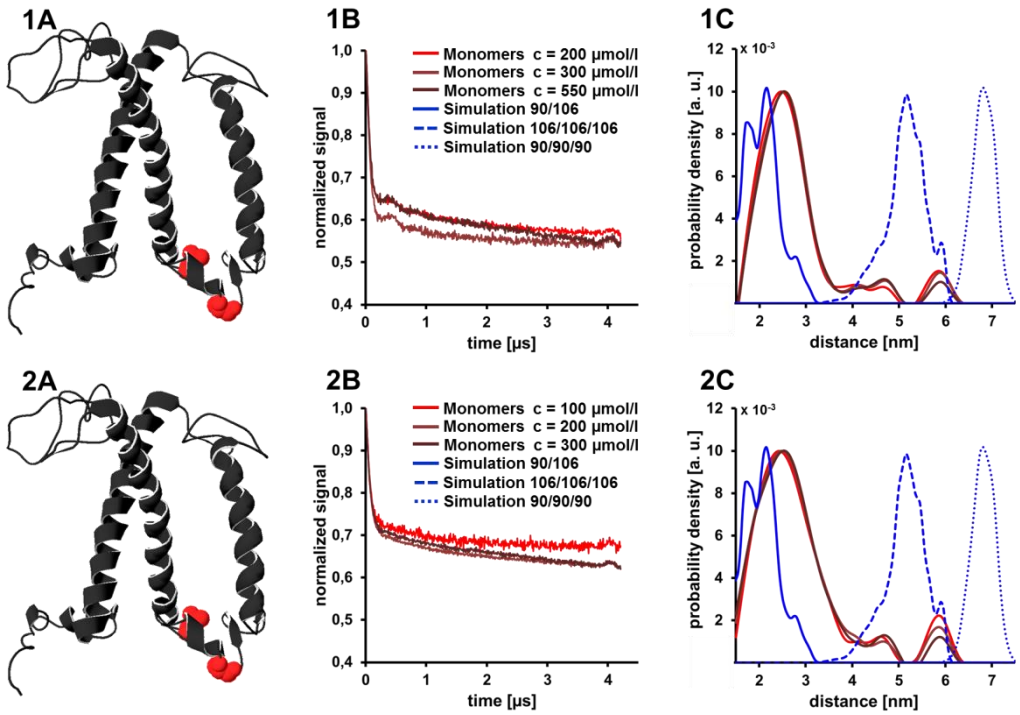

Figure 3.27: DEER-EPR results of a concentration row of the mutant V90C/S106Ch measured in Q-Band. 1: Reconstituted with total pigment extract. 2. Reconstituted with lipid-free single pigments. A: Labeled positions (red dots) within the protein-pigment complex. B: Original data. C. DEER distance-distribution.

3.4. Production of heterogeneous trimers

During the last years a lot of structural information of the LHCII, collected by EPR spectroscopy were compared with the X-ray data. For this purpose single and double Cys-mutants were prepared, PROXYL labeled, and measured. Double labeled mutants are a suitable solution to measure intramolecular distances between two positions within a monomer, in turn; single labeled mutants are used for a triangulation in a trimeric assembly. Both assembly states have contributed considerably to get a deeper view inside the LHCII structure in detergent micelles (Dockter *et al*., 2011). However, for some aspects this is not enough: A direct comparison of domains in monomeric and trimeric assembly requires to measure intramolecular distances in both assembly states. But double labeled mutants in a trimeric assembly cannot be used because each of the six spin labels would couple with every other one, leading to 15 different signals. Thus, it is necessary that only one of three monomers is double labeled and the other two are unlabeled (heterogeneous labeled trimers). However, the production of heterogeneous trimers is difficult because changes of the protein should be as small as possible.

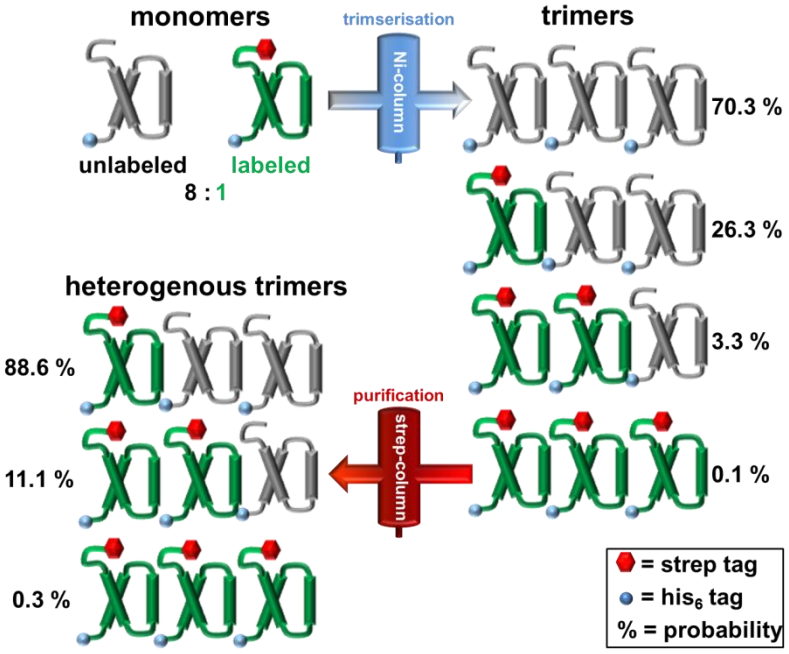

Figure 3.28: Schematic overview of the his-strep method to produce heterogeneous trimers. For the trimerization a Ni-IDA Sepharose column and for the purification of labeled trimers a Strep-Tactin column is used.

Nevertheless, a reproducible method should be developed including an acceptable time and material consuming production process. Initial success has already been achieved by using a streptactin-his_6 tag method (Dockter, 2009). This method is based on a mutant with an attached his_6 tag at the C-terminal domain and a strep tag II at the N-terminal

domain (Figure 3.28). The his_6 tag is needed to perform the trimerization of double labeled and unlabeled protein on a Ni-IDA Sepharose column (Ni-column) in a ratio of 1:8. As a result of statistic probabilities four kinds of trimers are formed: completely unlabeled trimers (70.3 %), trimers with one double labeled monomer (26.3 %), trimers with two double labeled monomers (3.3 %) and completely double-labeled trimers (0.1 %). To get rid of completely unlabeled trimers a second purification is needed. This is done by a strep tag that is attached exclusively to the double labeled mutants. This approach allows all trimers which consist of one or more labeled monomers to bind on the Streptactin-Sepharose column (Sp-Strep column). The majority of the resulting trimers now include one double-labeled monomer.

A particularly interesting part of the LHCII for a comparison in different assembly states is the N-terminal domain. This domain is incompletely resolved by crystallography and involved in a regulation process called state transition. Therefore, its conformation is of major interest. However, the reference method (Figure 3.28) could not be used because the strep tag attached to the N-terminal domain might influence its flexibility. An alternative preparation method is the liposome-his_6 tag method (Figure 3.29). This method is based on a trimerization without any tag by the proximity of monomers within liposomes. For a subsequent purification of the labeled trimers, a his_6 tag only attached to the C-terminal domain of the labeled protein was used.

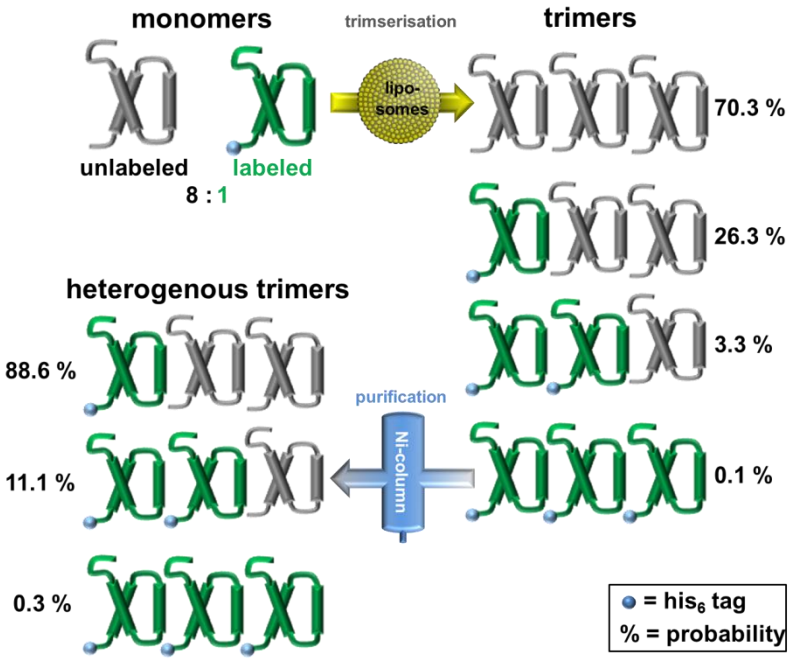

Figure 3.29: Schematic overview of the liposome-his method to produce heterogeneous trimers. The trimerization is performed in liposomes and for the purification of labeled trimers a Ni-IDA Sepharose column is used.

The following section provides a brief overview of the comparison of these methods. For detailed information, refer to the corresponding thesis of L. Kaufmann (2009). First experiments with the unlabeled protein revealed, that both methods are still working but further problems became more apparent. In particular, the liposome-his method is not only more time consuming but also includes a higher tendency for a contamination with aggregates. Therefore, a careful preparation was essential.

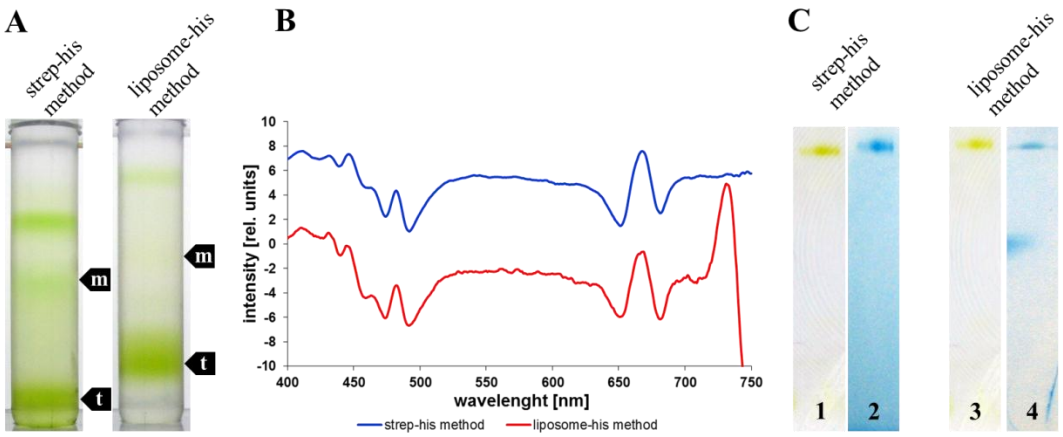

Figure 3.30: Analysis of heterogeneous trimers in direct comparison. Two kinds of preparations were used. A: Ultracentrifugation gradients (m: monomers; t: trimers); B: Circular-Dichroism spectra (staggered presentation); C: low denaturing gels unstained (1 and 3) and Coomassie stained (2 and 4).

At the end of the preparation processes, around 9.2 % (his-strep method) and 11.5 % (liposome-his method) of the theoretical possible heterogeneous trimers yield could be regained. In order to better detect the labeled amount of the produced heterogeneous trimers, further experiments were carried out with a Dy731 labeled protein (mutant stS106C/S160Ch). The gradients after the ultracentrifugation as well as the spectroscopic and gel-electrophoretic analysis looked very similar to those in Figure 3.30 and are therefore not presented. The amount of labeled protein in the trimers was calculated by denaturing gel-electrophoresis. For comparison, the labeled inclusion bodies as well as the unlabeled mutant C79Sh was also applied to the gel, then excited in the UV range, and the

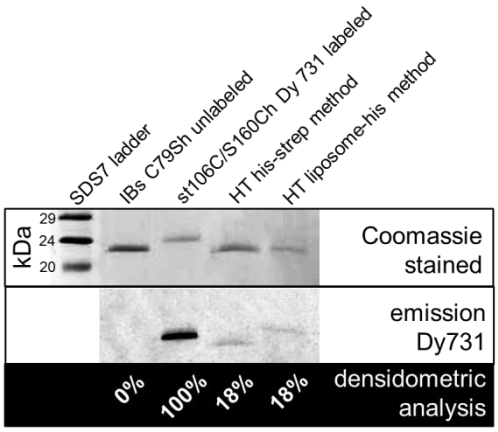

Figure 3.31: 15 % glycerol gel to calculate the amount of Dy 731 labeled monomers within heterogeneous trimers (HT). For direct comparison the samples were produced with the his-strep and liposome-his method. For the calculation of the densidometric analysis all protein bands were set to the same value.

fluorescence was detected at 700 nm (Figure 3.31). The fluorescence signals suggested that 18 % of the total protein amount was labeled and thus, did not match the theoretical value of 33 %. It must also be kept in mind that the densitometry analysis should be seen more as a qualitative rather than quantitative measure. In addition, the statistical probability indicates that the recovered sample is mainly composed of trimers with one single labeled monomer. However, in this experiment the yield was slightly lower than in the test with unlabeled protein. Only 6.6 % (strep-his_6 tag method) and 3.2 % (liposome-his_6 tag method) of the theoretical value could be regained but EPR samples were produced and measured anyway (Kaufmann, 2010). The results confirmed the suspicion that the strep tag II seemed to stabilize the N-terminal domain. But from an economic point of view, the strep-his method is better because of lower costs (half price) and less preparation time. A calculation based on the yield resulted in increased consumption of lipids and Bio-Beads, which made it relatively expensive, it showed a tendency for aggregation and the preparation took several days up to a week. Therefore a combination of both methods had to be found: a tag-less N-terminal domain but nevertheless two tags, one for the trimerization and the other for the purification. Thus a mutant was constructed with both tags at the C-terminal domain. It was unclear whether both tags positioned directly after one another might reduce the accessibility to the column material.

In order to check this, two Cys-free basic mutants were constructed (Figure 3.32). At the first one (C79Shst) the his_6 tag was directly attached to the C-terminal domain, followed by the strep tag II. At the other mutant (C79Ssth), two glycines served as a spacer, followed by the strep- II and then the his_6 tag.

Figure 3.32: Two kinds of LHCP double tag mutants. Left side: mutant with a his_6 and a strep tag at the C-terminal domain (hst); right side: additional spacer between the tags and the C-terminal domain, tags are orientated upside down (sth).

After that both of them were characterized biochemically. For detailed information, refer to the corresponding thesis of L. Lauf (2012). Regarding the reconstitution yield they did not show any significant difference versus the standard clone. But a key factor was the binding affinity to both types of column material. Firstly the interaction between the his_6 tag and the Ni-column material was analyzed. For that purpose both apoproteins were solubilized analogously to the detergent exchange method but without the cofactors

(pigments) to prevent folding. After they had been loaded on the column the flow of the loading step, of the washing steps, and of the elution step were collected, analyzed by a denaturing gel electrophoresis and the amount calculated densitometrically.

The standard C79Sh and the double tag mutant C79Ssth showed with 89 % in the elution fraction the highest binding affinity to the column material. In contrast, the double tag mutant C79Shst revealed a decrease of approximately 22 % in its binding affinity (Figure 3.33). This suggests that the strep tag influences the interaction of the his_6 tag to the Ni-column if it is at the end of the C-terminal amino acid chain.

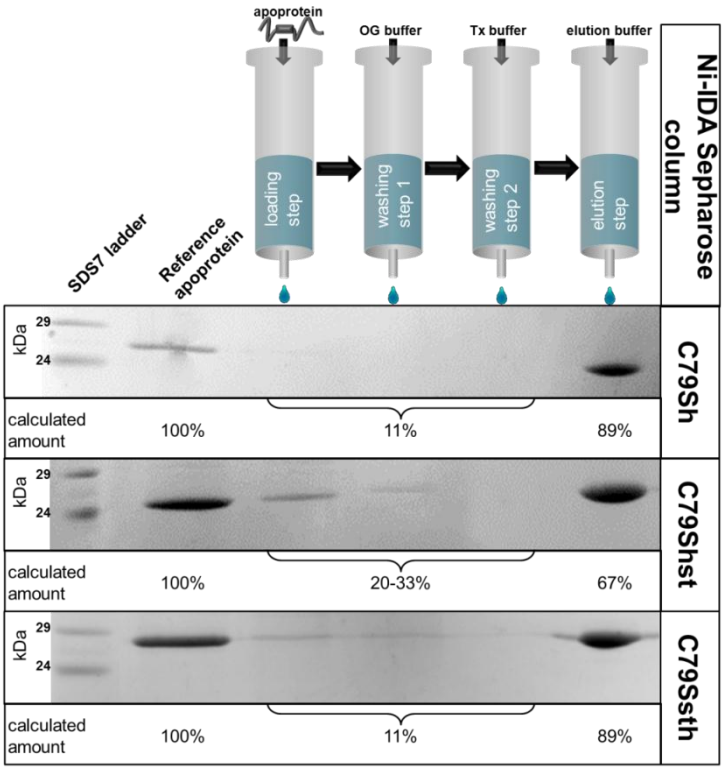

Figure 3.33: Binding affinity of two different double tag mutants in comparison to a reference mutant with a single tag to the Ni-IDA Sepharose column. In this experiment the denatured OG solubilized proteins were used. All fractions were loaded onto a 15 % glycerol gel and the amount calculated by densidometry in relation to the total volume.

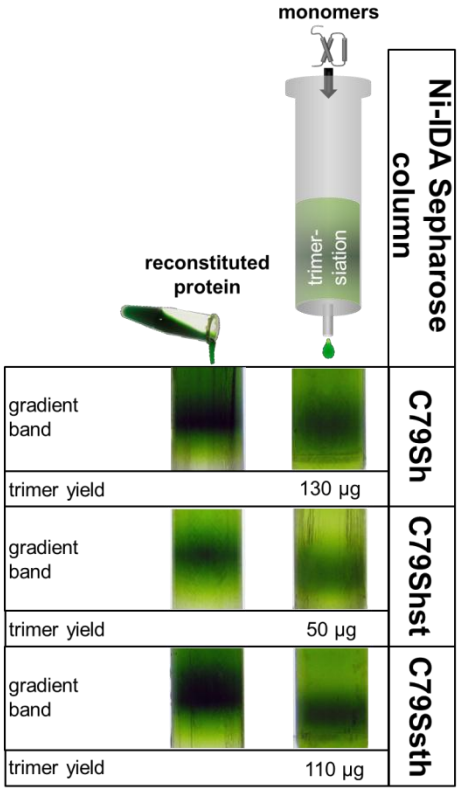

Besides this first indication, the trimerization yield was even more important. Therefore, a similar experiment with reconstituted protein was performed. 1 mg protein of each mutant was reconstituted and for a trimerization loaded on the Ni-column. The trimers in the elution fraction were purified by ultracentrifugation and the amount calculated photometrically. It could be shown that 13 % of the reference mutant C79Sh, 11 % of the double tag mutant C79Ssth, and 5 % of the other double tag mutant C79Shst trimers could be isolated as trimers (Figure 3.34).

Figure 3.34: Purificated monomeric and trimeric bands in ultracentrifugation gradients of two different double tag mutants in comparison to a reference mutant with a single tag. In each case 1 mg apoprotein was used for reconstitution.

Another important aspect was the binding affinity to the Sp-Strep column that was needed for purification. In a first step the binding affinity of the OG solubilized apoprotein was tested (Figure 3.35). In the loading step 80 % of all mutants bound to the column material and 20 % passed it. 10 % could be found in the washing step fraction. In the elution fraction different amounts could be calculated: 22 % at the reference mutant (C79Sst), 18 % at the double tag mutant with the strep tag II at the end (C79Shst), and 13 % at the double tag mutant with the his_6 tag at the end. Therefore, 50 % of the loaded protein could not be eluted by using D-Desthiobiotin. Biotin might work better but it destroys the column material irreversibly and thus, it was not used. However, these results may change if reconstituted protein is used and this is much more of interest.

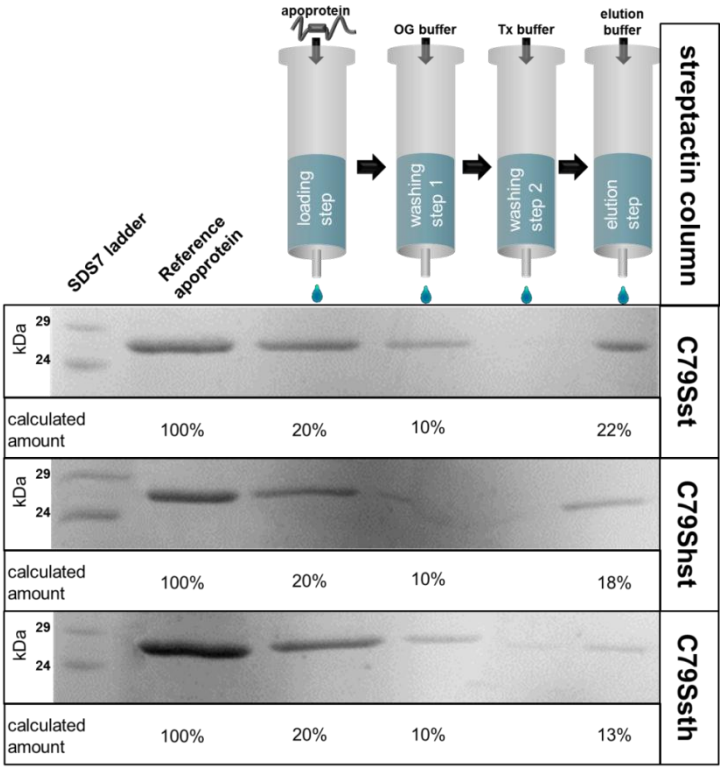

Figure 3.35: Binding affinity of two different double tag mutants in comparison to a reference mutant with a single tag to the Sp-Strep column. In this experiment the denatured OG solubilized proteins were used. All fractions were loaded onto a 15 % glycerol gel and the amount calculated by densidometry in relation to the total volume.

In a second step homogeneous trimers were formed using the refolded recombinant monomers of the mutants C79Ssth and C79Shst. These trimers were purified by ultracentrifugation in LM sucrose gradients and then loaded on the Sp-Strep column. The results (data not shown) showed that despite using a sufficient amount of column material most of the trimers did not attach to it: 60 to 80 % were found in the loading- and wash fractions. This strong decrease of the binding capacity suggested that the accessibility to the tag was reduced in refolded samples. Comparing the elution fraction of both mutants C79Ssth (16 %) showed a significantly higher amount of trimers than those of C79Shst (6 %). In previous experiments C79Ssth showed also a higher binding affinity to the Ni-column, thus, further tests were only performed with this mutant.

In a third step it was essential to improve the binding capacity to the Sp-Strep column. To achieve this goal, the column material, all steps, and chemical ingredients of the different buffers had to be analyzed. One key factor supposedly was the detergent because the stability of the refolded protein depends strongly on it and in addition, the Sp-Strep column material is based on a protein-protein interaction and thus, the usage of detergent

is much more limited. The manufacturer`s specifications differ a lot according to the maximum amounts for various detergents but it was unclear whether these data fit to our system (Table 3.5).

Table 3.5: Overview of non-ionic and ionic detergents that can be used with the Streptactin column material and amount of detergent in the needed buffers. Manufacturer specifications means the maximum concentration.

			concentration				
Reagents	**manufacturer`s (IBA) specifications**	**reconstitution buffer**	**elution buffer Ni column**	**OG buffer ST column**	**Tx buffer ST column**	**elution buffer ST column**	**centrifugation gradient**
Non-Ionic Detergents							
LM (N-dodecyl-ß-D-maltoside)	2,00%	none	none	none	none	none	0,10%
OG (N-octly-ß-D-glucopyranoside)	2,34%	1,00%	none	1,00%	none	none	none
TX (Triton X-100)	2,00%	none	0,05%	none	0,05%	0,05%	none
Ionic Detergents							
SDS (Sodium-N-dodecyl sulfate)	0,10%	<1.00%	none	none	none	none	none

At first sight, the necessary buffers do not exceed the permitted tolerance limits. But further experiments showed that the used detergent LM limited the number of regeneration cycles of the Sp-Strep column material. Without LM a purification of trimers after the Ni-column was not practicable because other detergents (OG or Tx) were not well suitable. One more critical step could be identified: During the first washing step (OG buffer) on the Sp-Strep column a substantial degeneration of the trimers could be detected. Two options were considered: the OG buffer contained no lipids, but lipids were important because they worked as a molecular glue between the monomers. This could either lead to a decay of the trimers or the OG micelles carried the pigments (cofactors) away. The main task of this step was to remove unspecific bound trimers from the column. This could also be done by Tx buffer containing of PG, thus, the OG washing step was replaced by one additional Tx washing step. In this way and by an increase of the Sp-Strep column volume (10 ml/1 mg protein instead of 1 ml/1 mg) losses were substantially reduced but were still present. In contrast, a negative impact of the OG washing step at the Ni-column during the trimerization could not be detected. Therefore, the buffers were varied to improve the yield of heterogeneous trimers.

To determine the yield of the different steps an SDS denaturing gel electrophoresis was prepared and then analyzed by densitometry. The intensity of each band was set into relation of the loading and total volume (Figure 3.36). It could be shown that 19 % of the protein got lost during the trimerization. Therefore, 81 % were loaded on the Sp-Strep column. During the loading and washing steps 16 % (in relation to the loaded Ni-column eluate) got lost. 12 % (in relation to the loaded Ni-column eluate) of the protein could be

detected in the eluate. These results suggested that a large fraction (72 %) of the protein presumably was denatured and remained on the column in the form of aggregates although the OG step had been eliminated. A further indication for a degeneration of trimers was the content of labeled protein in the elution fraction. 43 % were too high, implicating that trimers were broken down into monomers. Besides this, a formation of aggregates could be an indication of lost pigments because the sample was scattered through a huge column volume and during the washing step a loss of pigments was irreparable. To prevent this, 0.05 mg/ml pigments as well as glycerol (10 % v/v concentration) for protection were added to the Tx and elution buffer in further experiments. After that 50 % of the theoretical expected amount could be identified in the elution fraction.

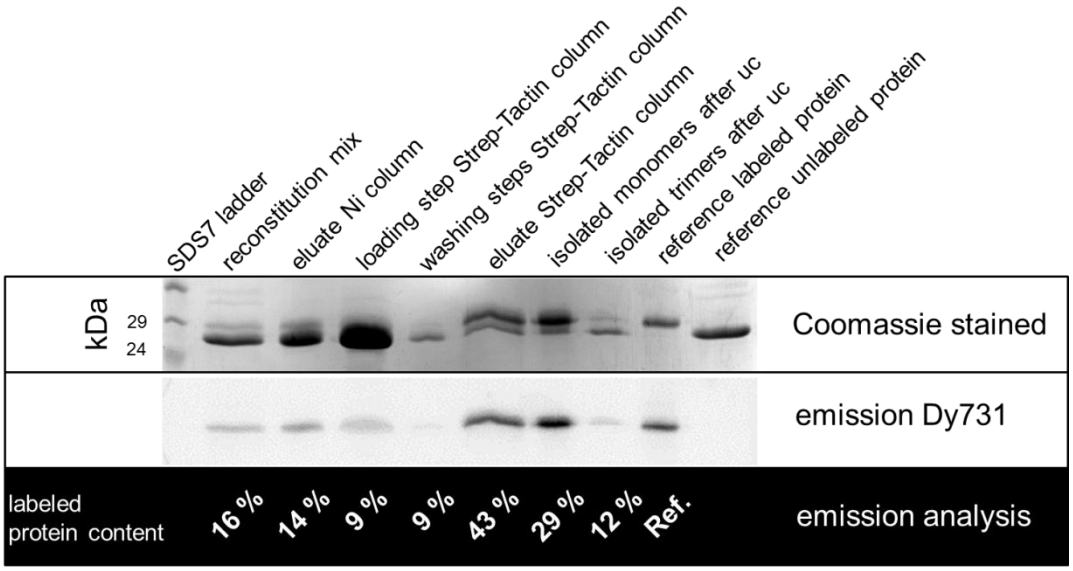

Figure 3.36: Production of heterogeneous trimers by using the strep-his method. For the purification with the Sp-strep column the tenfold amount of column material (10 ml/ 1 mg protein) was used. All samples were loaded onto a 15 % SDS denaturing gel. The upper band in the Coomassie stained gel is the Dy731 labeled protein, the lower band the unlabeled. The calculation of the total protein amount was taken into consideration of the applied and total volume. The labeled protein content was calculated by using a reference with a defined protein concentration. The percentage value describes the amount of labeled protein in relation to the total protein value.

These results sounded promising but they caused other problems: The ten-fold increase of Strep-Tactin column material also involved a tenfold increase of the elution volume. For a preparation of an EPR sample two mixtures of 40 mg unlabeled, 5 mg labeled protein, and 50 ml Strep-Tactin column material were needed. The elution was performed through two column volumes of elution buffer. Thus, 100 ml elution buffer was needed. On one hand the amount of protein per volume was very low and on the other hand only 4.5 ml could

be purified per ultracentrifugation run. For 100 ml 22 ultracentrifugation runs would be necessary, which was inacceptable. Therefore, the elution fraction was concentrated up to 10 or 5 ml. However, besides the trimers most of the detergent was concentrated too. Further tests showed that not 100 % but 74 % of the Tx was retained during the reduction of the elution buffer volume. The Tx concentration in the elution buffer was 0.1 % and after the reduction to 10 ml up to 0.74 %, accordingly upon volume reduction to 5 ml up to 1.5 % Tx was expected. The detergent (LM) concentration in sucrose gradients was also 0.1 %. Thus, the high Tx concentration prevented a purification and pass of the LHCII into the LM micelles. To reduce the Tx concentration Bio-Beads were added but care had to be taken that the Tx concentration did not fall below 0.1 % because this would lead to a precipitation of the LHCII.

To establish a controlled reduction of Tx, firstly a 30 ml stock solution with a Tx concentration of 0.74 % (Figure 3.37), and secondly a 15 ml stock solution with a Tx concentration of 1.5 % (Figure 3.38) were prepared and then divided equally (3 x 10 ml and 3 x 5 ml) into three identical tubes. After that 0.5 g, 1 g and 2 g fresh degased Bio-Beads were added. Each mixture was incubated for three hours at 4°C in a rotating apparatus and the decrease of Tx photometrical analyzed each 30 min..

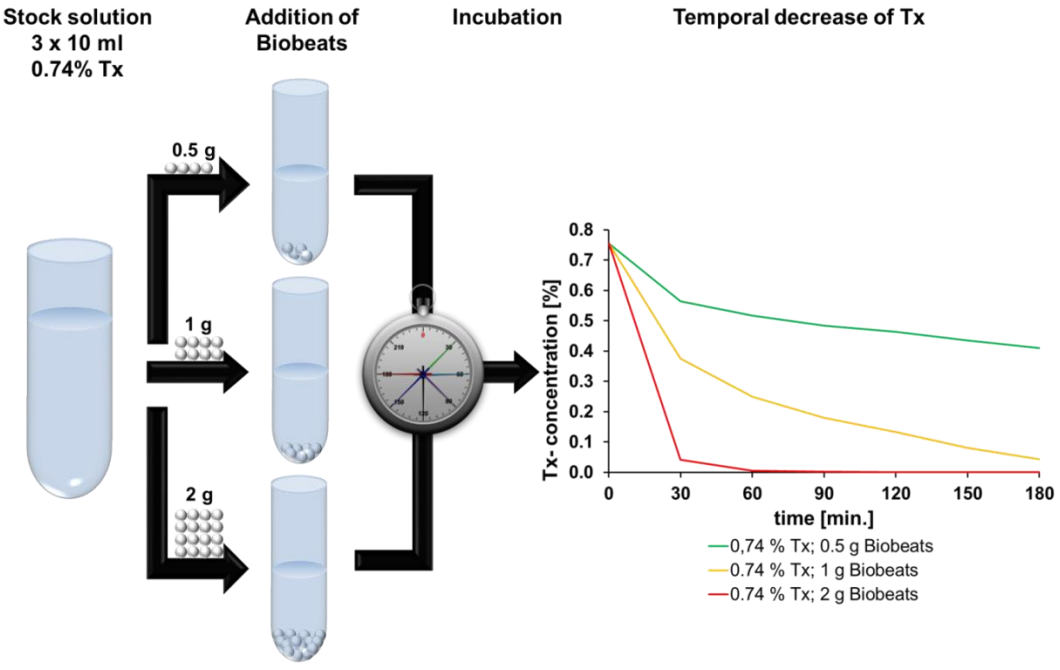

Figure 3.37: Results of a controlled reduction of Tx by using different amount of Bio-Beads. The stock solution contained 0.74 % Tx in 10 ml. After adding 0.5, 1 and 2 g Bio-Beads the temporal decrease of Tx was monitored within 3 h.

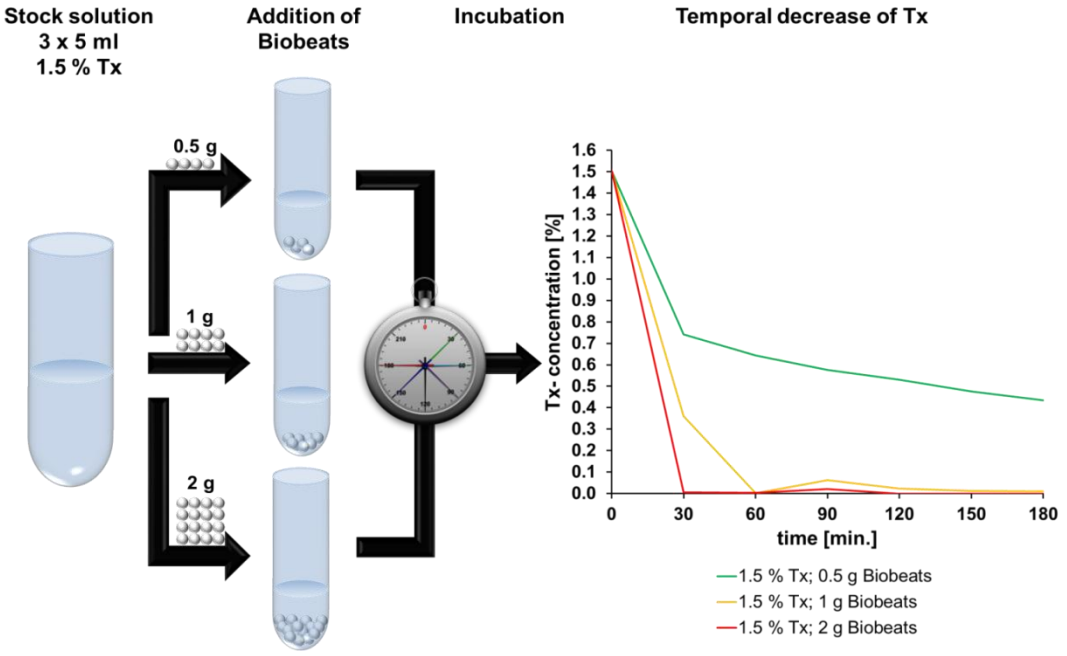

Figure 3.38: Results of a controlled reduction of Tx by using different amount of Bio-Beads. The stock solution contained 1.5 % Tx in 5 ml. After adding 0.5, 1 and 2 g Bio-Beads the temporal decrease of Tx was monitored within 3 h.

Within 30 min. nearly 100 % of the Tx was absorbed in both mixtures (Figure 3.37, Figure 3.38; red line), thus, it was difficult to determine the right moment to stop the reaction. In contrast with 0.5 g Bio-Beads it took over three hours to reach the needed concentration of Tx between 0.2 and 0.1 % (Figure 3.37, Figure 3.38; green line) but the decrease after 30 min. seemed to be nearly linear. The best compromise between fast but controlled absorption could be reached in the 10 ml solution (0.74 % Tx) containing 1 g Bio-Beads (Figure 3.37; orange line).

In further tests these results were applied to an LHCII sample. To this end, 5 mg of the wildtype similar mutant C3.2h was used. The detailed sample preparation is shown in Figure 2.5. All samples had been produced from one reconstitution in order to ensure that the yield of refolded protein was the same. The results showed that the amount of Tx strongly influences the purification quality (Figure 3.39, A). The reconstitution and trimerization yield were good, led to well isolated bands in the gradients, and to typical CD and fluorescence spectra (Figure 3.39, sample 1 and 2). A dilution with the Strep-Tactin elution buffer at a ratio of 1:1 did not result in a disintegration of the trimers (Figure 3.39, sample 3). In contrast, a very high Tx concentration deteriorated the purification quality a lot: instead of isolated bands, only a green area could be detected in the gradients, the CD spectrum was typical for LHCII in Tx micelles, and the fluorescence

spectrum showed a Chl *b* shoulder (Figure 3.39, sample 5). All four samples that had been incubated for a different time period with 1 g Bio-Beads showed that after 90 min. the best Tx concentration was reached (Figure 3.39, sample 8). A shorter or longer incubation time did not lead to a distinct band (Figure 3.39, sample 6, 7, and 9). Thus, the time frame for absorption seemed generally limited. It should be pointed out, nonetheless, that a dilution, concentration, and subsequent removal of detergent meant stress for the trimers. The yield of trimers was reduced to 1/8 of the original sample. It could therefore be concluded that this way led to heterogeneous trimers, but the optimized yield of 50 % as a result of a tenfold column volume was counterbalanced by the complicated concentration procedure reducing the yield to 10 %.

Besides this, the usage of pigment in the Tx- and elution buffer prevented a loss of LHCII-coordinated pigments but included a regeneration problem of the Sp-Strep column. To get rid of these pigments usually different washing steps with ethanol would be necessary. For the Ni-column this was no problem but by contrast ethanol destroyed the binding site of the Strep-Tactin column.

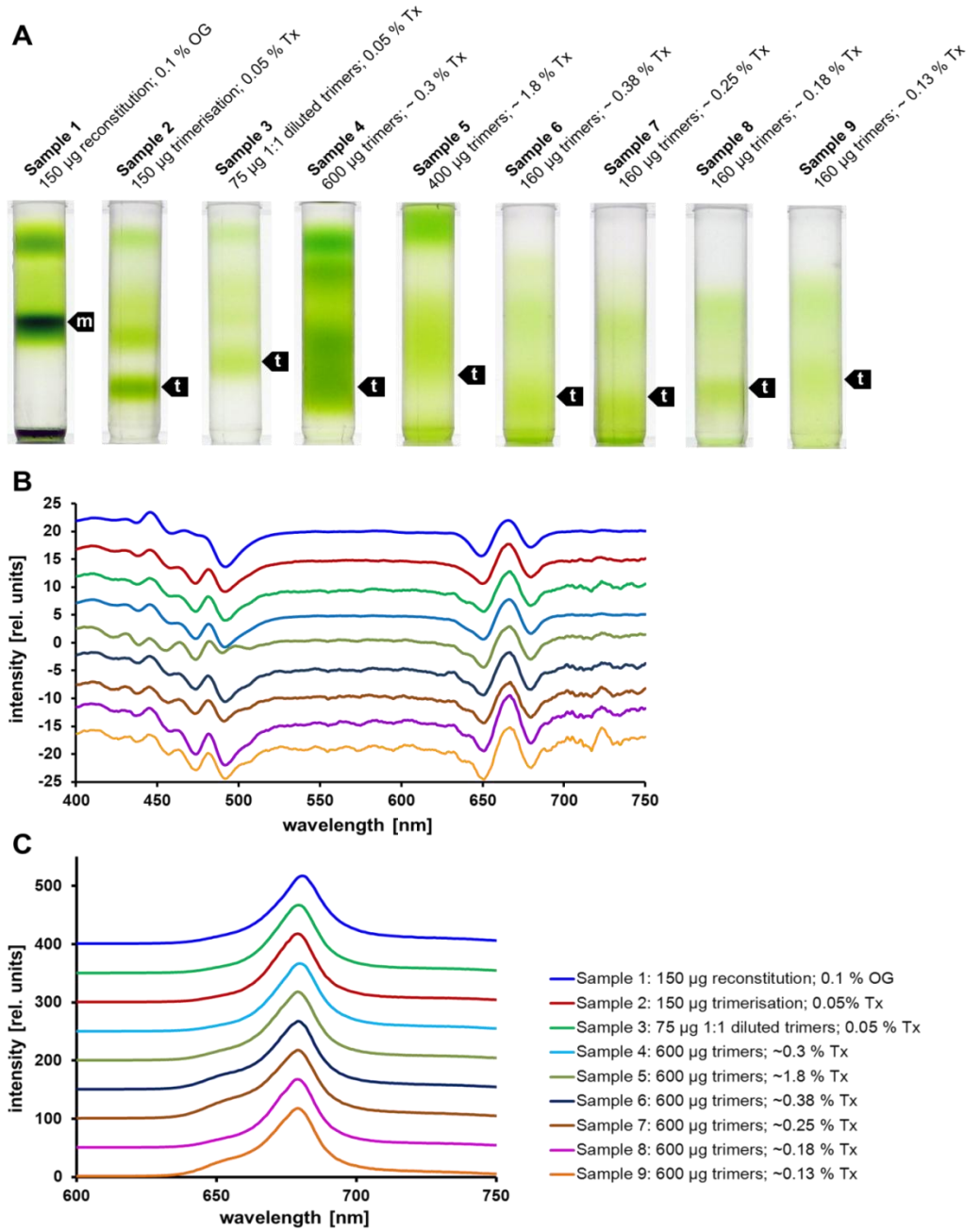

Figure 3.39: Preparation of trimers with various Tx amounts before the purification by ultracentrifugation. 5 mg of the wildtype similar mutant C3.2h was reconstituted (sample 1) and most of it used for a trimerization with the Ni-column (sample 2). The Ni-column eluate was diluted step by step (sample 3-5) and concentrated with elution buffer to reach different amounts of Tx. In the end 1 g Bio-Beads were added to four fractions (each consists of 0.74 % Tx in 2.5 ml solution) and incubated for 30, 60, 90 and 120 min. (sample 6-9) until they were purified by ultracentrifugation. A: ultracentrifugation gradients (m: monomers; t: trimers); B: CD-spectra (staggered presentation); C: fluorescence emission spectra (staggered presentation).

In order to find a solution for the time and material consuming production of heterogeneous trimers two different column materials were compared: Strep-Tactin Sepharose and a very new product called Strep-Tactin Macroprep. Both of them consist of the same binding site, a mutated streptavidin (Strep-Tactin) but differ in their basic material. Sepharose is a cross-linked agarose with a rough surface; Macroprep is a synthetic polymethacrylate that should be less prone to interact with pigments. For comparison purposes, firstly different loading steps (gravimetrically vs. batch) of both materials were analyzed, secondly heterogeneous trimers as well as a homogeneous negative control were compared, thirdly the exact yield of heterogeneous trimers quantified by using a Dy731 labeled double tag mutant. For all experiments each step was meticulously documented, i.e.: the volumes of all steps were analyzed, the concentration quantified photometrical after purification by ultracentrifugation, and in relation to the volume the yield identified.

The first experiment a his_6 tag mutant (C79Sh) and a double tag mutant that consisted of an additional strep tag were reconstituted in a ratio of 8:1 and both solutions were mixed (Figure 3.40). Because of the different reconstitution yield (C79Sh = 95 % and K7C/S34Csth = 44 %) the ratio changed from 8:1 to 17:1. In total, about 20 mg of monomers were loaded on a Ni-column to initiate trimerization. The identified yield of trimers was very low: only 2.1 mg trimers could be detected. However, these trimers were absolutely clean ultracentrifugation-purified trimers and the 500 µl aliquot that was stored 4 h on ice for the subsequent purification and quantification contained imidazole, which might support the decay of some trimers during this time. Theoretical the Ni-column eluate should contain four kinds of trimers: homogeneous trimers without a strep tag II (84.2 %), heterogeneous trimers that consisted of one strep tag monomer (14.9 %), those that consisted of two (0.9 %) and homogeneous trimers that consisted of three strep tag II monomers (0.01 %). The listed probabilities based on a unlabeled monomer to labeled monomer ratio of 17:1. This mixture was then divided into four equal portions. Two portions were loaded directly onto 500 µl Sepharose- and Macroprep-Streptactin and two were firstly batched with 500 µl Streptactin material and secondly the material was filled in an empty column. For the Tx washing steps and the elution the optimized buffers (containing an additional 10 % glycerol) were used. Due to the low column volume and thus, the low buffer volumes no pigments were added.

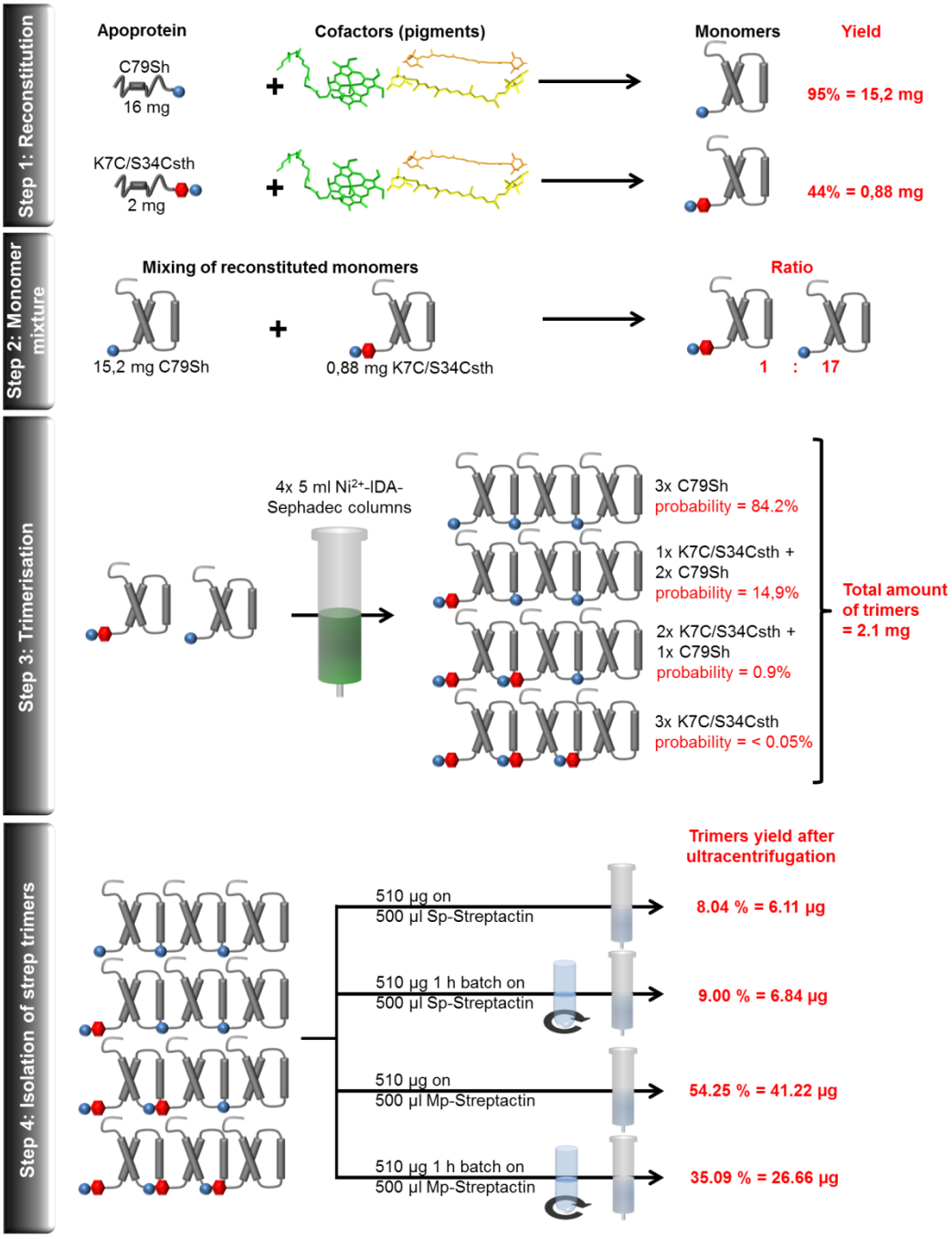

Figure 3.40: Schematic overview of the heterogeneous trimers production by using the Ni-column for trimerization and in direct comparison Sp-strep column vs. Mp-strep column material. The ratio of a single tag (C79Sh) and double tag (K7C/S34Csth) mutant was 8:1 (step 1). The different reconstitution yields of both mutants led to a diverging ratio of 17:1 (step 2). After trimerization (step 3) the Ni-column eluate was divided into four equal parts (step 4). Two were loaded onto a Sp-strep columns, the other two onto Mp-strep columns. The specified yields were calculated photometrical by using the purified samples after ultracentrifugation.

During this purification the large amount of homogeneous trimers without a strep tag should pass the column. Now, based on the probability most of heterogeneous trimers (94 %) should be those that consisted of one monomer with a strep tag II. After the ultracentrifugation a big difference between both column materials could be detected. While the Sepharose-Streptactin material led to very weak bands, the Macroprep material showed a clear trimeric band. Furthermore, the incubation on the column seemed to be better than the batch preparation and resulted in a recovery of 54.25 %. This indication could be confirmed during the biophysical and biochemical analysis. The CD-, fluorescence-emission spectrum as well as the low denatured gel electrophoresis showed trimeric typical results. At this point it was unclear whether these trimers were heterogeneous ones.

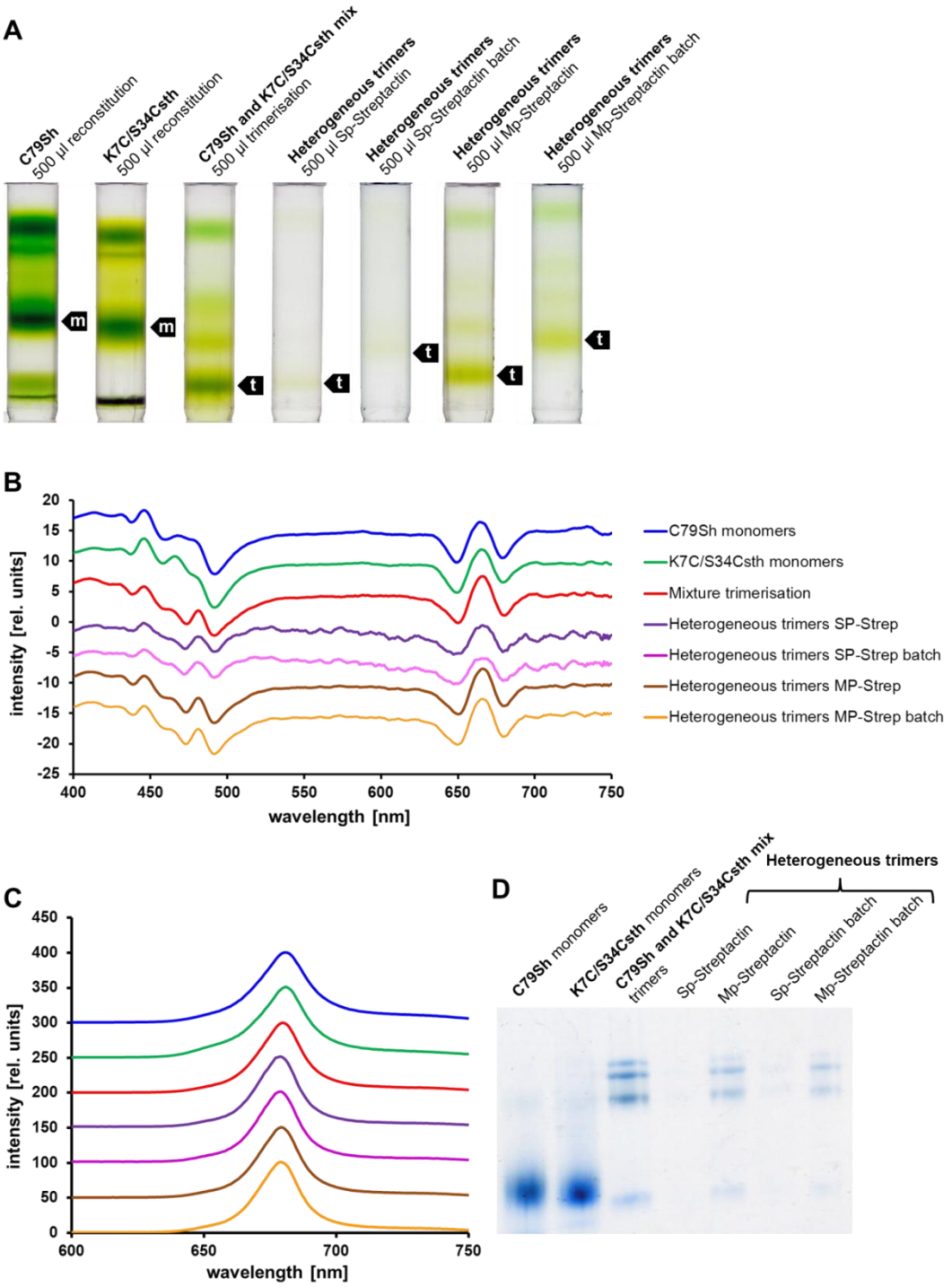

Figure 3.41: Results of the heterogeneous trimers production by using the Ni-column for trimerization and in direct comparison Sp-strep column vs. Mp-strep column material. A: ultracentrifugation gradients (m: monomers; t: trimers); B: CD-spectra (staggered presentation); C: Fluorescence emission spectra (staggered presentation); D: Coomassie stained low denatured 10% glycerol gel.

To exclude the possibility that an unspecific binding caused these results a similar experiment with a negative control was done, but only the Macroprep material was used. 8 mg of the his_6 tag mutant C79Sh and 1 mg of the double tag mutant K7C/S34Csth were reconstituted. The reconstitution yield was 69 % (5.51 mg) for C79Sh and 38 % (0.38 mg) for K7C/S34Csth. Immediately prior to the trimerization; the reconstitution solution of C79Sh was split into 2.5 mg for the negative control and 3 mg for the production of heterogeneous trimers. Thus, the monomer ratio of C79Sh to K7C/S34Csth was 8:1. After trimerization on the Ni-column the yield of the negative control was 25 % (631 µg) and of the heterogeneous mixture 23 % (777 µg) absolutely clean trimers. Both solutions were loaded onto two different 500 µl Macroprep-Streptactin columns, washed with Tx-buffer, and eluted with elution buffer. The volumes of all steps had been measured. The calculation of the yield was performed photometrical and the results set in relation to the volume after purification by ultracentrifugation. In relation to negative control (C79Sh homogeneous trimers) 70 % of the loaded trimers could be found in the loading step solution, 6 % in the Tx washing step, and 1 % in the elution fraction. 23 % trimers were missing and might be destroyed during the Strep- column process. In relation to the heterogeneous trimers (C79Sh and K7C/S34Csth in a ratio of 8:1) 41 % of the loaded trimers could be found in the loading step solution, 5 % in the Tx washing step, and 8 % in the elution fraction. Based on the probability by a ratio of 8:1 the heterogeneous trimers mixture should consist of 70.3 % homogeneous C79Sh trimers, 26.3 % trimers with one, 3.3 % with two and 0.1 % with three double tag monomers. The results would, in the best case, lead to a recovery of 29.7 % of the loaded trimers. Based on these calculations 29 % of the maximum possible yield could be recovered.

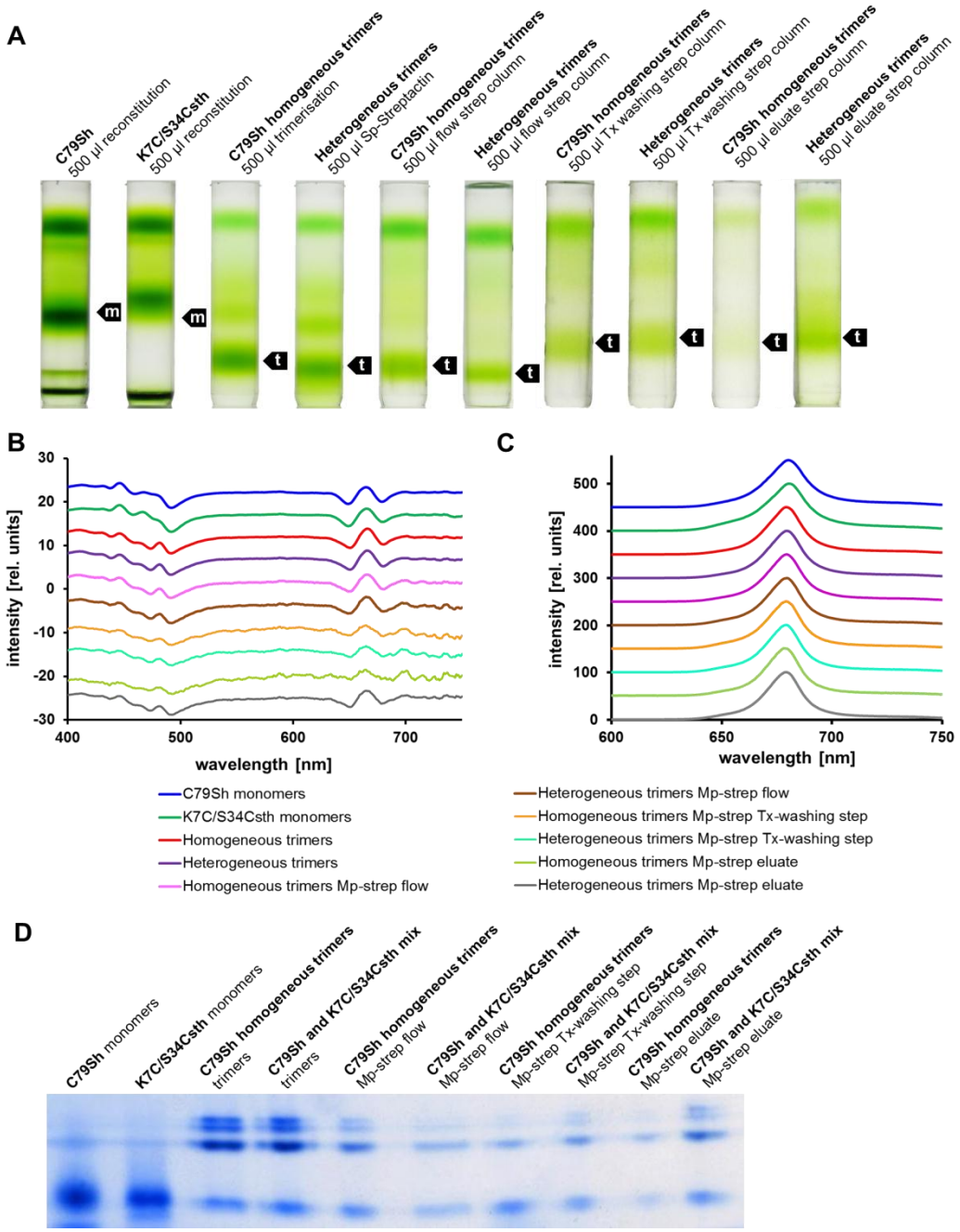

Figure 3.42: Specificity of the Mp-strep binding site to refolded strep tagged and strep less LHCII trimers. A: Ultracentrifugation gradients (m: monomers; t: trimers); B: CD-spectra (staggered presentation); C: Fluorescence emission spectra (staggered presentation); D: Coomassie-stained low denatured 10 % gel. After reconstitution two kinds of trimers were formed: homogeneous trimers consisting of three monomers carrying a his_6 tag and heterogeneous trimers whereas one of three monomers carries a his_6 and a strep tag II. By contrast to the heterogeneous trimers most of the homogeneous trimers could not bind to the strep column and led to a weak trimeric band in the gradient.

Finally 4 mg of an unlabeled (C79Sh) and 1 mg of a Dy731 labeled (S3Csth) mutant was reconstituted and both loaded on a low denaturing 10 % gel to identify the reconstitution yield. This should help to ensure that the aspired ratio (1:8) depended on the reconstituted monomers and not on the apoprotein. The reconstitution yield of the unlabeled C79Sh mutant was 84 % and of the Dy731 labeled S3Csth 44 %. After that both solutions were mixed, trimerized and loaded onto a 500 µl Mp-Strep column. In order to clarify the ratio of labeled and unlabeled protein in each fraction, a defined volume was loaded on a denatured 15 % gel and analyzed densitometrically. The reconstitution and trimerization yield as well as the total amount of monomers and trimers in each fraction was determined photometrical after purification by ultracentrifugation. All samples were analyzed by CD spectroscopy and fluorescence emission spectroscopy and were normal (data not shown).

Based on the isolated and purified trimers a trimerization yield of 20.44 % could be identified. 13 % of the Ni-column eluate could be identified as Dy731 labeled protein (Figure 3.43 B). This fits very well with the expected theoretical probability. The Ni-column eluate, consisting of 740 µg trimers, was halved and then loaded onto two 500 µl Mp-Strep columns. At the first column 32 % (118 µg) of the trimers and at the second 34 % (127 µg) could be detected in the flow. The amount of labeled protein in these fractions of column 1 and 2 was 6 % (column 1 shown in Figure 3.43 B). The first column was washed with four and the second with two column volumes of Tx buffer to find out whether four column volumes were really necessary. In the washing fraction of the first column 9 % (34 µg) and of the second one 5 % (19 µg) trimers could be determined. The amount of labeled protein was 6 % for column 1(Figure 3.43 B) and 10 % for column 2 (data not shown). Based on the probability by a mixing ratio of 1:8, round about 30 % (111 µg) of the loaded trimeric solution consists of single, double or threefold labeled monomers that should bind to the strep column. At the first column 56 % (62 µg) and at the second 65 % (72 µg) of these theoretical possible heterogeneous trimers could be regained. In both strep column eluates the amount of labeled protein was 28 %. Furthermore the number of labeled protein in the purified trimers was 29 %. This fits very well with the expected value of 33 %.

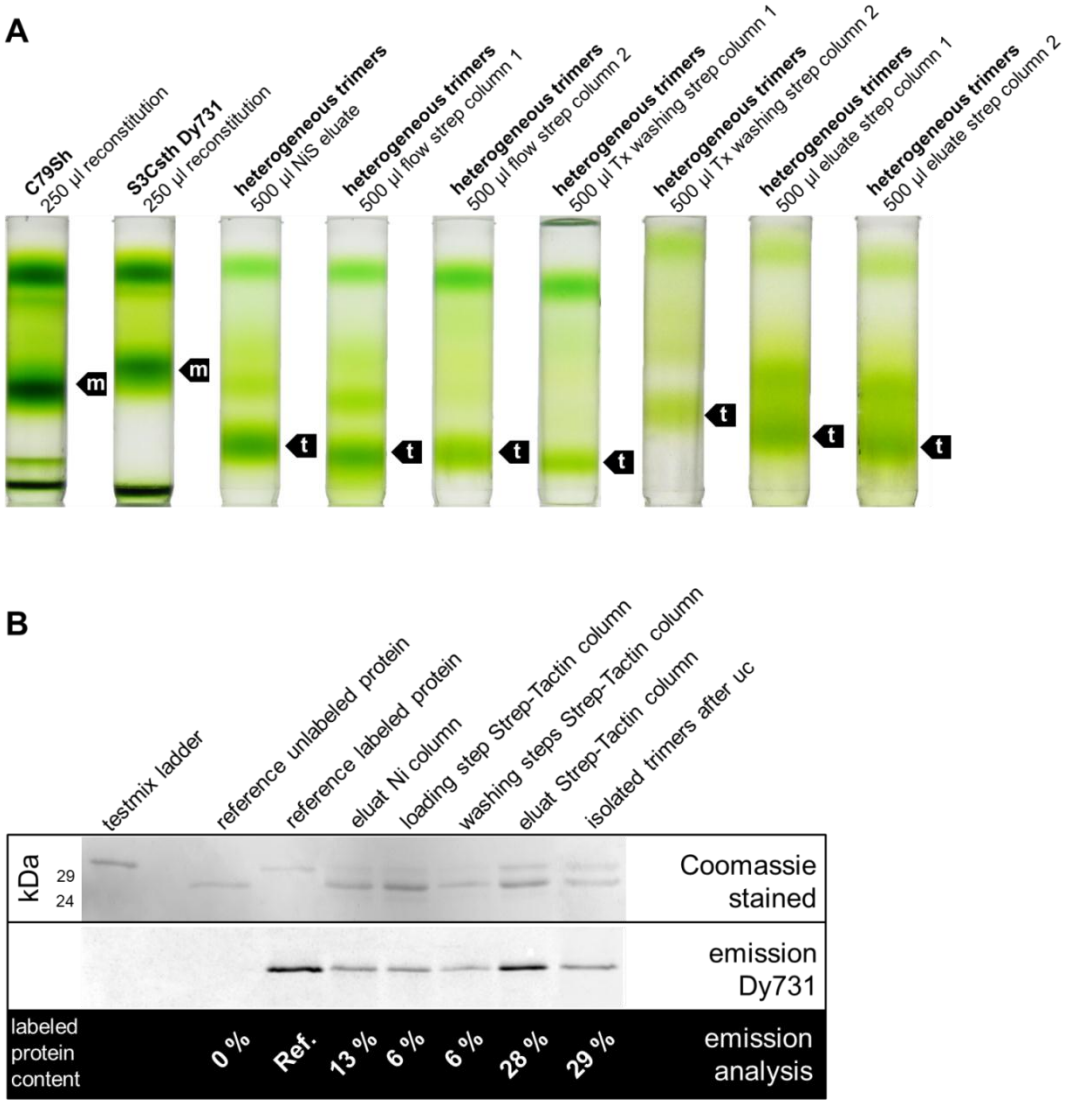

Figure 3.43: Heterogeneous trimers that were prepared with an unlabeled single-tag and a Dy731 labeled double-tag mutant. A: Ultracentrifugation gradients (m: monomers; t: trimers); B: 15 % denaturing SDS-solubilized glycerol gel (uc: ultracentrifugation). The upper band in the Coomassie stained gel is the Dy731 labeled protein, the lower band the unlabeled. The calculation of the total protein amount was taken into consideration of the applied and total volume. The labeled protein content was calculated by using a reference with a defined protein concentration. The percentage value describes the amount of labeled protein in relation to the total protein value.

The last problem that was to be solved is the regeneration of the column material. It was necessary to find an alternative way without ethanol. By contrast to the Sp-Strep material the content of remained pigments after the elution step is lower at the Mp-Strep material (Figure 3.44). Nevertheless, the Mp-strep material is also colored green after the elution step. To get rid of these pigments recombinant chlorophyllase was expressed, purified,

tested, and then incubated with the column material to cut off the phytol chain of the pigments. It took one week until the pigments had been spliced and could be washed out with water and 0.1 % SDS solution. However, an alternative and faster way without chlorophyllase would be better. If some amount of this enzyme remains on the column, it will lead to fatal consequences by the next preparation of heterogeneous trimers. Further experiments could show that an incubation of the column material in elution buffer and then in 1 % TX solution (both overnight in an incubator shaker at 4°C) could dissolve these pigments and their aggregates. The white cleaned Mp-strep material was then regenerated. Now the binding of HABA (column changes its color to red) could be detected very well.

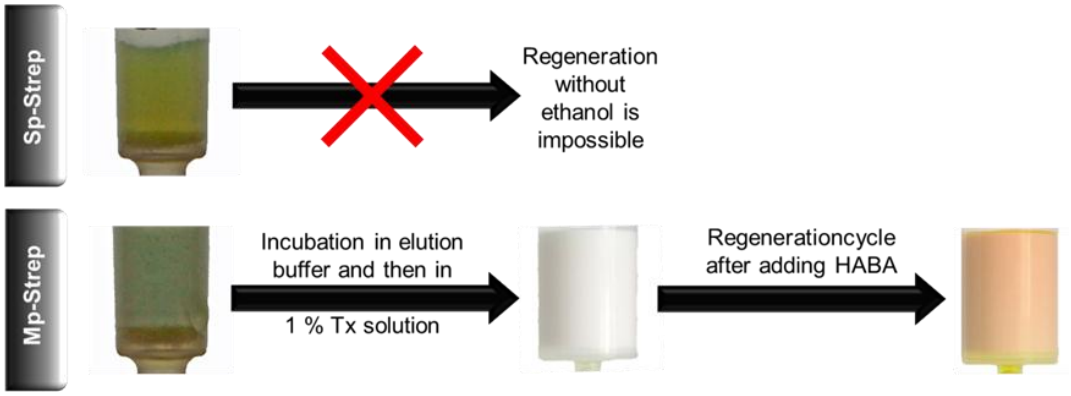

Figure 3.44: Streptactin column material after elution of the heterogeneous trimers and its regeneration. A clean column material is necessary to identify the binding of HABA (color changes to red) during the regeneration cycle because this color change is an indication for an active binding site.

3.5. Insertion of the recombinant LHCII into liposomes

In 2005 the best-known X-ray structure of the LHCII could be resolved at 2.5 A (Standfuss *et al*., 2005). Further structural information of the detergent-solved LHCII in a liquid system could be monitored by EPR spectroscopy (Dockter *et al*., 2011). Both methods revealed similar results. The hydrophobic core seems to be very rigid; by contrast the N- and C-terminal domain as well as loop regions seem to be more flexible. But both kind of analysis might not show the real *in vivo* situation because neither crystals nor detergent micelles are really close to the *in vivo* situation (Figure 3.45).

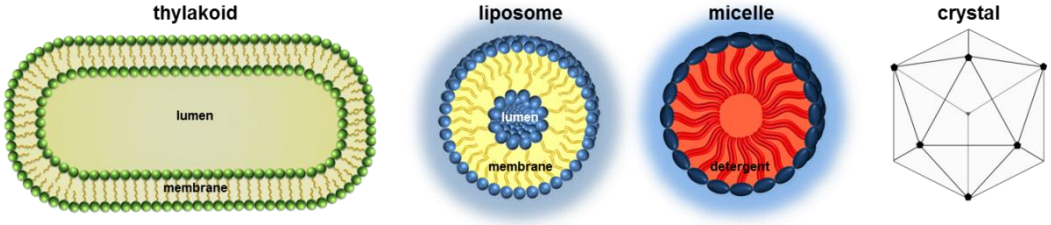

Figure 3.45: *In vivo* environment of the LHCII in comparison to different *in vitro* solutions for biochemical or structral analysis (graphics are not true to scale).

For micking the *in vivo* situation, liposomes are very useful because they shape spherical vesicles composed of a lipid bilayer and their lipid composition can be varied. In addition with EPR spectroscopy that works in a liquid system, this would be a powerful combination to uncover further information, and thus, structural changes under different conditions, for example regulation processes, would be observable. However, such experiments require a directed insertion of the LHCII into liposomes, firstly, to measure spin-spin distances of each labeled LHCII molecule in the same orientation, and secondly, to be sure that simulated *in vivo* situations (for example a different pH value inside and outside the membrane) effect in the same way to each labeled LHCII molecule.

During the last years a lot of experiments were done to reach a unidirectional insertion of the LHCII into liposomes. Common problems seemed to be the similar hydrophobicity of both terminal domains as well as a low protein concentration in liposomes. To increase the hydrophilicity of the N-terminal domain, a large hydrophilic protein (green fluorescent protein) was attached to the N-terminal domain but nevertheless, this did not work (Boggasch, 2006). By contrast if the membrane protein is attached to a modified two-dimensional surface, a directed insertion might work but would never reach an adequate protein concentration for EPR measurements. Thus, in this work another way was tested

to enable a directed insertion. The recombinant LHCII has a his_6 tag which binds reversible to Ni^{2+}-modified surfaces. To increase the protein concentration instead of a two- a three-dimensional surface was chosen (Figure 3.46). Such a three-dimensional surface might be Ni-IDA Sepharose column material (Ni-column) because it is well known that the recombinant his_6 tagged LHCII binds reversible to this column and such an immobilization might be usable to support a directed insertion. Therefore, on the basis of the Cys-free mutant C79S two kinds of LHCII mutants were prepared (2.6): One with a his_6 tag at the N-terminal domain (hNC79S) and one with a his_6 tag at the C-terminal domain (C79Sh). The insertion method based on different steps. In a first step the apoprotein was refolded by using the detergent-exchange method. In a second step the refolded protein was immobilized on a Ni-column, washed with liposome buffer, incubated with liposomes, and at last eluted by using imidazole. After this procedure the previously immobilized domain should be pointed outwards (Figure 3.47).

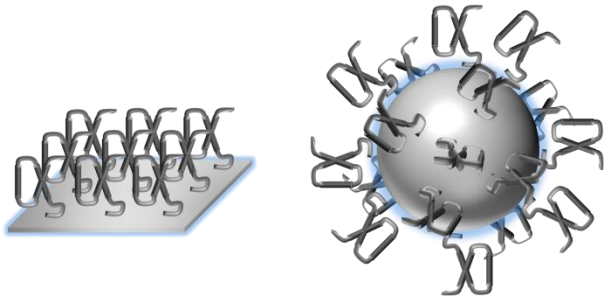

Figure 3.46: Comparison of the surface-bound LHCII on a two-dimensional (left) vs. three-dimensional surface. On a three-dimensional surface the amount of immobilized protein and the access to the protein is much higher.

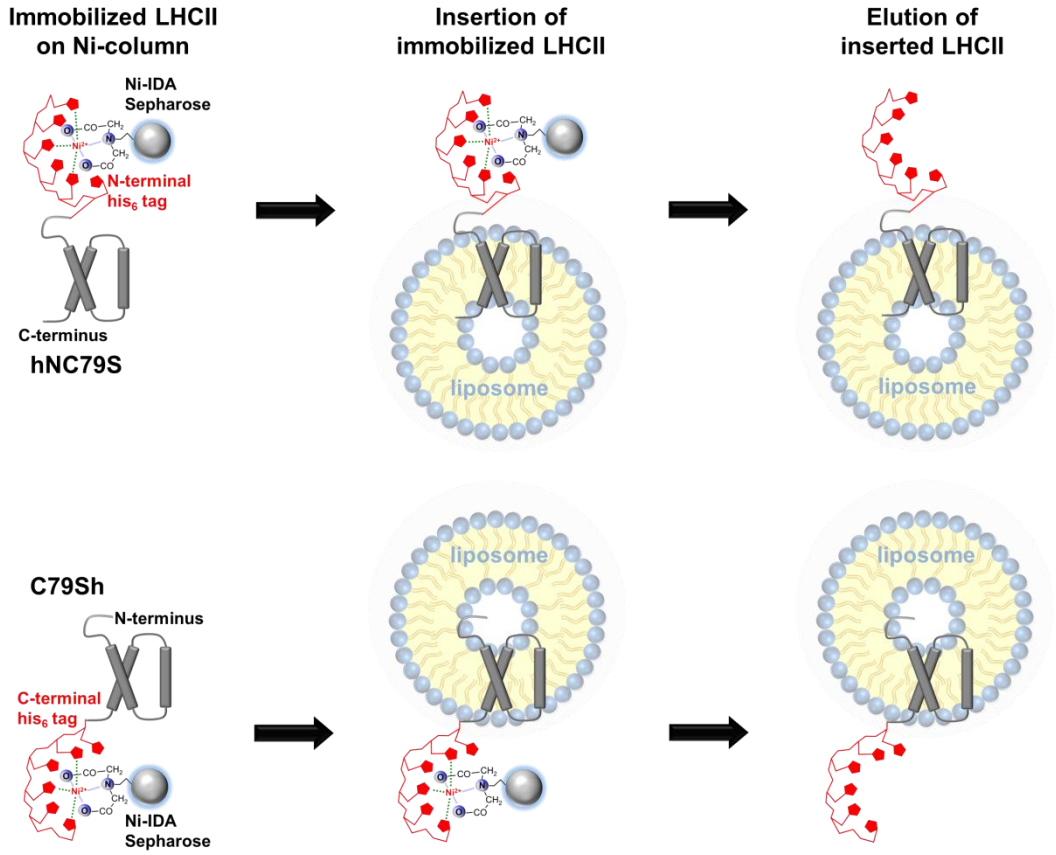

Figure 3.47: Principle of the directed insertion based on the surface immobilized protein. The his_6 tag of the protein interacts with the Ni-loaded IDA Sepharose and fixes the protein. After the detergent micelles have been replaced by liposomes the protein is eluted. The location of the his_6 tag (hNC79S: N-terminal; C79Sh: C-terminal) defines the insertion direction.

The orientations of the inserted proteins were checked by a digestion with the protease trypsin. Trypsin is a serine protease produced in the pancreas of many vertebrates with a molecular weight of 23.6 kDa. It cleaves peptide chains at the carboxyl side of the amino acids lysine or arginine and it will digest the unfolded LHCP totally. But trypsin is a hydrophilic protein that cannot pass a lipid bilayer membrane. Therefore, the refolded LHCII in liposomes will be attacked at its N-terminal domain, leading to a 1-2 kDa smaller product. The C-terminal domain does not contain any lysine or arginine and will not be digested. Thus, trypsin should not be able to digest the inserted hNC79S mutant but by contrast the C79Sh mutant, provided that the principle of a directed-insertion works (Figure 3.48).

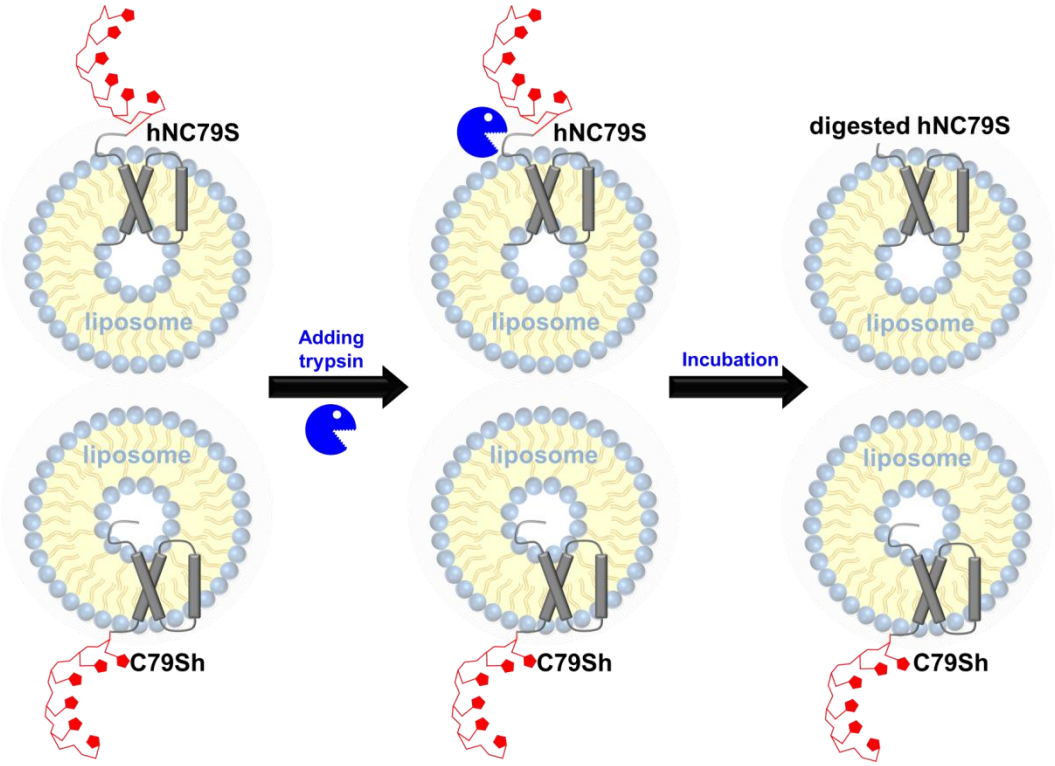

Figure 3.48: Principle of trypsin digestion to check the direction of insertion. The protease trypsin cleaves the N-terminal domain but cannot pass a lipid-bilayer and thus, the N-terminal domain should not be digested if it is pointed to the lumen of the liposome.

The mutants C79Sh and hNC79S were reconstituted and immobilized on a Ni-column. Unbound pigments were removed by two washing steps with OG- and Tx-buffer. After that the detergent of the washing steps had been removed, because a high contamination of detergent in liposomes might lead to a passage of the protease over the membrane, and thus, the insertion check by digestion would not work. Therefore, a row of liposome samples with reduced concentrations of detergent (0.1 %, 0.08 %, 0.06 %, 0.04 %) were used to clean the attached proteins step by step. The lipid to protein ration (LPR) was 300:1. The elution was performed with a mixture of 0.02 % detergent, PG liposomes, and 300 mmol/l imidazole. The eluate was measured by circular dichroism spectroscopy and showed a typical spectrum of LHCII monomers. In this experiment the orientations of both mutants were checked by a digestion with trypsin in different concentrations (0.1, 0.05, 0.005 and 0.001 mg/ml) for 30 minutes on ice, thermolysin was not used. The digestion was stopped by adding ¼ volume of SDS denaturing mix and boiling for 2 minutes. All samples were loaded on a 15 % denaturing SDS gel.

The first results proposed that the directed insertion was successful (Figure 3.49, left gel). Both undigested mutants as well as the digested C79Sh mutant were at the same gel level. By contrast, the band of the digested hNC79S mutant was at a lower level, which might be a result of a trypsin access to its N-terminal domain. Nevertheless it remarkable that all bands were at a higher level than suggested because the denatured LHCII has a molecular weight of 26 kDa.

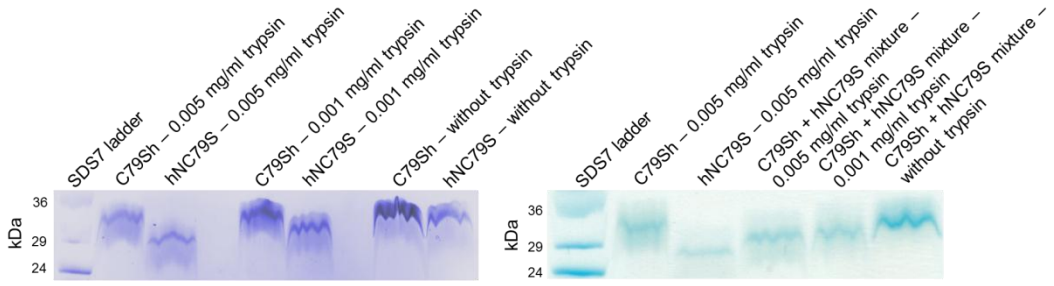

Figure 3.49: SDS-PAGE of trypsin digested LHCII samples after insertion into PG liposomes by using a combination of Ni-column and washing steps to replace the detergent.

To verify these results the digested samples of C79Sh and hNC79S were mixed and loaded on a new 15 % denaturing SDS gel (Figure 3.49, right gel). It became evident once again that the bands of the digested samples C79Sh and hNC79S led to different gel levels. A successful insertion and thus, a different digestion of both mutants, should lead to two different bands after mixing these solutions in a ratio of 1:1. However, instead of the expected two bands the mixture showed one band at 29 kDa.

These contradictory results of the denatured gels might be caused by incompletely destroyed liposomes. Thus, the amount of SDS was increased from 1 % to 2 % to be sure that all liposomes were diluted completely. A further 15 % gel (data not shown) showed much more clear bands at the same gel level, indicating that the directed insertion did not work at all.

To exclude any artefacts during gel-electrophoresis analysis the amount of SDS was increased. Two kinds of insertions were compared. The first method based on an accidental insertion. In this procedure detergent-solved monomers were mixed with PG liposomes and the monomers were transferred into liposomes by adding Bio-Beads to remove the detergent. The second procedure for an insertion was done in the same way as before (immobilization on Ni-column). For both insertions the mutants C79Sh and hNC79S were used. The trypsin digestion was performed in two different concentrations and the reaction was stopped by adding ½ volume of SDS denaturing mix and boiling for 2 minutes.

The results showed (Figure 3.50) much better and clear bands in the gel caused by the higher amount of SDS. According to the accidental insertion (B.B.: Bio-Beads) approximately 30 % of the protein was digested by trypsin, indicating an accidental insertion as expected. However, the protein that was inserted by using the Ni-column (d.i.) was also digested to approximately 90 %. The digested product of the mutant hNC79S showed bands at a lower gel level than the mutant C79Sh. This is caused by the N-terminal his_6 tag which is within the range of digestion. By contrast the digestion with 0.001 mg/ml trypsin showed a lower amount of digested protein independently from the insertion method. It seemed that a directed insertion of the LHCII into liposomes by using the Ni-column did not work, but possible causes were many and diverse. Besides the digestion, the CD spectrum after insertion raised questions. Principally a trimeric spectrum instead of a monomeric one was expected. Usually the physical proximity of immobilized monomers on the Ni-column leads to a trimerization and the lipid PG affects as a molecular clue. Thus, it is curious that an insertion with the Ni-column by using PG liposomes did not lead to trimers. In this experiment the LPR was 300:1. This might be too low. Perhaps the liposomes isolated all the monomers and they had no chance to come close enough together. Another reason might be the temperature during the insertion. PG consists of a C16 fatty-acid, thus, the phase-transition temperature should be below 0°C but is never known exactly. Perhaps it works better at a higher temperature.

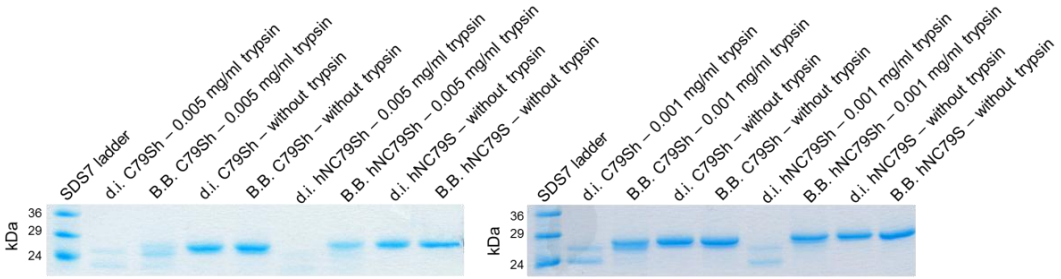

Figure 3.50: SDS-PAGE of trypsin digested LHCII samples after insertion into PG liposomes by using a combination of Ni-column and washing steps to replace the detergent.

To check these purposes further tests were performed. Two different LPRs (80:1 and 300:1) were compared as well as different incubation temperatures (4°C and 20°C). The insertion was done by using liposomes in combination with the N-column and by using liposomes in combination with Bio-Beads. The results looked very similar to those before, with one exception. The CD spectrum of the LHCII that had been inserted at 20°C by using the Ni-column showed a trimeric typical spectrum (Figure 3.51). This spectrum differed from those that were measured in detergent micelles but was similar to those that could be monitored in liposomes (Yang *et al.*, 2006). According to the digestion no differences could be detected. Neither the LPR nor the temperature had any effect to the insertion. Half of the detergent-solved LHCII, which was transferred into liposomes by using Bio-Beads to remove the detergent, was digested. This is an indication for accidental insertion as expected. Nearly 90 % of the samples that had been inserted by using the Ni-column were digested by trypsin as seen in the experiment before. This high amount of digested protein in several independent experiments could not be accidently and raised two suspicions: Neither the liposomes were still contaminated by detergent, which facilitated the invasion of the protease into liposomes, nor the PG formed lipid sheets instead of enclosed liposomes (Figure 3.52). It should be noted that the used PG lipid is a chemical product and that PG liposomes differs a lot from the lipid composition in the thylakoid membrane. Nevertheless, it was chosen because detergent-solubilized LHCII monomers in combination with a detergent removal by Bio-Beads insert PG liposomes very well and form trimers. However, this liposome composition might not be carried over to a protein insertion by using a three dimensional surface. Therefore, further experiments contained a series of changes. The lipid composition, the production of liposomes, the removal of

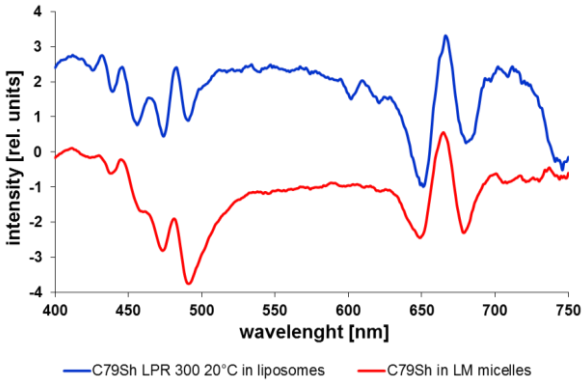

Figure 3.51: CD spectra of LHCII trimers in micelles in comparison to LHCII trimers in PG liposomes.

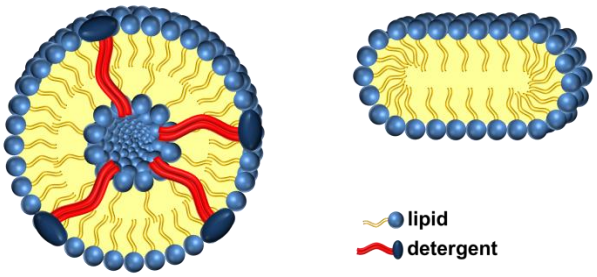

Figure 3.52: Spheric liposomes contaminated by detergent (left) and non-pheric sheets of liposomes (right).

detergent, and the kind of protein structure during insertion were varied step by step. For detailed information, refer to the corresponding diploma thesis of H. Berger (2009).

The thylakoid membrane in plant cells consists of 50 % monogalactosyldiacylglyceride (MGDG), 30 % digalactosyldiacylglyceride (DGDG), and 5-12 % sulfoquinovosyldiacyl-glyceride (SQDG) as well as 5-12 % phosphatidylglyceride (PG) (Murata and Siegenthaler, 1998). Thus, further productions of liposomes were performed by using the plant-extracted lipids DGDG, SQDG, and PG in a ratio of 61.9 : 16.7 : 21.4 (w/w). MGDG is a non-bilayer forming lipid and thus, was not used. To ensure that all liposomes had the same size they were extruded to a size of 100 nm.

Reconstituted and detergent-solubilized monomers of the mutants C79Sh and hNC79S were immobilized on the Ni-column. The detergent was removed in several washing steps with the liposome mixture. The elution was performed by using a liposome solution that contained imidazole. Not all of the samples could be eluted from the column material. A green band remained in the upper part which might be an indication for aggregates. This band had to be eluted with detergent. The measured CD spectra of both mutants that were eluted with liposome solution showed a typical spectrum for trimers in liposomes (Figure 3.53). The eluted green band (contained liposome-detergent mixture) led to a similar CD spectrum.

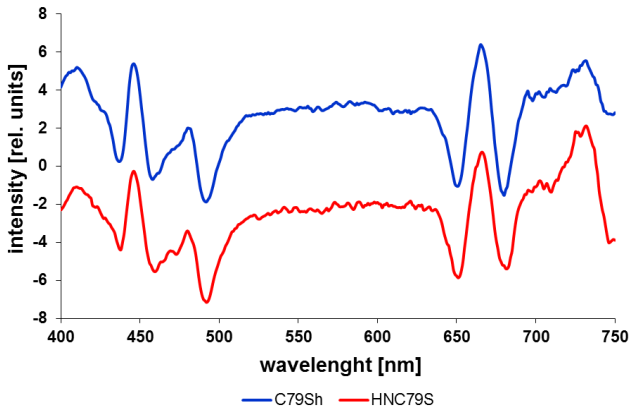

Figure 3.53: CD spectra of LHCII samples inserted into DGDG-SQDG-PG liposomes.

In the following trypsin digestion nearly all of both samples were digested by trypsin (Figure 3.54). Thus, the varied composition of the liposomes turned out to be unsuccessful.

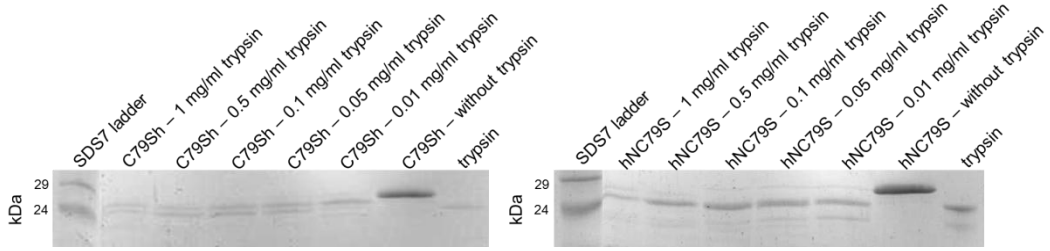

Figure 3.54: SDS-PAGE of trypsin-digested LHCII samples after insertion into DGDG-SQDG-PG liposomes by using a combination of Ni-column and washing steps to replace the detergent.

In order to answer the question whether the liposomes were contaminated by detergent, Bio-Beads in a high concentration were added to the eluate of the Ni-column and at last the product was measured by CD. It is well known that such a fast removal of detergent would lead to a degradation of the LHCII if there are still detergent micelles in the mixture. If the LHCII is integrated in liposomes by contrast, the Bio-Beads would not have any effect to the LHCII structure. A comparison of the sample before and after Bio-Beads incubation by CD showed big differences. Instead of a typical trimeric spectrum noise was detected, indicating a complete degradation of the LHCII and thus, a contamination of detergent in the initial eluate. These results combined with the tendency of the LHCII to aggregate during the washing steps on the column, required to rethink the kind of detergent removal.

Another possibility to get rid of the detergent is dialysis. Therefore the reconstituted and detergent-solubilized monomers were immobilized on the Ni-column material. Instead of washing steps the column material was transferred into dialysis tubes with liposome solution. Bio-Beads were used to remove the detergent slowly. After this procedure the LHCII was eluted, analyzed, and a trypsin digestion was started. This time the whole sample could be eluted and the CD spectra were typical for liposome-solubilized trimers. But the trypsin digestion led one more time to a totally digestion of both inserted mutants. It seemed that not all of the detergent could be removed by dialysis. This suspicion could be supported by adding Bio-Beads, which resulted in a loss of the CD signal. Furthermore, the digestion was not only limited to the N-terminal domain, it seems that some part of the protein was totally cleaved by trypsin. This happens when the protein is unfolded and not inserted in liposomes or detergent micelles. One possible explanation could be a loss of pigments and therefore, a decay of the protein.

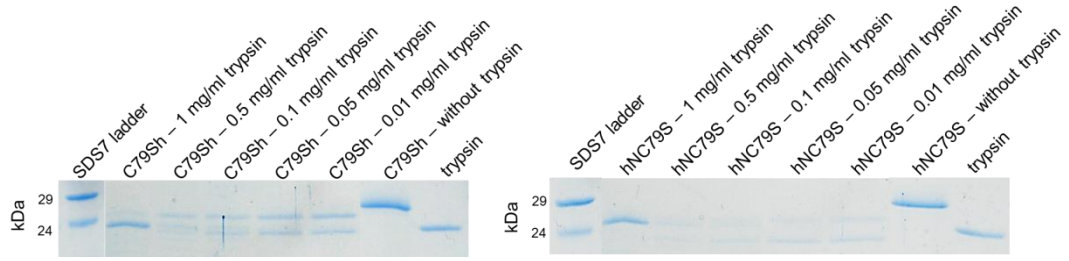

Figure 3.55: SDS-PAGE of trypsin-digested LHCII samples after insertion into DGDG-SQDG-PG liposomes by using a combination of Ni-column and dialysis to replace the detergent.

To verify these notions pigment-loaded liposomes were prepared and the further experiment was repeated. However, the results were identical to the previous.

Overall it seems that all directed-insertion experiments had something common. The LHCII was digested totally caused by an incompletely removal of detergent. The control samples by contrast which were prepared with liposomes and Bio-Beads showed an expected digestion. Half of the protein was digested caused by a non-directed insertion. Neither washing steps nor dialysis seems to be suitable to remove the detergent. Thus, it was tried to combine both methods. In a further experiment the refolded LHCII was immobilized on the Ni-column material. Then the column material was dissolved in a solution that contained pigments and detergent. The liposomes were added and the detergent was removed slowly by dialysis with the help of Bio-Beads. But this kind of insertion method led to aggregates. Therefore, it is unclear whether the partly digestion of the protein was caused by these aggregates or by a better insertion. But either way, there was still an amount of digested protein and thus, it could be concluded that the LHCII was non-directedly inserted.

3.6. EPR analysis of the rigid core, flexible terminus, and lumenal loop of the LHCII

The LHCII is an excellent model to get more information about membrane protein function. In this work Electron Paramagnetic Resonance (EPR) was used to get more information about the dynamic and interaction of the LHCII under functional conditions (1.2.5). For this purpose several amino acids were replaced by cysteine, the functionality of these mutants checked, free sulfhydryl groups spin labeled, mutants refolded and measured by EPR.

In a first step rigid positions were measured and compared with the X-ray data (3.6.1). In a second step flexible domains, like the unresolved N-terminal domain, were analyzed in different assembly states to get a deeper view inside the LHCII structure (3.6.1 and 3.6.2). In a third step the lumenal loop of the LHCII was monitored at different conditions to get more information about this controversially discussed region (3.6.3).

3.6.1. Rigid core and flexible terminus

Rigid Core and Flexible Terminus

STRUCTURE OF SOLUBILIZED LIGHT-HARVESTING CHLOROPHYLL a/b COMPLEX (LHCII) MEASURED BY EPR[*][S]

Received for publication, October 6, 2011, and in revised form, November 24, 2011 Published, JBC Papers in Press, December 6, 2011, DOI 10.1074/jbc.M111.307728

Christoph Dockter[‡1,2], **André H. Müller**[‡1,2], **Carsten Dietz**[‡3], **Aleksei Volkov**[§4], **Yevhen Polyhach**[¶], **Gunnar Jeschke**[¶], **and Harald Paulsen**[‡5]

From the [‡]*Institut für Allgemeine Botanik der Johannes Gutenberg-Universität Mainz, 55099 Mainz, Germany, the* [§]*Max-Planck-Institut für Polymerforschung, 55021 Mainz, Germany, and the* [¶]*Laboratorium für Physikalische Chemie, Eidgenössische Technische Hochschule, 8093 Zürich, Switzerland*

Background: Structural changes of LHCII may be required for its roles beyond light harvesting.
Results: EPR distance mapping reveals a high flexibility of the N-proximal protein domain.
Conclusion: The N-terminal domain in LHCII adopts various conformations in an aqueous environment.
Significance: The flexibility of hydrophilic domains in LHCII is compatible with potential structural changes of the protein between its various functional states.

The structure of the major light-harvesting chlorophyll *a/b* complex (LHCII) was analyzed by pulsed EPR measurements and compared with the crystal structure. Site-specific spin labeling of the recombinant protein allowed the measurement of distance distributions over several intra- and intermolecular distances in monomeric and trimeric LHCII, yielding information on the protein structure and its local flexibility. A spin label rotamer library based on a molecular dynamics simulation was used to take the local mobility of spin labels into account. The core of LHCII in solution adopts a structure very similar or identical to the one seen in crystallized LHCII trimers with little motional freedom as indicated by narrow distance distributions along and between α helices. However, distances comprising the lumenal loop domain show broader distance distributions, indicating some mobility of this loop structure. Positions in the hydrophilic N-terminal domain, upstream of the first trans-membrane α helix, exhibit more and more mobility the closer they are to the N terminus. The nine amino acids at the very N terminus that have not been resolved in any of the crystal structure analyses give rise to very broad and possibly bimodal distance distributions, which may represent two families of preferred conformations.

The light-harvesting complex LHCII[6] largely increases the efficiency of the photosynthetic process in green plants by collecting light energy and conducting it to a photosynthetic reaction center where light-driven charge separation takes place. LHCII is accumulated at high amounts in plant chloroplast membranes, making it the most abundant membrane protein on earth (1). A total of 18 chromophores are noncovalently bound to the apoprotein and warrant absorption of solar radiation over much of the visible spectrum. These chromophores are eight chlorophyll (Chl) *a*, six Chl *b*, and four carotenoid molecules. The crystal structure of the functional, trimeric form of LHCII is known in atomic detail (2, 3). Each monomer possesses three transmembrane helices H1, H3, and H4 spanning the thylakoid membrane and creating a central scaffold where the chromophores are bound in their specific positions at a high density (Fig. 1*A*). Only a segment of the N-terminal domain remains elusive in the atomic structures (2, 3).

Besides its main light-harvesting function, LHCII is involved in several regulatory processes to optimize photosynthesis and to prevent photo-damage of the photosystems (PS) in changing light conditions. It is assumed by some but not by others that the switch from one functional state to another may require a conformational change of some domains of the apoprotein. Under high light conditions, LHCII is involved in the short term protection of the photosynthetic system, which is referred to as the energy-dependent component (*qE*) of nonphotochemical quenching or feedback de-excitation (4). Triggered by the acidification of the thylakoid lumen, the carotenoid violaxanthin is converted to zeaxanthin by a lumenal de-epoxidase, and the excess energy is dissipated as heat. The protonation of lumen-exposed acidic residues under low pH conditions has been suggested to trigger a conformational change of helix H3 and the lumenal loop domain, resulting in an active energy-trapping

* This work was supported in part by Deutsche Forschungsgemeinschaft Grants SFB 625, TP B10 (to G. J. and H. P.), and Pa 324/9-1 (to H. P.) and Swiss National Science Foundation Grant 200020-103550/1 (to G. J.).
[S] This article contains supplemental "Methods," Figs. S1–S5, and additional references.
[1] Both authors contributed equally to this work.
[2] Present address: Carlsberg Laboratory, Gamle Carlsberg Vej 10, DK-1799 Copenhagen V, Denmark.
[3] Supported by the Max Planck Graduate Center, Johannes Gutenberg-Universität Mainz.
[4] Present address: BASF SE, 67063 Ludwigshafen, Germany.
[5] To whom correspondence should be addressed: Institut für Allgemeine Botanik der Johannes Gutenberg-Universität Mainz, Müllerweg 6, 55099 Mainz, Germany. Tel.: 49-6131-3924633; Fax: 49-6131-3923787; E-mail: paulsen@uni-mainz.de.

[6] The abbreviations used are: LHCII, light-harvesting chlorophyll *a/b* complex; DEER, double electro-electron resonance; PROXYL, 3-(2-Iodoacetamido)-2,2,5,5-tetramethyl-1-pyrrolidinyloxy; Chl, chlorophyll; PS, photosystem; ESEEM, electron spin echo envelope modulation; PDB, Protein Data Bank; PG, phosphatidylglycerol.

site composed of xanthophyll cycle carotenoids and a Chl *a* dimer (2). According to another model of nonphotochemical quenching, LHCII interacts with the protein PsbS in the photosynthetic membrane at low lumen pH, which results in a conformational change of LHCII, an altered configuration of its pigments, and consequently, a switch to the dissipative state (5). Ruban et *al.* (6) postulated an alternative model for energy dissipation in LHCII. Based on the twist in the configuration of the LHCII-bound carotenoid neoxanthin, the structure of LHCII is changed into the dissipative state, and excess energy is transferred from Chl *a* to a lower energy carotenoid lutein.

To date, the structural basis of nonphotochemical quenching in LHCII is unclear and controversially discussed. Kühlbrandt and co-workers (3) proposed alternative models for quenching mechanisms without conformational changes of LHCII. First, the simple replacement of violaxanthin by zeaxanthin in the binding pocket of LHCII itself can cause an effective quenching of excess energy without any structural changes. Second, the interaction between LHCII and PsbS monomers creates a quenching unit of transiently bound pigments that then function as a channel for the safe dissipation of energy (7). Miloslavina *et al.* (8) proposed another model involving a Chl-Chl charge transfer state as a quenching unit. The prerequisite for their model is the formation of inter-trimer Chl-Chl pairs at the interface of LHCII oligomers. Recently, Avenson *et al.* (9) suggested a carotenoid radical cation model for energy dissipation. Minor LHCs, positioned between LHCII and PSII, provide the quenching sites by binding zeaxanthin. Electrons can be transferred from Chl to zeaxanthin, which then undergoes charge separation.

Besides this energy-dissipating function, LHCII is involved in the balanced distribution of excitation energy between the photosystems by dissociating from PSII and binding to PSI in high light conditions. This short term process is referred to as state transition and is regulated by phosphorylation of the N-terminal protein domain in LHCII by the thylakoid kinase STN7 (10–12). Different binding specificities of phosphorylated LHCII for both photosystems have been proposed, but the molecular basis of the redistribution of LHCII complexes between PSII and PSI remains unknown as yet (13). Among several hypotheses that have been put forward, a conformational switch of the N-terminal conformation has been discussed (14). A light-induced conformational change of the N-terminal region was shown by an increase of its accessibility to tryptic cleavage and was also suggested in connection with the phosphorylation process (15).

Yet another function of LHCII is the organization of chloroplast membranes in chloroplast grana stacks, which is thought to be mediated by interactions between N-terminal LHCII domains. The recently published cryoelectron tomography of thylakoid membranes supports a Velcro-like interaction of LHCII trimers in grana thylakoids (16) as it was suggested earlier (3). According to the model, grana stacks are held together by the electrostatic interaction between the positively charged N-terminal domains of one trimer with the negatively charged stromal surface of the opposite trimer. For such an interaction, some flexibility in the N-terminal domain, including the positive charge cluster, would be advantageous but was never confirmed experimentally. A flexible N terminus in LHCII has also been proposed to explain the low resolution in this segment of the LHCII crystal structure (16).

Structural information on proteins in solution, their flexibility, and their conformational changes can be gathered by various techniques of EPR in combination with site-directed spin labeling. The apoprotein of LHCII is recombinantly expressed in *Escherichia coli* (17) and therefore can easily be spin-labeled in specific positions (18). Adding pigments to the apoprotein in detergent solution induces the spontaneous assembly of monomeric (17, 19, 20) or trimeric LHCII (21). Double electron-electron resonance (DEER) spectroscopy allows the measurement of distances between two spin-labeled residues in the range of 2–8 nm (22, 23). This technique is especially useful for assessing structure dynamics. The distribution of protein conformations observed in a frozen sample represents the variety of conformations that are accessible to the protein at physiological temperatures (24–27). Distance mapping of individual protein domains in LHCII revealed a two-state structural behavior of the N-terminal domain in monomers and trimers (24). DEER recently provided insight into the refolding process of LHCII *in vitro* (20). Additional information about the accessibility of single residues in various domains of LHCII monomers was obtained by comparison of conventional continuous wave and pulsed EPR measurements (18).

In this study, we used DEER for a refined and extended distance mapping to obtain information about LHCII structure in solution, particularly the positioning and flexibility of the N-terminal domain. Spin-labeled versions of LHCII were refolded and purified in their monomeric or trimeric form, and distances were monitored between spin label pairs in the core region and the N-terminal domain of LHCII. Based on the EPR distance map, we compared the structure of LHCII in detergent solution with the structure predicted from crystal data (3), including a PROXYL rotamer library based on a molecular dynamics simulation (28).

EXPERIMENTAL PROCEDURES

Protein Preparation and Site-directed Spin Labeling—Proteins used in this study were C-terminally His_6-tagged derivatives of the Lhcb1*2 (AB80) gene from pea (*Pisum sativum*) (29) with its single Cys in position 79 replaced with Ser. In EPR measurements, different mutant versions were used, each containing either one or two Cys replacing Ser at positions 3, 11, 12, 14, 29, 34, 59, 106, 123, and 160; Ala at positions 4 and 10; Lys at position 7, or Val at positions 9, 22, 90, and 196. All derivatives have either been described in earlier studies (18, 20, 24) or were constructed by using the QuikChange mutagenesis kit (Stratagene). Bacterial expression of the derivatives (17) and labeling of the protein with PROXYL spin labels (3-(2-iodoacetamido)-PROXYL, Aldrich) were performed as described in the supplemental material.

Reconstitution of Spin-labeled LHCII with Pigments—Plant pigments for reconstitution of spin-labeled LHCII were extracted from pea thylakoids according to Ref. 17. All spin-labeled versions of LHCII were reconstituted in their monomeric form using the detergent-exchange procedure as

described previously (30), except that 10 mM β-mercaptoethanol was used as a reductant.

Singly labeled versions of LHCII were immobilized on nickel-chelating Sepharose via a C-terminal His_6 tag to prepare trimeric LHCII complexes (24), and doubly labeled LHCII samples were purified in their monomeric form. Purification of monomeric and trimeric LHCII was performed by ultracentrifugation on 0.1–1 M sucrose density gradients containing 0.1% (w/w) *n*-dodecyl-β-D-maltoside (Merck) and 5 mM Tris-HCl (pH 7.8) (Serva). After spinning for 16 h at 230,000 × *g* at 4 °C, the bands containing monomeric or trimeric LHCII were collected and concentrated in centrifugal filter units (30 kDa) (Millipore). LHCII samples exhibiting a protein concentration of about 600 μM were mixed at a 1:1 volume ratio with 80% glycerol as a cryoprotectant, loaded onto EPR tubes, and flash-frozen in liquid nitrogen. The quality of EPR samples was checked by fluorescence emission spectroscopy (31) and CD spectroscopy in the visible domain (21), as described in the supplemental material. High glycerol concentrations did not alter the functional structure of LHCII as shown previously (20).

EPR Spectroscopy—X-band (9 GHz) pulse EPR measurements were performed on a Bruker Elexsys E580 EPR spectrometer using a Bruker Flexline split-ring resonator ER 4118X_MS3 overcoupled to $Q \sim 100$. Sample temperature was kept constant at 50 K with liquid helium cooling using an Oxford CF935 cryostat with an Oxford ITC4 temperature controller.

The four-pulse DEER experiments were performed as described by Jeschke *et al.* (24) with an interpulse delay τ_2 between 2000 and 2500 ns depending on the transverse relaxation times, an optimum repetition time between 3 and 6 ms depending on saturation behavior, and a total measurement time of ~8 h. The quality of EPR samples was checked by electron spin echo measurements and T_2 relaxation measurements as described previously (18).

Three-pulse ESEEM measurements were performed as described by Volkov *et al.* (18), using a home-written Bruker Pulse SPEL program for accessibility measurements that is available on request. A sequence $(\pi/2) - \tau - (\pi/2) - T - (\pi/2) - \tau$-echo was used with fixed $\tau = 344$ ns, corresponding to a proton blind spot, and $\pi/2$ pulse lengths of 16 ns. The variable time T was incremented in steps of 8 ns starting at $T_0 = 80$ ns. ESEEM traces of 1024 points with a total length of 8.184 μs were acquired. To eliminate echo crossings, a $((+x,+x) - (-x,+x) - (+x,-x) + (-x,-x))$ phase cycle was applied to the final two $\pi/2$ pulses.

Data Analysis—DEER data were analyzed using the "DeerAnalysis" program (32), which is available on line. A background function was fitted to the data at dipolar evolution times $t > t_b$. Starting time t_b was determined automatically as described by Jeschke *et al.* (32). After background correction of the data by an exponential decay function, the distance distribution was determined by Tikhonov regularization with an optimum regularization parameter determined by the L curve criterion. Significance of features at long distances was checked with the validation tool in "DeerAnalysis." ESEEM data were analyzed as described in Volkov *et al.* (18) using a home-written Matlab program that is available on request.

Rotamer Library Simulations—Distance distributions were predicted from the crystal structure (PDB code 2BHW (3)) with rotamer library modeling of spin label conformations (28) as implemented in the software MMM, which is available on line. The DEER window in MMM was used to check to what extent three-spin effects (33) influence analysis in terms of distance distributions at the observed modulation depths. For the qualitative and semi-quantitative discussions in this work and at the reduced modulation depths compared with samples with 100% labeling efficiency, such an influence was found to be negligible. The DEER window in MMM was also used to test whether DEER data simulated from the crystal structure were in agreement with experimental data.

RESULTS

Distances between Positions Near the LHCII Core—The LHCII structure in detergent solution was analyzed by pulsed EPR distance measurements and compared with that in stacked two-dimensional crystals (3). EPR distances were defined by the nitroxide of PROXYL spin labels attached to engineered Cys residues in positions 59, 90, 106, 123, 160, or 196 as shown in Fig. 1, *B* and *C*. Except for positions 59 and 106, these labeling sites were located within the hydrophobic core of the complex (18) and thus inside the detergent micelle. The labeling sites were chosen in the periphery of the LHCII core, facing toward the LHCII surface to avoid steric clashes and structural perturbations. Spin labeling of unfolded apoproteins was optimized as described previously and found to be higher than 90% for mutants containing a singular Cys (supplemental Fig. S1). The actual labeling efficiency was somewhat smaller due to partial reduction of the labels under the conditions of LHCII reconstitution. A reduced spin labeling efficiency will only affect the intensity of the expected DEER signal but not give rise to false signals.

Spin-labeled apoproteins of LHCII were reconstituted with pigments according to the standard procedure (30), and the purified and concentrated complexes in their monomeric or trimeric form were compared with those reconstituted with the nonlabeled WT protein. Neither CD spectra in the visible range nor the intramolecular energy transfer from Chl *b* to Chl *a* showed any difference, demonstrating that spin labeling of the chosen sites did not affect the structure or function of LHCII (18, 20). When LHCII samples were thawed after EPR measurements, they gave fluorescence and CD spectra very similar to those obtained before the measurements (supplemental Figs. S2–S4), indicating that neither the addition of glycerol as cryoprotectant (40% (w/v) final concentration) nor the shock freezing step affected the functional structure of the pigment-protein complexes. A 1:1 mixture of two singly labeled monomers did not result in any appreciable DEER signal (supplemental Fig. S5) (20, 24) proving the notion that DEER signals originate from dipole-dipole interaction between electron spins within the same protein in doubly labeled complexes or between singly labeled monomers in trimeric samples but not from intermolecular spin-spin interactions due to aggregation of the complexes. However, one of the control samples (monomers labeled in position 59, supplemental Fig. S5*B*) exhibited a minor but significant DEER signal with a modulation depth of 0.17,

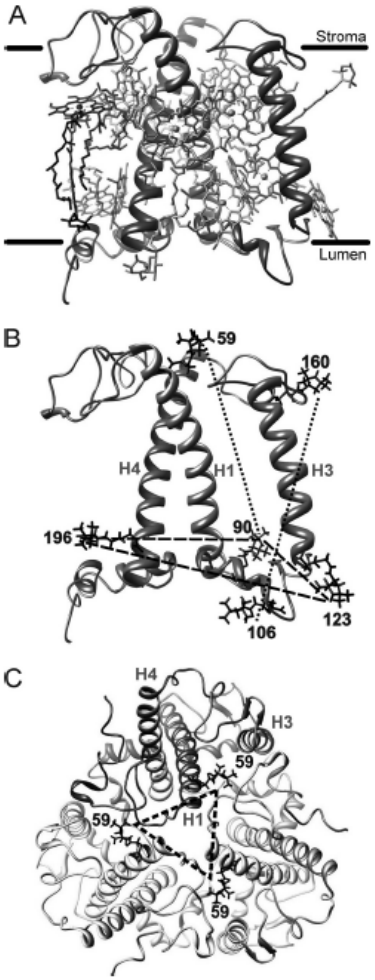

FIGURE 1. **Protein structure and labeling sites of monomeric and trimeric LHCII.** *A*, side view of monomeric LHCII with bound pigments based on the latest crystal structure (PDB entry 2BHW). *Dotted* and *dashed traces* highlight interspin distances measured in doubly labeled monomers (*B*) or trimers assembled with three singly labeled monomers (*C*, stromal top view).

indicating that unwanted protein aggregation or oligomerization to a minor extent cannot be excluded in the sample preparation procedure (see "Discussion").

The core structure of detergent-solubilized LHCII monomers was assessed by measuring two distances parallel to the trans-membrane helices, one alongside helix H1 (59/90) and one between the lumenal and stromal loops (*106/160, dotted lines*, Fig. 1*B*) as well as several distances parallel to the lumenal surface of the complex (90/123, 90/196, and 123/196), providing information on the position of the trans-membrane helices to each other (*dashed lines*, Fig. 1*B*). Additionally, distances within trimeric LHCII were measured between monomers spin-labeled either in position 59 (*stromal side*, Fig. 1*C*) or 106 (lumenal side). Three spin-spin distances are present in each of these trimers; however, because of the 120° symmetry in the trimeric structure, these three distances are expected to be the same.

To obtain interspin distances from the raw DEER data, these (Fig. 2*B*, *black lines*) were background-corrected and used to calculate spin-spin distance probability distributions (Fig. 2*C*, *black lines*). The width of the distance distributions reflects the unknown conformation distribution of the protein domains carrying the spin labels and the conformation distribution of the spin labels themselves. The latter adds a distance uncertainty between two given points in the protein of ±0.5 nm per spin label, *i.e.* ±1 nm uncertainty for each spin-spin distance, assuming complete conformational freedom for the nitroxide labels. In most cases, this freedom will be restricted due to steric hindrance by the protein and pigment environment of the labels. This restricted conformation distribution of the spin labels has been modeled into the crystal structure (28) identifying allowed orientations and estimating their probability by a rotamer library (Fig. 2*A*). The resulting predicted distance distributions, taking into account only conformation distribution of the label but no flexibility in the protein domains (*dotted lines*, Fig. 2*C*), were used for simulating the expected EPR dipolar evolution signals (*gray curves*, Fig. 2*B*). Those distances in our analysis that exhibit a larger deviation from the crystal structure than what is expected because of spin label conformational distribution can be detected by significant differences between measured and simulated dipolar evolution function and distance distributions (Fig. 2, *B* and *C*, respectively).

The distance distribution obtained with the spin pair on either end of helix H1 (59/90) is very narrow, consistent with the expected low protein flexibility in an α helix, and it coincides very well with the one resulting from the rotamer library (maxima of 4.9 and 4.8 nm, respectively). The measured distance distribution is even narrower than the one predicted from the rotamer library, indicating that the simulation overestimates the rotational freedom of the spin labels. The parallel distance between the stromal and lumenal loops (106/160) also yielded a distance distribution very similar to the predicted one, although in this case the EPR-measured distribution is somewhat broader. This may reflect some mobility of the loop domains, which is expected to be higher than that of the α helices (7).

The distance measurements on the lumenal surface of LHCII yielded a similar agreement between the EPR-measured data and those predicted from modeling. The measurement between helices H1 and H4 (90/196) resulted in a very narrow main peak, as expected for the rigid labeling positions in the helices. The same is true for the separation between helices H1 and H3 (90/123), where the measured distance distribution again is narrower than the modeled one and the H3-H4 separation (123/196). These three distance distributions contain, next to the main peaks corresponding to the expected separation, additional peaks on the shorter and longer distance sides. The 59/90 measurement also yielded an additional peak at shorter distances compared with the main distance peak. These may reflect artifacts due to protein aggregation and will be dis-

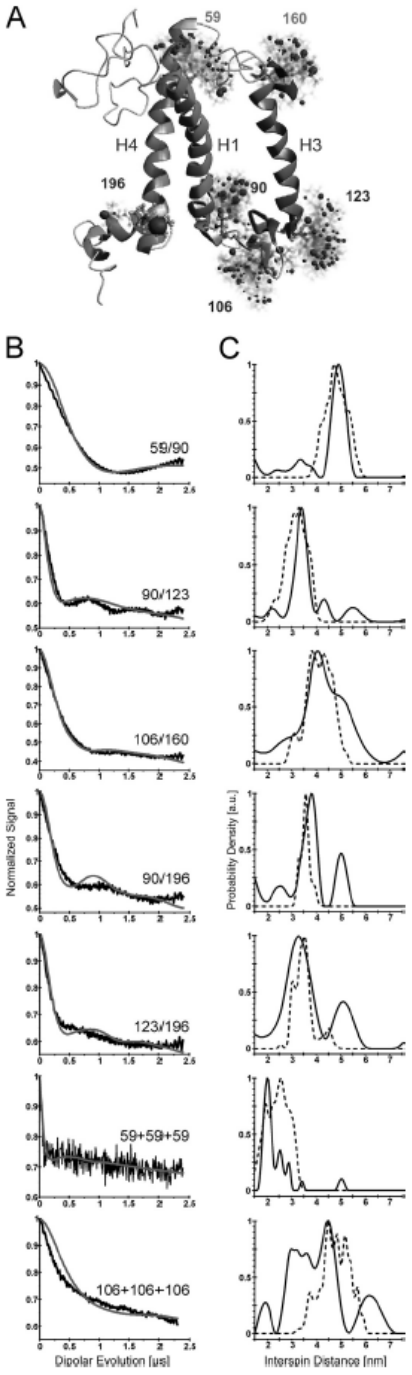

cussed below. Taken together, these data show that the hydrophobic core domain of LHCII in detergent-solubilized monomers adopts a structure very similar or identical to the one seen in crystallized LHCII trimers.

Reasonable agreement between the EPR-measured distances and the crystal structure was also seen when trimeric LHCII was analyzed with spin labels attached to position 59, *i.e.* to the N-proximal end of helix H1 (59 + 59 + 59 in Fig. 2). The sharp peak at 2.1 nm overlaps with the range of spin-spin distances resulting from the rotamer library, but the latter predicts a distance of 2.6 nm as the most frequently adopted one. The distance distribution between the three lumenal loops in the trimeric structure (106 + 106 + 106) shows a broad major peak between 2.5 and 5.3 nm. Part of this broad distribution may stem from some mobility of the loop structure, but some of it is due to a larger mobility of the spin label as compared with the one seen in the α-helical labeling positions, as deduced from the broader modeled distance distribution. Although the peak maxima of the measured and predicted data coincide, the predicted range of distances is shifted to larger values (3.5–6 nm). The EPR measurement of LHCII labeled in the three lumenal loop domains yielded extra peaks on the shorter and longer distance side (1.9 and 6.2 nm, respectively). Again, these may be artifacts (see "Discussion").

Distances Extending to N-terminal Domain—The N terminus of LHCII up to residue 10 has not been resolved even in the latest crystal structure, which has been interpreted to indicate a certain degree of flexibility of this domain (7). Two series of experiments were performed to investigate the structure of the N-terminal domain in LHCII monomers and trimers. In one line of experiments, we measured distances between parts of the N-terminal protein domain and the rigid LHCII core. In the other series, the positioning of the three N termini relative to each other in trimeric LHCII was assessed.

The five N-terminal distances 29/59, 14/29, 3/59, 3/29, and 3/14 in LHCII monomers were assessed by DEER EPR (Fig. 3). In the case of 29/59, the predominant distances calculated from the DEER data correlate with the prediction based on the rotamer library between 2.5 and 3.8 nm. In addition, shorter and longer distances are detected indicating either a higher degree of label delocalization or peptide flexibility at position 29. In sample 14/29, hardly any correlation exists between DEER data and prediction. Here, a narrow distribution of spin-spin distances between 1.5 and 2.5 nm is expected from the simulation, although a broad range of distances between 1.5 and 5.5 nm results from the DEER experiment. The extension of the measured distance distribution toward longer distances cannot be explained by an underestimation of conformation distribution of the label, as was checked with the "Any rotamers?" feature of the software MMM, which demonstrates that distances longer than 3 nm cannot be reconciled with the back-

FIGURE 2. **DEER results for monomeric and trimeric LHCII samples labeled in core positions and in the stromal and lumenal loops.** *A*, crystal structure (PDB entry 2BHW) of monomeric LHCII with possible acetamido-PROXYL rotamers. *B*, normalized dipolar evolution (*black line*) and rotamer library simulation (*gray line*). *C*, distance distribution calculated from the data in *B* with a regularization parameter $\alpha = 10$ and a dipolar evolution time of 2.5 µs (*black line*) and determined from a rotamer library-based simulation (*dotted line*).

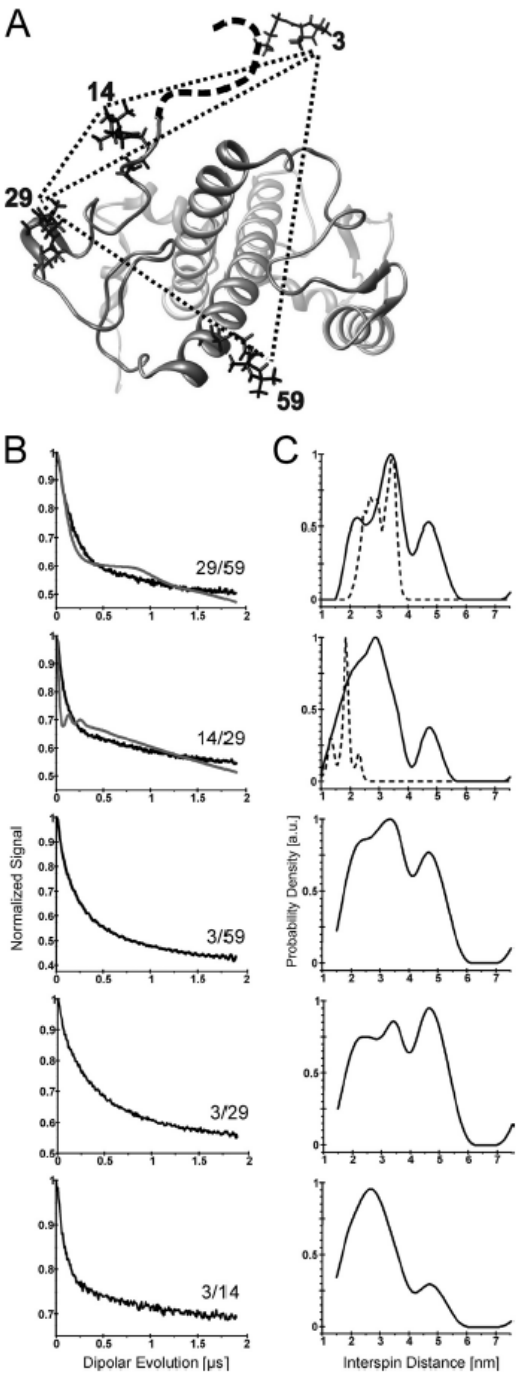

bone coordinates of residues 14 and 29 in the crystal structure. Hence, monomeric samples in solution display conformations of the N-terminal domain that deviate from the known crystal structures (2, 3).

Broad distributions are also found for distances 3/59, 3/29, and 3/14. Residue 3 is the only one among these labeling positions that is not resolved in the crystal structure. Therefore, a distance prediction between residue 3 and residues 14, 29, and 59, and thus a comparison with the DEER distance distribution, is not possible. However, the broad distance distributions again cannot be explained by only conformation distribution of the label and thus indicate a considerable flexibility of the domain. Again, a side peak at ~5 nm is detected in all monomeric samples labeled at N-terminal positions (see "Discussion").

The second series of DEER experiments assessed 12 different interspin distances between the three N-terminal domains of trimeric LHCII as displayed in Fig. 4. Here, an extensive Cys-walk toward the N terminus was performed, to detect possible deviations between the structures of LHCII in solution and in crystals and to assess the flexibility of individual segments of this domain. As the fixed point in these measurements, position 59 at the N-proximal end of helix H1 was chosen as part of the rigid core of LHCII.

The consistency between measured and predicted data remains fairly good going from position 59 to position 12. The only exception is position 22 where both the measurement and the structure simulation yield narrow distance distributions, but the peak maxima (at 5 and 6 nm, respectively) differ by 1 nm. The rotamer library prediction for this site is rather insensitive to repacking of the side groups in the LHCII structure with SCWRL4 (34); however, the "Any rotamers?" feature of MMM can reconcile the experimentally observed and simulated distance distributions, except for the minor noise-related peak at about 3 nm. Remarkably, in the 12 + 12 + 12 measurement, the EPR distance measurement yields a main peak that is narrower than the predicted distribution. The measured data do include an additional peak at 3.5 nm, which was found to be insignificant by validation and is probably noise related.

Up to position 12, the simulations can still be reconciled with experimental data considering the combined uncertainties; starting at residue 11 this is clearly no longer possible. The measured distance distribution becomes much broader than those distributions seen at the more distal labeling points and also broader than the predicted distribution. Moreover, the peak maximum in the measured distance distribution is shifted toward shorter distances in comparison with that of the predicted data (5 and 6.5 nm, respectively). This shift is even more pronounced in the 10 + 10 + 10 measurement (5.1 and 7.1 nm). In positions 10 and 11, the rotamer simulations possibly predict distributions that are somewhat too broad, as the spin label conformations may be restricted by side groups of the first nine

FIGURE 3. **DEER results for monomeric LHCII doubly labeled in the N-terminal domain.** *A*, stromal top view of monomeric LHCII (PDB entry 2BHW) with interspin distances measured in the N-terminal domain (*dotted lines*). *B*, normalized dipolar evolution (*black line*) and rotamer library simulation (*gray line*). *C*, distance distribution calculated from the data in *B* with a regularization parameter $\alpha = 10$ and a dipolar evolution time of 2.5 µs (*black line*) and determined from a rotamer library-based simulation (*dotted line*).

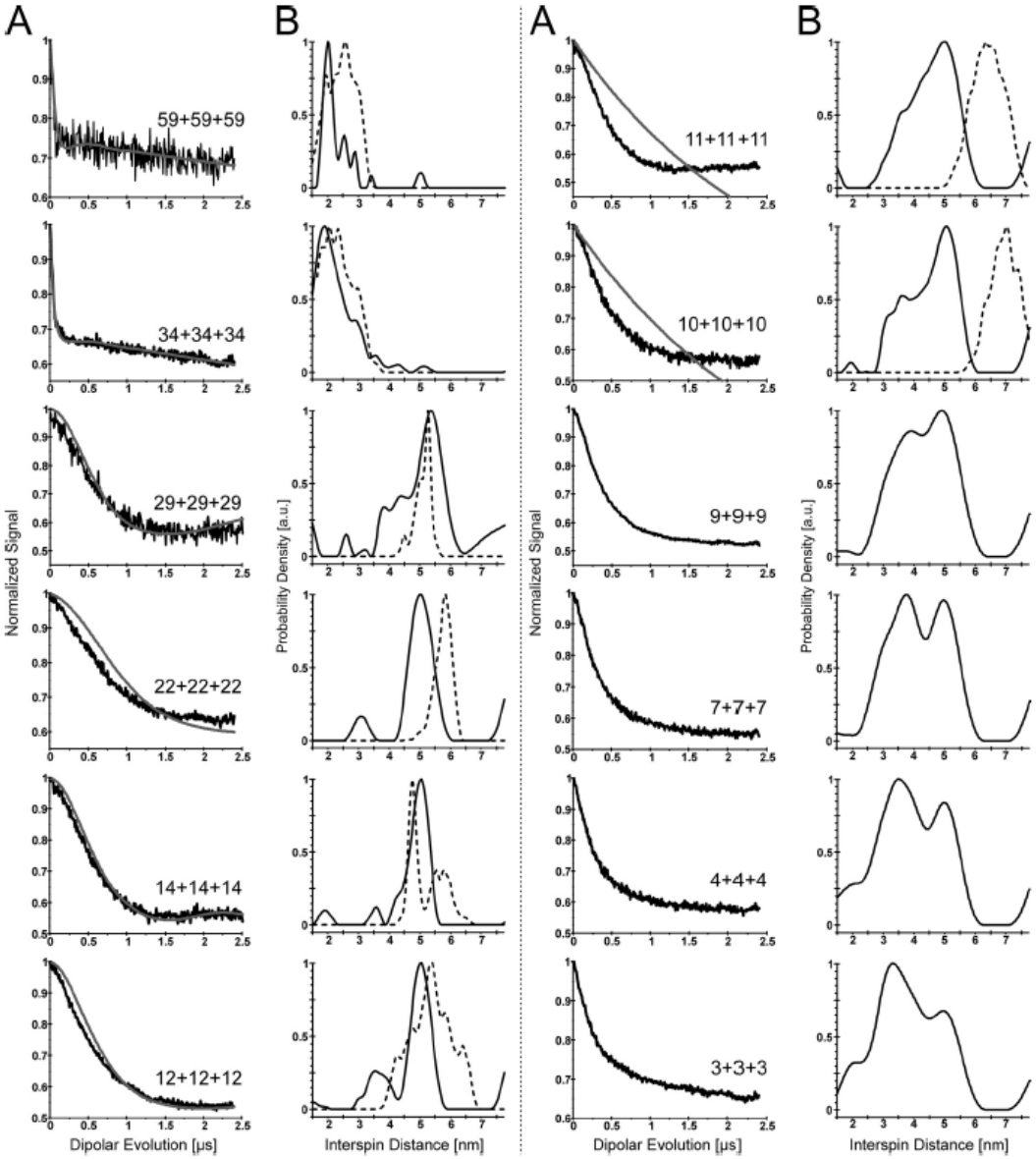

FIGURE 4. **DEER results obtained for trimeric LHCII labeled in the N-terminal domain.** *A* (*1st column* and continues in *3rd column*), normalized dipolar evolution (*black line*) and rotamer library simulation (*gray line*). *B* (*2nd column* and continues in *4th column*), distance distributions calculated from the data in *A* with a regularization parameter $\alpha = 10$ and a dipolar evolution time of 2.5 μs (*black line*) and determined from a rotamer library-based simulation (*dotted line*).

residues that are not resolved in the structure and thus disregarded in the simulations. However, the strong discrepancy between simulated and experimental data for these sites cannot be explained by this uncertainty, as the difference in the mean distances is larger than the total width of the conformational distribution for an unrestricted label, as tested with the "Any rotamers?" feature of MMM. Distances shorter than 4.7 nm for site 11 and shorter than 5.2 nm for site 10 are inconsistent with the backbone coordinates of these residues in the crystal structure. Possible suppression of long distances in the experimental

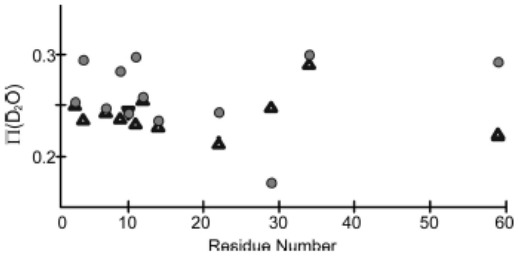

FIGURE 5. **Water accessibility parameter $\Pi(D_2O)$ based on deuterium ESEEM as a function of residue number.** *Black triangles* denote trimer data, and *gray dots* denote monomer data.

distribution by background correction cannot explain the results either, because the presence of the short distances that are inconsistent with the crystal structure can be inferred already from the fast decay of the initial part of the uncorrected dipolar evolution data at times smaller than 1 μs. Clearly, this part of the N-terminal domain is shifted toward the symmetry center of the LHCII trimer in comparison with the crystal structure. For the amino acid positions closer to the N terminus (positions 9, 7, 4, and 3), no comparison is possible with data predicted from the crystal structure because this protein segment has not been resolved crystallographically. The measured data clearly show that the distance distributions become even broader, indicating an increasing protein mobility toward the N terminus. Moreover, the maxima in the distributions further shift toward smaller distances, indicating that in the most frequently adopted structure the N termini extend toward the symmetry center of the trimer.

Water Accessibility to N-terminal Amino Acid Residues—ESEEM EPR was used to localize the N-terminal residues in monomers and trimers with respect to the water environment and the hydrophobic core of the detergent micelle. In this experiment, the hyperfine interaction of spin labels with deuterium nuclei of heavy water was measured for the 12 N-terminal residues, and the water accessibility parameter $\Pi(D_2O)$ was calculated as described previously (Fig. 5, *gray dots* and *black triangles*, respectively) (18).

Earlier experiments showed that residues near the LHCII core, which reside inside the hydrophobic micelle, exhibit a very low water accessibility parameter $\Pi(D_2O)$ (0.075–0.12), whereas the free label in detergent-containing buffer exhibits $\Pi(D_2O) = 0.35$ (18). Uncertainty of the experimental values is $\Delta\Pi(D_2O) \approx \pm 0.02$. Overall, N-terminal positions have enhanced access to the hydrophilic environment, but in some cases differences between monomers and trimers appear. Residues (34, 14, 12, 10, 7, and 3) in monomers and trimers exhibit identical water accessibility, so they reside in similar environments. Monomeric samples 59, 22, 11, 9, and 4 show slightly but significantly enhanced water accessibility as compared with their trimeric equivalents, whereas the environment of residue 29 is slightly but significantly more hydrophobic in monomers than in trimers. Although the change in sample 59 can be due to the labeling position close to the interface between two monomers in a trimer, the other positions can hardly be affected by oligomerization and thus show conformational change of the N-terminal protein domain in response to the state of oligomerization.

In the trimer, water accessibility is roughly the same in samples 14, 12, 11, 9, 7, 4, and 3. This indicates that the localization of these residues with respect to detergent and lipid headgroups remains approximately the same throughout this section. The mean conformation of this section thus runs nearly parallel to the headgroup layer.

DISCUSSION

Core Structure of LHCII in Solution—The x-ray crystal structures of LHCII from spinach and pea (2, 3) can be superimposed to yield an almost perfect overlap of the main chain polypeptide atoms of residues 14–231. Additionally, the three trans-membrane helices of LHCII superimpose almost perfectly with the polypeptide backbones of LHCI apoproteins, corroborating the assumption of a conserved core structure of LHCs with little flexibility between individual α helices (7).

In our EPR study, the core structure of monomeric and trimeric LHCII in detergent solution was analyzed to scan the LHCII interior for flexible protein domains. Recently, DEER distance mapping was shown to be an excellent technique to analyze structural dynamics of proteins in solution (20, 25, 26). Therefore, interspin distances were measured between PROXYL labels, attached to each of the trans-membrane helices of LHCII, and these distances were compared with distances determined in a simulation based on label rotamers in the structure of trimeric LHCII crystals (28).

The DEER distance map of LHCII in aqueous solution displays a core structure identical to that seen in crystals with regard to both the sizes and the arrangement of membrane-spanning helices. Measured distance distributions between positions near the LHCII core are even narrower than the ones predicted from the rotamer library, indicating that spin labels have less rotational freedom than expected and verifying the tight packing of the complex in detergent solution. As pointed out by Barros and Kühlbrandt (7), a rigid scaffold fixing the pigments in their optimum position for both anisotropic light absorption and efficient energy transfer is a prerequisite for proper light harvesting.

The side peaks at 5.1 nm in the distance distributions 90/196 and 123/196 (Fig. 2) are puzzling. In both cases, the maximum peak of the EPR distance distribution coincides nicely with the maximum peak of distances predicted by the rotamer simulation, but the 5.1 nm side peaks exceed these maxima by more than 1 nm and therefore cannot be due to the spin mobility simply being larger than expected from the molecular model. A distance change of this size in a subpopulation of LHCII would require either an altered tilt or partial unfolding at the lumenal end in at least one of the trans-membrane helices. This would jeopardize proper binding of the Chls situated between the trans-membrane helices or bound to ligands near the lumenal surface, respectively. Either appears highly unlikely in a functional LHCII structure.

An alternative explanation for the existence of side peaks is the accidental formation of LHCII trimers or aggregates due to the high LHCII concentration in the EPR sample (300 μM), which is approximately the concentration of LHCII trimers in

the mother liquor of typical crystallization experiments (35). Highly concentrated LHCII monomers can form trimers in the presence of phosphatidylglycerol (PG) (36), of which trace amounts are contained in the pigments used for reconstituting LHCII. However, in CD and PAGE analyses of these LHCII solutions, no significant amounts of trimerized complexes were detectable (supplemental Figs. S2–S4). In the CD spectra and in partially denaturing electrophoresis, LHCII trimers would have shown up as a trimer signal at 473 nm (37) and as a distinct band with a higher molecular mass as compared with monomeric LHCII, respectively (supplemental Figs. S3 and S4) (21). Moreover, a spin-spin distance of 5.1 nm would not be expected in the trimeric complexes. For instance, in LHCII trimers labeled at positions 123 and 196, the expected intra- and intermonomer distances are 2.3, 3.3, 4.5, and 5.8 nm but not 5.1 nm. A similar argument holds for the 90/196 measurement. Structure simulations in MMM (28), including multispin effects (33), did not reproduce a 5.1-nm peak either, not even for pure trimers.

The formation of LHCII aggregates would also bring monomers in sufficiently close proximity to lead to intermonomer EPR signals. Control measurements with singly labeled LHCII monomers at the same concentrations in many cases gave clean exponentially decaying background signals confirming that, as expected, no significant spin-spin interaction took place. However, in some cases aggregation was seen, *e.g.* in the case of monomers labeled in position 59 (supplemental Fig. S5*B*), which exhibited a modulation depth as large as 0.17. Only crystalline aggregates would yield few distinct spin-spin distances, whereas in irregularly structured aggregates a large multitude of intermonomer spin-spin separations would be expected. Although LHCII trimers are known to form crystalline two-dimensional aggregates at high concentrations, displaying an alternating up/down orientation of the complexes (7), LHCII monomers have never been observed to crystallize. However, this does not exclude the possibility that a small part of the monomeric complexes forms ordered aggregates in a regularly alternating up/down orientation. Because in both samples 90/196 and 123/196 the spin labels are attached to the same side of the monomers, the intermonomer distances between neighboring monomers would then correspond to somewhat more than the distance between the stromal and lumenal faces of LHCII, which is consistent with the 5.1-nm side peak. Alternatively, a 5.1-nm distance peak due to aggregation of LHCII monomers may be an artifact resulting from the evaluation of our EPR measurements. Because of the properties of Tikhonov regularization, a broad peak will split into several more narrow peaks, if some other feature in the distance distribution, in this case the main peak, is narrow. Furthermore, contributions from longer distances are suppressed by background correction. Hence, we cannot exclude that the 5.1 nm peak is the remainder of a broad aggregate peak.

Structure and Flexibility of Loop Domains—By contrast to the rigid core domains, loop regions revealed more flexibility. As noted before, part of the broad distance distributions found in monomeric sample 106/160 and trimeric sample 106 + 106 + 106 may stem from a larger mobility of the spin labels than the one seen in α-helical labeling positions, as deduced from the broader modeled distance distribution. However, the DEER distance distributions measured were even broader than the predicted ones. Consistently, a certain degree of flexibility of LHCII loop regions has been deduced from comparing the two crystal structures and from inspecting crystallographic *B* factors (7). No bimodal distance distributions were seen in these EPR measurements, so these data do not support the notion of a co-existence of preferred conformers. Conformational changes in the lumenal loop and core structures of LHCII, triggered by lumen acidification and leading to nonphotochemical quenching, have been proposed by some (2, 6) and doubted by others (7). The EPR data presented here indicate a considerable flexibility in an aqueous environment of the apoprotein in its loop domains but not in the hydrophobic core where the chlorophylls are bound.

Structure and Flexibility of the N-terminal Domain of LHCII in Solution—To discuss the structure and flexibility of the N terminus of monomeric and trimeric LHCII in solution, the domain will be divided into three individual sections, proceeding from the N-proximal end of the first trans-membrane helix toward the N terminus, and each section will be compared with the structural data published in the latest x-ray studies (2, 3).

The flexibility of the first section, covering the polypeptide backbone from residue 59 to 26, is low in LHCII crystals and in solubilized trimers. Interestingly, only this section of the N terminus could be traced out in the first LHCII structure in two-dimensional crystals at 3.4 Å resolution (38), a first evidence for a low flexibility of the section in trimeric LHCII. According to the crystal structure, residues 51 to 42 form a short loop that submerges into the lipophilic membrane environment. In this loop, the polar headgroup of the lipid PG is in contact with Tyr-44, and one of its fatty acid chains expands deeply into the core of the trimer along the interface of two monomers, probably undergoing hydrophobic interactions (36). Thus, PG may anchor the first N-terminal section to the rigid core of LHCII, which may explain the rigid structure of this part of the N-terminal protein domain in trimeric LHCII.

The second section, covering amino acid residues 26 to 14, was more difficult to resolve in crystallography and was defined only by the newer x-ray studies by Liu *et al.* (2) (PDB code 1RWT) and by Standfuss *et al.* (3) (PDB entry 2BHW). EPR measurements of trimeric LHCII in solution confirm the low flexibility expected from the crystal data, whereas the broadened distance distribution in sample 14/29 indicates a less defined and more flexible structure for this section in monomeric LHCII. The main peak in the distance distribution of the same sample is shifted in LHCII monomers compared with trimers, and the water accessibility parameter in positions 29 and 22 show significant differences, both indicating this protein domain to adopt a slightly different structure in monomers compared with that in trimers. This is not unexpected because according to the crystal structure of LHCII trimers, amino acid Tyr-24 is the protein ligand for the central Mg^{2+} of Chl 9. The pigments Chl 9 and violaxanthin and the lipid PG, which run parallel to each other, are positioned in monomer-monomer interfaces in the trimer and are only weakly, if at all, bound to monomers. Therefore, in monomeric LHCII, these contact sites may be missing Chl 9 and thus the middle section in the

N-terminal domain, rendering it more flexible in comparison with its situation in LHCII trimers.

The last section of the N-terminal domain covers residues 14 to 1 of which the first nine residues have not been resolved in the x-ray studies. Thus, for these positions, we cannot compare the EPR data to the x-ray structure. Residues 14 to 10 were resolved in structure 2BHW only, featuring strongly enhanced *B* factors, and at least for residues 11 and 10 it is safe to state that their mean location with respect to the C_3 symmetry axis of the trimer in solution differs strongly from the one observed in crystals. We have also tested whether the width of the distance distributions for sites 11, 10, 9, 7, 4, and 3 can be explained by any well defined conformation of the N-terminal domain and conformation distribution of the spin label. The full width at half-height of the distance distributions simulated for completely unrestricted label conformation varies slightly with the distance between the labeled residues and their relative orientation. However, this width is typically 1.5–1.7 nm and in no case exceeds 2 nm, whereas all experimental distance distributions in this section are at least as broad as 3 nm. We therefore conclude that in aqueous solution the backbone of the N-terminal domain in this section exhibits a spatial distribution between 0.5 and 1.5 nm. A flexible N terminus in LHCII has been proposed to explain the low resolution in this segment of the LHCII crystal structure (3), but it was never confirmed experimentally for LHCII. The DEER distance mapping in our study provides evidence for a highly disordered domain-terminal protein section in both monomeric and trimeric LHCII. This is the protein section that carries the phosphorylation site in LHCII (Thr-5 and -6). LHCII phosphorylation triggers the so-called state transition, a re-distribution of LHCII to balance the excitation energy flow between PSI and PSII (39). A different EPR structural study on the N-terminal domain of the CP29, one of the monomeric minor light-harvesting complexes of PSII, also indicated that the phosphorylation site is located in a mobile protein domain (40). This local flexibility of the substrate protein may be a prerequisite for its interaction with its cognate kinase.

In the distance distributions in the trimeric complexes labeled in positions 9, 7, 4, and 3, two maxima can be noted. These do not immediately suggest a bimodal distance distribution because there is no base-line separation between the two peaks. However, some of the primary EPR data show a kink in the time trace that does indicate bimodality. There is a trend when going from 9 to 7 and 4 to 3 for this kink to become more pronounced. This may indicate two families of preferred conformations, with the difference between the families increasing toward the N terminus, confirming our earlier notion of two preferred conformations of the N-terminal LHCII domain (24). However, as long as such conformations have not been correlated with functional states such as the phosphorylated and nonphosphorylated state or the attachment to PSI or PSII, their significance remains unclear.

The structural information on LHCII presented here refers to the complex in aqueous detergent solution. It has been shown that detergent micelles are able to mimic the membrane environment quite well for at least some membrane proteins (41). LHCII like many other membrane proteins is able to adopt its functional structure in aqueous detergent solution, taking efficient intra-molecular energy transfer from Chl *b* to Chl *a* as a criterion for functionality. It is difficult to decide whether the LHCII environment in crystals used for x-ray analyses is a better approximation to the one provided by the thylakoid membrane. On the one hand, the stacked two-dimensional crystals containing lipids of pea LHCII (3) or the icosahedral proteoliposomes of spinach LHCII (2) contain a more or less continuous hydrophobic phase in which the complexes are inserted rather than individual micelles enclosing the hydrophobic section of each LHCII. On the other hand, the non-natural up/down orientation of neighboring LHCII trimers as well as crystal packing effects may distort parts of the protein, particularly hydrophilic domains. In the detergent situation, those hydrophilic domains protrude into a truly aqueous environment. Consequently, differences seen between the LHCII crystal structures and structural data derived from EPR measurements should be taken as a reminder that the native structure of membrane-embedded LHCII may still be different from what we have seen so far. Because of the improved sensitivity of Q-band EPR, it may soon be possible to perform structural studies on LHCII embedded in thylakoid membranes.

Acknowledgments—We thank Professor H. G. Spiess for helpful discussion and R. Tschaggelar for technical support.

REFERENCES

1. Peter, G. F., and Thornber, J. P. (1991) Biochemical composition and organization of higher plant photosystem II light-harvesting pigment proteins. *J. Biol. Chem.* **266,** 16745–16754
2. Liu, Z., Yan, H., Wang, K., Kuang, T., Zhang, J., Gui, L., An, X., and Chang, W. (2004) Crystal structure of spinach major light-harvesting complex at 2.72 Å resolution. *Nature* **428,** 287–292
3. Standfuss, J., Terwisscha van Scheltinga, A. C., Lamborghini, M., and Kühlbrandt, W. (2005) Mechanisms of photoprotection and nonphotochemical quenching in pea light-harvesting complex at 2.5 Å resolution. *EMBO J.* **24,** 919–928
4. Andersson, J., Wentworth, M., Walters, R. G., Howard, C. A., Ruban, A. V., Horton, P., and Jansson, S. (2003) Absence of the Lhcb1 and Lhcb2 proteins of the light-harvesting complex of photosystem II. Effects on photosynthesis, grana stacking, and fitness. *Plant J.* **35,** 350–361
5. Pascal, A. A., Liu, Z., Broess, K., van Oort, B., van Amerongen, H., Wang, C., Horton, P., Robert, B., Chang, W., and Ruban, A. (2005) Molecular basis of photoprotection and control of photosynthetic light harvesting. *Nature* **436,** 134–137
6. Ruban, A. V., Berera, R., Ilioaia, C., van Stokkum, I. H., Kennis, J. T., Pascal, A. A., van Amerongen, H., Robert, B., Horton, P., and van Grondelle, R. (2007) Identification of a mechanism of photoprotective energy dissipation in higher plants. *Nature* **450,** 575–578
7. Barros, T., and Kühlbrandt, W. (2009) Crystallization, structure, and function of plant light-harvesting Complex II. *Biochim. Biophys. Acta* **1787,** 753–772
8. Miloslavina, Y., Wehner, A., Lambrev, P. H., Wientjes, E., Reus, M., Garab, G., Croce, R., and Holzwarth, A. R. (2008) Far-red fluorescence. A direct spectroscopic marker for LHCII oligomer formation in nonphotochemical quenching. *FEBS Lett.* **582,** 3625–3631
9. Avenson, T. J., Ahn, T. K., Zigmantas, D., Niyogi, K. K., Li, Z., Ballottari, M., Bassi, R., and Fleming, G. R. (2008) Zeaxanthin radical cation formation in minor light-harvesting complexes of higher plant antenna. *J. Biol. Chem.* **283,** 3550–3558
10. Lemeille, S., and Rochaix, J. D. (2010) State transitions at the crossroad of thylakoid signaling pathways. *Photosynth. Res.* **106,** 33–46

11. Pesaresi, P., Hertle, A., Pribi, M., Schneider, A., Kleine, T., and Leister, D. (2010) Optimizing photosynthesis under fluctuating light. The role of the *Arabidopsis* STN7 kinase. *Plant Signal. Behav.* **5,** 21–25
12. Tikkanen, M., Grieco, M., and Aro, E. M. (2011) Novel insights into plant light-harvesting complex II phosphorylation and "state transitions." *Trends Plant Sci.* **16,** 126–131
13. Kargul, J., and Barber, J. (2008) Photosynthetic acclimation. Structural reorganization of light harvesting antenna. Role of redox-dependent phosphorylation of major and minor chlorophyll *a*/*b*-binding proteins. *FEBS J.* **275,** 1056–1068
14. Nilsson, A., Stys, D., Drakenberg, T., Spangfort, M. D., Forsén, S., and Allen, J. F. (1997) Phosphorylation controls the three-dimensional structure of plant light harvesting complex II. *J. Biol. Chem.* **272,** 18350–18357
15. Zer, H., Vink, M., Keren, N., Dilly-Hartwig, H. G., Paulsen, H., Herrmann, R. G., Andersson, B., and Ohad, I. (1999) Regulation of thylakoid protein phosphorylation at the substrate level. Reversible light-induced conformational changes expose the phosphorylation site of the light-harvesting complex II. *Proc. Natl. Acad. Sci. U.S.A.* **96,** 8277–8282
16. Daum, B., Nicastro, D., Austin, J., 2nd, McIntosh, J. R., and Kühlbrandt, W. (2010) Arrangement of photosystem II and ATP synthase in chloroplast membranes of spinach and pea. *Plant Cell* **22,** 1299–1312
17. Paulsen, H., Rümler, U., and Rüdiger, W. (1990) Reconstitution of pigment-containing complexes from light-harvesting chlorophyll *a*/*b*-binding protein overexpressed in *E. coli*. *Planta* **181,** 204–211
18. Volkov, A., Dockter, C., Bund, T., Paulsen, H., and Jeschke, G. (2009) Pulsed EPR determination of water accessibility to spin-labeled amino acid residues in LHCIIb. *Biophys. J.* **96,** 1124–1141
19. Plumley, F. G., and Schmidt, G. W. (1987) Reconstitution of chlorophyll *a*/*b* light-harvesting complexes. Xanthophyll-dependent assembly and energy transfer. *Proc. Natl. Acad. Sci. U.S.A.* **84,** 146–150
20. Dockter, C., Volkov, A., Bauer, C., Polyhach, Y., Joly-Lopez, Z., Jeschke, G., and Paulsen H. (2009) Refolding of the integral membrane protein light-harvesting complex II monitored by pulse EPR. *Proc. Natl. Acad. Sci. U.S.A.* **106,** 18485–18490
21. Hobe, S., Prytulla, S., Kühlbrandt, W., and Paulsen, H. (1994) Trimerization and crystallization of reconstituted light-harvesting chlorophyll *a*/*b* complex. *EMBO J.* **13,** 3423–3429
22. Pannier, M., Veit, S., Godt, A., Jeschke, G., and Spiess, H. W. (2000) Dead-time free measurement of dipole-dipole interactions between electron spins. *J. Magn. Reson.* **142,** 331–340
23. Jeschke, G., and Polyhach, Y. (2007) Distance measurements on spin-labeled biomacromolecules by pulsed electron paramagnetic resonance. *Phys. Chem. Chem. Phys.* **9,** 1895–1910
24. Jeschke, G., Bender, A., Schweikardt, T., Panek, G., Decker, H., and Paulsen, H. (2005) Localization of the N-terminal domain in light-harvesting chlorophyll *a*/*b* protein by EPR measurements. *J. Biol. Chem.* **280,** 18623–18630
25. Altenbach, C., Kusnetzow, A. K., Ernst, O. P., Hofmann, K. P., and Hubbell, W. L. (2008) High resolution distance mapping in rhodopsin reveals the pattern of helix movement due to activation. *Proc. Natl. Acad. Sci. U.S.A.* **105,** 7439–7444
26. Klein, J. C., Burr, A. R., Svensson, B., Kennedy, D. J., Allingham, J., Titus, M. A., Rayment, I., and Thomas, D. D. (2008) Actin-binding cleft closure in myosin II probed by site-directed spin labeling and pulsed EPR. *Proc. Natl. Acad. Sci. U.S.A.* **105,** 12867–12872
27. Hilger, D., Polyhach, Y., Jung, H., and Jeschke, G. (2009) Backbone structure of transmembrane domain IX of the Na^+/proline transporter PutP of *Escherichia coli*. *Biophys. J.* **96,** 217–225
28. Polyhach, Y., Bordignon, E., and Jeschke, G. (2011) Rotamer libraries of spin-labeled cysteines for protein studies. *Phys. Chem. Chem. Phys.* **13,** 2356–2366
29. Cashmore, A. R. (1984) Structure and expression of a pea nuclear gene encoding a chlorophyll *a*/*b*-binding polypeptide. *Proc. Natl. Acad. Sci. U.S.A.* **81,** 2960–2964
30. Paulsen, H., Finkenzeller, B., and Kühlein, N. (1993) Pigments induce folding of light-harvesting chlorophyll *a*/*b*-binding protein. *Eur. J. Biochem.* **215,** 809–816
31. Hobe, S., Niemeier, H., Bender, A., and Paulsen, H. (2000) Carotenoid-binding sites in LHCIIb. Relative affinities towards major xanthophylls of higher plants. *Eur. J. Biochem.* **267,** 616–624
32. Jeschke, G., Chechik, V., Ionita, P., Godt, A., Zimmermann, H., Banham, J., Timmel, C. R., Hilger, D., and Jung, H. (2006) Deer Analysis 2006. A comprehensive software package for analyzing pulsed ELDOR data. *Appl. Magn. Reson.* **30,** 473–498
33. Jeschke, G., Sajid, M., Schulte, M., and Godt, A. (2009) Three-spin correlations in double electron-electron resonance. *Phys. Chem. Chem. Phys.* **11,** 6580–6591
34. Krivov, G. G., Shapovalov, M. V., and Dunbrack, R. L., Jr. (2009) Improved prediction of protein side-chain conformations with SCWRL4. *Proteins* **77,** 778–795
35. Kühlbrandt, W. (1987) Three-dimensional crystals of the light-harvesting chlorophyll *a*/*b* protein complex from pea chloroplasts. *J. Mol. Biol.* **194,** 757–762
36. Nussberger, S., Dörr, K., Wang, D. N., and Kühlbrandt, W. (1993) Lipid-protein interactions in crystals of plant light-harvesting complex. *J. Mol. Biol.* **234,** 347–356
37. Rühle, W., and Paulsen, H. (2011) Preparation of native and recombinant light-harvesting chlorophyll *a*/*b* complex. *Methods Mol. Biol.* **684,** 113–125
38. Kühlbrandt, W., Wang, D. N., and Fujiyoshi, Y. (1994) Atomic model of plant light-harvesting complex by electron crystallography. *Nature* **367,** 614–621
39. Rochaix, J. D. (2011) Reprint of: Regulation of photosynthetic electron transport. *Biochim. Biophys. Acta* **1807,** 878–886
40. Kavalenka, A. A., Spruijt, R. B., Wolfs, C. J., Strancar, J., Croce, R., Hemminga, M. A., and van Amerongen, H. (2009) Site-directed spin-labeling study of the light-harvesting complex CP29. *Biophys. J.* **96,** 3620–3628
41. Roth, M., Lewit-Bently, A., Michel, H., Deisenhofer, J., Huber, R., and Oesterhelt, D. (1989) Detergent structure in crystals of a bacterial photosynthetic reaction center. *Nature* **340,** 659–662

3.6.2. Comparison of the conformation of the N-terminal domain in a monomeric and trimeric assembly by using heterogeneous trimers

The N-terminal domain of the LHCII is involved in a regulation process called state transition (Nilsson *et al*., 1997; Zhang and Scheller, 2004; Standfuss *et al*., 2005). This region is still incompletely resolved by X-ray analysis (Standfuss *et al*., 2005); perhaps, caused by a high flexibility. Previous measurements of double labeled mutants in a monomeric assembly as well as single labeled mutants in a trimeric assembly suggested a reduced flexibility in trimers (Müller, 2008; Dockter *et al*., 2011). In order to confirm these indications a direct comparison of intramolecular distances in both assembly states was required. For this purpose, a reproducible method for the preparation of heterogeneous trimers was established (details see 3.4) and a series of double labeled mutants prepared. Therefore, reconstituted double labeled mutants that contained a strep and an additional his_6 tag at the C-terminal domain were mixed in a ratio of 1:8 with unlabeled mutants that contained only a his_6 tag at the C-terminal domain. The his_6 tag was used to immobilize monomers onto the Ni-column, leading to four kinds of trimers, either consisting of completely unlabeled monomers or consisting of one, two or three labeled monomers. In order to get rid of incompletely unlabeled trimers, the Ni-column eluate was immobilized on the Mp-strep column until immobilized and labeled trimers were eluted and purified by ultracentrifugation. Labeling positions were located at the amino acids 3, 7, 11, 34, and 59. The amino acids 34 and 59 were chosen as reference points from where potentially flexible positions within the loop region could be measured because multiscale modeling of macromolecular systems (MMM) simulation predicted these positions as relatively rigid. Corresponding amino acids, forming a spin-spin pair with the reference points, were located at positions 3, 7, and 11. All produced samples were characterized biochemically by fluorescence emission and CD spectroscopy as well as denaturing gel electrophoresis. Biochemical data were not shown because they were identical to those in Figure 3.42.

Measurements between both reference points (34/59) led to approximately identical distance distributions in monomers and trimers (Figure 3.57-red and blue lines), containing a similar main distance peak between 1.5 and 3 nm. Overall, measured distance distributions were between 1.5 and 5 nm and thus broader than the theoretically predicted distance distribution, which was between 1.5 and 3 nm (Figure 3.57-green line). The distance peaks above 5 nm were caused by aggregation and/or incorrect background correction. The arrangement and flexibility of the backbone seemed to be identical with regard to the rigid predicted anchor positions and independently of the assembly state.

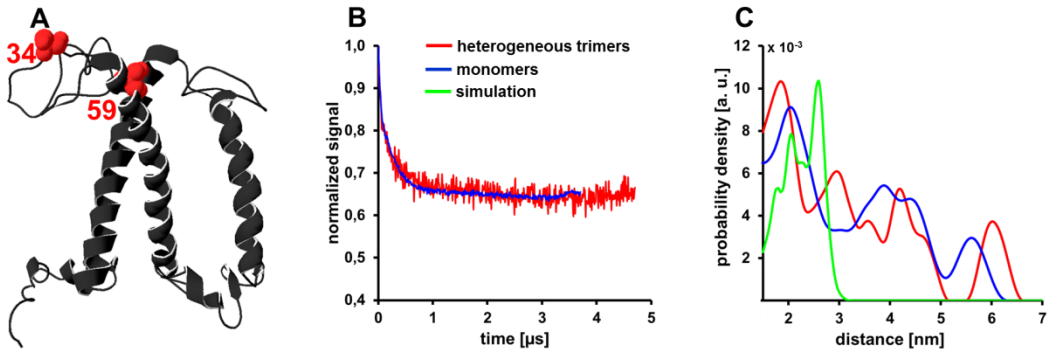

Figure 3.56: DEER-EPR measurements of the N-terminal domain of the detergent-solved LHCII to compare flexibility in a monomeric and trimeric assembly. Monomers (blue line) and trimers (red line) of the PROXYL-labeled mutant 34/59 showed similar distance distributions, independently of the assembly state but were broader than predicted by MMM simulation (green line). A: Labeled positions within in the X-ray structure are marked as red dots; B: Primary EPR data; C: Distance distributions.

A comparison between monomeric and trimeric distance distributions of those mutants that had one label inside the unresolved region of the N-terminal domain (positions 3, 7 and 11) by contrast showed clear differences. Details of the main peaks are listed in Table 3.6. Measurements in a monomeric assembly led to broader distance distributions, whereas distance distributions in a trimeric assembly tend to shorter distances, indicating a reduced flexibility, which became clear by the results of the mutants 3/59 (Figure 3.57-4), 7/59 (Figure 3.57-5) and 11/59 (Figure 3.57-6). Results of the mutant 7/34 (Figure 3.57-2) confirmed these data but a comparison of both assembly states of the complete 34 dataset was impossible, caused by broken samples of the 3/34 (Figure 3.57-1) monomers as well as 11/34 (Figure 3.57-3) heterogeneous trimers. Furthermore, the distance distributions at the beginning of the domain (Figure 3.57-1 and 4) were very broad and became smaller in the further course (Figure 3.57-2, 3, 5 and 6). Thus, flexibility at the beginning of the N-terminal domain seemed to be high and to decrease in the further course (Figure 3.57-6 and Figure 3.56-1) independently of the assembly state. Distance peaks above 6 nm were caused by aggregation and/or incorrect background correction. A comparison with the crystal structure by MMM simulation was not possible for mutants containing PROXYL labels at the positions 3, 7 and 11 caused by unresolved structural data.

Table 3.6: Detailed numbers of distance distributions of all double labeled mutants in a monomeric and trimeric assembly. Listed distances were limited to the main peak. MMM simulation was limited to the resolved part of the protein.

labeled positions	assembly state	distance distribution main peak	maximum of the main peak
34/59	MMM-simulation	1.50 - 3.00 nm	2.60 nm
	monomeric	1.50 - 5.00 nm	2.00 nm
	trimeric	1.50 - 5.00 nm	1.80 nm
3/34	monomeric	sample was broken	
	trimeric	1.50 - 5.40 nm	2.10 - 3.00 nm
7/34	monomeric	1.50 - 5.50 nm	2.25 - 4.00 nm
	trimeric	1.50 - 5.00 nm	2.50 - 3.30 nm
11/34	monomeric	1.50 - 5.60 nm	2.05 nm
	trimeric	sample was broken	
3/59	monomeric	1.50 - 5.50 nm	2.00 nm
	trimeric	1.50 - 5.10 nm	1.50 nm
7/59	monomeric	1.50 - 5.25 nm	2.85 nm
	trimeric	1.50 - 3.70 nm	2.05 nm
11/59	monomeric	1.50 - 5.35 nm	2.25 nm
	trimeric	1.50 - 4.80 nm	2.25 nm

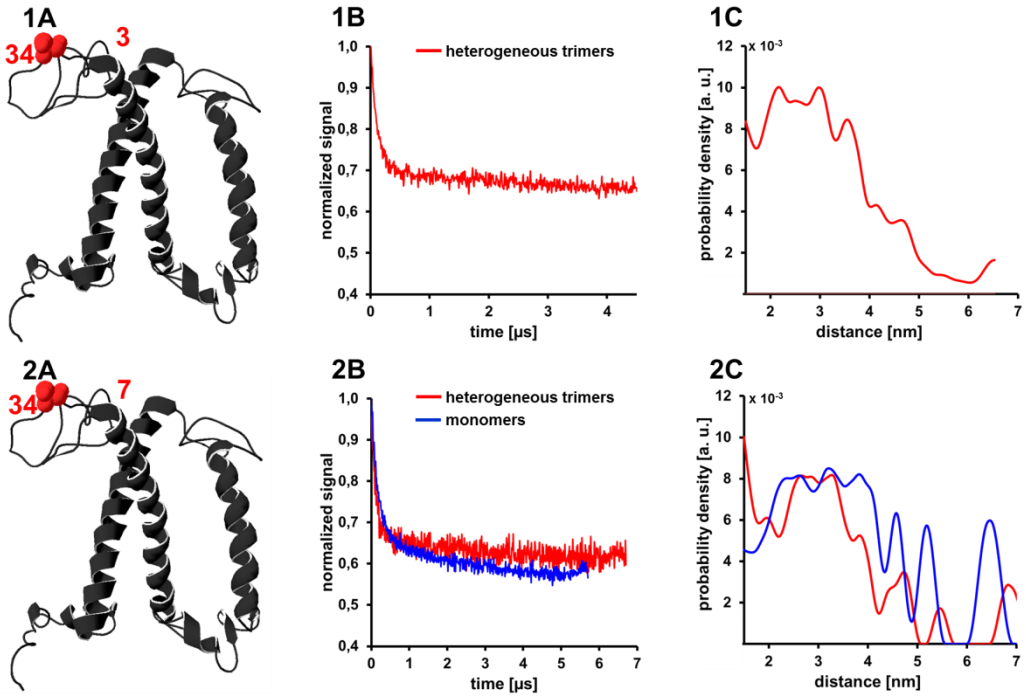

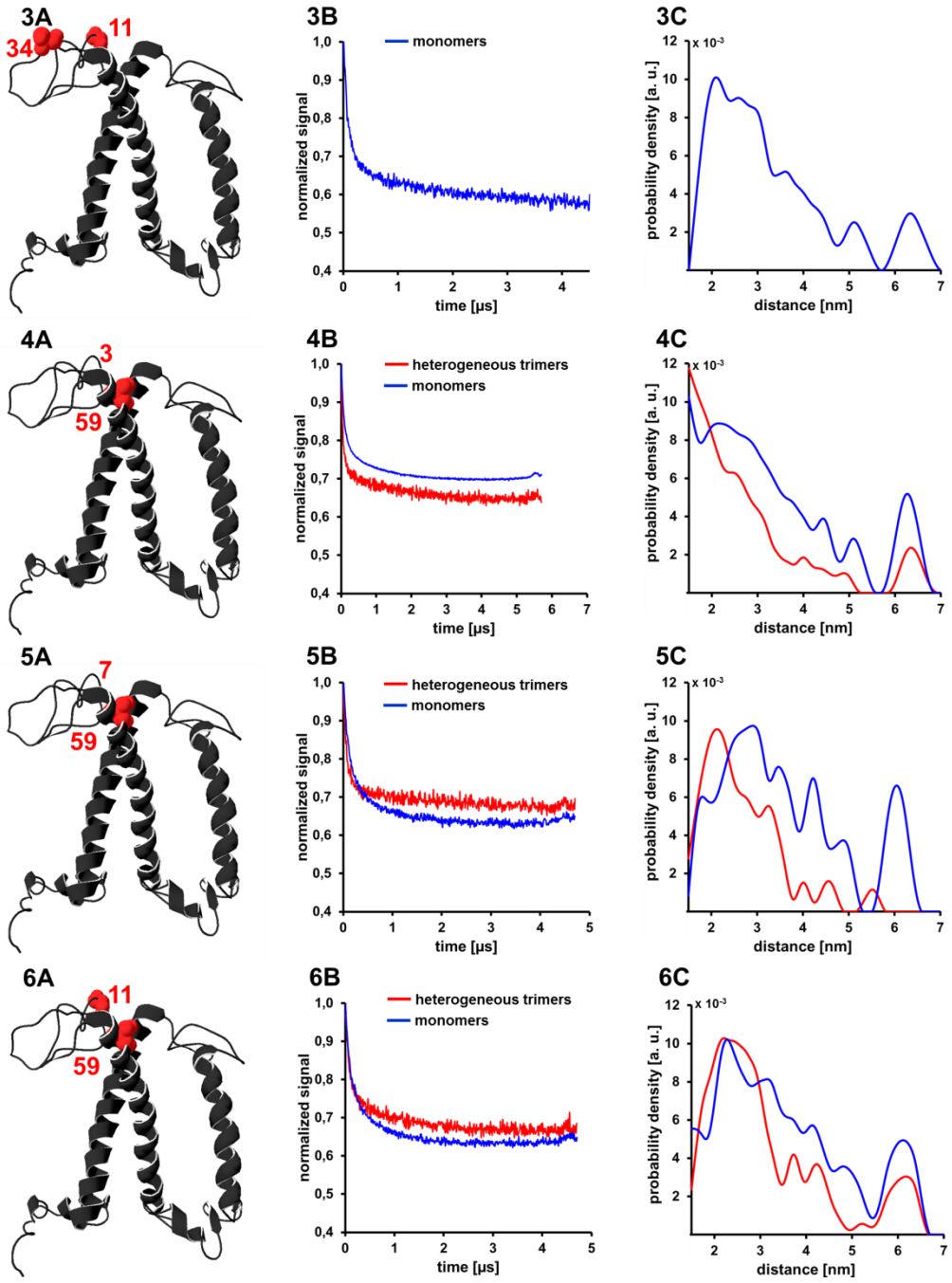

Figure 3.57: DEER-EPR measurements of the N-terminal domain of the detergent-solved LHCII to compare flexibility in a monomeric and trimeric assembly. PROXYL-labeled amino acids 34 and 59 were used as anchor positions. Amino acids 3, 7 and 11 were located in the unresolved part (X-ray crystallography) of the protein, replaced by Cys and spin labeled. A: Labeled positions within in the X-ray structure are marked as red dots as far as possible; B: Primary EPR data; C: Distance distributions of monomers (blue), heterogeneous trimers (red) and MMM simulation (green). MMM simulation was limited to resolved parts of the protein.

3.6.3. The lumenal loop of the LHCII

The lumenal loop of the LHCII supposedly is involved in a regulation mechanism called non-photochemical quenching (NPQ) to protect the protein-pigment complex under stress conditions. Effects of the pH value to the loop region are discussed controversially (1.2.3.2). It is still unclear whether or not a conformation change takes place. Besides NPQ there are further unanswered questions. Refolded and fully-pigmented LHCII mono- and trimers show a typical fingerprint in CD spectroscopy (Figure 3.6). If neoxanthin (neo) is lacking, monomers look like trimers and trimers show a much deeper 470 nm peak in CD. Furthermore, trimerization on the Ni-column might lead to a loss of the lipid DGDG, which could influence the conformation.

In order to analyze the lumenal loop region, several amino acids within and near this region were replaced by cysteins, spin labeled, and refolded. Results of the biochemical characterizations are shown in Figure 3.6. Rigidity of each labeled position was checked by measuring intermolecular distances of single labeled mutants in a trimeric assembly.

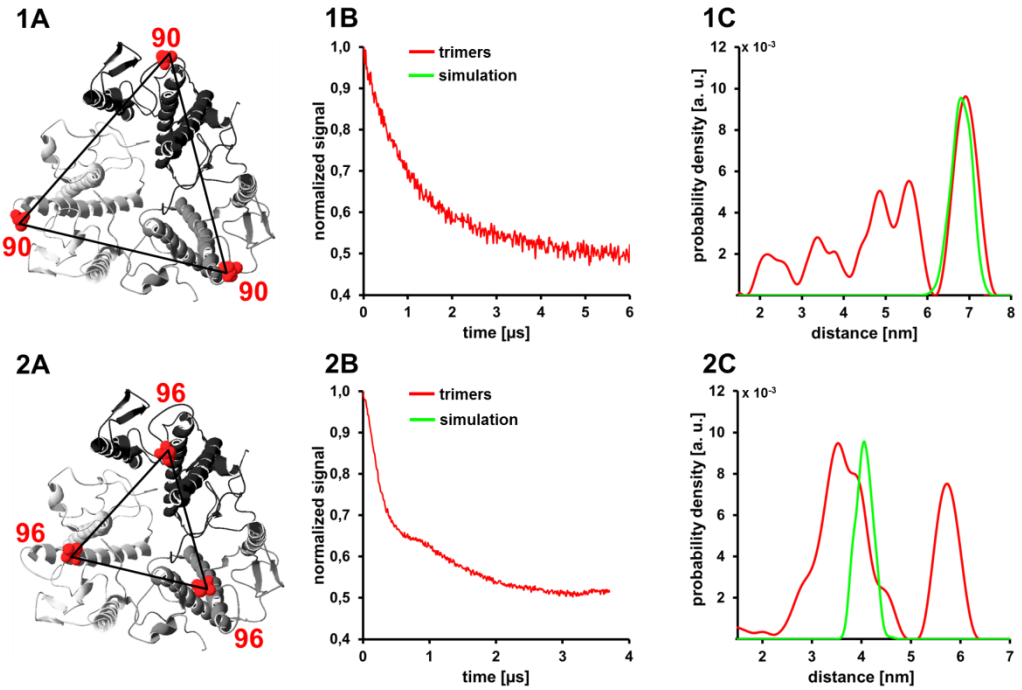

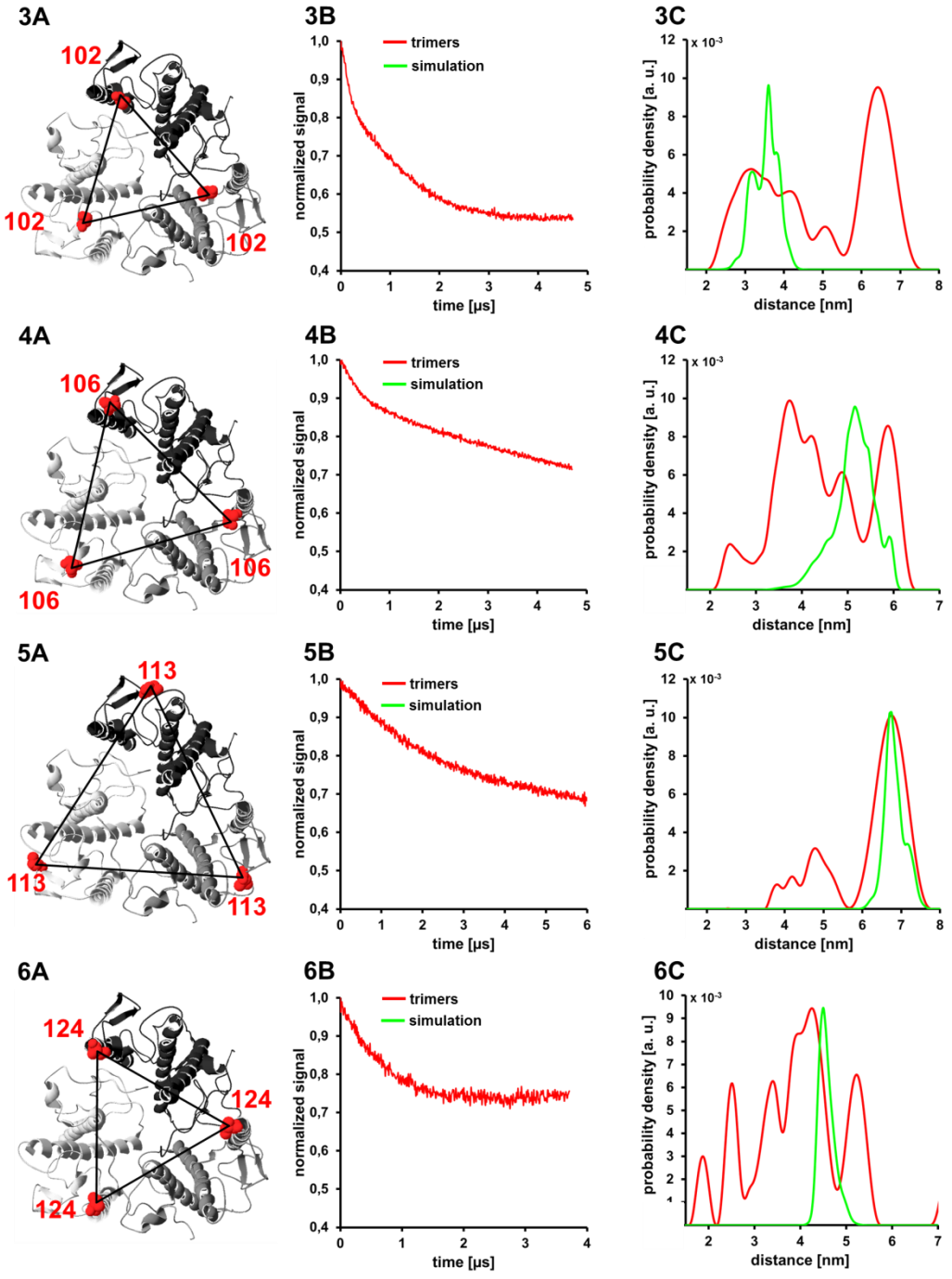

Figure 3.58: DEER-EPR measurements of detergent-solved LHCII trimers and their comparison to the MMM simulated distributions. A: Labeled positions within in the X-ray structure are marked as red dots; B: Primary EPR data; C: Distance distributions of trimers (red) and MMM simulation (green).

Main peaks of the positions 90, 96, 102, and 113 were similar to the predicted distance distribution by MMM simulation, whereas positions 106 and 124 deviated. Results of the mutants 106 and 124 were critical because a background correction affected the shape and appearance of the distance distributions. All other trimeric samples showed a broader distance distribution with more peaks than predicted by MMM simulation. It must be taken into account that these data should be seen as a first indication because a correction of three- and/or higher order contributions (aggregates) in the trimer signals were not taken into account and corrections are still in progress. A removal of these contributions combined with reduced amounts of aggregates might lead to distance distributions that correspond much better to the main peaks.

Previous analysis of lumenal loop data (Dietz, 2008; Berger, 2011) showed first indications for a deviated conformation and it was suggested that a loss of the lipid DGDG during the trimerization process might be the reason (Dockter, 2009). Thus, sample 96 was additionally prepared by adding a molecular excess of plant extracted DGDG to the trimerization buffers.

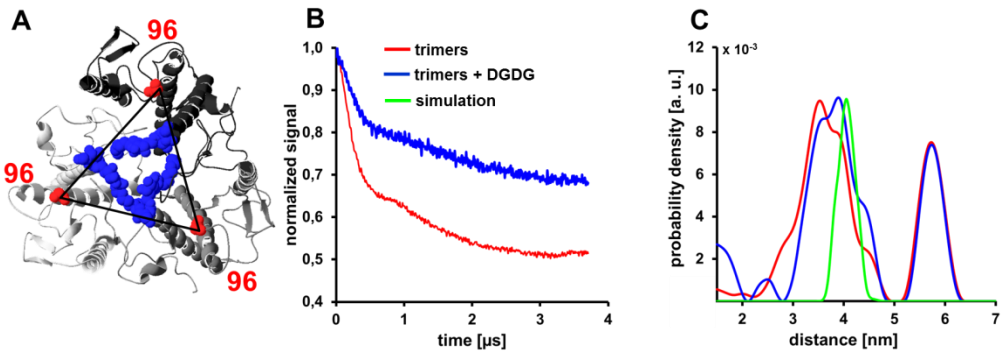

Figure 3.59: Comparison of DEER-EPR measurements of detergent-solved LHCII trimers labeled at position 96 that was trimerized with (blue) and without (red) additional lipid (DGDG) as well as the MMM simulation (green) A: Labeled positions within in the X-ray structure are marked as red dots, the position of the lipid DGDG is shown in blue; B: Primary EPR data; C: Distance distributions.

Results could show that both preparation methods led to similar distance distributions. The peaks at 5.8 nm were caused by aggregates. The mutant that was trimerized with additional DGDG had a worse signal no noise ratio. Both distance distributions were broader than predicted by MMM simulation.

In order to analyze effects of a pH shift and the composition of pigments, double labeled monomers were used. Samples that were prepared under *in vivo* similar conditions (fully-pigmented at pH 7.8) were compared with protein-pigment complexes that were isolated

at pH 4.5 and those lacking neo. For a better overview results of mine and of my diploma student (Berger, 2009) are shown.

All constructed mutants were spin labeled within or near the lumenal loop region. MMM simulation predicted the positions 90 (helix 1) and 124 (helix 3) as rigid positions, thus they were chosen as reference points from where potentially flexible positions within the loop region could be measured. In order to determine flexible regions as precisely as possible, several positions in the loop domain were chosen to form spin pairs with either reference points. Position 96 is located directly between the helices 1 and 2, position 102 inside the helix 2, position 106 between the helix 2 and the ß-sheet, and position 113 inside the ß-sheet.

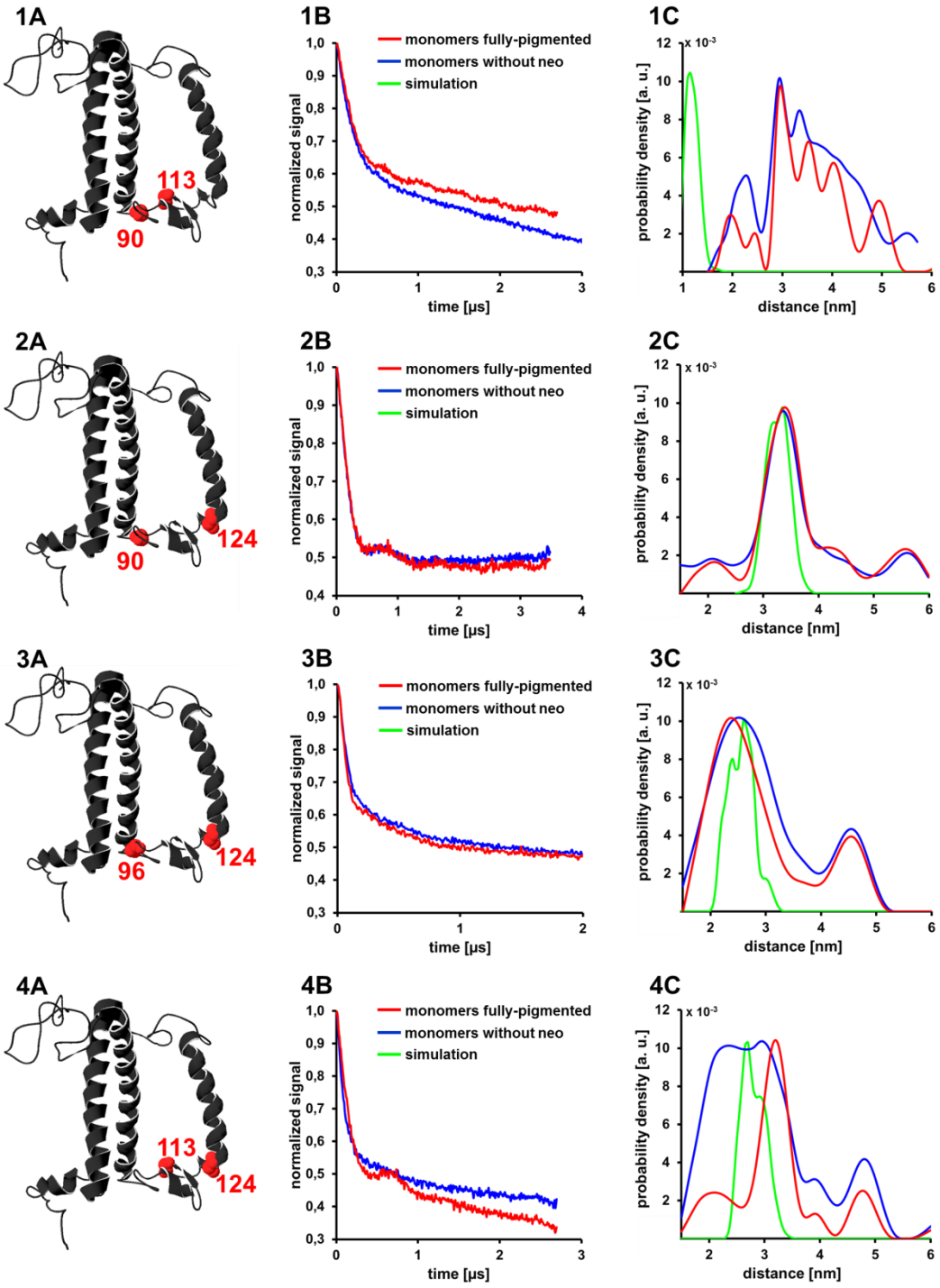
1A
113
90
1B
monomers fully-pigmented
monomers without neo
simulation
normalized signal
time [µs]
1C
x 10-3
probability density [a. u.]
distance [nm]
2A
124
90
2B
monomers fully-pigmented
monomers without neo
simulation
normalized signal
time [µs]
2C
x 10-3
probability density [a. u.]
distance [nm]
3A
124
96
3B
monomers fully-pigmented
monomers without neo
simulation
normalized signal
time [µs]
3C
x 10-3
probability density [a. u.]
distance [nm]
4A
113
124
4B
monomers fully-pigmented
monomers without neo
simulation
normalized signal
time [µs]
4C
x 10-3
probability density [a. u.]
distance [nm]

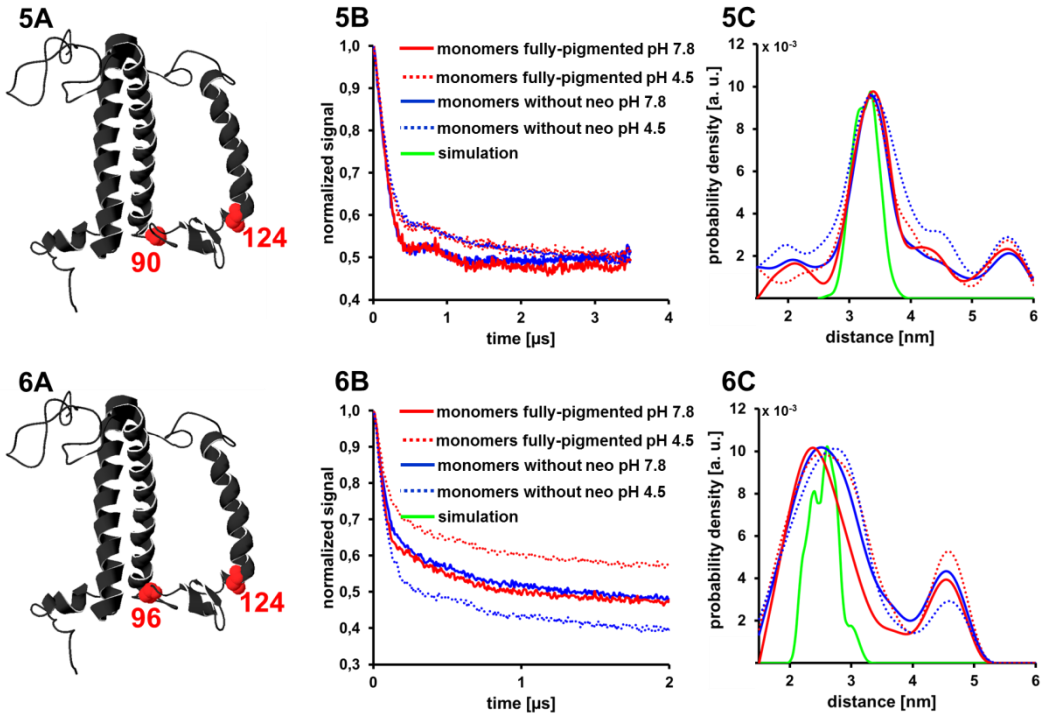

Figure 3.60: DEER-EPR measurements of detergent-solved LHCII monomers and their comparison to the MMM simulated distributions. A: Labeled positions within in the X-ray structure are marked as red dots; B: Primary EPR data; C: Distance distributions of fully-pigmented monomers (red), neo-free monomers (blue) and MMM simulation (green). Dotted lines (only mutants 90/124 and 96/124): variations of the pH value.

The main distance peaks of the mutants 90/124 (Figure 3.60-2) and 96/124 (Figure 3.60-3) were similar to those predicted by MMM simulation. Both were a somewhat broader and showed one more distance peak in the longer-distance range (above 4 nm), due to a contamination by aggregates. Variations of the pH value and pigment composition (with or without neoxanthin) did not influence distance distributions of these mutants (Figure 3.60-5 and 6). Detailed numbers of the distance distributions and maxima are shown in Table 3.7. All mutants that contained a spin label at position 113 by contrast differed from the predicted distance distributions. The width of the fully-pigmented sample 113/124 (Figure 3.60-4) was similar to MMM simulation but the maximum showed a 0.5 nm longer distance. The distance distribution of the neo-free mutant was much broader and showed a higher amount of shorter distances. Measurements of the mutant 90/113 (Figure 3.60-1) differed a lot from MMM simulation, which predicted distances that were beyond the detection limit of DEER-EPR (1.15 nm). Both prepared samples showed a much broader distance distribution with a maximum of the main peak near 3 nm. The distance distributions were similar but in order to check the amount of shorter distances near the

prediction of MMM simulation, the field sweep spectrum was taken into account because short distances (of about 1 nm) are represented by a spin-spin interaction shoulder.

Table 3.7: Detailed numbers of distance distributions of all double labeled mutants and MMM simulations. Listed distances were limited to the main peak.

labeled positions	pigment composition	pH value	main peak	
			distance distribution	maximum
90/124	MMM-simulation	7.8	2.60 - 3.80 nm	3.30 nm
	fully-pigmented		2.50 - 3.90 nm	3.35 nm
	without neo		2.50 - 3.90 nm	3.35 nm
	fully-pigmented	4.5	2.50 - 4.20 nm	3.30 nm
	without neo		2.30 - 4.20 nm	3.35 nm
96/124	MMM-simulation	7.8	2.00 - 3.35 nm	2.54 nm
	fully-pigmented		1.50 - 3.40 nm	2.35 nm
	without neo		1.50 - 3.80 nm	2.45 nm
	fully-pigmented	4.5	1.50 - 3.65 nm	2.52 nm
	without neo		1.50 - 3.65 nm	2.68 nm
113/124	MMM-simulation	7.8	2.25 - 3.45 nm	2.70 nm
	fully-pigmented		2.50 - 3.70 nm	3.16 nm
	without neo		1.50 - 4.20 nm	2.20 - 2.90 nm
90/113	MMM-simulation	7.8	1.00 - 1.65 nm	1.15 nm
	fully-pigmented		2.62 - 4.47 nm	2.95 nm
	without neo		1.55 - 5.00 nm	2.92 nm

A comparison of the field sweep spectra showed indications for a higher amount of shorter distances in the fully-pigmented sample caused by the appearance of spin-spin interactions shoulders (Figure 3.61-red arrows). It seemed that the presence or absence of neo influenced distance distributions, if position 113 was involved. Therefore, a comparison of position 113 in a trimeric assembly at varied pigment composition was done (Figure 3.62). Results showed differences in the distance distributions. The main peak of the fully-pigmented sample was between 5.5 and 7.5 nm with a maximum at 6.7 nm and thus, similar to the MMM simulation, which predicated a distance distribution between 6 and 7.5 nm with a maximum at 6.7 nm. The

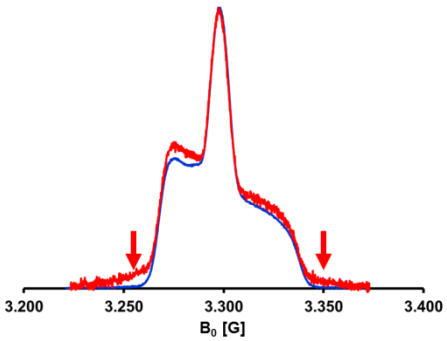

Figure 3.61: Field sweep of the mutant 90/113 with (red) and without (blue) neoxanthin. The neo free sample showed spin-spin interaction shoulder (marked by red arrows). B_0: magnetic field.

main peak of the neo-free mutant by contrast was between 5.5 and 6.5 nm with a maximum at 6.1 nm. Additional peaks of both samples in lower distance ranges were caused by aggregation.

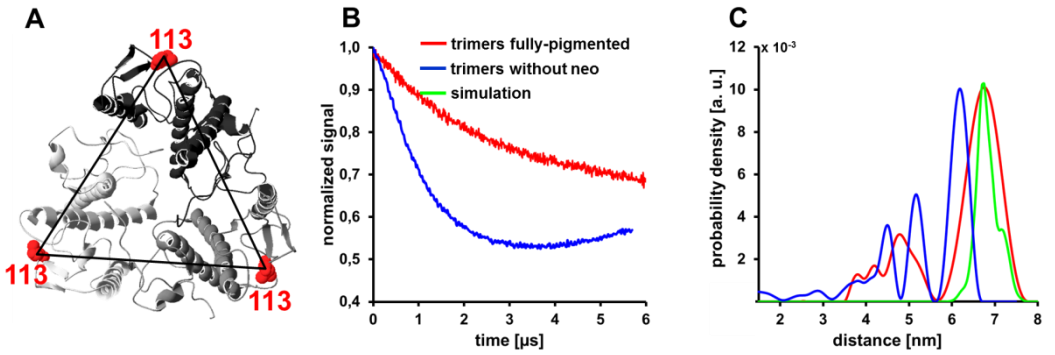

Figure 3.62: DEER-EPR measurements of the mutant 113 in a trimeric assembly with varied pigment composition. A: Labeled positions within in the X-ray structure are marked as red dots; B: Primary EPR data; C: Distance distributions of fully-pigmented monomers (red), neo-free monomers (blue) and MMM simulation (green).

4. Discussion

4.1. Construction and characterization of new LHCII mutants

Replacements of amino acids in order to produce Cys mutants are essential for EPR labeling. Site directed mutagenesis in comparison to traditional methods like restriction and ligation of fragments already containing the mutated sequence is faster (Dockter, 2009; Müller, 2008) but also more expensive. However, costs could be sufficiently reduced by using half volumes of the PCR-mixture as well as XL1-blue super competent cells. Instead of 33.18 € per reaction (status 2012, Stratagene), costs could be reduced to 16.59 € per reaction. The yield of bacteria cells containing the new construct decreased to 60-70 %, but a couple of mutagenesis reactions were problematic independently from the used mixture volume. A specific reason could not be identified but the usage of the tenfold amount of template combined with a longer incubation time of DpnI could compensate problematic mutagenesis with low yields.

In contrast, multiple replacements within one reaction were critical (3.1.2 – mutant A10S/S12P/P15S/C79Sh). The manufacturer pointed out (personal comment, Stratagene) that this was not tested and thus, no information was available. Nevertheless, a multiple replacement was tested, because changes were limited to three DNA bases in order to construct the new mutant (Table 4.1). However, five attempts were needed to produce this tetra-serine mutant. Probably the attachment of the primers was less, although overhangs on both sites were long enough. Finally, the tenfold amount of template combined with a longer DpnI digestion was successful, but the yield was low and thus, three single replacements would be more efficient. It can be concluded that mutation of one site works perfect, but efficiency decreases drastically when more sites are targeted simultaneously (Seyfang and Jin, 2004). Multiple site-directed mutagenesis methods (Michaelian and Sergeant, 1992; Bhat, 1996) require multiple rounds of PCR (Lee *et al*., 2002), leading to a higher risk of undesired reactions. An alternative procedure was described, allowing more than ten simultaneously

Table 4.1: Amino acid changes in order to construct the mutant A10S/S12P/P15S/C79Sh. Changed amino acids respectively DNA bases are labeled in red.

position lhcb sequence		10	11	12	13	14	15
template	aminoacid	Ala	Ser	Ser	Gly	Ser	Pro
	codon	GCG	AGC	TCT	GGA	AGC	CCA
mutant	aminoacid	Ser	Ser	Pro	Gly	Ser	Ser
	codon	TCG	AGC	CCT	GGA	AGC	TCA

mutagenesis, which can use double-stranded DNA, and is performed in a single round (Seyfang and Jin, 2004). This method, which is a combination of mutagenesis by using phosphorylated primers with a long binding sequence and ligation, seems to be more suitable for multiple mutagenesis reactions, which was also shown by the construction of mutants, either with additional tags or inserted amino acids.

All constructed mutants showed usual yields in the overexpression with one exception: overexpression of the mutant SSPGSSNC79Sh failed, although the sequence including the TATA-box was correct. In mutagenesis reactions care should be taken that frequent codons are preferred (Table 2.3). A low frequent codon (Hénaut *et al*. 1996) in the sequence was detected and replaced but this had no effect (Richard, 2011). The same problem was observed and analyzed with the mutant hNC79Sts, which has the motif in the C-terminal domain (Richard, 2011). Transformation in another bacterial strain *E. coli* (Rosetta^{TM}) did not led to an overexpression. However, the third tetra serine mutant (A10S/S12P/P15S/C79Sh) could be overexpressed and for lack of time, the source of error was not analyzed in detail (Richard, 2011).

During the characterization a couple of refolded mutants showed untypical CD spectra. It was proposed that these deviations might be caused by untypical replacements of the amino acids leucin and isoleucin (Berger, 2010). On one hand these kinds of mutations were done in other proteins without any influences. In F-Actin (Scoville *et al*., 2009) and arrestin (Hanson *et al*., 2007) leucine were replaced, respectively without any problems. On the other hand the replacement of isoleucine at position 143 had no influence. It seems that incorrect refoldings as well as trimerization and protein instabilities are limited to critical regions. This view is supported by the results of lumenal loop mutants, the mutant V196Ch (Dockter, 2009) and some N-terminal domain mutants (Müller, 2008) independently of specific replaced amino acids. Lumenal loop mutants were affected in particular exhibiting reduced refolding yields and reduced protein-pigment complex stabilities. The lumenal loop region contains several amino acids, particularly the acid ones that could not be replaced without a loss of function (Mick, 2004). Further critical positions are between the amino acids 97-101, consisting of the sequence WFXAG which is highly conserved in all chl-binding proteins (Green and Pichersky, 1994). The mutant stL113C/I124Ch was instable at pH 4.5, leading to a reaction of chl *a* to phaeophytin (Berger, 2010). The pH sensitivity correlates with a reduced CD signal at 680 nm (Geister, 2003), which was monitored at the mutant stL113C/I124Ch (Figure 3.6 A). Further deviations were observed with the mutants S106Chc, S123Ch (Dietz, 2008), E107V, D111V (Yang *et al*., 2008), stV102C/I124Ch, stV90C/L113Ch, stI124Ch (Figure 3.6 A), which showed typical spectra for neoxanthin lacking mutants (Hobe *et al*., 2006). Without

neoxanthin the peak at 472 (-) nm was more pronounced (Figure 3.6 B). Structural effects, caused by these mutations are discussed in 4.5.2.

The trimerization yield was mostly comparable to the wild-type similar mutant C3.2h, with the exception of the lumenal mutants S106Chc, S123Ch (Dietz, 2008), stI124Ch (Berger, 2011) and some N-terminal domain mutants (Müller, 2008). Between the amino acids 16-21 the trimerization motif is located (Hobe *et al*., 1995) and it was already shown that changes within this motif resulted in a decrease or loss of trimerization (Müller, 2008; Dockter, 2009). Replaced residues of the tetra-serine motif mutant A10S/S12P/P15S/C79Sh were not within but directly near the trimerization motif and this mutant did not form trimers, neither by using the Ni-column nor by using the liposomes (Richard, 2011). Alanine and proline are non-polar amino acids, whereas serine is polar. The replacement of two non-polar against two polar residues (A10S and P15S) seems to cause the loss of trimerization because changes are close to the trimerization motif and hydrophobic interactions between the non-polar amino acids of the N-terminal domain and pigments (Liu *et al*., 2004) as well as the lipid PG (Nußberger *et al*., 1993) are also essential for trimerization. Replaced amino acids of the lumenal loop mutants are by contrast far away from the trimerization motif. It is conceivable that the same replacements, for example mutant stL113C/I124Ch, where two non-polar amino acids were replaced by two polar cysteine, led to changed interactions with pigments, which could influence trimerization (Liu *et al*., 2004). This proposition is supported by extended sensitivity of the mutant stL113C/I124Ch at low pH values.

4.2. The quality of EPR samples depends on several conditions

EPR techniques that are used for protein analyses require site-directed spin labels attached to the protein sample. In the end 30-40 µl of protein solution is needed. EPR signal quality on a given EPR spectrometer depends on many factors and the most important are: protein labeling efficiency, inversion efficiency (number of flipped spins), detection quality (depends on the pulse settings and on the spectrometer quality), stability of the spin label, concentration of the protein solution as well as sample purity. In the DEER experiment, the labeling efficiency (f) and inversion efficiency (λ) affect the value of the modulation depth (Δ) caused by the correlation: $\Delta = 1-\lambda \bullet f$ (for a two spin system) or $\Delta = 1-(1-\lambda)^{N-1}$ (for a multi-spin system) providing that $f < 1$. The higher the protein concentrations the higher the numbers of detectable spins in the probe volume and hence signal intensity but

too large concentration leads to an increased relaxation and supports aggregation. Effects to the DEER experiments are a steeper DEER trace decay, reduced precision, the detection of long distances becomes difficult, and background correction is difficult (Polyhach *et al.*, 2012). Therefore, highly purified protein samples are necessary to get rid of partly or unfolded protein. Usually, in X-band EPR (~9.5 GHz, B_0 = 3500 G) a protein concentration of approximately 200 µmol/l and in Q-band (~34.5 GHz, B_0 = 12200 G) of approximately 50 µmol/l (personal comment Dr. Y. Polyhach, ETH Zürich, 2012) is needed for a very good signal to noise ratio with a good compromise between amount of detectable spins labels and not too much increased relaxation.

Detailed analyses of three different sizes of sucrose gradients (3.3.1) showed that the purification quality depends highly on the size and preparation method of the sucrose gradients formed by freeze thaw cycles. As the number of freeze-thaw cycles increased, the purification quality decreased (Figure 3.9) because the steepness of the gradient was doubled by three freeze-thaw cycles and tripled by fife cycles in comparison to one freeze-thaw cycle. Thus, at the top of the ultracentrifugation tube the sucrose concentration was zero and loaded samples sunk in deeply, leading to blurred areas instead of clear isolated bands after ultracentrifugation, which includes a higher risk of contamination content. However, a separation of unfolded aggregates and monomers requires a longer passage of the sample through the sucrose gradient. Thus, variations of the sucrose concentration combined with small gradients seem to be the best solution because the surface is small and applied volume low. It was shown that purification quality decreases as the gradient sizes and the time period between the thaw process and its usage increases (Figure 3.10). This effect can be explained by diffusion processes. Based on the first Fick`s law the flux goes from regions of high concentration to regions of low concentration, with a magnitude that is proportional to the concentration gradient. The diffusion coefficient in liquid solutions is described by the Stokes-Einstein formula. Decisive factors are the viscosity and temperature of the solution as well as the hydrodynamic radius of the solvent. According to Einstein, the diffusion course is proportional to the square root of the time ($\lambda_x = \sqrt{2DT}$). Calculated with the diffusion coefficient for sucrose solution in water ($D = 5.22 \cdot 10^{-10}$ m^2/s), the diffusion course of sucrose molecules within one hour is 1.94 mm and within 24 hours 9.5 mm. Diffusion processes increase as the gradient size increases, which was extremely represented in the large (SW28) gradients. Due to the large diameter, ultracentrifugation tubes are difficult to handle, vibrations are inevitable and during acceleration as well as deceleration of the rotor susceptibility to disturbances is increased. Thus, small gradients should be preferred. The only disadvantage is a lower amount of purified protein but this can be compensated by stronger EPR spectrometer. For monomeric sample preparation additional sucrose concentrations should be tested,

because the passage through the gradients and thus, separation of monomers and trimers could be increased by using 0.55 mol/l sucrose. Probably special gradients for monomers and a collection of monomers, which is limited to the lower part of the band might solve this problem and is tested by N. Fehr.

After an EPR sample is measured, primary data are processed by Fourier transformation, Thikonow regularization and background correction, leading to the distance distribution spectrum. This distance distribution can be compared with the predicted theoretical distance distribution by using multiscale modeling of macromolecular systems (MMM) simulation, which bases on crystal structure data. Thus, distance distributions of mutants that were labeled within the rigid core should be very similar to experimental data (Dockter *et al.*, 2011) but previous experiments showed that besides the predicted main distance peaks often further unexpected distance peaks were determined. On one hand these peaks might represent real distances or they could be caused by unwanted side effects, like artifacts from the background correction or higher oligomerization states of protein. An increased amount of these peaks appeared in particular in monomeric samples and seemed to depend in most cases on the protein concentration (Bender, 2004; Dietz, 2008; Müller, 2008; Dockter, 2009; Berger, 2010; Kaufmann, 2011; Lauf, 2012), which is an indication for unwanted side effects. A formation of aggregates might be caused by different detergent concentrations in the EPR samples because the initial protein concentrations of the purified bands in the sucrose gradients vary from 2 – 8 µmol/l. Thus, some samples require a stronger increasing step of the concentration until the final EPR sample concentration is reached than others and during this step approximately 75 % of the detergent remains in the sample (3.4). The higher the content of detergent, the higher the risk that pigments move into empty detergent micelles, leading to an aggregation of protein-pigment complexes. However, a series of refolded LHCII samples with increasing concentrations could not confirm this suggestion. All samples led to identical CD spectra (Figure 3.24). Any indications for protein aggregates, which form a negative band in the chl *a* region around 438 nm (Ruban *et al*., 1997) or an additional peak upon 700 nm were not determined. Due to the high amount of monomers, spontaneously formed trimers are an alternative procedure but they would be detectable by an increased CD signal at 470 nm, which was not the case. Furthermore, neither low denaturing gel electrophoresis nor the separated bands of the ultracentrifugation gradients showed any indications for aggregates or trimers within the purified colored protein bands. EPR measurements of these samples by contrast showed a content of 10 – 20 % of non-predicted peaks (Figure 3.27), which is comparable to older samples (Bender, 2004). It is highly unlikely that spontaneous formed trimers caused these non-predicted peaks because the usage of phospholipase A_2 (Nußberger *et al*., 1993; Bender, 2004) or lipid free pigment extract

avoids a trimerization process efficiently but nevertheless, non-predicted peaks also appeared in PG lacking samples.

If neither trimers nor aggregates of refolded protein cause the contamination of EPR samples, non-pigmented protein aggregates might be the reason. This hypothesis is confirmed by obtained results because these aggregates are not colored and therefore, not distinguishable in the sucrose gradients and not detectable in CD spectroscopy, which bases on pigment interactions (Ruban *et al*., 1997). In EPR spectroscopy by contrast labeled and unfolded protein aggregates would lead to non-predictable distances. This scenario could also explain that contamination occurs preferably in monomeric samples because current results (Fehr, unpublished data) showed that the distance between unfolded aggregates and trimers within the sucrose gradient is larger. A further indication is the kind of the ultracentrifugation gradient that is used for purification. Monomeric samples that were purified in the medium (SW40/SW41) gradients (Lauf, 2012) contained a higher content of non-predicted peaks than monomeric samples that were purified in small (SW60) gradients, which showed a higher purification quality. Current results (Fehr, unpublished data) of the mutant 34/59 showed that the lower monomeric gradient band did not lead to non-predicted peaks, whereas the upper band did. Thus, unfolded protein aggregates seem to be close to the monomeric band.

Beside a potential aggregation, EPR measurements revealed a lower modulation depth as well as a decay rate that did not correspond to the nominal concentration. A decrease of the experimental modulation depth indicates a low labeling efficiency. Protein labeling efficiency was analyzed biochemically and should be over 90 % (Dockter, 2009). However, a confirmation by EPR spectroscopy seems to be unavoidable and is currently tested by N. Fehr. Nevertheless, high labeling efficiency, well purified protein samples and less contamination are essential for a good signal to noise ratio in EPR experiments but become less important, if the PROXYL label is losing its radical status within the biological system. Pioneer research about nitroxides and radicals was published three decades ago (Forrester *et al*., 1968; Rozantsev, 1970; Balaban, 1971; Rozantev and Scholle, 1971; Aurich and Heiss, 1976; Janzen, 1971). Several nitroxide radical labels in order to use them in EPR studies were analyzed and results published in an overview (Keana, J. F. W., 1977). Most stable nitroxide free radicals are secondary amine N-oxides in which there are no hydrogens attached to the α-carbon atoms. In contrast, one or more hydrogen atoms attached to the α-carbon atom of the nitroxide group supports a disproportionation reaction of the radical (Bowman *et al*., 1971; Martinie-Hombrouck and Rassat, 1974), producing a nitrone and N-hydroxyamine, either or both of which may undergo further reaction (Keana, J. F. W., 1977). Today, a large number of nitroxide free

radicals are chemically stable and the used PROXYL-IAA label complies with all requirements. However, influences of all chemical ingredients to the PROXYL label during labeling and reconstitution process were never tested but important because evidences for a reduction process were determined.

During the labeling process TCyEP is the standard reducing agent because it contains no SH-groups and thus, does not compete with cysteins for the binding of the label. Nevertheless, for comparison ß-me was also checked (Figure 3.21). Both reducing agents led to a similar decrease of the PROXYL signal. It is interesting that in reference 3 that was incubated for 12h but contained no reducing agent, the PROXYL signal also decreased to 87 %. Studies about the stability of pyrrolodin nitroxides showed that the spin label dissolved in buffer (pH 7) and incubated at 20°C as well as at 37°C was stable over ten weeks (Kroll, 1999). The manufacture (Sigma Aldrich) points out that PROXYL-IAA is light and heat sensitive but samples were boiled before the label was added and always kept dark. Thus, a decrease of the signal during the labeling process seems to be inevitable. Alternative reducing agents, for example TCcEP that is also used in combination with the LHCII (Gundlach, 2010) are not suitable. TCcEP contains three carboxylic acid groups, supporting a reduction of the pH value. Intensive studies could show that nitroxide EPR labels are highly instable at low pH levels (Kroll, 1999). Piperidinoxides were particularly vulnerable. Their EPR signal decreased within several minutes to zero. However, pyrrolnitroxides were much more stable but 50% of the signal was also lost. This reaction is reversible but nevertheless; further reactions destroyed some amount of the label irreversible. In order to precipitate the labeled protein, acetone should be used instead of 5 % trichloroacetic acid (TCA) to avoid a low pH value.

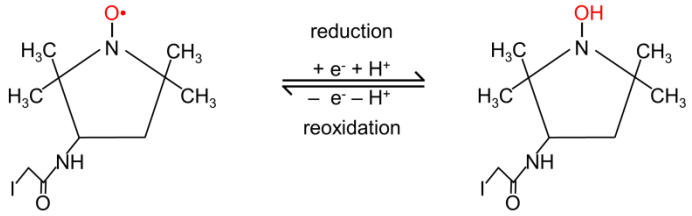

Figure 4.1: Reduction and re-oxidation process of the PROXYL-IAA.

During the reconstitution process ß-me is used as standard reducing agent and preparation is done in the dark to protect pigments and avoid the production of reactive oxygen species.

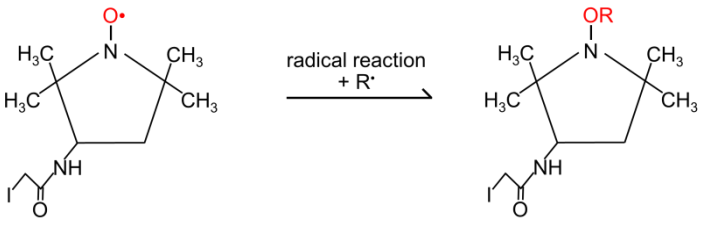

Figure 4.2: Radical reaction process of the PROXYL-IAA

The decrease of the PROXYL signal of all samples that did not contain any reducing agent was moderate. This is astonishing because neither sunlight nor UV light could influence PROXYL stability. It would have been possible that light energy support a radical reaction and thus, a loss of signal. Furthermore, it is astonishing that a combination of reducing agent and sunlight had a much stronger effect on the signal. UV light is able to destroy organic bonds but this seems not to be the fact here because otherwise the samples without reducing agent should show a similar loss of EPR signal.

Besides a radical reaction, molecules containing a radical are able to react in two directions: reduction (Figure 4.1) or oxidation (Figure 4.3). However, the oxidation of the PROXYL label seems to be unlikely, because if an oxidation had taken place, all mixtures containing reducing agents should show a stronger EPR signal in the end, caused by a protection effect of the reducing agent but the opposite turned out to be the case. In living cells it could be determined that hydroxylamines were oxidized to nitroxides in the presence of oxygen (Chen and Swart, 1990). Lipid-soluble hydroxylamines were oxidized much faster than water-soluble ones. Furthermore, indications were found that this process is enzyme-linked. In the case of the LHCII reconstitution, neither living cells were used nor were enzymes located in the micelles. Therefore, two possibilities remain. Either the radical label was reduced to a hydroxylamine and had no chance for a re-oxidation or a radical reaction caused by a combination of UV light and dissolved oxygen, leading to reactive oxygen species had taken place. Without further experiments it is impossible to find the exact reason but in an additional experiment it could be shown that the reconstitution process led to similar yields without using any reducing agent (Figure 3.23). The mutant C3.2h, containing a free cysteine could be reconstituted with either ß-me or TCyEP as well as TCcEP with a very good yield. As already described and discussed TCcEP should be avoided in the presence of PROXYL labels. In contrast, without reducing agent the yield decreased to 50 %. That could have been expected because disulfide bonds were not broken. The labeled mutant as well as the unlabeled cysteine-free mutant could be reconstituted with approximately 100 %. In combination with the results above, the best way to reduce any risks according to the spin label is a reconstitution without any reducing agent.

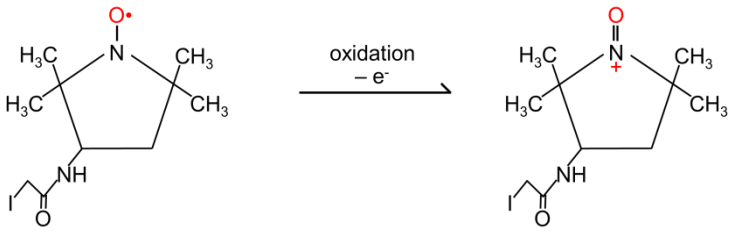

Figure 4.3: Oxidation process of the PROXYL-IAA.

4.3. Insertion process of immobilized LHCII into liposomes

Analyses of membrane proteins are difficult caused by their tendency to aggregate and precipitate in the absence of membranes. Famous examples for *in vitro* refolded and studied membrane proteins are the voltage-dependent anion channel (Engelhardt *et al*., 2007), the mammalian G protein-coupled receptor (Michalke *et al*., 2010), bacteriorhodopsin (Huang *et al*., 1981) and the LHCII (Plumley and Schmidt, 1987; Paulsen *et al*., 1990). For micking the *in vivo* situation, incorporation into liposomes would be a promising solution. A non-directed insertion of the LHCII into liposomes could be still established (Boggasch, 2006; Yang *et al*., 2006) but is not suitable for EPR measurements. A unidirectional insertion is essential, on one hand to avoid confusing signals of the attached spin labels and on the other hand to mimic regulation processes like the non-photochemical quenching by preparing a pH gradient over the membrane. One membrane protein that could be inserted unidirectedly is the F_0F_1-ATPase (Richard *et al*., 1990; Levy *et al*., 1992; Rigaud and Pitard, 1995). However, several factors influence an insertion: the characteristic of the protein, the composition of lipids, the detergent, the lipid to protein ratio (lpr), and the principle of insertion.

The F_0F_1-ATPase consists of two substantially different hydrophobic termini, which considerably simplify insertion. According to the LHCII differences are limited; the N-terminal domain contains 57 % hydrophilic and 43 % hydrophobic amino acids, the C-terminal domain 69 % hydrophilic and 31 % hydrophobic amino acids. An attachment of a large hydrophilic green fluorescence protein (GFP) to the LHCII, in order to support a directed insertion failed (Boggasch, 2006). Thus, in this work two LHCII mutants, carrying the his_6 tag at different termini were immobilized on column material and inserted into liposomes. The insertion was monitored by a trypsin digestion and gel electrophoresis. A unidirectional insertion into phosphatidylglyceride (PG) liposomes failed. Possible causes might be on one hand that the stability of the LHCII seems to be reduced in pure phospholipid environment (Boggasch, 2006; Yang *et al*., 2006) and on the other hand that PG liposomes differs a lot from *in vivo* membranes, although the phase behavior of PG is similar to digalactosyldiacylglyceride (DGDG) and sulfoquinovosyldiacyl-glyceride (SQDG) (Sprague and Staehlin, 1984; Selstam, 1998; Williams, 1998). It is known that transmembrane helices of membrane proteins differ in their size and shape and stabilization requires a mixture of lipids with varied package

parameter (Chapman, 1984). Thus, an insertion of the LHCII into liposomes, consisting of 61,9 % DGDG, 21,4 % PG, and 16,7 % SQDG, should be better suited, caused by its similarity to the thylakoid membrane, which consists of 50 % monogalactosyldiacylglyceride (MGDG), 30 % DGDG, and 5-12 % SQDG as well as 5-12 % PG (Murata and Siegenthaler, 1998) and by the specific combination of head groups and fatty acid chains, which stabilize integrated proteins (Hobe *et al*., 1995; Kruse *et al*., 2000; Hagio *et al*., 2000; Sato *et al*., 2000; Latowski *et al*., 2004; Steffen *et al*., 2005; Hölzl *et al*., 2006). However, results could not confirm this hypothesis because variation of the liposome composition did not lead to a unidirectional insertion (Berger, 2011), suggesting that experimental problems, which will be discussed in this chapter, seems to influence the insertion process.

4.3.1. Liposomes are contaminated by detergent

LHCII was firstly reconstituted in OG micelles, secondly immobilized on the Ni-column, and thirdly washed with liposome solution. Detergent was removed by adding Bio-Beads to the eluate. A contamination of detergent would produce holes, which support a penetration of trypsin into the liposomes and thus, enable a digestion from both sides. Bio-Beads were still used in combination with other proteins to absorb OG (Park *et al*., 2004) but it is unclear if all detergent would be removed. An indication that it is not completely removed could be shown by CD measurements. All liposome samples showed negative peaks at 437 and 458 nm (Boggasch, 2002 and 2006; Yang *et al*., 2006; Berger, 2011) and it was proposed that these peaks are typical for LHCII in liposomes (Yang *et al*, 2006). However, the addition of OG and therefore, disintegration of liposomes did not lead to a typical CD spectrum of LHCII in detergent micelles, it remained unchanged. These two peaks were also monitored by pigment aggregates (Ruban *et al*., 1997; Fender, 2001). In order to determine a contamination of detergent some hydrophobic dyes, showing different fluorescence in liposomes and detergent might be suitable. Those dyes should be very hydrophobic to ensure an effective incorporation into liposomes and they should not contain reactive or charged groups. For this purpose three commercially available dyes might be suitable: nile red, solvent red 26 (oil red EGN), solvent blue 14 (oil blue N).

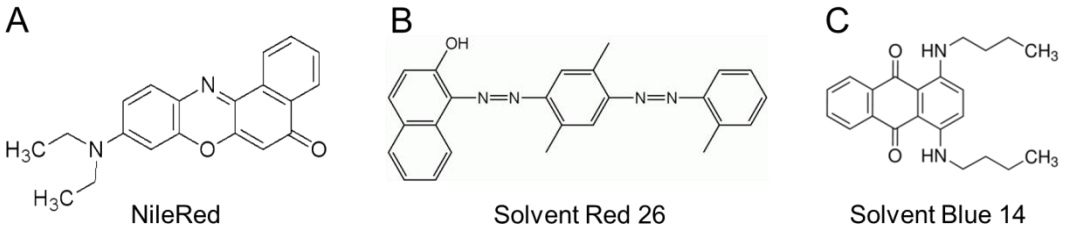

Figure 4.4: Three commercial dyes to detect a contamination of detergent.

Another possibility to remove OG is via dialysis but experiments led to the same CD signal and result of digestion (Berger, 2011). It is published that the orientation of inserted proteins depends on the reconstitution method. The reconstitution of the lactose transporter (LacS) from Streptococcus thermophiles or of the di-tripeptide transporter (DtpT) from Lactococcus lactis could show that the detergent highly influences either a unidirected or a random insertion (Knol *et al*., 1998; Fang *et al*., 1999). According to the LHCII OG could be replaced by Tx, which seems to be very suitable because it can be totally removed by Bio-Beads (Figure 3.37 and Figure 3.38) and seems to support a unidirected insertion by using a lipid to protein ratio of 1000 (Boggasch, 2006).

4.3.2. Influence of the lipid to protein ratio and disintegration of the LHCII

Previous experiments could show that insertion of protein decreased as the lipid to protein ratio (lpr) increased (Boggasch, 2006). It was proposed that less protein interaction might support disintegration. The maximum lpr for monomers seemed to be 1000, whereas trimers were stable up to 1 million. During the production of heterogeneous trimers refolded LHCII formed aggregates or was disintegrated caused by a loss of pigments (3.4). This scenario is also conceivable for the LHCII in liposomes, especially for monomers that are less stable than trimers. The results of the trypsin digestion might be influenced by this procedure because trypsin is able to attack unfolded LHCII efficiently. Furthermore, it should be noted that the reconstitution mix, which was used for an insertion into liposomes, is contaminated by unfolded protein, which was also immobilized onto the Ni-column. An purification step at this point, like it was proposed by Berger (2011) might help but results of monomeric EPR analysis (4.2) raised the suspicion that the monomeric band after ultracentrifugation might contain unfolded aggregates. Thus, it would be better to use trimers, because of their higher stability and better purification quality. One more critical point is aggregation that depends on the lpr.

If the lpr is too low, the protein tends to aggregate. Such a formation of cluster could be monitored by atomic force microscope and was seen at an lpr below 1000 (Boggasch, 2006). This is a big problem because on one hand the lpr should be high enough to avoid aggregation and on the other hand low enough to limit the risk of disintegration. Furthermore, it is not possible to raise the protein concentration of liposomes, thus detection by EPR might be critical if the lpr is too high.

4.3.3. The surface of the Ni-column avoids an unidirected insertion

A comparison of the Sepharose and Macroprep strep column (4.4.2) revealed a smoother surface of Macroprep and thus, less interaction with pigments. The Ni-column consists of the same basic material, the cross-linked, beaded-form of a polysaccharide polymer material. In this work liposomes were prepared by extrusion with a maximal diameter of 100 nm. According to the Ni-column, the manufacturer points out that the diameter of each Sepharose bead is between 45-165 µm. The exact roughness of the surface is unknown but if pits are deep enough, it might be possible that LHCII monomers, having a distance between both terminal domains of ~8 nm are shielded partly from liposomes (Figure 4.5). Thus, a smoother surface of the column material might be useful to ensure a better insertion. For this purpose the Macroprep strep column could be used. Besides this, further experiments should be done with purified LHCII trimers to get rid of unfolded or aggregated apoprotein, to ensure a higher stability of the protein and to have a larger leeway for the lpr. According to the detergent, Tx seems to be more suitable, caused by a better removal and its tendency to support unidirected insertion.

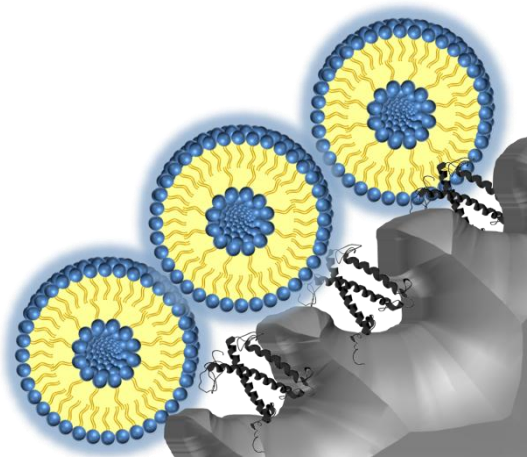

Figure 4.5: LHCII monomers, immobilized in pits of the Ni-column material might be shielded against liposomes.

4.4. Immobilization processes of the LHCII on different column materials

The immobilization of proteins on column materials is a suitable solution for different biochemical applications. According to the LHCII it can be used to form trimers and to purify a mixture of heterogeneous and homogeneous trimers. Since the beginning of the eighties protein tags have been developed but several factors limit their usage, especially in combination with the LHCII. The refolded protein-pigment complex is a comparatively small protein with a limited biochemical tolerance. Therefore, tags like the GST tag cannot be used, caused by its size and other tags like the Arg tag do not fit to the biochemical tolerance of the LHCII because it might influence its tertiary structure and has to be eluted under alkali conditions. Thus, only two protein tags, which are listed in Table 4.2 are suitable for the LHCII: the his_6 tag and the strep tag II.

Table 4.2: List of several selected protein tags and their characteristics (Terpe, 2003)

tag	length	sequence	size	pros and cons
Arg tag	5	RRRRR	0,80 kDa	pros: small cons: influence to tertiary structure; works under alkali conditions
His_6 tag	6	HHHHHH	0,84 kDa	pros: small; works under physiological conditions; cheap
Strep tag II	8	WSHPWFEK	1,06 kDa	pros: small; very specific and high binding affinity cons: expensive
GST tag	211	protein	26 kDa	pros: works under physiological conditions; supports protein solubility cons: tendency to form dimers

The his_6 tag has been used for many years to immobilize tagged LHCII monomers onto the Ni-column to form trimers. However, the preparation of heterogeneous trimers requires an immobilization of LHCII trimers either to the Ni-column (liposome-his_6 tag method; Seimetz, 2004; Dockter, 2005) or to the strep column (streptactin-his_6 method; Kaufmann, 2010; Lauf, 2012) but a lot of these experiments could show that the binding affinity of purified LHCII samples was drastically reduced, independently of the column

material. This is astonishing because the principal of binding is completely different. The interaction of the his_6 tag to the Ni-column bases on complexation, whereas the Strep-tag/Strep-Tactin-system bases on a short peptide, which binds selectively to Strep-Tactin, an engineered streptavidin. For the Ni^{2+}-NTA matrix a binding capacity of 5-10 mg protein/ml of matrix resin with a binding affinity of $K_d = 10^{-13}$ mol/l for a six residue histidine tag at pH 8.0 is published (Schmitt *et al*., 1993). The binding affinity decreases, if the LHCII is refolded, caused by reduced accessibility (4.4.1) but is still strong enough to immobilize monomers efficiently. According to the strep tag II the manufacturer points out that the binding affinity to Strep-Tactin is approximately 100 times higher ($K_d = 10^{-6}$ mol/l) than to streptavidin (IBA BioTAGnology). After first binding tests to the strep column (double tag mutant stS106C/S160Ch) it was proposed that nearly 100 % of the refolded protein attached to the column material. Even so, the yield of the heterogeneous trimeric EPR sample in the end was very low (Dockter, 2009). Other binding experiments showed that solely 6.6 % of the theoretical value could be regained (Kaufmann, 2010). Additional suggestions were identified by using two other double tag mutants (Figure 3.31). 70 % of the apoprotein and ~20 % of trimers could be immobilized on the strep column (Lauf, 2012). Deviations of these results are high, inconsistent and therefore, difficult to interpret. It is unclear where a mismatch occurred. The manufacturer (IBA BioTAGnology) points out that the capacity depends on the fused recombinant protein and normally lies between 50 and 100 nmol protein per 1 ml column volume. According to the LHCII 1.3 mg up to 2.6 mg protein should bind to 1 ml column material. In all experiments 1 ml column material per 1 mg protein was used, which should be sufficient to ensure binding. Besides this, it is astonishing that immobilized apoprotein eluted only partly (Lauf, 2012). In nature biotin is the binding partner for streptavidin. It is known that streptavidin homo tetramers have an extremely high affinity for biotin (Figure 4.6B) with a dissociation constant (K_d) of 10^{-14} mol/l (Green, 1975), which is a result of several factors (Weber *et al*., 1989) and one of the strongest non-covalent interactions known in nature. Thus, it can be used to elute strep-column immobilized proteins but the interaction is so strong that a regeneration of the column material is impossible. A suitable alternative is the biotin analogue D-desthiobiotin that binds less tightly to Strep-Tactin (Hirsch *et al*.,

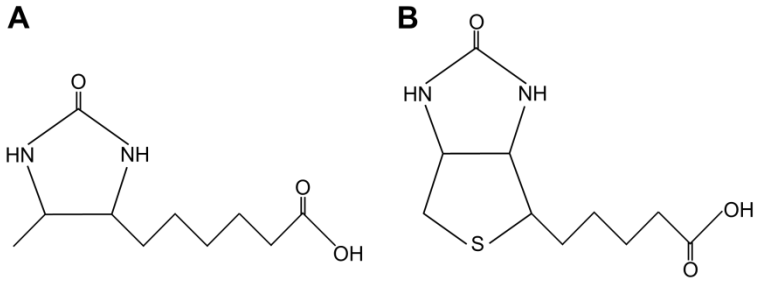

Figure 4.6: Formula of D-Desthiobiotin (A) and Biotin (B).

2002). Therefore, it was used in all LHCII Strep-Tactin experiments. The dissociation constant for D-desthiobiotin is described as 10^{-13} mol/l (Green, 1975; Kylie *et al*., 2009), which is lower than biotin but it should be strong enough to replace protein that is bound to Strep-Tactin efficiently. Thus, it is difficult to find a clear argument that could explain non-eluted LHCP. However, the major aim was the immobilization of refolded protein; thus, further experiments with the apoprotein were not carried out. Nevertheless, for the preparations of heterogeneous trimers reasons are required that could explain the low binding affinity of refolded samples. Several aspects that might influence these processes will be discussed in this chapter.

4.4.1. Influence of steric effects

It was proposed that a re-immobilization of his_6 tagged LHCII might not work caused by a steric hindrance and therefore, a limited accessibility to the tag in refolded samples (Dockter, 2009). However, a preparation of a mutant with an N-terminally attached his_6 tag did not lead to an increase of rebound protein. Several studies of the N-terminal domain attribute to this protein part a high flexibility (Jeschke *et al*., 2005; Daum *et al*., 2010; Dockter *et al*., 2011). This domain is essential for trimerization (Hobe *et al*., 1995) and in trimers interactions between the individual N-terminal domains seemed to reduce flexibility (4.5.1) but nevertheless, flexibility is high enough that the first ten amino acids could not be monitored by X-ray analyses (Standfuss *et al*. 2005). Furthermore, reduced binding affinity was determined in both assembly states and a usage of another column material (IDA- Fractogel), which is characterized by tentacle-like binding sites did not lead to an improvement (Dockter, 2009). Thus, it seems to be highly unlikely that steric hindrances cause a reduced rebinding of purified and refolded LHCII samples to the Ni-column.

However, the situation is somewhat different by double tag mutants, whose first binding affinities were compared. It was found that the amount of immobilized protein (mutant C79Shst) decreased, if the his_6 tag was bordered by the protein and the strep tag II (Lauf, 2012). An explanation is the arrangement of the his_6 tag. For the coordination of the protein a geometric adaption to the coordination sphere of the central ion is required (Schön, 2003). In the mutant C79Shst the conformational flexibility of the captured his_6 tag seems to limit interactions between the histidines and the complexed Ni^{2+} atoms of the column material. The situation for the strep tag II differs: its position (C79Shst: terminal location vs. C79Ssth: captured position) seems to have solely a small influence to the binding capacity. Schmidt *et al*. (1996) analyzed the strep tag II in detail and found out

that the backbone conformation of the residues His-Pro-Gln-Phe-Glu in the strep tag II was that of a 3_{10}-helix. Furthermore, an intramolecular hydrogen bond could be detected between Ser and Glu (Figure 4.7). Thus, the flexibility of the strep tag II by contrast to the his_6 tag is much more limited and therefore, less important for binding. Within a 3_{10}-helix the amino acids are arranged in a right-handed helical structure with a 360° turn each third residue caused by hydrogen bonds between the N-H group of an amino acid and the C=O group of the amino acid three residues earlier. Therefore, the position of the strep tag II is less important for a high binding capacity to the column material, providing unrestricted accessibility.

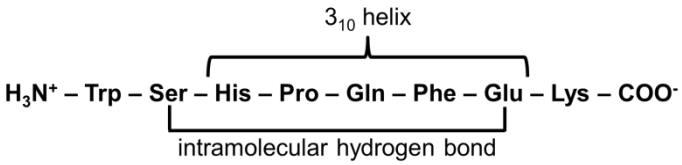

Figure 4.7: Interactions within the strep tag II. Figure bases on Schmidt et al. (1996).

4.4.2. Influence of contaminants

Interactions of the tag with the affinity material should be highly specific but it is known that contaminating proteins as well as non-protein contaminants can bind non-specifically to the column material or the tagged protein of interest itself (Kess *et al*., 2000). Thus, a reduced re-binding affinity of his_6 tagged LHCII to the Ni-column caused by a contamination of Ni^{2+} that remained at the tag of eluted samples should not be excluded from the outset. Experiments of C. Dockter (2009) could show that the binding affinity decreased as $NiCl_2$ increased. Nevertheless, it was concluded that such a high contamination seems to be unlikely, which corresponds to the results in this work. Purified LHCII samples were loaded onto columns that consisted to one half of Ni-IDA Sepharose and to the other half of Ni-free IDA Sepharose. In both cases LHCII samples preferred to bind at the Ni-Sepharose, indicating that a potential contamination was, if at all, low. These results could be confirmed in an additional experiment with varied concentrations of $NiCl_2$ on the IDA-Sepharose (Figure 3.16). As seen before, LHCII samples preferred to bind to the IDA-Sepharose containing the highest amount of $NiCl_2$. Thus, an effect of contaminates is highly unlikely. In direct comparison it seems that the Strep-Tactin system has an advantage caused by its very specific interaction. However, it was shown that a contamination on the strep column does not apply to the protein but to the column material. Pigments tended to form aggregates that remained at the Sepharose-strep column. This effect decreased by using Macroprep-strep column material. Sepharose is a

cross-linked, beaded-form of a polysaccharide polymer material, whereas Macroprep is a synthetic polymethacrylate that seems be to interact less with pigments, perhaps as a result of a smoother surface. Impurities can be significantly reduced by using organic solvent (Kess *et al.*, 2000) but this cannot be used with refolded LHCII and strep column material. On one hand pigments would get lost and on the other hand the binding site of the strep column material gets destroyed. Nevertheless, a completely regeneration of the strep column is possible (4.4.5).

4.4.3. Influence of the pH value

The Strep-Tactin system allows one-step purification of almost any recombinant protein under physiological conditions, thus preserving its bioactivity (IBA BioTAGnology). Variation of the pH value is not useful, because it might destroy its binding activity. In contrast the pH value is an important key factor for a re-immobilization of his_6 tagged LHCII to the Ni-column. After refolding, the protein is dissolved in reconstitution buffer with a pH of 9.0 and after the purification step in sucrose gradient solution with a pH of 7.8. In direct comparison the yield could be increased by 19 % to 26 % (Figure 3.17). This effect is explainable with the protolysis balance of the amino acid histidin (Figure 4.8) and the binding principle to the Ni-IDA column. If the pH value is above 6.0, the nitrogen of the imidazole ring has a free electron pair which is essential for an interaction with the Ni^{2+} atom of the column. At a low pH level by contrast, the nitrogen is protonated and an interaction is impossible.

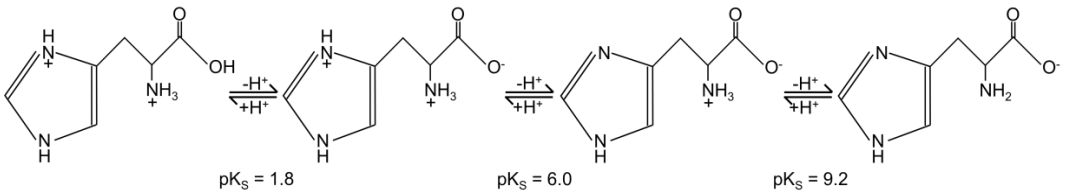

Figure 4.8: Protolyse balance of the amino acid histidin

It must be noted that the binding affinity to the column at both compared pH levels (7.8 and 9.0) should be equal but firstly variations cannot be excluded, secondly the pH level within the micelles might differ (Dockter, 2009), and thirdly differences of both yields were small.

4.4.4. Influence of detergent micelles

Besides the pH value, the composition of the detergent micelles has a big influence to both column materials. With regard to the Ni-column, Dockter (2009) could reach the highest amount of rebound protein (25 %) by removal of the detergent LM and dissolving the protein in mock-buffer, containing all ingredients of a reconstitution without protein. Despite this improvement, 75 % of the protein got lost. One critical step seems to be the removal of the detergent LM by using Bio-Beads because aggregation as well as adsorption processes could be determined (Boggasch, 2006). Furthermore, a removal is a time consuming step. In contrast, a mixing of detergents, leading to LM-OG micelles is faster and limits risks of aggregation. In combination with a threefold volume of column material and a fourfold re-application of the sample led to a yield of 85 % in the eluate and to 45% after second ultracentrifugation (Figure 3.19). It is obvious that differences between the yield of the eluate and of secondly purified trimers are caused by protein degradation. On one hand it was shown previously that LHCII trimers degraded into monomers in the presence of OG (Nußberger *et al*., 1993) and on the other hand a loss of pigments during the dilution with OG or during the washing steps also supports degradation. In the crystal structure of Kühlbrandt *et al*. (1994) the chl *b* molecules 11 and 12 could not be identified, perhaps caused by loose binding to the LHCII. However, in LHCs chl *b* is required for stabilization (Paulsen *et al*., 1993; Yang *et al.*, 2003; Horn and Paulsen 2004; Takabayashi *et al*., 2011). A counter-argument was given by Horie *et al*. (2009). They published that an incubation of a LHCII trimer with NYC1-LIKE chlorophyll b-reductase (NOL) resulted in a stable trimer without chl molecules. Overall, a loss of loosely bound pigments is the most likely hypothesis because similar results were obtained during the production of heterogeneous trimers with the help of the strep column. Nevertheless, this could be avoided by adding either pigments (Dockter, 2009; Lauf, 2012) or glycerol (Lauf, 2012; 3.4). Thus, adding pigments or glycerol seems to be promising in order to further increase the yield.

According to the strep column, another point of view is essential, caused by different interactions between the tag and its belonging column material. The immobilization of the his_6 tag bases on complexation whereas the strep tag II as a peptide sequence interacts with the protein streptavidin respectively Strep-Tactin. Ionic interactions and hydrogen bonds via two water molecules play important roles (Schmidt *et al*., 1996). Thereby, this interaction is very specific but also includes a heightened sensitivity to chemical ingredients. A verification of the used detergents in combination with the strep column showed differing results as the manufacturer points out (Table 3.5). Everything seemed to suggest that LM reduced the performance and thus, the lifetime of the column material.

Generally non-ionic detergents are mild and do not affect important structural features. Nevertheless, an inactivation cannot be excluded (Maire *et al*., 2000), what is particularly the case for short (C_7-C_{10}) hydrocarbon chain and octylglucoside, which are often more inactivating than corresponding detergents with an intermediary (C_{12}-C_{14}) hydrocarbon chain length (Lund *et al*., 1989). LM is often used in solubilization of membrane proteins with retention of functional properties (Tanford *et al*, 1974; Van Aken *et al*., 1986; Lund *et al*, 1989, Fleming *et al*., 1997). Physical properties of used detergents are listed in Table 4.3 and their structure is figured out in Figure 4.9.

Table 4.3: Physical properties of used detergents (data bases on Maire *et al*., 2000).

Name	Monomer mass	CMC	Aggregation number
N-octyl-ß-D-glucopyranoside (OG)	292	$1.9 – 2.5 \cdot 10^{-2}$	~90
Triton X-100 (Tx)	625	$2.5 \cdot 10^{-4}$	75-165
N-dodecyl-ß-D-maltoside (LM)	511	$1.8 \cdot 10^{-4}$	110-140

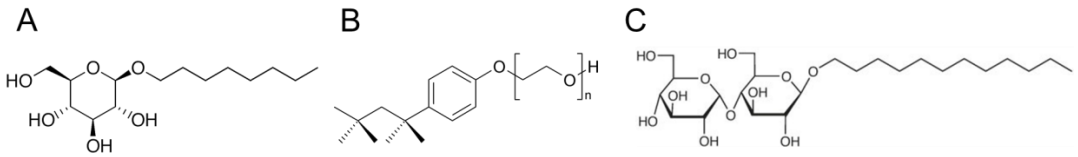

Figure 4.9: Structure of used detergents. A: Octylglucoside (OG); B: Triton X-100 (Tx); C: Laurylmaltoside (LM)

Thus, an inactivation or degradation of LHCII trimers by OG can be expected and was already shown (Nußberger *et al*., 1993). LM by contrast combines two main properties that are needed for membrane proteins: it is a mild, non-ionic detergent and with its long hydrocarbon chain inactivation should be low. According to the LHCII this is the case but it is surprising that it seems to inactivate Strep-Tactin. In a previous user manual the maximum amount of LM was specified with 0.01 % but manufacturer (IBA BioTAGnology) points out that 2 % is the correct value. Nevertheless, my experiences could not confirm this. Thus, neither OG nor LM should be used in combination with the strep column, whereas Tx can be used without any problems. However, an immobilization of ultra-centrifuged samples onto the strep column is critical. Tx can be used in ultracentrifugation gradients but a loss of four chl molecules per LHCII must be taken into

account (Boggasch, 2004), which is unacceptable because an increased loss of pigments are a problem anyway. Therefore, the eluate of the Ni-column, which contained trimers dissolved in Tx-micelles should be not ultra-centrifuged, it should be loaded directly onto the strep column and the OG washing step should be replaced by a Tx washing step.

4.4.5. Influence of ethanol during regeneration

The regeneration of column materials is an important point for a satisfactory cost-benefit ratio. The Ni-column in combination with the LHCII is an excellent example because immobilization works specifically and material fatigue is low. In contrast, the strep column has a limited number of regeneration cycles of approximately six under ideal conditions. However, a contamination of the column material is a big problem (4.4.2). Chlorophylls tend to aggregate in polar solvents. Typical causes are hydrophobic interaction of the phytol chains or π-π interaction of the porphyrin rings. The binding energy of such interaction is low (Kooyman, 1979). Nevertheless, removing pigment aggregates requires ethanol washing steps, which is well suitable for the Ni-column but destroys the binding site of the strep column (Lauf, 2012). In comparison to the Sp-strep column, interactions of the Mp-strep column and aggregates are reduced but still present. Besides ethanol the enzyme chlorophyllase can be used to destroy chlorophyll aggregates. This enzyme is the catalyst for the hydrolysis of chlorophyll to produce chlorophyllide by splitting chlorophyll into the phytol chain and porphyrin ring (Yi *et al.*, 2006). Recombinant chlorophyllase was used successfully to clean the column material but it took several days. The main problem seems to be a limited access to the pigments within aggregate arrangement. More suitable is an incubation of the column material with detergent (Tx) solution, which allows to remove pigments within one day.

In conclusion, the binding experiments by using both kinds of tags were modified in such a way that losses were reduced drastically, although the exact cause for a reduced re-binding affinity was not found but some promising indications. It seems that a combination of several aspects influence these processes.

4.5. Conformational flexibility of LHCII

The structure and conformational flexibility of the LHCII was analyzed by pulsed EPR measurements and compared with the crystal structure. Previous and current results showed that the core of LHCII seems to be very similar to the crystal structure but deviations were monitored within the N-terminal domain and loop regions (Dockter *et al*., 2011). In addition to these published data, further results of the N-terminal domain and the lumenal loop, which are directly involved in regulation processes, will be discussed in this chapter.

4.5.1. A comparison of monomers and heterogeneous trimers showed that the assembly state of the LHCII influences the flexibility of the N-terminal domain

DEER-EPR measurements of this domain by using double labeled monomers and single labeled trimers as well as ESEEM-EPR measurements gave first indications that the flexibility and thus, the conformation depends on the assembly state (Jeschke *et al.,* 2005; Müller, 2008; Dockter, 2009; Dockter *et al.*, 2011). An essential step for a direct comparison was the preparation of heterogeneous trimers. In previous experiments (Dockter, 2009) heterogeneous trimers could be prepared but were not suitable for analyses of the N-terminal domain, caused by tag modifications of the N-terminal domain, which influenced its flexibility (Kaufmann, 2010). In this work interactions between the his_6 tag and the Ni-column as well as between the strep tag II and the Sp- respectively MP-strep column were analyzed in detail and already discussed in 4.4. Results were used to establish a reproducible preparation of heterogeneous trimers without modifying the N-terminal domain (3.4) by constructing mutants with a double tag at the C-terminus, consisting of a spacer (two glycine), a strep tag II (eight amino acid long sequence), and a his_6 tag. With this method 65 % of theoretically possible trimers could be regained, which was a tenfold increase of the yield in comparison to further results (Kaufmann, 2010). The signal to noise ratio of all prepared heterogeneous samples seems to confirm biochemical results (3.4). The amounts of additional distance peaks, which are an indication for aggregates, are lower than in corresponding monomers. Although additional peaks in DEER-EPR measurements were analyzed (4.2) and identified as spin-spin interactions of unfolded apoprotein, aggregation peaks were unavoidable because samples were prepared before the kind of contamination was identified. Furthermore, it is important to note that in some cases current and previous measurements of the same mutant differed. Results of

the monomeric mutant 3/59 (previous data: Dockter et al., 2011 – figure 3; current data: Figure 3.57 - 4) will be presented as an example to explain these deviations before results of the N-terminal domain in both assembly states will be discussed.

In both data sets the distances were unstructured between 1.5 and 5.5 nm and biggest differences were monitored in long and short distance ranges. Current data showed less distances at 5 nm, an additional aggregation peak at 6.3 nm and a dominating amount of shorter distances. These differences may be related to the sensitivities of the spectrometers, to the dipolar evolution times and to the amounts of aggregates. Older data were measured in less sensitive X-band EPR and current data in stronger Q-band EPR, which has stronger detection pulses. The shorter the pulses, the broader are excitation bandwidths, resulting in a better determination of higher frequencies. Thus, short distances (below 2 nm) are much better detectable. The dipolar evolution time or free induction decay (FID) describes the spin-spin relaxation time; the longer it is, the longer is it possible to detect the echo. The concentration of the older sample was much higher, leading to strong signal decay and therefore, to a shorter dipolar evolution time (current data: 5 µs, older data: 1.8 µs). Effects on the distance distributions are: the stronger the signal decay, the higher is the effect of the background correction and the longer the dipolar evolution time, the greater the likelihood to detect long distances more precisely. Effects on the distance distribution of the newer data set were that distances around 5 nm became less intense but they extended to longer values (around 6.3 nm). The most critical point is the amount of aggregates. The older preparation had a higher sample concentration, which might (3.3.4) lead to more aggregates. Further indications for aggregates are the modulation depths (current data: 0.3, older data: 0.6). If the modulation depth is higher than 0.2, the risk for a contamination is increased. Thus, the protein concentration in addition to a higher modulation depth strongly indicates a higher amount of aggregates in the older sample. In order to verify the significance of both distance distributions, a further aggregation-free preparation of this mutant is advisable.

In order to compare the N-terminal domain in both assembly states, this protein part is divided into three sections (Dockter *et al*, 2011): section 1 is between the amino acids 26 and 59, section 2 between 26 and 14, and section 3 between 14 and 1. The flexibility within the first section should be low because it contains two stabilizing parts: A short loop (residues 51-42) that

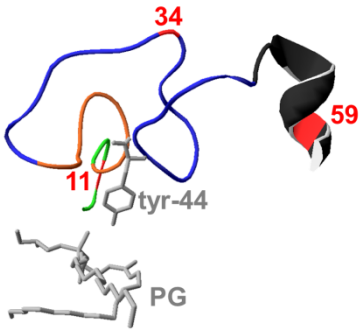

Figure 4.10:Three sections of the N-terminal domain. Section 1 (residues 59-26) is colored in blue, 2 (residues 26-14) in orange, and 3 (residues 14-1) in green. Labeled amino acids are colored in red.

submerges into the lipophilic membrane environment and an interaction between tyr-44 and the polar headgroup of the lipid PG, whose fatty acid chain expands into the core of the trimer (Nussberger *et al.*, 1993). Thus, MMM simulation predicted a small distance distribution between the residues 34 and 59 (Figure 3.56). The widths of the measured samples seem to be caused by aggregates. First indication is the high amount of short distances near the predicted peak of MMM simulation. Second indication is the spectrum of an almost aggregation-free preparation of the mutant 34/59 in a monomeric assembly (N. Fehr, unpublished data), which was prepared after the reason for contamination was identified (3.3.4). It showed that distances above 3 nm decreased, whereas shorter distances increased, leading to a spectrum that was very similar to MMM simulation. It is highly suspected, therefore, that longer distances in the heterogeneous trimer spectrum might also decrease by avoiding aggregates. This hypothesis is confirmed by the trigonometric data of the trimers 59 and 34 (Dockter *et al.*, 2011 – figure 4), which showed high similarity to the MMM simulation. Although previous biochemical experiments could not demonstrate conclusively the presence of PG in monomers (Bender, 2004), it is known that the affinity of PG to monomers is high (Nussberger et al., 1993). All these data indicates that the assembly state does not influence the conformation of the N-terminal domain within the first section. Consequently, it is likely that the short loop and the interaction between PG and tyr-44 stabilize this section in monomers and trimers.

Previous results (Dockter *et al.*, 2011) suggested a higher flexibility of section 2 (residues 26 to 14) in monomers caused by weakly bound chl 9, which is in contact with tyr-22, violaxanthin (vio), and the lipid PG (Figure 4.11). A broadened distance distribution of the sample 14/29 as well as the water accessibility parameters of both positions confirmed these suggestion (Dockter *et al.*, 2011) but a direct comparison of this section in both assembly states by using heterogeneous trimers was not done in this work, caused by a lack of time.

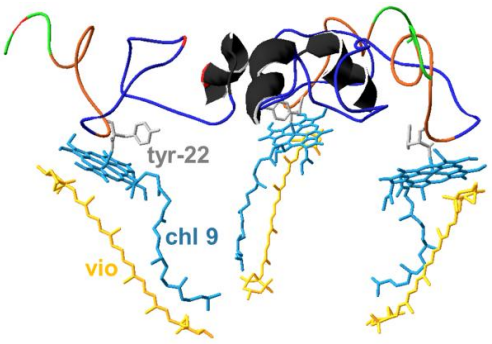

Figure 4.11: Section 2 (residues 26-14; orange) of the N-terminal domain is stabilized by chl 9 that is in interaction with tyr-22 and by vio.

Within the third section (residues 14 to 1) a higher flexibility was already expected because this part is still unresolved by X-ray analysis (Standfuss *et al.*, 2005) and trigonometric measurements of single labeled mutants in a trimeric assembly showed

broad distance distributions including indications for two maxima (Dockter *et al*., 2011 – figure 4). Intramolecular distance distributions taken from double labeled mutants in both assembly states that were labeled within the third section could on one hand confirm a higher flexibility at all and on the other hand showed that flexibility seems to be increased in monomers (Figure 3.57). In comparison to trigonometric measurements two maxima did not appear. This is not a contradiction because some conformational changes might affect to the distance distributions taken from triangulated trimers, without any influences to the intramolecular distances taken from heterogeneous trimers (Figure 4.12).

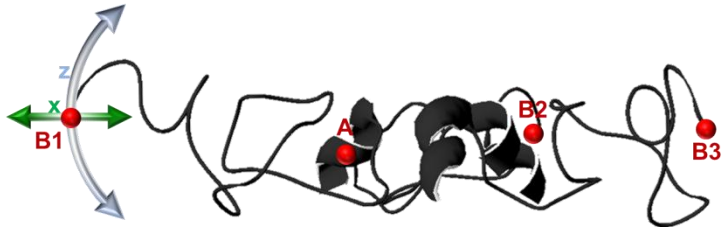

Figure 4.12: Distance distributions taken from triangulation (distances between B1, B2, and B3) that show a bimodal spectrum might be caused by a movement of the labels in x- (green arrow) or z-axis (blue arrow). Distance distributions taken from intramolecular distances (distances between B1 and A) of heterogeneous trimers can lead to a similar bimodal spectrum, if the label moves along the x-axis but by contrast can also show a spectrum with one peak, if the label moves along the z-axis.

The data set of the mutant 34 row should be completed by a new preparation of broken samples. If all measurements are complete, including aggregation free monomers, it should be possible to model the position of the residues in section 3. A simple and provisional modeling is shown in Figure 4.13 to get a first impression of the residues 7 and 3 in section 3. The intersection of both maxima of the main peaks shows that the N-terminal domain seems to be oriented to helix 1 and thus, a bit less exposed to the aqueous environment. This suggestion is confirmed by the ESEEM data, which showed a higher accessibility of position 11 to the aqueous environment than position 3 (Dockter, 2009).

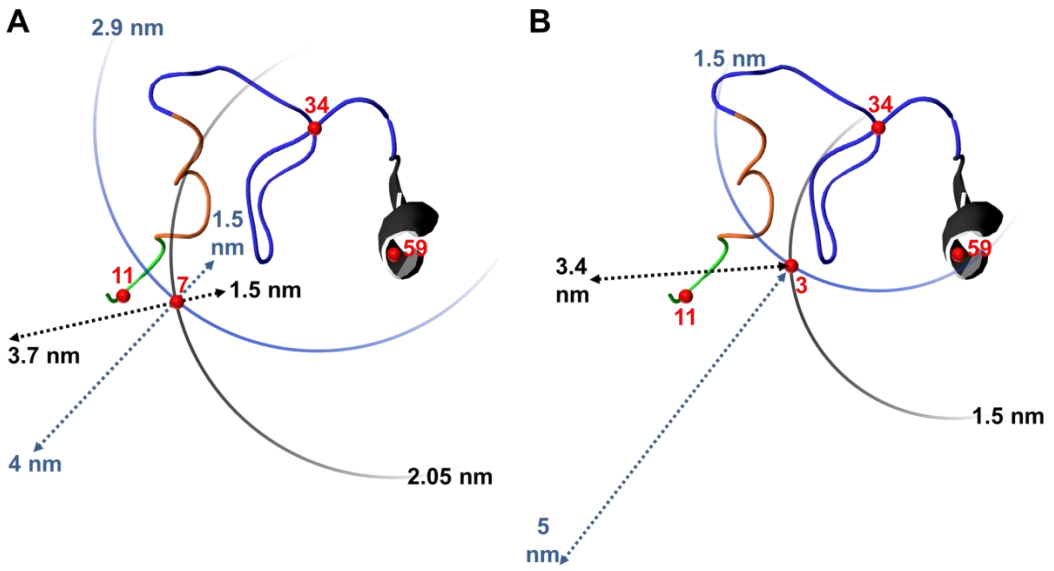

Figure 4.13: Calculated positions of the residues 7 (A) and 3 (B) in a trimeric assembly. The blue circles symbolize the maxima of the main peak of the distance distributions in relation to position 34, the black circles in relation to position 59. Dotted arrows symbolize the widths of both distance distributions.

At this point, it can be concluded that the comparison of the N-terminal domain in a monomeric versus trimeric assembly state by using heterogeneous trimers confirmed previous DEER data of triangulated trimers (Dockter *et al.*, 2011) and ESEEM data (Müller, 2008; Dockter, 2009; Dockter *et al.*, 2011). Flexibility in section 1 (residues 59-26) is limited and very similar in both assembly states, section 2 (residues 26-14) was not analyzed by using heterogeneous trimers, and the mobility of section 3 (residues 14-1) is very high, in monomers significantly higher than in trimers.

In order to increase the significance, an aggregation-free preparation of the monomeric samples is advisable and broken samples (34/11 heterogeneous trimers, 3/34 monomers) should be prepared again. The mobility of section 2 could be monitored by measuring the distance between the reference point 59 and residue 14. Further interesting information of the N-terminal domain require a directed insertion of the LHCII into liposomes to analyze the domain in a mimicked native environment and the isolation of a kinase to phosphorylate the domain in a larger scale (Gorleku, 2007; Schneider, 2008).

4.5.2. In fully-pigmented LHCII the pigment composition but not the pH value influence the conformation of the lumenal loop region

The lumenal loop region and its interaction with the xanthophyll cycle is one of the most controversially discussed topics of the LHCII (Liu *et al*., 2004; Holt *et al*., 2005; Standfuss *et al*., 2005; Pascal *et al*., 2005 and 2010; Ruban *et al*., 2007; Barros and Kühlbrandt, 2009; Zaks *et al*., 2012). A varity of methods, like Raman spectroscopy (Bassi et al., 2008), X-ray crystallography (Standfuss et al., 2005), CD spectroscopy (Liu *et al*., 2008) and EPR spectroscopy (Dietz, 2008; Dockter, 2009, Berger, 2011; Dockter *et al*., 2011) were used to get a deeper view inside this region. DEER-EPR allows analyzing the protein conformation in aqueous solution, thus, it is one of the most suitable methods for this purpose. In previous DEER-EPR experiments the conformation of the lumenal loop region of the detergent-solved LHCII was monitored initially (Dietz, 2008) and now analyzed in detail under varied conditions by using several spin labeled mutants that were distributed over the whole region.

The data sets of fully-pigmented lumenal loop mutants in a monomeric and trimeric assembly suggest that this region consists of rigid and flexible parts but indications for different conformations were not found. A loss of neoxanthin by contrast seems to change the conformation. At this point it should be mentioned that significances of the trimeric measurements are reduced, caused by a contamination of aggregates that led to additional distance peaks and data analyses that are still in progress.

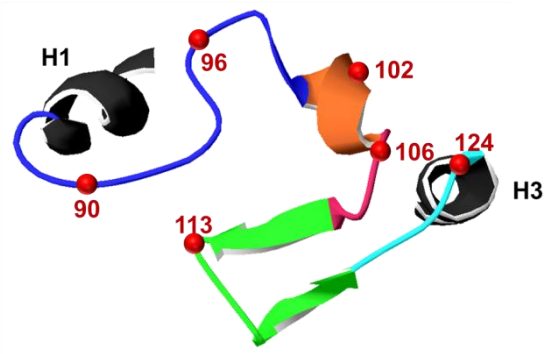

Figure 4.14: Bottom view to classified sections of the lumenal loop region. Blue: section 1 (residues 84-100), orange: section 2 (residues 101-104), magenta: section 3 (residues 105-109), green: section 4 (residues 110-120), cyan: section 5 (residues 121-124); red dots: spin labeled residues; H: helix. Figure was prepared with the swiss pdb viewer (PDB entry: 2BHW).

For a better interpretation of individual distance distributions, the lumenal loop region will be classified into five sections (Figure 4.14). Section 1 is between the residues 87-100, section 2 (residues 101-104) is symbolized by helix 2, section 3 is between the residues 105-109, section 4 contains the ß-sheet (residues 110-120), and section 5 is between the residues 121-124. Section 1 seems to be rigid at its beginning and gets somewhat more flexible in its further course, concluded from the mean distance devices and widths of the main

peaks of the mutants 90 and 96 (Figure 3.58 – 1 and 2) in comparison to MMM simulation. This hypothesis is confirmed by the monomer data of the double labeled mutants 90/124 and 96/124. Experimental data of 90/124 (Figure 3.60 – 2) are nearly identical to MMM simulation. Mutant 96/124 (Figure 3.60 – 3) has a similar mean distance device but a broader distance distribution in comparison to MMM simulation. Position 90 is close to the transmembrane helix 1, thus, rigidity is consistent to the data set taken from the hydrophobic core (Dockter *et al.*, 2011). Neither a pH shift nor the composition of pigments influenced the conformation (Figure 3.60). A loss of the lipid DGDG on the Ni-column during the trimerization process was another proposed hypothesis (Dockter, 2009) for broader or deviated distance distribution because an incubation of trimers in 1.2 % OG for two days showed on one hand a disintegration of trimers and on the other hand a loss of DGDG (Nußberger *et al.*, 1993). The polar headgroup of DGDG is attached to the transmembrane helix 4 and its hydrophobic tail near the C-terminal domain (Standfuss *et al.*, 2005). Position 96 is with 1.35 nm the closest distance between a labeled residue and the lipid (Figure 4.15) but the comparison of trimers produced by using the standard protocol and by using additional plant-extracted DGDG had a minimal, non-significant effect to the distance distribution (Figure 3.59).

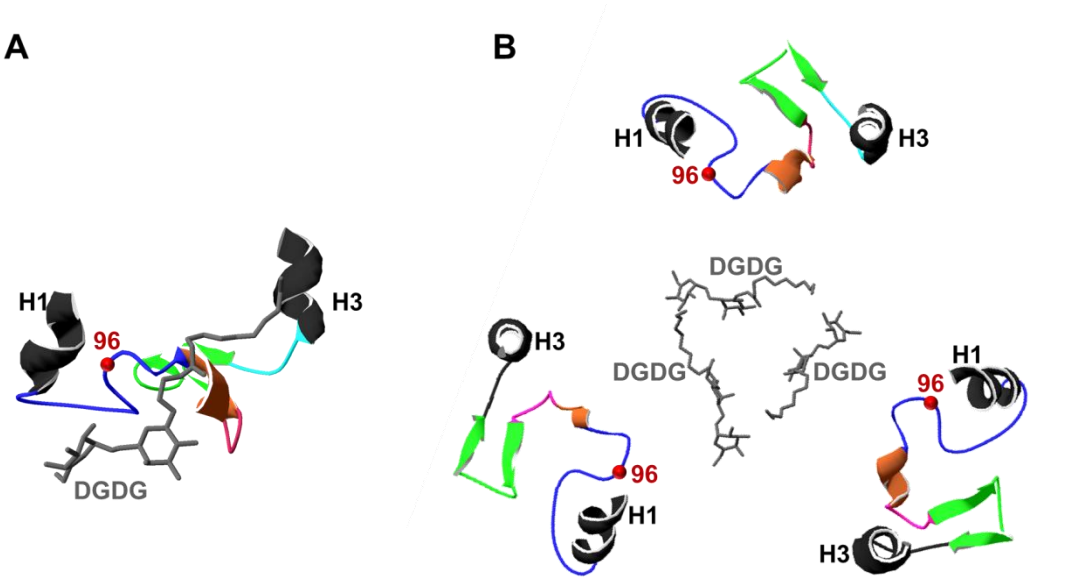

Figure 4.15: Lumenal loop region and its interaction with the lipid DGDG. A: Monomeric front view; B: Trimeric top view. Blue: section 1, orange: section 2, magenta: section 3, green: section 4, cyan: section 5; red dots: spin labeled residues; H: helix. Figure was prepared with the swiss pdb viewer (PDB entry: 2BHW).

In section 2 an increased mobility was detected, even though position 102 is located within helix 2. The α-helix itself should be rigid; rather it seems that flexible areas in front of and behind the helix cause the monitored mobility in trimers. Liu *et al.* (2004) suggested a mechanism for NPQ that includes a conformational change of the helices 2 and 5 triggered by protonation of lumen exposed amino acids. DEER-measurements of the mutants 96/124 and 102/124 (Berger, 2011) at pH 4.5 by contrast did not show any indications for conformational changes. It should be noted that it is impossible to mimic a pH gradient in detergent micelles but nevertheless, lumen exposed amino acids should be protonated at this low pH value. Most reliable information requires EPR measurements of the LHCII in the thylakoid membrane or liposomes.

The width of the distance distribution of position 106, located in section 3 (behind the helix), suggests a sharply increased mobility. Previous data confirm these results: triangulation in trimers as well as the monomeric mutant 106/160 (Dockter *et al.*, 2011 – figure 2) showed broad distance distributions. Differences between the current and older data of the 106 trimers may be related to the sensitivities of the spectrometers, to the dipolar evolution times, and to the amounts of aggregates. All these points were already discussed in 4.5.1. On one hand a larger mobility of the spins labels than the ones in α-helical labeling positions could cause broader distance distributions, on the other hand pigments located nearby seem to influence the mobility of concerned residues in a different degree. A view inside the X-ray structure (Figure 4.16) shows that the xanthophylls lutein (lut) and neoxanthin (neo) as well as the chlorophylls (chls) 6 and 10 limit the mobility of position 96, whereas position 106 is not affected as strongly.

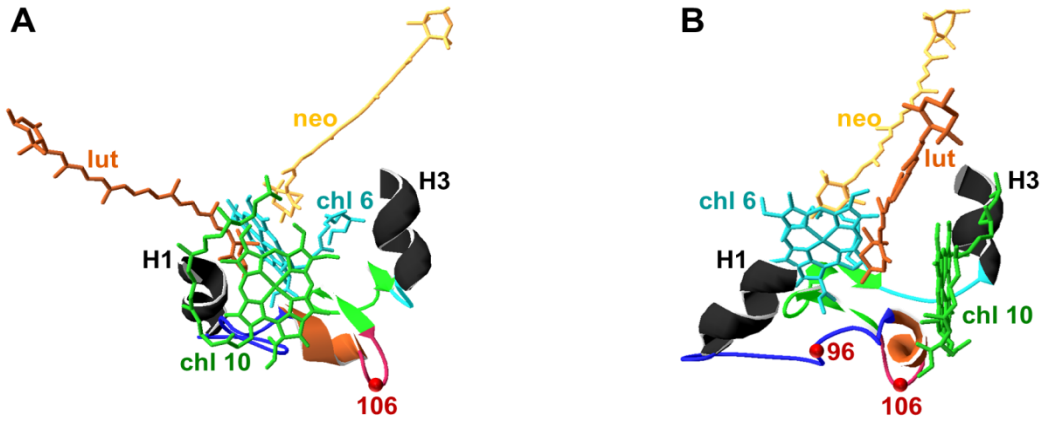

Figure 4.16: Front view (A) and side view (B) to the lumenal loop region. Several pigments (lut: lutein, neo: neoxanthin, chl: chlorophyll) seem to limit the mobility of the spin labels as well as of the residues of the positions 96 and 106 in a different degree. Blue: section 1, orange: section 2, magenta: section 3, green: section 4, cyan: section 5; red dots: spin labeled residues; H: helix. Figure was prepared with the swiss pdb viewer (PDB entry: 2BHW).

Section 4 seems to be the most interesting part. In a trimeric assembly neither flexibility nor a different conformation seems to be present. The width as well as the main peak of the distance distribution were very similar to the predicted distance distribution of MMM simulation. In a monomeric assembly by contrast deviations were monitored. Longer distances that were determined in fully-pigmented LHCII indicate an increased mobility. In comparison to trimeric distances, taken from triangulation, two scenarios are conceivable: Either the conformation in monomers differs or mobility is limited to a direction that does not influence the triangulated distance. However, it should be noted that differences might not be as great as it seems. On one hand predicted distances of the mutant 90/113 are beyond the detection limit of DEER EPR and in the field sweep spectrum a higher amount of shorter distances was detected, on the other hand deviations of the mutant 113/124 are so small (0.5 nm) that they could be caused by rotation of the spin label. The high density of pigments might lead to a preferred orientation of the spin label away from position 124. A further indication for this suggestion is the width of the distance distribution, which is nearly identical to the predicted one. A view inside the X-ray structure (Figure 4.17) shows that the chls 13 (attached to residue 131), 14 (attached to residue 119), and neo limit the space for mobility. This effect is intensified by the chls 6 and 10 (Figure 4.16). Effects of aggregates should also be taken into account. A new aggregation-free preparation of these mutants is needed to increase the significance of these measurements.

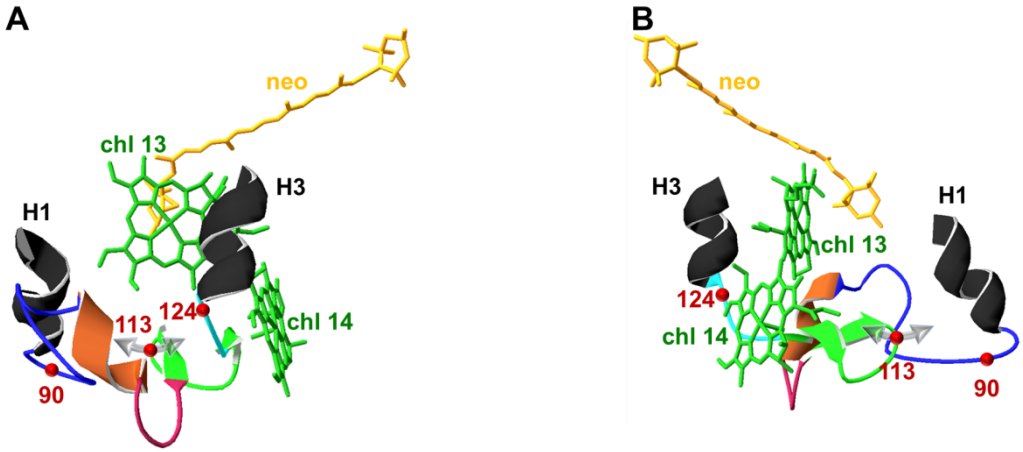

Figure 4.17: Front view (A) and back view (B) to the lumenal loop region. Neoxanthin (neo) and the chlorophylls (chl) 13 and 14) seem to limit the mobility of the spin labels and ß-sheet into a direction that is symbolized by the grey arrow. Blue: section 1, orange: section 2, magenta: section 3, green: section 4, cyan: section 5; red dots: spin labeled residues; H: helix. Figure was prepared with the swiss pdb viewer (PDB entry: 2BHW).

It is interesting that the absence or presence of neo seems to influence the conformation of the ß-sheet. The field sweep spectrum of the mutant 90/113 shows a higher amount of shorter distances, if neo is present, whereas the absence of neo seems to pull the conformation away from its normal fold. This indication is confirmed by the results of the monomeric mutant 113/124 and triangulated trimeric mutant 113. In a trimeric assembly the distance between residues 113 decreased without neo and in a monomeric assembly the distance distribution between the residues 113 and 124 was broader and showed a higher amount of shorter distances in the absence of neo. A view inside the X-ray structure shows that a loss of neo leaves empty space, leading on one hand to an increased mobility of the ß-sheet and on the other hand the ß-sheet moves a little bit into the trimeric core. Pascal *et al.* (2005) and Ruban *et al.* (2007) proposed a mechanism for NPQ that bases on a repositioning of the chls 10 and 13 caused by a twist of neo. CD spectra of the neo-free mutants 113, 113/124 showed a significant increase of the signal at 472 nm in comparison to the wildtype similar mutant C3.2h. Thus, in combination with the EPR results, a repositioning of the chls cannot be excluded but the question is, whether a twist of neo is comparable to its absence. In direct comparison to the other proposed mechanisms for NPQ an interaction of the xanthophyll cycle with lumen exposed amino acids together with the PsbS protein seems likely. Thus, it can be concluded that section four is the most flexible and influenced part of the lumenal loop region in particular in a monomeric assembly state. In fully-pigmented mutants a higher mobility was determined but nevertheless the conformation was similar to the crystal structure. In neo lacking mutants by contrast strong indications were found that the conformation was pulled away from its normal fold.

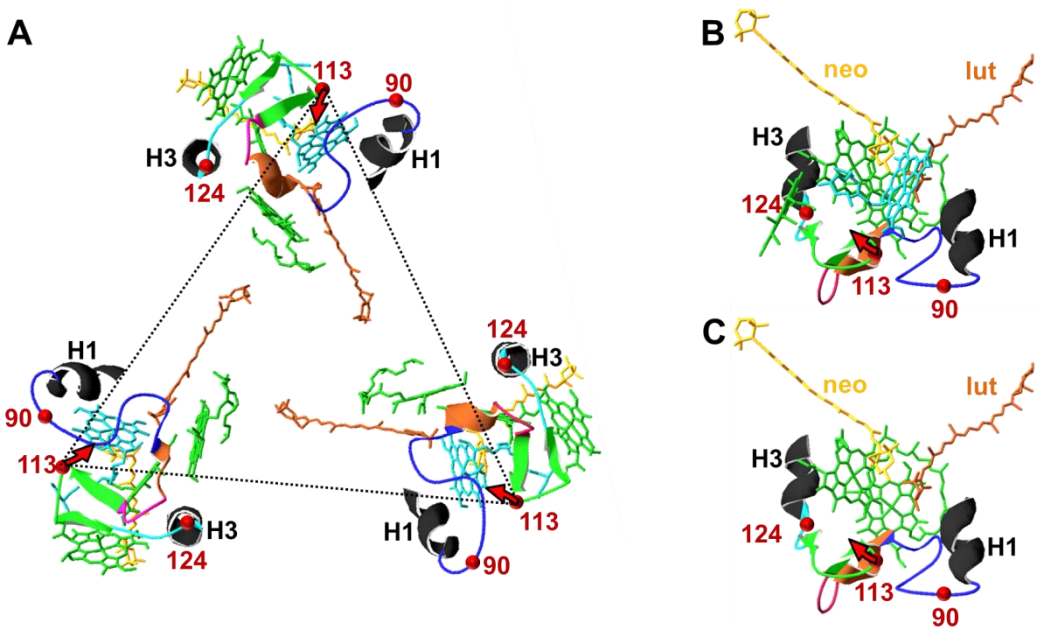

Figure 4.18: Bottom view to the triangulated trimer 113 (A) and two backside views to the lumenal loop region (B and C). In the absence of neo the residue 113 seems to move into the core of the trimer (A – red arrow) and the distance between 113 and 124 seems to decrease (B – red arrow). Pascal *et al.* (2005) and Ruban *et al.* (2007) proposed a mechanism of NPQ that includes a twist of neo, leading to a repositioning of the chls 10 and 13 (C).

Section 5 seems to be rigid. Although the distance distribution of the trimeric mutant 124 differed from MMM simulation, distance distributions of the double labeled monomers 90/124 and 96/124 showed distance distributions that were very similar to MMM simulation. Results of the trimeric mutant 124 seem to be non-significant because the main peak of the triradical is broader and shifted 1 nm into longer distance ranges. Usually the mobility of the spin label and residue should be reduced by the pigments in the surroundings. Furthermore, position 124 is directly in front of the transmembrane helix 3 and should be very rigid. Furthermore, previous results (Dockter, 2009) showed a shift of the triangulated trimer 123 into shorter distance ranges and double labeled mutants, containing one label at position 123 also led to different distance distributions than predicted by MMM simulation. It is difficult to imagine that a spin label and/or the residue 123 are orientated into the trimeric core, whereas position 124 is located into the opposite direction. A real shift of 1 nm would have a massive effect to the structure (Figure 4.19).

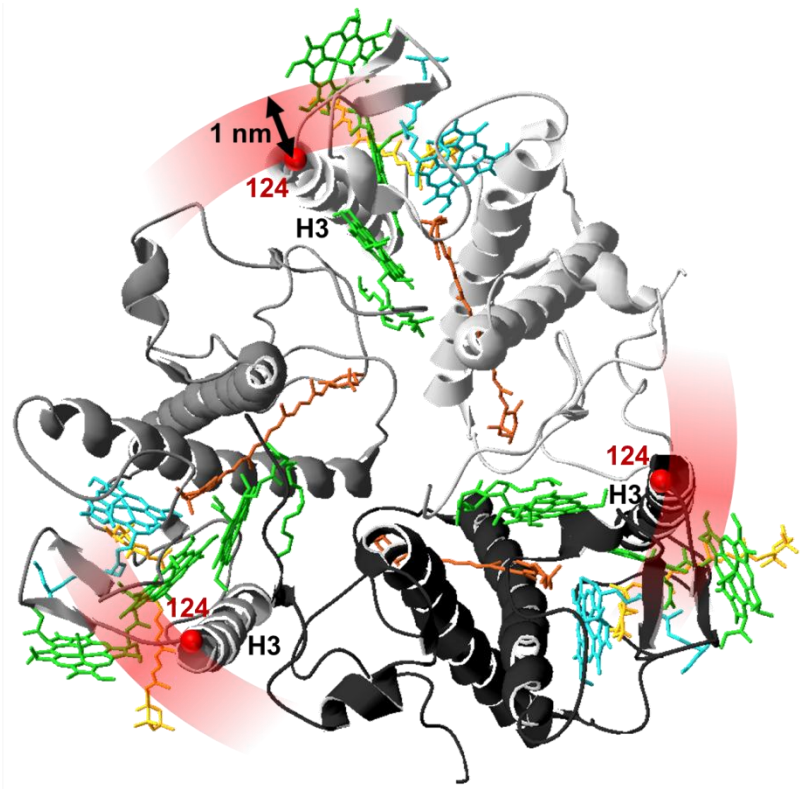

Figure 4.19:Trimeric LHCII labeled at position 124 (red dot). The inner margin of the red circle symobilzes distances that are predicted by MMM simulation, whereas the outer margin of the cycle the measured distances. Figure was prepared with the swiss pdb viewer (PDB entry: 2BHW).

In summary, the lumenal loop region consists of rigid and flexible parts. Within sections 1 and 5 mobility is limited, in section 2 increased and in section 4 sharply increased, as deduced from the width of distance distributions. Section 3 (mutant 106) as well as the results of trimeric mutant 124 are difficult to interpret and should be repeated. A loss of the lipid DGDG during trimerization and influences to the distance distribution seems unlikely. Variations of the pH value did not influence the conformation. However, strong indications were detected that the absence of neo pulled the conformation away from its normal fold and causes deviated CD spectra of neo lacking mutants.

5. Summary

The major light harvesting complex II (LHCII) of higher plants is the most abundant membrane protein on earth and located in the thylakoid membrane of chloroplasts. It is a perfect model system to analyze membrane protein function because 96 % of its structure is resolved by X-ray crystallography and its recombinant version can be refolded *in vitro*, leading to a full-functional protein-pigment complex that is nearly identical to the *in vivo* version.

Electron paramagnetic resonance (EPR) spectroscopy is a very sensitive and well suited method to analyze structural dynamics of proteins. EPR requires a site-directed spin labeling to Cys residues that replace carefully chosen amino acids of the LHCII without influencing its function.

In this work the stability of the spin label and the quality of labeled samples was optimized by analyzing each preparation step. Results were used to establish a method, which avoids the risk of protein aggregation and a loss of EPR signal extremely. In combination with Q-band EPR low concentrated LHCII samples are now detectable. Furthermore, a reproducible method for the production of heterogeneous trimers, consisting of one double labeled monomer and two unlabeled monomers, was established. Heterogeneous trimers were used to compare the incompletely resolved N-terminal domain in both assembly states. On one hand results of both assembly states showed a limited mobility in the section near to the rigid core and an increasing flexibility in its further course to the N-terminus. On the other hand results confirmed the suggestion that sections near the N-terminus are less flexible in trimers than in monomers. Comparisons of several mutants under varied pH values and pigment compositions were used to analyze the controversially discussed lumenal loop region of the LHCII. Measurements showed that this region consists of rigid and flexible parts independently of the pH value, whereas a loss of neoxanthin by contrast changes the conformation. Additional analyses of the structural dynamic of the LHCII by mimicking the *in vivo* situation were impossible because a unidirectional insertion of the refolded protein into liposomes failed.

6. Zusammenfassung

Der Haupt-Lichtsammenkomplex II (LHCII) höherer Pflanzen ist das häufigste Membranprotein der Welt und in die chloroplastidäre Thylakoidmembran integriert. Der LHCII kann als Modellsystem genutzt werden, um die Funktionsweise von Membranproteinen besser zu verstehen, da 96 % seiner Struktur kristallografisch aufgelöst ist und er in rekombinanter Form *in vitro* rückgefaltet werden kann. Hierbei entsteht ein voll funktionaler Protein-Pigment.Komplex, der nahezu identisch mit der *in vivo* Variante ist.

Elektronenparamagnetischen Resonanz (EPR) Spektroskopie ist eine hoch sensitive und ideal geeignete Methode, um die Strukturdynamik von Proteinen zu untersuchen. Hierzu ist eine ortsspezifische Markierung mit Spinsonden notwendig, die kovalent an Cysteine binden. Möglich wird dies, indem sorgfältig ausgewählte Aminosäuren gegen Cysteine getauscht werden, ohne dass die Funktionsweise des LHCII beeinträchtigt wird.

Im Rahmen dieser Arbeit wurden die Stabilität des verwendeten Spinmarkers und die Probenqualität verbessert, indem alle Schritte der Probenpräparation untersucht wurden. Mithilfe dieser Erkenntnisse konnte sowohl die Gefahr einer Proteinaggregation als auch ein Verlust des EPR Signals deutlich vermindert werden. In Kombination mit der gleichzeitigen Etablierung des Q-Band EPR können nun deutlich geringer konzentrierte Proben zuverlässig vermessen werden. Darüber hinaus wurde eine reproduzierbare Methode entwickelt, um heterogene Trimere herzustellen. Diese bestehen aus einem doppelt markierten Monomer und zwei unmarkierten Monomeren und erlauben es, die kristallografisch unvollständig aufgelöste N-terminale Domäne im monomeren und trimeren Assemblierungsgrad zu untersuchen. Die Ergebnisse konnten einerseits die Vermutung bestätigen, dass diese Domäne im Vergleich zum starren Proteinkern sehr flexibel ist und andererseits, dass sie in Monomeren noch mobiler ist als in Trimeren. Zudem wurde die lumenale Schleifenregion bei unterschiedlichen pH Werten und variierender Pigmentzusammensetzung untersucht, da dieser Bereich sehr kontrovers diskutiert wird. Die Messergebnisse offenbarten, dass diese Region starre und flexiblere Sektionen aufweist. Während der pH Wert keinen Einfluss auf die Konformation hatte, zeigte sich, dass die Abwesenheit von Neoxanthin zu einer Änderung der Konformation führt. Weiterführende Analysen der strukturellen Dynamik des LHCII in einer Lipidmembran konnten hingegen nicht durchgeführt werden, da dies eine gerichtete Insertion des rückgefalteten Proteins in Liposomen erfordert, was trotz intensiver Versuche nicht zum Erfolg führte.

7. Appendix

7.1. Abbreviations

ac	**Amino acid**
1b code	1 letter code amino acids
ß-me	ß-mercaptoethanol
bp	Base pair
BSA	Bovine serum albumin
CD	Circular dichroism
chl	Chlorophyll
da	dalton
ddNTP	Didesoxynucleotidtriphosphat
DEER	Double electron electron resonance
DGDG	Digalactosyldiacylglycerol
DMF	Dimethylformamid
DMSO	Dimethylsulfoxid
dNTP	Desoxynucleotidtriphosphat
DTT	Dithiothreitol
EDTA	Ethylendiamintetraacetat
EPR	Electron paramagnetic resonance
ESEEM	Electron spin echo envelope modulation
EtOH	Ethanol
his_6 tag	Hexa histidyl tag
IB	Inclusion bodies
IPTG	Isopropyl-β-D-thiogalactopyranosid
KCl	Potassium chloride
KDS	Potassium dodecylsulfate
LB	Luria Bertani
LDS	Lithiumdodecylsulfate
LHCII	Light harvesting complex II
LM	n-Dodecyl-β-D-Maltosid
lut	Lutein
µg	Microgram
mg	Milligram
$MgCl_2$	Magnesium chloride
MGDG	Monogalactosyldiacylglycerol
MMM	Multiscale modeling of macromolecular systems

N_2	Nitrogen
NaOH	Sodium hydroxide
neo	Neoxanthin
ng	Nanogram
$NiCl_2$	Nickel chloride
Ni column	Nickel column
NPQ	Non photochemical quenching
OD	Optical density
OG	n-Octyl-β-D-glucopyranosid
p.a.	Per analysi
PAA	Polyacrylamide
PAGE	Polyacrylamide gel electrophoresis
PCR	Polymerase chain reaction
PG	Phosphatidylglycerol
PROXYL-IAA	[3-(2-Iodacetamido)-2,2,5,5-tetramethyl-1-pyrrolidinyloxy], free radical
PsbS	Subunit S of photosystem II
PSI	Photosystem I
PSII	Photosystem II
qT, qI, qE	Forms of photochemical quenching
rpm	Rounds per minute
SDS	Sodiumdodecylsulfate
SH	Sulfhydryl
TCA	Trichloraceticacid
TCyEP	Tris-(2-cyanoethyl)phosphine
TCcEP	Tris-(2-carboxyethyl)phosphine
Tx	Triton X-100
U	Units
VDE	Violaxanthindeepoxidase
vio	Violaxanthin
w/v	weight / volume
w/w	weight / weight
zea	Zeaxanthin

7.2. Amino acids three- and one-letter codes

Amino acid	3L code	1L code	Amino acid	3L code	1L code
Alanine	Ala	A	**Leucine**	Leu	L
Arginine	Arg	R	**Lysine**	Lys	K
Asparagine	Asn	N	**Methionine**	Met	M
Aspartic acid	Asp	D	**Phenylalanine**	Phe	F
Cysteine	Cys	C	**Proline**	Pro	P
Glutamine	Gln	Q	**Serine**	Ser	S
Glutamic acid	Glu	E	**Threonine**	Thr	T
Glycine	Gly	G	**Tryptophane**	Trp	W
Histidine	His	H	**Tyrosine**	Tyr	Y
Isoleucine	Ile	I	**Valine**	Val	V

7.3. Description of mutant titles

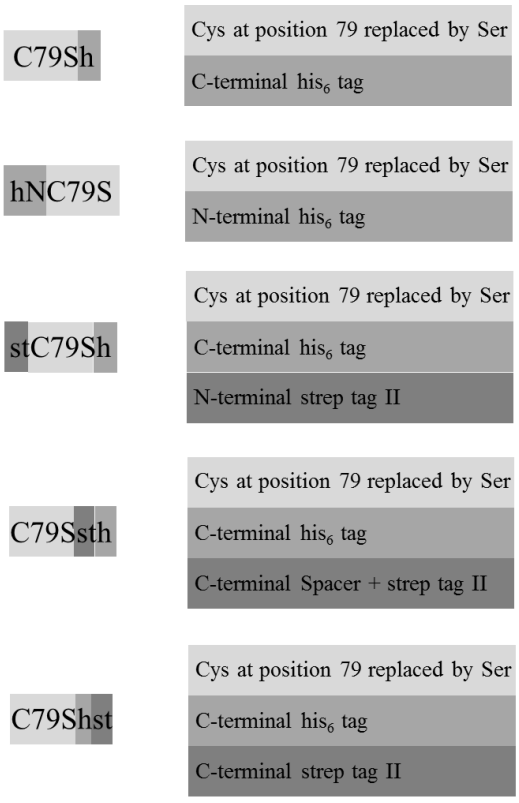

7.4. LHCII sequence, DNA base code, amino acids, replacements and insertions

st (strep tag II): TGG AGC CAC CCG CAG TTC GAA AAA
hN (his$_6$ tag): CAC CAT CAC CAT CAC CAT

S3C: Cys (TGT) K7C: Cys (TGT) 10: Ser (AGT)

Position	START	1	2	3	4	5	6	7	8	9	10
AC 3L-Code		Arg	Lys	Ser	Ala	Thr	Thr	Lys	Lys	Val	Ala
AC 1L-Code		R	K	S	A	T	T	K	K	V	A
Base code	ATG	CGT	AAA	TCT	GCT	ACC	ACC	AAG	AAA	GTA	GCG
Protein part	N-terminal domain										

S11C: Cys (TGC) 12: Pro (CCT) 15: Ser (CCT)

Position	11	12	13	14	15	16	17	18	19	20
AC 3L-Code	Ser	Ser	Gly	Ser	Pro	Trp	Tyr	Gly	Pro	Asp
AC 1L-Code	S	S	G	S	P	W	Y	G	P	D
Base code	AGC	TCT	GGA	AGC	CCA	TGG	TAC	GGA	CCA	GAC
Protein part	N-terminal domain									

Position	21	22	23	24	25	26	27	28	29	30
AC 3L-Code	Arg	Val	Lys	Tyr	Leu	Gly	Pro	Phe	Ser	Gly
AC 1L-Code	R	V	K	Y	L	G	P	F	S	G
Base code	CGT	GTT	AAG	TAC	TTA	GGC	CCA	TTC	TCC	GGT
Protein part	N-terminal domain									

S34C: Cys (TGC)

Position	31	32	33	34	35	36	37	38	39	40
AC 3L-Code	Glu	Ser	Pro	Ser	Tyr	Leu	Thr	Gly	Glu	Phe
AC 1L-Code	E	S	P	S	Y	L	T	G	E	F
Base code	GAG	TCT	CCA	TCC	TAC	TTG	ACT	GGA	GAG	TTC
Protein part	N-terminal domain									

Position	41	42	43	44	45	46	47	48	49	50
AC 3L-Code	Pro	Gly	Asp	Tyr	Gly	Trp	Asp	Thr	Ala	Gly
AC 1L-Code	P	G	D	Y	G	W	D	T	A	G
Base code	CCC	GGT	GAC	TAC	GGT	TGG	GAC	ACT	GCC	GGA
Protein part	N-terminal domain									

S59C: Cys (TGC)

Position	51	52	53	54	55	56	57	58	59	60
AC 3L-Code	Leu	Ser	Ala	Asp	Pro	Glu	Thr	Phe	Ser	Lys
AC 1L-Code	L	S	A	D	P	E	T	F	S	K
Base code	CTC	TCT	GCT	GAC	CCA	GAG	ACA	TTC	TCC	AAG
Protein part	N-terminal domain				Helix H1					

Position	61	62	63	64	65	66	67	68	69	70
AC 3L-Code	Asn	Arg	Glu	Leu	Glu	Val	Ile	His	Ser	Arg
AC 1L-Code	N	R	E	L	E	V	I	H	S	R
Base code	AAC	CGT	GAG	CTT	GAA	GTC	ATC	CAC	TCC	AGA
Protein part	Helix H1									

Position	71	72	73	74	75	76	77	78	79	80
AC 3L-Code	Trp	Ala	Met	Leu	Gly	Ala	Leu	Gly	Cys	Val
AC 1L-Code	W	A	M	L	G	A	L	G	C	V
Base code	TGG	GCT	ATG	TTG	GGT	GCT	TTG	GGA	TGT	GTC
Protein part	Helix H1									

V90C: Cys (TGT)

Position	81	82	83	84	85	86	87	88	89	90
AC 3L-Code	Phe	Pro	Glu	Leu	Leu	Ser	Arg	Asn	Gly	Val
AC 1L-Code	F	P	E	L	L	S	R	N	G	V
Base code	TTC	CCA	GAG	CTT	TTG	TCT	CGC	AAC	GGT	GTT
Protein part	Helix H1						lumenal loop region			

V96C: Cys (TGC)

Position	91	92	93	94	95	96	97	98	99	100
AC 3L-Code	Lys	Phe	Gly	Glu	Ala	Val	Trp	Phe	Lys	Ala
AC 1L-Code	K	F	G	E	A	V	W	F	K	A
Base code	AAA	TTC	GGC	GAA	GCT	GTG	TGG	TTC	AAG	GCA
Protein part	lumenal loop region									

S102C: Cys (TGT)

S106C: Cys (TGT)

Position	101	102	103	104	105	106	107	108	109	110
AC 3L-Code	Gly	Ser	Gln	Ile	Phe	Ser	Glu	Gly	Gly	Leu
AC 1L-Code	G	S	Q	I	F	S	E	G	G	L
Base code	GGA	TCT	CAA	ATC	TTT	AGT	GAG	GGT	GGA	CTT
Protein part	Helix H2				lumenal loop region					

L113C: Cys (TGC)

Position	111	112	113	114	115	116	117	118	119	120
AC 3L-Code	Asp	Tyr	Leu	Gly	Asn	Pro	Ser	Leu	Val	His
AC 1L-Code	D	Y	L	G	N	P	S	L	V	H
Base code	GAT	TAC	TTG	GGC	AAC	CCA	AGC	TTG	GTC	CAT
Protein part	ß-sheet							ß-sheet		

I124C: Cys (TGC)

Position	121	122	123	124	125	126	127	128	129	130
AC 3L-Code	Ala	Gln	Ser	Ile	Leu	Ala	Ile	Trp	Ala	Thr
AC 1L-Code	A	Q	S	I	L	A	I	W	A	T
Base code	GCT	CAA	AGC	ATC	CTT	GCC	ATA	TGG	GCC	ACT
Protein part	lumenal loop region			Helix H3						

V138C: Cys (TGC)

Position	131	132	133	134	135	136	137	138	139	140
AC 3L-Code	Gln	Val	Ile	Leu	Met	Gly	Ala	Val	Glu	Gly
AC 1L-Code	Q	V	I	L	M	G	A	V	E	G
Base code	CAG	GTT	ATC	TTG	ATG	GGA	GCT	GTC	GAA	GGT
Protein part	Helix H3									

I143C: Cys (TGT)

Position	141	142	143	144	145	146	147	148	149	150
AC 3L-Code	Tyr	Arg	Ile	Ala	Gly	Gly	Pro	Leu	Gly	Glu
AC 1L-Code	Y	R	I	A	G	G	P	L	G	E
Base code	TAC	CGT	ATT	GCC	GGT	GGG	CCT	CTC	GGT	GAG
Protein part	Helix H3			stromal loop region						

Position	151	152	153	154	155	156	157	158	159	160
AC 3L-Code	Val	Val	Asp	Pro	Leu	Tyr	Pro	Gly	Gly	Ser
AC 1L-Code	V	V	D	P	L	Y	P	G	G	S
Base code	GTG	GTT	GAT	CCA	CTT	TAC	CCA	GGT	GGA	AGC
Protein part	stromal loop region									

Position	161	162	163	164	165	166	167	168	169	170
AC 3L-Code	Phe	Asp	Pro	Leu	Gly	Leu	Ala	Asp	Asp	Pro
AC 1L-Code	F	D	P	L	G	L	A	D	D	P
Base code	TTT	GAT	CCA	TTG	GGC	TTA	GCT	GAT	GAT	CCA
Protein part	stromal loop region									

A174C: Cys (TGT)

Position	171	172	173	174	175	176	177	178	179	180
AC 3L-Code	Glu	Ala	Phe	Ala	Glu	Leu	Lys	Val	Lys	Glu
AC 1L-Code	E	A	F	A	E	L	K	V	K	E
Base code	GAA	GCA	TTC	GCA	GAA	TTG	AAG	GTG	AAG	GAA
Protein part	Helix H4									

Position	181	182	183	184	185	186	187	188	189	190
AC 3L-Code	Leu	Lys	Asn	Gly	Arg	Leu	Ala	Met	Phe	Ser
AC 1L-Code	L	K	N	G	R	L	A	M	F	S
Base code	CTC	AAG	AAC	GGT	AGA	TTA	GCC	ATG	TTC	TCA
Protein part	Helix H4									

Position	191	192	193	194	195	196	197	198	199	200
AC 3L-Code	Met	Phe	Gly	Phe	Phe	Val	Gln	Ala	Ile	Val
AC 1L-Code	M	F	G	F	F	V	Q	A	I	V
Base code	ATG	TTT	GGA	TTC	TTC	GTT	CAA	GCT	ATT	GTA
Protein part	Helix H4									

Position	201	202	203	204	205	206	207	208	209	210
AC 3L-Code	Thr	Gly	Lys	Gly	Pro	Leu	Glu	Asn	Leu	Ala
AC 1L-Code	T	G	K	G	P	L	E	N	L	A
Base code	ACT	GGA	AAG	GGT	CCT	TTG	GAG	AAC	CTT	GCT
Protein part									Helix H5	

Position	211	212	213	214	215	216	217	218	219	220
AC 3L-Code	Asp	His	Leu	Ala	Asp	Pro	Val	Asn	Asn	Asn
AC 1L-Code	D	H	L	A	D	P	V	N	N	N
Base code	GAT	CAT	CTT	GCA	GAC	CCA	GTC	AAC	AAC	AAT
Protein part	Helix H5			C-terminal domain						

Position	221	222	223	224	225	226	227	228	229	230
AC 3L-Code	Ala	Trp	Ser	Tyr	Ala	Thr	Asn	Phe	Val	Pro
AC 1L-Code	A	W	S	Y	A	T	N	F	V	P
Base code	GCA	TGG	TCA	TAT	GCC	ACC	AAC	TTT	GTT	CCC
Protein part	C-terminal domain									

Position	231	232	STOP
AC 3L-Code	Gly	Lys	
AC 1L-Code	G	K	
Base code	GGA	AAA	TAA
Protein part			

Ch (his$_6$ tag): CAC CAT CAC CAT CAC CAT

Chst (his$_6$ tag and strep tag II): CAC CAT CAC CAT CAC CAT TGG AGC CAC CCG CAG TTC GAA AAA

Csth (spacer (2 Gly), strep tag II, and his$_6$ tag): GGT GGT TGG AGC CAC CCG CAG TTC GAA AAA CAC CAT CAC CAT CAC CAT

tS (tetra serine motif): AGC AGC CCG GGA AGC AGC

7.5. Statutory Declaration

I hereby declare that I wrote the dissertation submitted without any unauthorized external assistance and used only sources acknowledged in the work. All textual passages which are appropriated verbatim or paraphrased from published and unpublished texts as well as all information obtained from oral sources are duly indicated and listed in accordance with bibliographical rules. In carrying out this research, I complied with the rules of standard scientific practice as formulated in the statutes of Johannes Gutenberg-University Mainz to insure standard scientific practice.

Mainz, 28.12.2012

7.6. Curriculum Vitae

Personal information

Name	Carsten Dietz
Place of birth	Wetzlar

Education

11/2008 – 12/2012	Doctorate studies at the department of biology of the Johannes-Gutenberg University, Mainz
09/2009 – 09/2012	Scholarship holder of the Max-Planck-Graduate Center with the Johannes-Gutenberg University (MPGC), Mainz
	Degree: Dr. rer. nat.
10/2003 – 09/2008	Academic studies at the Johannes-Gutenberg University, Mainz
	Degree: Diploma (Biology)
09/1998 – 10/2003	Academic studies at the Johannes-Gutenberg University, Mainz
	Without degree (Pharmacy)

8. References and notes

A:

Adamska I. (1997) ELIPs — light-induced stress proteins, Physiologia. Plantarum. 100; 794–805.

Allen, J. F., Forsberg, J. (2001) Molecular recognition in thylakoid structure and function. Trends Plant Sci., 6, 317-326.

Aurich, H. G. and Heiss, W. (1976) Topics in Current Chemistry", Vol. 59, F. L. Boschke, Ed., Springer-Verlag, New York, N.Y.,

B:

Balaban, A. T. (1971) Rev. Roum. Chim., 16, 725

Bals T., Dünschede B., Funke S., Schünemann D. (2010) Interplay between the cpSRP pathway components, the substrate LHCP and the translocase Alb3: An in vivo and in vitro study. FEBS Letters 584; 4138–4144.

Barros, T., Kühlbrandt, W. (2009) Crystallisation, structure and function of plant Light-Harvesting Complex II, Biochim. Biophys. Acta, 1787, 753-772.

Bassi, R., Sandonà, D. & Croce, R. (1997) Novel aspects of chlorophyll a/b proteins. Physiol. Plant. 100, 769–779.

Bassi, R. und Caffari, S., (2000) LHC proteins and the regulation of photosynthetic light harvesting function by xanthophylls. Photosynthesis research, 64, 243-256.

Bender A. (2004) Konformationsanalyse und Lipidbindung am rekombinanten Lichtsammlerprotein LHCIIb höherer Pflanzen. Dissertation am Fachbereich Biologie, Johannes Gutenberg-Universität, Mainz.

Bhat (1996) K.S. Multiple site-directed mutagenesis, Methods Mol. Biol. 57, 269–277.

Boggasch, S. (2006) Immobilisierung von rekombinantem Haupt-Lichtsammlerkomplex LHCIIb in Liposomen, an Affinitätsmaterialien und Nanokristallen - biochemische und einzelmolekülspektroskopische Untersuchungen. Dissertation am Fachbereich Biologie, Johannes Gutenberg-Universität, Mainz.

Bowman, D.F., Gillan, T. and Ingold, K. U. (1971), J. Am. Chem. SOC., 93,6555

Broglie R., Bellemare G., Bartlett S. G., Chua N. H., Cashmore A. R. (1981) Cloned DNA sequences complementary to mRNAs encoding precursors to the small subunit of ribulose-1,5-bisphosphate carboxylase and a chlorophyll a/b binding polypeptide, Proc. Natl. Acad. Sci. U. S. A. 78; 7304–7308.

Bujard, H., Gentz, R., Lanzer, M., Stueber, D., Müller, M., Ibrahimi, I., Hauptle, M. T., Doberstein, B. (1987) A T5 promoter-based transcription-translation system for the analysis of protein in vivo and in vitro. Meth. Enzymol., 155, 416–433.

Butler, P. J. G., Kühlbrandt, W. (1988) Determination of the aggregate size in detergent solution of the light-harvesting chlorophyll-a/b-protein complex from chloroplast membranes. Proc. Natl. Acad. Sci. USA, 85, 3797-3801.

C:

Caffarri, S., Kouril, R., Kereiche, S., Boekema, E.J. and Croce, R. (2009) Functional architecture of higher plant photosystem II supercomplexes. EMBO J. 28: 3052–3063.

Cashmore, A. R. (1984). Structure and expression of a pea nuclear gene encoding a chlorophyll a/b-binding polypeptide. Proc. Natl. Acad. Sci. USA, 81, 2960-2964.

Chapman, D. (1984) Biological Membranes. Academic Press.

Chen, K.; Swart, H.M. (1990) Oxidation of hydroxylamines to nitroxide spin labels in living cells. Biochim. Biophys. Acta 1034, 285-289

Camm E. L., Green B. R. (2004) How the chlorophyll–proteins got their names, Photosynth Res. 80 (2004) 189–196.

Connelly JP, Müller MG, Hucke M, Gatzen G, Mullineaux CW, Ruban AV, Horton P. (1997) Ultrafast spectroscopy of trimeric light harvesting complex II from higher plants. J Phys Chem, 101: 1902−1909

Coruzzi G., Broglie R., Cashmore A., Chua N. H. (1983) Nucleotide sequences of two pea cDNA clones encoding the small subunit of ribulose 1,5-bisphosphate carboxylase and the major chlorophyll a/b-binding thylakoid polypeptide, J. Biol. Chem. 258; 1399-1402.

Cross, B. C., Sinning, I., Luirink, J., and High, S. (2009) Delivering proteins for export from the cytosol. Nat. Rev. Mol. Cell Biol. 10, 255–264

D:

Daum, D., Nicastro, D., Austin, J. II, McIntosh, R., and Kühlbrandt, W. (2010) Arrangement of photosystem II and ATP synthase in chloroplast membranes of spinach and pea. Plant Cell, 22, 1299-1312

Deisenhofer, J., Epp, O., Miki, K., Huber, R. und Michel, H. (1985) Structure of the protein subunits in the photosynthetic reaction center of Rhodopseudomonas Viridis at 3A resolution. Nature 318, 618-324

Dekker, J. P., Boekema, E. J. (2005) Supramolecular organization of thylakoid membrane proteins in green plants. Biochim. Biophys. Acta, 1706, 12-39.

Demmig-Adams B (1990) Carotenoids and photoprotection in plants: a role for the xanthophyll zeaxanthin. Biochim Biophys Acta 1020: 1–24

Di Valentin M., Biasibetti F., Ceola S., Carbonera D. (2009) Identification of the Sites of Chlorophyll Triplet Quenching in Relation to the Structure of LHC-II from Higher Plants. Evidence from EPR Spectroscopy J Phys Chem B 113, 13071-13078.

Dockter, C. (2005) Konformationsuntersuchungen an rekombinantem Lichtsammlerprotein (LHCII) mittels elektronenparamagnetischer Resonanz (EPR). Diplomarbeit am Fachbereich Biologie, Johannes Gutenberg-Universität, Mainz.

Dockter C. (2009) Untersuchung der Struktur und Assemblierung des Lichtsammelkomplexes II höherer Pflanzen mittels elektronenparamagnetischer Resonanz (EPR). Dissertation am Fachbereich Biologie, Johannes Gutenberg-Universität, Mainz.

Dockter C., Volkov A., Bauer C., Polyhach Y., Joly-Lopez Z., Jeschke G., Paulsen H. (2009) Refolding of the integral membrane protein light-harvesting complex II monitored by pulse EPR. Proc. Natl. Acad. Sci. U.S.A. 106, 18485–18490.

Dockter C., Müller A. H., Dietz C., Volkov A., Polyhach Y., Jeschke G., and Paulsen H. (2011) Rigid Core and Flexible Terminus. THE JOURNAL OF BIOLOGICAL CHEMISTRY VOL. 287, NO. 4, pp. 2915–2925.

Dreuw A., Fleming G. R. and Head-Gordon M. (2003) Chlorophyll Fluorescence Quenching by Xanthophylls. Phys. Chem. Chem. Phys., 5, 3247-3256.

Duysens, L.N.M. and Amesz, J. (1962) Function and identification of two photochemical systems in photosynthesis. Biochim. Biophys. Acta. 64, 243–260.

E:

Engelhardt H., Meins T., Poynor M., Adams V. (2007) High-Level Expression, Refolding and Probing the Natural Fold of the Human Voltage-Dependent Anion Channel Isoforms I and II. J Membrane Biol (2007) 216:93–105

F:

Falk S., Sinning I. (2010) cpSRP43 Is a Novel Chaperone Specific for Light-harvesting Chlorophyll a,b-binding Proteins. THE JOURNAL OF BIOLOGICAL CHEMISTRY VOL. 285, NO. 28, pp. 21655–21661.

Fang, G., Friesen, R., Lanfermeijer, F., Hagting, A., Poolman, B. und Konings, W.N. (1999) Manipulation of activity and orientation of membrane-reconstituted di-tripeptide transport protein DtpT of Lactococcus lactis. Mol. Membr. Biol. 16: 297-304.

Fanucci G. E., Lee J. Y., and Cafiso D. S. (2003) Specroscopic evidence that osmolytes used in crystallization buffers inhibit a conformation change in a membrane protein. Biochemistry, 2003; 42: p. 13106-13112.

Field CB, Behrenfeld MJ, Randerson JT, Falkowski P (July 1998) Primary production of the biosphere: integrating terrestrial and oceanic components. Science 281 (5374): 237–40.

Forrester, A. R., Hay, J. M. and Thomson, R. H. (1968) Organic Chemistry of Stable Free Radicals", Academic Press, New York, N.Y.

Frank H. A., Cogdell R. J. (1996) Carotenoids in photosynthesis. Photochem. Photobiol. 63, 257-264.

G:

Geister, S. (2003) Stabilität des Lichtsammlerkomplexes LHCIIb: Mutationsanalyse der luminalen Schleife. Diplomarbeit im Fachbereich Biologie der Universität Mainz

Gilmore AM, Yamamoto HY (1992) Dark induction of zeaxanthin-dependent nonphotochemical fluorescence quenching mediated by ATP. Proc Natl Acad Sci USA 89: 1899–1903.

Gorleku, O. (2007) Trennung und Charakterisierung von phosphoryliertem und nicht phosphoryliertem LHCII. Diplomarbeit am Fachbereich Biologie, Johannes Gutenberg-Universität, Mainz.

Gradinaru CC, Özdemir S, Gülen D, van Stokkum IHM, van Grondelle R, van Amerongen H. (1998) The flow of excitation energy in LHCII monomers: Implications for the structural model of the major plant antenna. Biophys J., 75: 3064−3077

Green, NM (1975) Avidin. Advances in protein chemistry 29: 85–133.

Green, B.R., Dunford, D. G. (1996) The chlorophyll-carotenoid proteins of oxygenic photosynthesis. Annu. Rev. Plant Physiol. Plant Mol. Biol., 47, 685-714.

Green, B. R. and Pichersky, E. (1994) Hypothesis for the evolution of three-helix Chl a/b and Chl a/c light harvesting antenna proteins from two-helix and four-helix ancestors. Photosynth. Res. 39, 149-162

Grudnik, P., Bange, G., and Sinning, I. (2009) Protein targeting by the signal recognition particle. Biol. Chem. 390, 775–782

Gundlach, K. (2010) Pflanzlicher Lichtsammler (LHCII) in Hybridkomplexen mit organischen Farbstoffen und anorganischen Halbleiter-Nanokristallen (Quantum dots). Dissertation am Fachbereich Biologie, Johannes Gutenberg-Universität, Mainz.

H:

Hager A (1969) Light dependent decrease of pH-value in a chloroplast compartment causing enzymatic interconversion of violaxanthin to zeaxanthin—relations to photophosphorylation. Planta 89: 224–243

Hagio M., Gombos Z., Varkonyi Z., Masamoto K., Sato N., Tsuzuki M., Wada H. (2000) Direct evidence for requirement of phosphatidylglycerol in photosystem II of photosynthesis. Plant Phys. 124 (2): 795-804

Hankamer, B., Barber, J. & Boekema, E.J. (1997) Structure and membrane organization of photosystem II from green plants. Ann. Rev. Plant Phys. Plant Mol. Biol. 48, 641–672.DOI: 10.1146/annurev.arplant.48.1.641

Hanson, S. M., Van Eps, N., Francis, D. J., Altenbach, C., Vishnivetskiy, S. A., Arshavsky, V. Y., Klug, C. S., Hubbell, W. L., Gurevich, V. V. (2007) Structure and function of the visual arrestin oligomer. EMBO J., 26, 1726–1736.

Heinemann, B. (1999) Random mutations directed to trans-membrane and loop domains of light-harvesting chlorophyll a/b protein: Impact on complex formation and pigment binding. Dissertation. Institut für Allgemeine Botanik. Johannes Gutenberg-Universität, Mainz.

Hénaut A, Rouxel T, Gleizes A, Moszer I, Danchin A (1996) Uneven distribution of GATC motifs in the Escherichia coli chromosome, its plasmids und its phages. J. Mol. Biol 257:574–585

Henderson, R., Baldwin, J.M., Ceska, T.A., Zemlin, F., Beckmann, E., Downing, K.H. (1990). Model for the structure of bacteriorhodopsin based on high-resolution electron cryomicroscopy. J. Mol. Biol., 213, 899-929

Henry R. L. (2010) SRP: adapting to life in the chloroplast. Nature Structural & Molecular Biology 17, 676–677.

Hieber AD, Bugos RC, Yamamoto HY (2000) Plant lipocalins: violaxanthin de-epoxidase and zeaxanthin epoxidase. Biochim Biophys Acta 1482: 84–91

Hill, R. and Bendall, F. (1960) Function of the two cytochrome components in chloroplasts, a working hypothesis. Nature 186, 136–137

Hirsch JD, Eslamizar L, Filanoski BJ, Malekzadeh N, Haugland RP, Beechem JM, Haugland RP (2002) Easily reversible desthiobiotin binding to streptavidin, avidin, and other biotin-binding proteins: uses for protein labeling, detection, and isolation. Anal Biochem. Sep 15;308(2):343-57.

Hobe, S. (1995) Trimerisierung des in-vitro-rekonstituierten Lichtsammelkomplexes höherer Pflanzen und spektroskopische Untersuchungen zur Pigmentorganisation. Wissenschaftsverlag Mainz, Aachen.

Hobe, S., Förster, R., Klingler, J., Paulsen, H. (1995) N-Proximal sequence motif in lightharvesting chlorophyll a/b-binding protein is essential for the trimerization of lightharvesting chlorophyll a/b complex. Biochemistry 34, 10224–10228

Hobe, S., Niemeier, H.; Bender, A. und Paulsen, H. (2000). Carotenoid binding sites in LHCII – Relative affinities towards major xanthophylls of higher plants. Eur. J. Biochem. 267: 616-624.

Hobe, S., Trostmann, I., Raunser, S., Paulsen, H. (2006) Assembly of the major lightharvesting chlorophyll-a/b complex. Thermodynamics and kinetics of neoxanthin binding. J. Biol. Chem., 281, 25156–25166.

Hölzl G., Witt S., Kelly A. A., Zähringer U., Warnecke D., Dörmann P.; Heinz E. (2006) Functional differences between galactolipids and glucolipids revealed in photosynthesis of higher plants. PNAS 103, 7512–7517

Holt N. E., Zigmantas D., Valkunas L., Li X. P., Niyogi K. K., Fleming G. R. (2005) Carotenoid cation formation and the regulation of photosynthetic light harvesting. Science, 307: 433-436.

Hope, M. J., Bally, M. B., Webb, G. & Cullis, P. R. (1985) Production of large unilamellar vesicles by a rapid extrusion procedure. Characterization of size distribution, trapped volume and ability to maintain a membrane potential. Biochimica et Biophysica Acta, Biomembranes, 812, 55-65.

Horton P, Ruban AV (1992) Regulation of photosystem II. Photosynth Res 34: 375–385

Huang, K.-S., Bayley, H., Liao, M.-J., London, E. & Khorana, H. G. (1981). Refolding of an integral membrane protein.Denaturation, renaturation, and reconstitution of intact bacteriorhodopsin and two proteolytic fragments. J. Biol. Chem. 256, 3802–3809. Ishii T.M., Zerr P., Xia X.M., Bond C.T., Maylie J., Adelman J.P. (1998) Site-directed mutagenesis, Methods Enzymol. 293, 53–71.

Hubbel W. L., Cafiso D. S., Altenbach C. (2000) Identifying conformational changes with site-directed spin labeling. Nature Structural Biology 7 (9): p. 735-739.

J:

Jackowski, G., Kacprzak, K., Jansson, S. (2001) Identification of Lhcb1/Lhcb2/Lhcb3 heterotrimers of the main light-harvesting chlorophyll a/b-protein complex of photosystem II (LHC II). Biochim. Biophys. Acta, 1504, 340–345.

Jansson, S. (1994) The light-harvesting chlorophyll a/b-binding proteins. Biochim. Biophys Acta, 1184, 1-19.

Jansson, S. (1999) A guide to the Lhc genes and their relatives in Arabidopsis. Trends in Plant Science, 4, 236–240.

Janzen, E. G. (1971) For a review of the stereochemistry and conformational aspects of nitroxides, Top. Stereochem., 177-217

Jaru-Ampornpan, P., Chandrasekar, S. and Shan, S.O. (2007) Efficient interaction between two GTPases allows the chloroplast SRP pathway to bypass the requirement for an SRP RNA. Mol. Biol. Cell 18, 2636–2645.

Jeschke, G., Bender, A., Schweikardt, T., Panek, G., Decker, H., Paulsen, H. (2005) Localization of the N-terminal domain in light-harvesting chlorophyll-a/b-protein by electron paramagnetic resonance measurements. J. Biol. Chem., 280, 18623-18630.

K:

Kaufmann, L. (2010) Heterogen markierter trimerer Lichtsammelkomplex (LHCII) zur strukturellen Charakterisierung mittels elektronenparamagnetischer Resonanz (EPR). Staatsexamensarbeit, am Fachbereich Biologie, Johannes Gutenberg-Universität, Mainz.

Keana, J. F. W. (1977) Newer Aspects of the Synthesis and Chemistry of Nitroxide Spin Labels, Chemical Reviews, Vol. 78, No. 1

Kees L., Franken C., Hoebert S., Hiemstra, van Meijgaarden K. E., Subronto Y., den Hartigh J., Ottenhoff T. H. M., Drijfhout J. W. (2000) Purification of His-Tagged Proteins by Immobilized Chelate Affinity Chromatography: The Benefits from the Use of Organic Solvent. Protein Expression and Purification 18, 95–99

Kessler, F., and Schnell, D. (2009) Chloroplast biogenesis: diversity and regulation of the protein import apparatus. Curr. Opin. Cell Biol. 21, 494–500.

Kim S., Sandusky P., Bowlby N. R., Aebersold R., Green B. R., Vlahakis S., Yocum C. F., Pichersky E. (1992) Characterization of a spinach psbS cDNA encoding the 22 kDa protein of photosystem II, FEBS Lett. 314; 67–71.

Kleima FJ, Gradinaru CC, Calkoen F, van Stokkum IHM, van Grondelle R, van Amerongen H. (1997) Energy transfer in LHC II monomers at 77K studied by sub-picosecond transient absorption spectroscopy. Biochemistry, 36: 15262−15268

Klimyuk, V. I., Persello-Cartieaux, F., Havaux, M., Contard-David, P., Schünemann, D., Meiherhoff, K., Gouet, P., Jones, J. D., Hoffman, N. E., and Nussaume, L. (1999) A chromodomain protein encoded by the arabidopsis CAO gene is a plant-specific component of the chloroplast signal recognition particle pathway that is involved in LHCP targeting. Plant Cell 11, 87–99

Knol, J., Sjollema , K., und Poolman B. (1998) Detergent-mediated reconstitution of membrane proteins. Biochemistry 37(46):16410-5.

Kooyman R. P. H., Schaafsma T. J., Jansen G., Clarke R. H., Hobart D. R., Leenstra W. R. (1979) A comparative study of dimerization of chlorophylls and pheophytins by fluorescence and odmir. Chem. Phys. Lett., 68,65

Krause G. H., Weis E. (1991) Chlorophyll fluorescence and photosynthesis: The basics. Annu. Rev. Plant Physiol. Plant Mol. Biol. 42: 313-350.

Kroll, C. (1999) Analytik, Stabilität und Biotransformation von Spinsonden sowie deren Einsatz im Rahmen pharmazeutisch-technologischer und biopharmazeutischer Untersuchungen. Dissertation, Humboldt-Universität Berlin.

Kruse O., Hankamer B., Konczak C., Gerle C., Morris E., Radunz A., Schmid G. H., Barber J. (2000) Phosphatidylglycerol is involved in the dimerization of photosystem II. J. Biol. Chem. 275, 6509-6514

Kühlbrandt, W., Wang, D. N., Fujiyoshi, Y. (1994) Atomic model of plant light harvesting complex by electron crystallography. Nature, 367, 614-621.

Kunkel T.A. (1985) Rapid and efficient site-specific mutagenesis without phenotype selection, Proc. Natl. Acad. Sci. USA 82, 488–492.

Kylie D. Barker, Amanda L. Eckermann, Matthew H. Sazinsky, Matthew R. Hartings, Carnie Abajian, Dimitra Georganopoulou, Mark A. Ratner, Amy C. Rosenzweig, and Thomas J. Meade (2009) Protein Binding and the Electronic Properties of Iron(II)

Complexes: An Electrochemical and Optical Investigation of Outer Sphere Effects. Bioconjugate Chem., 20, 1930–1939

L:

Lampoura S. S., Barzda V., Owen G. M., Hoff A. J., van Amerongen H. (2002) Aggregation of LHCII leads to a redistribution of the triplets over the central xanthophylls in LHCII. Biochemistry 41; 9139-9144.

Latowski D., Åkerlund H-E., Strza]ka K. (2004) Violaxanthin De-Epoxidase, the Xanthophyll Cycle Enzyme, Requires Lipid Inverted Hexagonal Structures for Its Activity. Biochemistry 43, 4417-4420

Lauf, L. (2012) Herstellung & strukturelle Charakterisierung heterogen markierter trimerer Lichtsammelkomplexe (LHCII) mittels elektroparamagnetischer Resonanz (EPR) und LHCII Degradierung durch die Chl b Reduktase. Erweiterte Staatsexamensarbeit, am Fachbereich Biologie, Johannes Gutenberg-Universität, Mainz.

Lee G.-C., Lee L.-C., Sava V., Shaw J.-F. (2002) Multiple mutagenesis of non-universal serine codons of the Candida rugosa LIP2 gene and biochemical characterization of purified recombinant LIP2 lipase overexpressed in Pichia pastoris, Biochem. J. 366, 603–611.

Levy, D., Gulik, A., Bluzat, A., and Rigaud, J.-L. (1992) Reconstitution of the sarcoplasmic reticulum Ca^{2+}-ATPase: mechanisms of membrane protein insertion into liposomes during reconstitution procedures involving the use of detergents. BBA 1107, 283–298

Li X-P, Phippard A, Pasari J, Niyogi KK. (2002c) Structure function analysis of photosystem II subunit S (PsbS) in vivo. Functional Plant Biology 29, 1131–1139.

Li X-P, Gilmore AM, Caffarri S, Bassi R, Golan T, Kramer D, Niyogi KK. (2004) Regulation of photosynthetic light harvesting involves intrathylakoid lumen pH sensing by the PsbS protein. Journal of Biological Chemistry 279, 22866–22874.

Liu, Z., Yan, H., Kuang, T., Zhuang, J., Bui, L., Chang, W. (2004) Crystal structure of spinach major light-harvesting complex at 2.72 Å resolution. Nature, 428, 287-292.

Liu, C., Zhang, Y., Cao, D., He, Y., Kuang, T., Yang, C. (2008) Structural and functional analysis of the antiparallel strands in the lumenal loop of the major light-harvesting chlorophyll a/b complex of photosystem II (LHCIIb) by site-directed mutagenesis. J. Biol. Chem., 283, 487-495.

Lund S., Orlowski S., de Foresta B., Champeil P., le Maire M., Møller J. V. (1989) Detergent structure and associated lipid as determinants in the stabilization of solubilized Ca^{2+}-ATPase from sarcoplasmic reticulum. J. Biol. Chem. 264, 4907-4915.

M:

Maire M., Champeil P., Jesper V. Møller J. (2000) Interaction of membrane proteins and lipids with solubilizing detergents. Biochimica et Biophysica Acta 1508, 86-111

Martinie-Hombrouck, J. and Rassat, A. (1974), Tetrahedron, 30, 433

Marty, N.J., Rajalingam, D., Kight, A.D., Lewis, N.E., Fologea, D., Kumar, T.K., Henry, R.L. and Goforth, R.L. (2009) The membrane-binding motif of the chloroplast signal recognition particle receptor (cpFtsY) regulates GTPase activity. J. Biol. Chem. 284, 14891–14903.

McConnell M. D., Koop R., Vasil´ev S., Bruce D. (2002) Regulation of the Distribution of Chlorophyll and Phycobilin-Absorbed Excitation Energy in Cyanobacteria. A Structure-Based Model for the Light State Transition. Plant Physiology, Vol. 130, pp. 1201–1212.

Mc Dermott, G., Prince, S.N., F reer, A.A., Hawthornthwaite-Lawless, A.M., Papiz, M.Z., Cogdell, R.J., Isaacs, N.W (1995) Crystal structure of an integral membran light-harvesting complex from the photosythetic bacteria. Nature 374, 517-521 (1995).

Meyer G., Kloppstech K. (1984) A rapidly light-induced chloroplast protein with a high turnover coded for by pea nuclear DNA, Eur. J. Biochem. 138; 201–207.

Michaelian I., Sergeant A. (1992) A general and fast method to generate multiple site directed mutations, Nucleic Acids Res. 20, 376.

Michalke K., Huyghe C., Lichière J., Gravière M. E., Siponen M., Sciara G., Lepaul I., Wagner R., Magg C., Rudolph R., Cambillau C., Desmyter A. (2010) Mammalian G protein-coupled receptor expression in Escherichia coli: II. Refolding and biophysical

characterization of mouse cannabinoid receptor 1 and human parathyroid hormone receptor 1. Analytical Biochemistry 401; 74–80

Milsmann, M. H. W., Schwendener, R. A. & Weder, H. G. (1978) The preparation of large single bilayer liposomes by a fast and controlled dialysis. Biochimica et Biophysica Acta, Biomembranes, 512, 147-155.

Moore, M., Harrison, M.S., Peterson, E.C. and Henry, R. (2000) Chloroplast Oxa1p homolog albino3 is required for post-translational integration of the light harvesting chlorophyll-binding protein into thylakoid membranes. J. Biol. Chem. 275, 1529–1532.

Moore, M., Goforth, R.L., Mori, H. and Henry, R. (2003) Functional interaction of chloroplast SRP/FtsY with the ALB3 translocase in thylakoids: substrate not required. J. Cell Biol. 162, 1245–1254.

Mozzo M., Dall'Osto L., Hienerwadel R., Bassi R., Croce R. (2008) Photoprotection in the antenna complexes of photosystem II – role of individual xanthophylls in chlorophyll triplet quenching. J. Biol. Chem. 283; 6184-6192.

N:

Nilsson, A., Stys, D., Drakenberg, T., Spangfort, M. D., Forsén, S., und Allen, J. F. (1997) Phosphorylation controls the three-dimensional structure of plant light harvesting complex II. JBC 272, 18350 – 18357

Niyogi KK, Grossman AR, Bjo¨rkman O (1998) Arabidopsis mutants define a central role for the xanthophyll cycle in the regulation of photosynthetic energy conversion. Plant Cell 10: 1121–1134.

Niyogie K.K., Li X., Rosenberg V. and Jung H. (2004) Is PsbS the site of non-photochemical quenching in photosynthesis? Journal of Experimental Botany, 56, No. 411; p.375-382.

Nußberger, S., Dörr, K., Wang, D. N., Kühlbrandt, W. (1993) Lipid-protein interactions in crystals of plant light-harvesting complex. J. Mol. Biol., 234, 347-356.

O:

Olson, F., Hunt, C. A., Szoka, F. C., Vail, W. J. & Papahadjopoulos, D. (1979) Preparation of liposomes of defined size distribution by extrusion through polycarbonate membranes. Biochimica et biophysica acta, 557, 9-23.

P:

Papahadjopoulos, D. & Watkins, J. C. (1967) Phospholipid model membranes. II. Permeability properties of hydrated liquid crystals. Biochimica et Biophysica Acta, Biomembranes, 135, 639-652.

Park K. H., Berrier C., Martinac B., Ghazi A. (2004) Purification and Functional Reconstitution of N- and C-Halves of the MscL Channel. Biophys J.; April; 86(4): 2129–2136

Paulsen, H., Rümler, U., and Rüdiger, W. (1990) Reconstitution of pigment-containing complexes from light-harvesting chlorophyll a/b-binding protein overexpressed in *E. coli*. Planta 181, 204–211

Paulsen, H., Finkenzeller, B., Kühlein, N. (1993) Pigments induce folding of light-harvesting chlorophyll-a/b-binding protein. Eur. J. Biochem., 215, 809-816.

Perozo E., Cortes D. M., and Cuello L. G. (1999) Structural rearrangement underlying K^+-channel activation gating. Science; 285: p. 73-78.

Peter, G. F., and Thornber, J. P. (1991) Biochemical composition and organization of higher plant photosystem II light-harvesting pigment proteins. J. Biol. Chem. 266, 16745–16754

Pettersen, E. F., Goddard, T. D., Huang, C. C., Couch, G. S., Greenblatt,D. M.,Meng, E. C., Ferrin, T. E. (2004) UCSF chimera –Avisualization system for exploratory research and analysis. J. Comput. Chem., 25, 1605–1612.

Pfundel E, Bilger W (1994) Regulation and possible function of the violaxanthin cycle. Photosynth Res 42: 89–109.

Plumley, F. G., Schmidt, G. W. (1987) Reconstitution of chlorophyll a/b light-harvesting complexes: Xanthophyll-dependent assembly and energy transfer. Proc. Natl. Acad. Sci. USA, 84, 146-150.

Plunger, M. (2007) Herstellung heterogener Trimere des rekombinanten Lichtsammlerproteins (LHCII). Diplomarbeit am Fachbereich Biologie, Johannes Gutenberg-Universität, Mainz.

Polyhach, Y., Bordignon E., Tschaggelar R., Gandra S., Godt A. and Jeschke G. (2012) High sensitivity and versatility of the DEER experiment on nitroxide radical pairs at Q-band frequencies. Phys. Chem. Chem. Phys., 2012, 14, 10762–10773.

radical pairs at Q-band frequencies

Popot, J-L., Engelman, D.M. (2000). Helical Membrane Protein Folding, Stability, and Evolution. Annu. Rev. Biochem. 69, 881-922

R:

Richard, P., Rigaud, J.-L., and Graber, P. (1990) Reconstitution of CFoF1 into liposomes using a new reconstitution procedure. Eur. J. Biochem. 193, 921–925

Rigaud, J.-L., and Pitard, B. (1995) in: Liposomes as Tools in Basic Research and Industry (Phillippot, L. L., and Schuber, F., eds) CRC Press, Boca Raton, FL

Rozantsev, E. G. (1970) Free Nitroxyl Radicals", Plenum Press, New York, N.Y.,

Rozantsev, E. G. and Scholle, V. D. (1971) Synthesis, 190

Ruban, A. V., Calkoen, F., Kwa, S. L. S., Grondelle, R. va, Horton, P. and Dekker, J. P. (1997) Characterisation of LHCII in the aggregated state by linear and circular dichroism spectroscopy. BBA 1321, 61-70

Rühle, W., Paulsen, H. (2004) Preparation of native and recombinant light-harvesting chlorophyll-a/b complex, Methods in Molecular Biology, 274, Photosynthesis Research Protocols.

S:

Salvadori E., Di Valentin M., Kay C. W. M., Pedone A., Baronee V. and Carboneraa D. (2012) The electronic structure of the lutein triplet state in plant light-harvesting complex II. Phys. Chem. Chem. Phys., 14, 12238–12251.

Sanger, F., Nicklen, S., Coulsen, A. R. (1977). DNA sequencing with chain-terminating inhibitors. Proc. Natl. Acad. Sci. USA, 74, 5463-5467.

Sato N., Hagio M., Wada H., Tsuzuki M. (2000) Requirement of phosphatidylglycerol for photosynthetic function in thylakoid membranes. PNAS 97, 10655-10660

Schmid, V. H. R. (2008) Light-harvesting complexes of vascular plants. Cell. Mol. Life. Sci., 65, 3619-3639.

Schmidt T. G. M., Koepke J., Frank R., Skerra A. (1996) Molecular Interaction Between the Strep-tag Affinity Peptide and its Cognate Target, Streptavidin. J. Mol. Biol. 255, 753–766.

Schmitt J, Hess H, Stunnenberg HG (1993) Affinity purification of histidine-tagged proteins. Mol Biol Rep. 18(3):223-30.

Schneider, K. (2008) Trennung und Charakterisierung von phosphoryliertem und nicht phosphoryliertem LHCII. Diplomarbeit, Johannes Gutenberg-Universität, Mainz.

Schön P. (2003) Protein-modifizierte Elektroden: Immobilisierung und Elektronentransfer. Dissertation am Fachbereich Biologie, Universität Osnabrück.

Schuenemann, D., Gupta, S., Persello-Cartieaux, F., Klimyuk, V. I., Jones, J. D., Nussaume, L., and Hoffman, N. E. (1998) Proc. Natl. Acad. Sci. U.S.A. 95, 10312–10316

Schünemann, D. (2007) Mechanisms of protein import into thylakoids of chloroplasts. Biol. Chem. 388, 907–915.

Scoville, D., Stamm, J. D., Altenbach, C., Shvetsov, A., Kokabi, K., Rubenstein, P. A., Hubbell, W. L., Reisler, E. (2009) Effects of binding factors on structural elements in F-Actin. Biochemistry, 48, 370-378.

Seimetz, M. (2004) Abstandsmessungen am rekombinanten Lichtsammlerprotein mittels elektromagnetischer Resonanz (EPR). Einfluss von Xanthophyllen auf die Konformation des LHCIIb. Staatsexsamensarbeit am Fachbereich Biologie, Johannes Gutenberg-Universität, Mainz.

Selstam E. (1998) Development of thylakoid membranes with respect to lipids. In: Siegenthaler P-A.; Murata N. (eds) Lipids in Photosynthesis: Structure, Function and Genetics, 209-224. Kluwer, Dordrecht.

Soll, J., and Schleiff, E. (2004) Protein import into chloroplasts. Nat. Rev. Mol. Cell Biol. 5, 198–208

Sprague S. G., Staehelin L. A. (1984) Effects of reconstitution method on the structural organization of isolated chloroplast membrane lipids. BBA 777, 306–322.

Standfuss, J., Kühlbrandt, W. (2004) The three isoforms of the light-harvesting complex II. Spectroscopic features, trimer formation, and functional roles. J. Biol. Chem., 279, 35, 36884-36891.

Standfuss, J., Terwisscha van Scheltinga, A. C., Lamborghini, M., und Kühlbrandt, W. (2005) Mechanisms of photoprotection and nonphotochemical quenching in pea lightharvesting complex at 2.5 Å resolution. EMBO J., 24, 919–928.

Steffen R., Kelly A. A., Huyer J., Dörmann P., Renger G. (2005) Investigations on the Reaction Pattern of Photosystem II in Leaves from Arabidopsis thaliana Wild Type Plants and Mutants with Genetically Modified Lipid Content. Biochemistry 44, 3134-3142

Steinhoff H. J. (2002) Methods for study of protein dynamics and protein-protein interaction in protein-ubiquitination by electron paramagnetic resonance spectroscopy. Frontiers in Bioscience, 7: p. c97-110.

Stengel, K. F., Holdermann, I., Cain, P., Robinson, C., Wild, K., and Sinning, I. (2008) Structural basis for specific substrate recognition by the chloroplast signal recognition particle protein cpSRP43. Science 321, 253–256

Storf, S., Stauber, E., Hippler,M. and Schmid,V. H. R. (2004) Proteomic Analysis of the photosystem I light-harvesting antenna in tomato (Lycopersicon esculentum). Biochemistry 43, 9214–9224.

Sundström, V. (2000) Light in elementary biological reactions. Progress in Quantum Electronics 24, 187

Szoka, F., Jr. & Papahadjopoulos, D. (1978) Procedure for preparation of liposomes with large internal aqueous space and high capture by reverse-phase evaporation. Proceedings of the National Academy of Sciences of the United States of America, 75, 4194-4198.

T:

Takabayashi, A.,Kurihara, K., Kuwano, M., Kasahara, Y., Tanaka, R. and Tanaka, A. (2011) The Oligomeric States of the Photosystems and the Light-Harvesting Complexes in the Chl b-Less Mutant. Plant Cell Physiol. 52(12): 2103–2114

Terpe, K. (2003): Overview of tag protein fusions: from molecular and biochemical fundamentals to commercial systems. Appl. Microbiol. Biotechnol. 60: 523-533.

Timperio, A. M. and Zolla, L. (2005) Investigation of the lateral light-induced migration of photosystem II lightharvesting proteins by nano-high performance liquid chromatography electrospray ionization mass spectrometry. J. Biol. Chem. 280, 28858–28866.

Trémoliéres A., Dubacq J. P., Ambard-Bretteville F., RÈmy R. (1981) Lipid composition of chlorophyl–protein complexes: specific enrichment in trans-hexadecenoic acid of an oligomeric form of light-harvesting chlorophyll a/b protein, FEBS Lett. 130; 27–31.

Trémoilières, A. and Siegenthaler, P. A. (1998) Reconstitution of Photosynthetic Structures and Activities with Lipids. Kluwer Academic Publishers, 175-189

Trinkunas G, Connelly JP, Müller MG, Valkunas L, Holzwarth AR. (1997) Model for the excitation dynamics in the light-harvesting complex II from higher plants. J Phys Chem B, 101: 7313−7320

Trostmann, I. (2004) Neoxanthinbindung im majoren Lichtsammelkomplex (LHCIIb) höherer Pflanzen. Diplomarbeit, Johannes Gutenberg-Universität.

Tu, C. J., Peterson, E. C., Henry, R., and Hoffman, N. E. (2000) The L18 domain of light-harvesting chlorophyll proteins binds to chloroplast signal recognition particle 43. J. Biol. Chem. 275, 13187–13190

V:

Van der Vos, D. Carbonera, A.J. Hoff (1991) Microwave and optical spectroscopy of carotenoid triplets in light-harvesting complex LHCII of spinach by absorbance-detected magnetic resonance, J. Appl. Magn. Reson. 2; 179–202.

Visser HM, Kleima FJ, van Stokkum IHM, van Grondelle R, van Amerongen H. Probing the many energy-transfer processes in the photosynthetic lightharvesting complex II at 77

K using energy-selective sub-picosecond transient absorption spectroscopy. Chem Phys 1996, 210: 297−312

Volkov, A., Dockter, C., Bund, T., Paulsen, H., and Jeschke, G. (2009) Pulsed EPR determination of water accessibility to spin-labeled amino acid residues in LHCIIb. Biophys. J. 96, 1124–1141

W:

Weber, PC, Phlendorf, DH, Wendoloski, JJ Salemme, FR (1989) Structural origins of high-affinity biotin binding to streptavidin. Science Vol. 243 no. 4887 pp. 85-88.

Wedel N., Klein R., Ljungberg U., Andersson B., Herrmann R. G. (1992) The single-copy gene psbS codes for a phylogenetically intriguing 22 kDa polypeptide of photosystem II, FEBS Lett. 314; 61–66.

Weiner M.P., Costa G.L., Schoettlin W., Cline J., Mathur E., Bauer J.C. (1994) Site-directed mutagenesis of double-stranded DNA by the polymerase chain reaction, Gene 151, 119–123.

Williams W. P. (1998) The physical properties of thylakoid membrane Lipids and their relation to photosynthesis. In: Siegenthaler, P-A.; Murata, N. (eds) Lipids in Photosynthesis: Structure, Function and Genetics, 103-118. Kluwer, Dordrecht.

Woodle, M. C. & Papahadjopoulos, D. (1989) Liposome preparation and size characterization. Methods in Enzymology, 171, 193-217.

Y:

Yang, C., Boggasch, S., Haase, W. and Paulsen, H. (2006) Thermal stability of trimeric light-harvesting chlorophyll a/b complex (LHCIIb) in liposomes of thylakoid lipids. BBA 1757, 1642-1648

Yang, C., Lambrev, P., Chen, Z., Jávorfi, T., Kiss, A., Paulsen, H., Garab, G. (2008) The negatively charged amino acids in the lumenal loop influence the pigment binding and conformation of the major light-harvesting chlorophyll a/b complex of photosystem II. Biochim. Biophys. Acta, 1777, 1463–1470.

Yi Y, Kermasha S, Neufeld R (2006) Characterization of sol-gel entrapped chlorophyllase. Biotechnol. Bioeng. 95 (5): 840–9

Z:

Zaks J., Amaranth K., Kramer D. M., Niyogi K. K., and Fleming G. R. (2012) A kinetic model of rapidly reversible nonphotochemical quenching. PNAS. In print.

Zhang S., Scheller H. V (2004) Light-harvesting complex II binds to several small subunits of photosystem I. H. Biol Chem. 279, 3180-3187

Zinth, W., Huppman, P., Arlt, T. und Wachtveitl, J. (1998) Ultrafast spectroscopy of the electron transfer in photosythetic reaction centers: towords a better understanding of electron tranfer in biological systems. Phil. Trans. R. Soc. Lond. A 356, 465-476

Zolla, L., Rinalducci, S., Timperio, A. M. and Huber, C. G. (2002) Proteomics of light-harvesting proteins in different plant species. Analysis and comparison by liquid chromatography- electrospray ionization mass spectrometry. Photosystem I. Plant Physiol. 130, 1938–1950.

Zolla, L., Rinalducci, S.,Walcher,W. and Huber, C.G. (2003) Proteomics of light-harvesting proteins in different plant species. Analysis and comparison by liquid chromatographyelectrospray ionization mass spectrometry. Photosystem II. Plant Physiol. 131, 198–214.

Zolla, L., Rinalducci, S. and Timperio, A. M. (2007) Proteomic analysis of photosystem I components from different plant species. Proteomics 7, 1866–1876.